

**Functional characterization of the *Ustilago maydis*
effector genes *UMAG_11060* and *UMAG_05306***



Inaugural-Dissertation

zur

Erlangung des Doktorgrades der Naturwissenschaften

(Der.rer.nat.)

der Mathematisch-Naturwissenschaftlichen Fakultät

der Universität zu Köln

vorgelegt von

Luyao Huang

aus Chongqing

Köln, 2023

**Functional characterization of the *Ustilago maydis*
effector genes *UMAG_11060* and *UMAG_05306***

Inaugural-Dissertation

zur

Erlangung des Doktorgrades der Naturwissenschaften

(Der.rer.nat.)

der Mathematisch-Naturwissenschaftlichen Fakultät

der Universität zu Köln

vorgelegt von

Luyao Huang

aus Chongqing

Köln, 2023

Die Untersuchungen zur vorliegenden Arbeit wurden von Oktober 2018 bis Mai 2023 am Lehrstuhl für Terrestrische Mikrobiologie an der Universität zu Köln unter der Betreuung von Herrn Prof. Dr. Gunther Döhlemann durchgeführt.

Erstgutachter: Prof. Dr. Gunther Döhlemann

Zweitgutachter: Prof. Dr. Bart Thomma

Tag der mündlichen Prüfung: 07.08.2023

Summary

Ustilago maydis causes corn smut and triggers tumor formation in all aerial parts of maize. To adapt to the host plant and promote disease progression, *U. maydis* uses effector proteins that exhibit organ-specific expression and adaptation during infection. This study focuses on two of these effectors, *UMAG_11060* and *UMAG_05306*.

This study characterizes *UMAG_11060* (Chapter 2), which encodes the effector protein TOPLESS (TPL) interacting protein 6 (Tip6). The study shows that Tip6 interacts with the N-terminal region of ZmTPL2 through its two EAR (ethylene-responsive element binding factor-associated amphiphilic repression) motifs. These motifs are crucial for virulence function and alter the nuclear distribution pattern of ZmTPL2, disrupting host transcriptional regulation. This disruption leads to the down-regulation of 13 transcription factors in the AP2/ERF B1 subfamily. This study proposes a regulatory mechanism in which Tip6 uses repressive domains to recruit the corepressor ZmTPL2, thereby disrupting the transcriptional networks of the host plant.

The second part of the thesis focuses on the characterization of *UMAG_05306* (Chapter 3), which exhibits highly specific subcellular localization and appears as thick and twisted filament-like structures. The study shows that *UMAG_05306* interacts with four maize dynamin related proteins (DRPs) and is able to interact with both the N- terminal and C-terminal of ZmDRP5. Three DRPs are found to interact with maize tubulin. Furthermore, *UMAG_05306* directly interacts with tubulin. These findings shed light on their potential roles in *U. maydis* infection.

In conclusion, this study provides insight into the molecular mechanisms underlying *U. maydis* infection and reveals the importance of *UMAG_11060* and *UMAG_05306* effectors for virulence and tumor formation.

Abbreviations

Abbreviations

AvrBs3	avirulence protein triggering Bs3 resistance
AFP1	anti-fungal proteins 1
AFP2	anti-fungal proteins 2
AP2	APETALA2
AP2/ERF	APETALA2/ethylene-responsive element binding factor
AUX	Auxin
Ade	Adenine
Aa	Amino acid
Avr	Avirulence
Amp	Ampicillin
Aux/IAA repressor 7	IAA7
BAK1	BRASSINOSTEROID-INSENSITIVE-associated kinase 1
BZR1	brassinazole-resistant 1
BR	brassinosteroid
BD1	BRANCHED SILKLESS1
BFL1	BRANCHED FLORETLESS1
Babyboom	Bbm
CEBiP	chitin oligosaccharide-induced binding protein
CDPKs	calcium- dependent protein kinases
CERK1	chitin-inducible receptor kinase triple complex 1
CBD	chitinase-containing
Chi28	Chintinas 28
Cce1	cysteine-rich core effector
CWDEs	cell wall degrading enzymes
CC9	maize corn cystatin 9
4-coumaroyl CoA	coumaroyl coenzyme A
CRISPR	clustered regularly interspaced short palindromic repeats
Co-IP	Co-immunoprecipitation
CTLH	C-terminal LisH motif domain
CRA	CT11-RanBPM domain
CBB	Coomassie brilliant blue
CLSM	Confocal laser scanning microscopy
cLuc	carboxyl-terminal half of luciferase
Cbx	Carboxin
Carb	Carbenicillin
cDNA	complementary DNA
C-terminal	Carboxyterminal

Cmu1	Chorismate mutase 1
Δ	Deletion/Delta
DAMPs	damage-associated molecular patterns
dpi	days post-infection
DRE	dehydration response elements
DNA	Deoxyribonucleic acid
Da	Dalton
DEGs	Differentially expressed genes
DND1	Defense No Death 1
DND2	Defense No Death 2
DRPs	dynammin-related proteins
ddH₂O	Doubled distilled water
°C	Degree Celsius
DMSO	Dimethylsulfoxid
DTT	Dithiothreitol
EF-Tu	elongation factor thermolabile
EFR	EF-Tu receptor
ETS	effector triggered susceptibility
ETI	effector-triggered immunity
ER	endoplasmic reticulum
EWCA_s	effectors with chitinase activity
Erc1	enzyme required for cell-to-cell elongation
EAR motif	ERF-associated amphiphilic repression motif
ERE	ethylene response elements
ET	ethylene
ESR 1	ENHANCER OF SHOOT REGENERATION 1
ESR 2	ENHANCER OF SHOOT REGENERATION 2
EGB	Early golden bantam
EXPO4	Exportin-4
Fig.	Figure
FLS2	FLAGELLIN-SENSITIVE 2
FLS3	FLAGELLIN-SENSITIVE 3
FZP	FRIZZY PANICLE
Fly1	Fungalysin 1
FC	fold change
GmLHP1-2	heterochromatin protein 1-2
GmPHD6	homeodomain finger protein 6
GlcNAc	N-acetylglucosamine

Abbreviations

GH12	glycoside hydrolase family protein 12
GFP	green fluorescent protein
Gal4AD	Gal4 activation domain
Gal4BD	Gal4 DNA binding domain
GST	glutathione S-transferase
GO	Gene Ontology
β-glucuronidase	GUS
gDNA	genomic DNA
Gent	Gentamycin
GB	Golden bantam
g	Gram
HR	hypersensitive response
HDA19	histone deacetylases 19
HA	Haemagglutinin
His	Histidine
His6	hexahistidine 6
h/hrs	Hour
Hyg	Hygromycin
IAA	indole-3-acetic acid
IP	immunoprecipitation
in planta	inside the plant cell
IPTG	isopropyl-β-D-1-thyogalactopiranoside
JA	Jasmonic acid
JUB1	JUNGBRUNNEN1
Kana	Kanamycin
kDa	Kilodalton
LFQ	label-free quantitation
LPE	LEAFY PETIOLE
LysM	lysine motifs
Leu	Leucine
LisH	LIS1 homology domain
LYK4	LysM-containing receptor-like kinases 4
LYK5	LysM-containing receptor-like kinases 5
MAPK	mitogen-activated protein kinase
Mer1	Merope1
MS	mass spectrometry
ZmKWL1	maize protein Kiwellin 1
M	Molar
min	Minute(s)

ml	Millilitre
mM	Millimolar (mg/L)
mm	Millimeter
mRNA	messenger' RNA
MgCl₂	Magnesium chloride
NADPH	Nicotinamide adenine dinucleotide phosphate
NCER2	NEUTRAL CERAMIDASE 2
NLRs	nucleotide-binding leucine-rich repeat receptors
Nkd1	Naked1
Ni-NTA	Nickel-Nitrilotriacetic acid
NLS	nuclear localization signal
nLuc	amino-terminal half of luciferase
OFP1	ovate family protein 1
OFP6	ovate family protein 6
OG	oligogalacturonide
OD600	Optical density at 600 nm
PRRs	pattern-recognition receptors
PAMPs	pathogen-associated molecular patterns
PTI	pattern-triggered immunity
PR genes	pathogenesis-related genes
PL	proximity labeling
p	Statistical probability value
Pep1	protein essential during penetration 1
POX12	Peroxidase 12
Pit	proteins important for tumor formation
PLCPs	papain-like cysteine proteases
PLANT DEFENSIN1.2	PDF1.2
PCR	Polymerase chain reaction
PD	Potato dextrose
PEG	Polyethyleneglycol
RLKs	receptor-like kinases
RLPs	receptor-like proteins
RDA2	Resistant to DFPM-inhibition of Absciscic acid signaling 2
ROS	reactive oxygen species
R-protein	Resistance genes
RNAi	RNA-mediated silencing
Rsp3	repetitive secreted protein 3
Rip1	ROS interfering protein 1

Abbreviations

RNA-seq	RNA-sequencing
RNA	Ribonucleotide
Rif	Rifampicin
rpm	Rounds per minute
RT	Room Temperature
SGT1	suppressor of G2 allele of <i>skp1</i>
See1	Seedling efficient effector 1
Sts2	small tumor on seedlings 2
SA	Salicylic Acid
SP	Signal peptide
SD	synthetic defined
SEC	size exclusion chromatography
SDS-PAGE	sodium dodecyl sulfate–polyacrylamide gel electrophoresis
SNC1	suppressor of <i>npr1-1</i> , constitutive 1
s/sec	Seconds
TPL	TOPLESS
TFs	transcription factors
TPR	co-repressor TOPLESS-related co-repressor
Tay1	Taygeta1
Tin2	Tumor inducing 2
TALEs	Transcription activator-like effectors
Trp	Tryptophan
TEM	transmission electron microscopy
Tab.	Table
TAE	Tris-Acetate + Na ₂ -EDTA
TBE	Tris-Borate + Na ₂ -EDTA
TE	Tris-Cl + Na ₂ -EDTA
TEMED	Tetramethylethylenediamine
Tris	Trishydroxymethyl aminomethane
µg	Microgram
µm	Micrometer
µM	Micromolar
VIGS	virus-induced gene silencing
V	volts
WAK1	wall-associated kinase 1
WAK2	wall-associated kinase 2
Wuschel2	Wus2
XLP1	XEG1-like protein 1
Y2H	yeast two-hybrid

Contents

Summary.....	I
Abbreviations.....	II
Contents	VII
Chapter 1. Introduction.....	1
1. The importance of plant disease	1
2. Plant-pathogen interactions.....	1
2.1 The plant immune system.....	1
2.2 Effectors in plant-pathogen interaction	5
2.2.1 Effectors: key pathogenic factors	5
2.2.2 Manipulation of plant immunity in microbial interactions	7
3. The <i>Ustilago maydis</i>-maize interaction	10
3.1 The Life cycle of <i>U. maydis</i>	10
3.2 <i>U. maydis</i> as model organism for fungal pathology.....	13
3.3 Understanding the molecular functions of <i>U. maydis</i> effectors.....	14
3.3.1 Evasion of host target recognition.....	16
3.3.2 Inhibition of ROS burst.....	16
3.3.3 Targeting and inhibiting cysteine protease activity	17
3.3.4 Metabolic reprogramming by <i>U. maydis</i> effectors.....	18
3.3.5 Effectors for tumorigenesis.....	19
3.3.6 Targeting TOPLESS corepressors by <i>U. maydis</i> effectors.....	20
4. Aim of this thesis.....	23
Chapter 2. Functional characterization of UMAG_11060	24
1. Functional characterization of UMAG_11060 (Tip6)	24
1.1 Tip6 is required for full virulence of <i>U. maydis</i>	24
1.2 Host target of Tip6 during <i>U. maydis</i> infection.....	25
1.2.1 Identification of host targets of Tip6.....	25
1.2.2 Interactions of Tip6 with maize TPL proteins	27
1.2.3 Tip6 interacts with ZmTPL2 by Co-IP	28
1.2.4 Tip6 binds to the N-terminal of ZmTPL2	28
1.3 Tip6 interacts with ZmTPL2 through EAR motifs.....	34
1.4 EAR motifs are essential for the virulence function of Tip6.....	35
1.5 Impact of Tip6 on maize gene expression.....	36
1.6 Co-localization of Tip6 and ZmTPL2 in plant cells.....	43
1.6.1 Tip6 is localized in the nucleus and cytoplasm	43
1.6.2 Subcellular localization of ZmTPL2	44
1.6.3 Tip6 alters the localization of ZmTPL2	45

Contents

1.6.4 Tetramer formation of ZmTPL2 is required for its nuclear localization	49
1.6.5 Tip6 co-localization with ZmTPL1 and ZmTPL3	52
1.7 Tip6 has a functional ortholog in <i>S. reilianum</i>	53
2. Discussion	57
2.1 Tip6 uses EAR motifs to recruit ZmTPL2	57
2.2 LxLxLx-type EAR motifs of Tip6 are required for virulence	58
2.3 Tip6 perturbs ZmTPL2 and changes its distribution in cells	59
2.4 Tip6 binds to the N-terminus of ZmTPL2	60
2.5 Tip6 regulates expression of various host transcription factors	61
2.6 Tip6 regulates AP2/ERF B1 family of transcription factors	64
2.7 <i>U. maydis</i> uses different strategies to target ZmTPL2	67
2.8 Working model and future plans	69
Chapter 3. Functional characterization of UMAG_05306	73
1. The effector gene UMAG_05306	73
1.1 UMAG_05306 is required for virulence of <i>U. maydis</i>	73
1.2 Subcellular localization of UMAG_05306	74
1.2.1 UMAG_05306 localization in <i>N. benthamiana</i>	74
1.2.2 UMAG_05306 localization in <i>Z. mays</i>	75
1.2.3 Co-localization of UMAG_05306 with the actin marker Lifeact	78
1.2.4 UMAG_05306 localization in maize by transmission electron microscopy ..	79
1.3 UMAG_05306 targets dynamin related protein in the maize	81
1.3.1 UMAG_05306 interacts with four maize DRPs by CoIP	81
1.3.2 UMAG_05306 interacts with N- and C-termini of ZmDRP5	83
1.4 Maize DRPs and UMAG_05306 both interact with maize Tubulin	84
1.5 UMAG_05306 interacts with ZmDRP1C and ZmTubulin3 β in split luciferase assays	87
1.6 Subcellular localization of maize DRPs	88
2. Discussion	91
2.1 UMAG_05306 is a virulence factor for <i>U. maydis</i> infection	91
2.2 UMAG_05306 has specific localization <i>in planta</i>	92
2.3 UMAG_05306 interacts with multiple maize DRPs	93
2.4 DRPs interact with Tubulin	95
2.5 UMAG_05306 interacts with Tubulin	96
2.6 Perspectives	97
Chapter 4. Material and methods	99
4.1 Material and methods	99
4.1.1 Chemicals	99

4.1.2 Buffers and solutions	99
4.1.3 Enzymes, antibodies and IP trap beads.....	99
4.1.4 Commercial kits.....	99
4.2 Media and cultivation.....	101
4.2.1 Media for microbes	101
4.2.2 Cultivation of <i>E. coli</i> and <i>A. tumefaciens</i>	102
4.2.3 Cultivation of <i>U. maydis</i>	102
4.2.4 Cultivation of <i>S. cerevisiae</i>	103
4.2.5 Measurement of cell density.....	103
4.3 Strains, oligonucleotides and plasmids	103
4.3.1 <i>E. coli</i> strains.....	103
4.3.2 <i>A. tumefaciens</i> strains.....	103
4.3.3 <i>S. cerevisiae</i> strains.....	104
4.3.4 <i>U. maydis</i> strains	104
4.3.5 Oligonucleotides.....	105
4.3.6 Plasmids	105
4.4 Microbiological standard experiment methods	108
4.4.1 Competent cell preparation and transformation of <i>E. coli</i>	108
4.4.2 Protoplast preparation and transformation of <i>U. maydis</i>	109
4.4.3 Competent cell preparation and transformation of <i>A. tumefaciens</i>	110
4.4.4 Competent cell preparation and transformation of <i>S. cerevisiae</i>	110
4.4.5 Dropout assay for <i>S. cerevisiae</i>	111
4.4.6 Filamentous growth test for <i>U. maydis</i>	112
4.5 Molecular microbiological methods.....	112
4.5.1 Isolation of nucleic acids	112
4.5.2 Nucleic acid modification.....	114
4.5.3 Separation and detection of nucleic acids.....	116
4.6 Protein methods and biochemical assays.....	118
4.6.1 Protein heterologous protein expression in <i>N. benthamiana</i>	118
4.6.2 Protein overexpression in <i>E. coli</i> and purification	119
4.6.3 Protein extraction from <i>S. cerevisiae</i>	121
4.6.4 Protein extraction from maize or tobacco	122
4.6.5 Co-immunoprecipitation assay in plant.....	122
4.6.6 SDS polyacrylamide gel electrophoresis (SDS PAGE)	124
4.6.7 Western blot	125
4.6.8 Coomassie staining of proteins	126
4.7 Plant assays	127

Contents

4.7.1 <i>Zea mays</i> material	127
4.7.2 Cultivation of <i>Z. mays</i>	127
4.7.3 <i>U. maydis</i> infection of <i>Z. mays</i>	127
4.7.4 Cultivation of <i>N. benthamiana</i>	128
4.7.5 Infiltration of <i>N. benthamiana</i> with <i>A. tumefaciens</i>	128
4.7.6 Biolistic transformation of maize leave cells	128
4.7.7 Split-luciferase complementation assay	129
4.8 Confocal laser scanning microscopy	129
4.9 Bioinformatics methods.....	129
4.9.1 RNA-Seq analysis.....	129
4.9.2 GO enrichment analysis	130
4.9.3 Gene accession	130
5 Bibliography.....	131
6 Appendix	161
Erklärung zur Dissertation.....	170
Delimitation of own contribution.....	171
Acknowledgements	172
Curriculum Vitae	173

Chapter 1. Introduction

1. The importance of plant disease

As the global population exceeds 8 billion in 2022 and continues to grow, the problem of food security remains an increasingly pressing issue (*World Population Prospects 2022: Summary of Results*). Improving crop yields is crucial to address this challenge, and genetics and environmental factors play a significant role in achieving this goal. However, microorganisms such as fungi, oomycetes and bacteria can cause devastating crop diseases that threaten food production and security. These plant pathogenic microorganisms result in an estimated annual global economic loss of approximately US\$220 billion and yield losses of up to 16% globally, highlighting their significant impact on crop yield (*FAO - News Article*; Ficke et al., 2018). Therefore, to combat these plant diseases, it is crucial to gain a comprehensive understanding of plant-pathogen interactions, including the biological characteristics, pathogenic mechanisms, and target host tissues/proteins of plant pathogenic microorganisms. This knowledge can help to identify key components of the plant immune system. It can also help to develop targeted strategies to enhance plant resistance to disease by improving current breeding strategies and selecting crop varieties with higher disease resistance.

2. Plant-pathogen interactions

The innate immunity of plants is essential in protecting them from pathogens and other invaders, allowing them to survive and continue to produce food and other valuable resources for humans and animals. This immune response not only protects plants but also promotes ecological balance by limiting the spread of pathogens and controlling populations of plant-associated microorganisms (Hacquard et al., 2017). As concerns about food security grow, research on plant immunity has become increasingly crucial for improving crop resistance to pathogens and environmental stressors, ultimately enhancing yields and increasing resource efficiency.

2.1 The plant immune system

Plants have an innate immune system relying on immune receptors located on the surface

Introduction

and within cells, allowing them to recognize and respond to various microbial pathogens and defend against invasive organisms (Albert et al., 2020; Boutrot & Zipfel, 2017; Kourelis & van der Hoorn, 2018; Zhou & Zhang, 2020). Pattern-recognition receptors (PRRs) like receptor-like kinases (RLKs) and receptor-like proteins (RLPs) activate pattern-triggered immunity (PTI) by recognizing pathogen-associated molecular patterns (PAMPs), damage-associated molecular patterns (DAMPs), and plant-derived molecular patterns (such as phytocytokines) (Boller & Felix, 2009; Couto & Zipfel, 2016; Hou et al., 2021; Jones & Dangl, 2006; Macho & Zipfel, 2014; Zipfel, 2014).

The bacterial flagellin immunogenic epitope flg22 is one of the essential molecular patterns recognized by plant cells to indicate bacterial pathogen invasion. The two receptors FLAGELLIN-SENSITIVE 2 (FLS2) and BRASSINOSTEROID-INSENSITIVE 1-associated kinase 1 (BAK1) recognize the flg22 epitope and initiate the activation of the innate immune response (Chinchilla et al., 2007; Gómez-Gómez & Boller, 2000; Heese et al., 2007; Sun et al., 2013). Additionally, certain members of the Solanaceae plant family can detect flgII-28 through the FLAGELLIN-SENSING 3 (FLS3) receptor, initiating the activation of multiple defense responses (Cai et al., 2011; Clarke et al., 2013; Hind et al., 2016).

Chitin is a polysaccharide form of N-acetylglucosamine (GlcNAc) that serves as the primary structural component of fungal cell walls. It is hydrolyzed by plant chitin hydrolases to release chitin oligosaccharides, which act as PAMPs and are recognized by plant PRRs containing LysM domains, thereby initiating downstream immune responses in the host plant (Cao et al., 2014; Iizasa et al., 2010; Kaku et al., 2006; Miya et al., 2007; Wan et al., 2012; Zhang et al., 2007). The rice (*Oryza sativa*) chitin elicitor binding protein (CEBiP) was the first chitin receptor to be found (Kaku et al., 2006). In *Arabidopsis*, there are LysM-containing receptor-like kinases 4 (AtLYK4), 5 (AtLYK5) and a chitin-inducible receptor kinase triple complex 1 (AtCERK1) that bind to chitin (Cao et al., 2014; Miya et al., 2007; Petutschnig et al., 2010; Wan et al., 2008, 2012). Recently, a sphingolipid from the cell membrane of *Phytophthora infestans* (*P. infestans*) was found to stimulate defense

responses in *Arabidopsis* by being converted by ceramidase NEUTRAL CERAMIDASE 2 (NCER2) into a 9-methyl-branched sphingoid base, which is detected by RESISTANT TO DFP-M-INHIBITION OF ABSCISIC ACID SIGNALING 2 (RDA2), a type of lectin receptor-like kinase (Kato et al., 2022). Other pathogenic PAMPs, such as bacterial elongation factor thermolabile (EF-Tu) and oligogalacturonide (OG), and fungal cell walls that release pectin are recognized by the PRRs EF-Tu receptor (EFR), wall-associated kinase 1 (WAK1) and WAK2, respectively (Brutus et al., 2010; Kohorn et al., 2009; Kunze et al., 2004).

Recognition of PAMPs by plant PRRs initiates a signaling cascade that triggers plant immune responses, including the influx of calcium ions, the activation of calcium-dependent protein kinases (CDPKs), the phosphorylation of NADPH oxidases leading to the generation of a reactive oxygen species (ROS) burst, the activation of the mitogen-activated protein kinase (MAPK) cascade pathway, the expression of defense-related genes, the biosynthesis of antibacterial compounds and defense-related phytohormones, and the reinforcement of the cell wall (Ahuja et al., 2012; Ali et al., 2018; Kadota et al., 2014; Kazan & Lyons, 2014; Köster et al., 2022; Meng & Zhang, 2013; Ngou et al., 2022; Qi et al., 2017; Underwood, 2012; Yip Delormel & Boudsocq, 2019). However, these mechanisms may not be sufficient to defend against host-adapted pathogens that can produce effectors capable of suppressing the plant immune response, resulting in effector triggered susceptibility (ETS) (Jones & Dangl, 2006). Conversely, plants have evolved resistance (R) genes that encode nucleotide-binding leucine-rich repeat receptors (NLRs), which recognize effectors and activate plant immune responses very similar to PTI, known as effector-triggered immunity (ETI) (Jones & Dangl, 2006; Mur et al., 2008; Ngou et al., 2022) (**Fig. 1**). Recent studies have demonstrated that ETI enhances and prolongs the ROS responses triggered by PTI and amplifies PTI signaling components, resulting in increased transcription of PTI signaling components (Ngou et al., 2021; Yuan et al., 2021). PTI also ensures the normal function of ETI in the complete resistance mechanism through the activation of MAPKs and NADPH signaling pathways (Ngou et al., 2021; Yuan et al., 2021).

Introduction

In conclusion, the innate immune system of plants is essential for their survival. Understanding the mechanisms of plant-pathogen interactions, including the function of effectors, is crucial for gaining insights into the plant immune system.

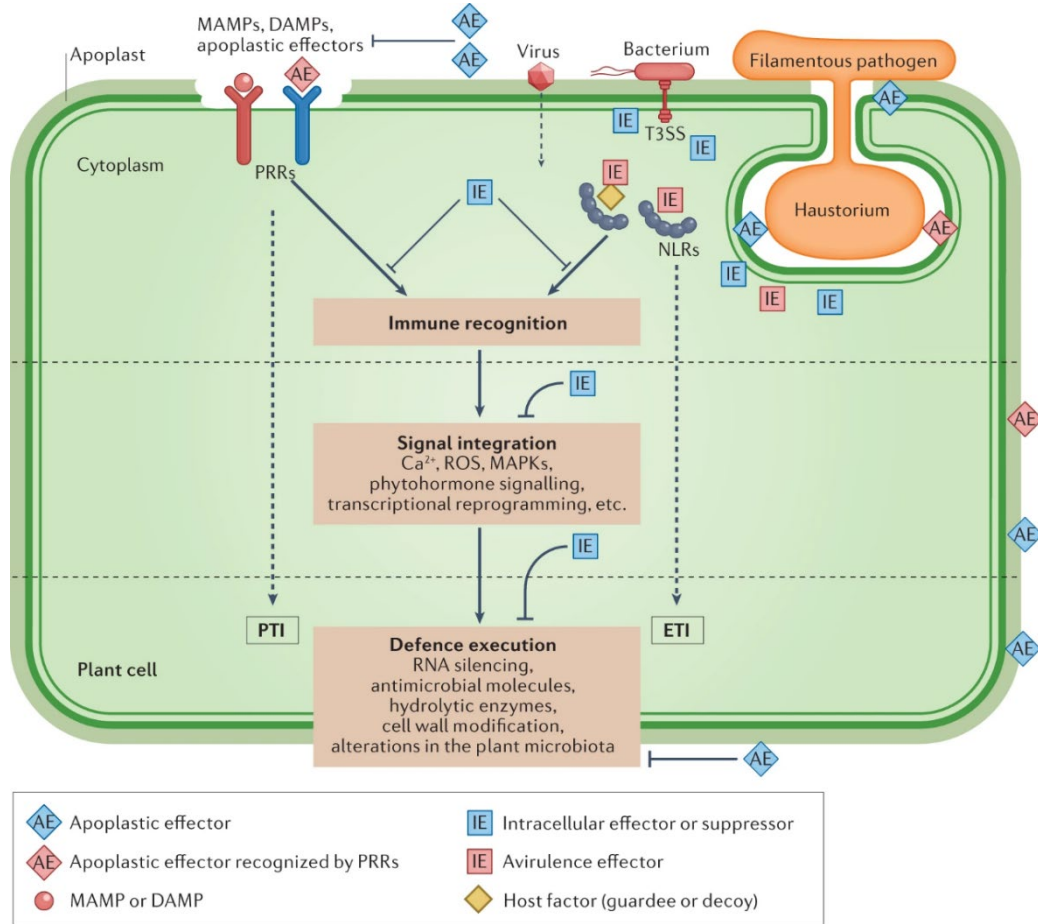


Fig. 1. Activation and phases of the plant innate immune system. The activation of the immune recognition process can be divided into three phases. During the first phase, plant cells utilize pattern-recognition receptors (PRRs) on the cell surface to recognize microorganism-associated molecular patterns (MAMPs), damage-associated molecular patterns (DAMPs) and apoplastic effectors released by pathogens. Intracellular nucleotide-binding leucine-rich repeat receptors (NLRs) recognize pathogenic avirulence effectors. In the second phase, numerous immune signaling events are initiated to coordinate an effective response against the invading pathogens. These events include calcium fluxes, the generation of reactive oxygen species (ROS) bursts, activation of the mitogen-activated protein kinase (MAPK) cascade pathway, activation of phytohormone signaling, and transcriptional reprogramming of host genes. In the third phase, plants execute a series of defense responses, such as RNA silencing, biosynthesis of antimicrobial compounds, secretion of protease and protease inhibitors, cell wall reinforcement, and maintenance of plant microbiota homeostasis. The plant immune system exhibits high resilience and robustness, enabling it to execute defenses quickly and efficiently in each cellular compartment to coordinate the appropriate host response against microbial infection. Picture taken from (Y. Wang et al., 2022).

2.2 Effectors in plant-pathogen interaction

2.2.1 Effectors: key pathogenic factors

Effector proteins are important pathogenic factors that can interfere with the immune response of plants in a variety of ways, thereby promoting pathogen infestation, spread and colonization (Lo Presti et al., 2015; Toruño et al., 2016; Win et al., 2012). For most phytopathogens, effector proteins account for between 5% to 10% of total proteins (Lo Presti et al., 2015). Effector proteins can be recognized by plant PRRs and NLRs and have the ability to inhibit PTI or ETI (Kourelis & van der Hoorn, 2018). Pathogens secrete effector proteins into the plant extracellularly and intracellularly (Lo Presti et al., 2015; Toruño et al., 2016). Most conventional effector proteins carry an N-terminal signal peptide and are secreted via an endoplasmic reticulum (ER)-Golgi-dependent secretory pathway (Lo Presti et al., 2015; Toruño et al., 2016). It is often possible to predict signal peptides and infer putative candidate effectors by bioinformatics (Almagro Armenteros et al., 2019; Arnold et al., 2009; Carreón-Anguiano et al., 2020; Petersen et al., 2011; Sonah et al., 2016; Sperschneider et al., 2016). Some effectors lack the typical N-terminal signal peptide and are transported to the extracellular space by bypassing the ER-Golgi-mediated pathway, and these effectors are secreted via unconventional pathways, including vesicular and non-vesicular pathways (Ding et al., 2012; Giraldo et al., 2013; Nickel & Rabouille, 2009; Rabouille, 2017; Rabouille et al., 2012). In addition, small RNAs and fungal secondary metabolites can also act as effectors to regulate plant immunity and promote infection (Collemare et al., 2019; Huang et al., 2019; Wang et al., 2015).

Based on subcellular localization, effectors are classified into two major categories: apoplastic extracellular effectors and cytoplasmic intracellular effectors (Giraldo et al., 2013; Wang et al., 2017). Several tools have been developed for the prediction of effector protein localization (Briesemeister et al., 2010; Sperschneider et al., 2017, 2018). The oomycete family of cytoplasmic effector proteins is categorized according to conserved motifs in amino-terminal sequences into the RxLR, crinkler (CRN) and CHxC classes of effectors, which contribute to their translocation into host cells (Haas et al., 2009; Jiang et

Introduction

al., 2008; Schornack et al., 2010; Win et al., 2007). Recent reports have shown that RxLR effectors from *P. infestans* and cytoplasmic effectors from *Magnaporthe oryzae* (*M. oryzae*) are translocated into plant cells through clathrin-mediated endocytosis (Oliveira-Garcia et al., 2023; H. Wang et al., 2023). Approximately 80% of the candidate secretory effector proteins of powdery mildew share the N-terminal tripeptide motif Y/F/WxC downstream of the signal peptide (Godfrey et al., 2010; Koeck et al., 2011). Whereas some fungal effectors are usually small cysteine-rich proteins with undefined motifs and structural domains (Gan et al., 2013; O'Connell et al., 2012; Stergiopoulos & de Wit, 2009). The cysteine residues in these effectors may form disulfide bonds, thereby enhancing protein stability, especially in the apoplastic spaces to overcome plant proteases (D. Wang et al., 2020).

Effector proteins face direct conflicts with the plant immune system, making their evolution a crucial factor in optimizing their virulence while evading detection (Lo Presti et al., 2015). However, it is important to control the process of genome evolution; the genome should not evolve indefinitely (Lo Presti et al., 2015). Many phytopathogens use gene-sparse genomic regions, rich in highly repetitive elements and transposons to regulate the rate of evolution (Dutheil et al., 2016; Raffaele & Kamoun, 2012; Singh et al., 2021; Torres et al., 2021). Transposon activity leads to gene dispersion, which promotes the development of gene diversity (Dutheil et al., 2016; Raffaele & Kamoun, 2012; Torres et al., 2021).

Although some core effector proteins remain highly conserved across pathogenic species, most effector proteins lack structural or functional domains, making it difficult to trace and elucidate their evolutionary roots (Seong & Krasileva, 2023; Sperschneider et al., 2015). For example, in *Ustilago maydis*, almost 40% of candidate secreted proteins are novel (Lanver et al., 2017; Schuster et al., 2018). The widespread use of structure prediction software, such as OmegaFold, ESMfold and AlphaFold, in computational structural genomics may help provide a deeper understanding of effector proteins (Seong & Krasileva, 2023). Some effector proteins with vastly different sequences may have

similar protein structure predictions and folding (Guillen et al., 2015; Lazar et al., 2022; Outram et al., 2022; Seong & Krasileva, 2021).

2.2.2 Manipulation of plant immunity in microbial interactions

2.2.2.1 Evade recognition of chitin by the plant immune system

To evade recognition of chitin by the plant immune system, fungal pathogens use various strategies and secrete diverse effector substances. For example, *Cladosporium fulvum* (*C. fulvum*) secretes the LysM-containing effector protein Ecp6, which binds chitin oligomers with ultra-high affinity, preventing host immune receptors from recognizing chitin fragments and triggering an immune response (Bolton et al., 2008; de Jonge et al., 2010; Sánchez-Vallet et al., 2013). Other fungi, including *M. oryzae*, *Colletotrichum higginsianum*, *V. dahlia*, *Rhizoctonia solani*, and *Rhizophagus irregularis*, also secrete LysM effectors, such as MoSlp1, ChElp1, ChElp2, Vd2LysM, RsLysM, and RiSLM, which impede chitin-activated immune responses (Dörfors et al., 2019; Kombrink et al., 2017; Mentlak et al., 2012; Takahara et al., 2016; Zeng et al., 2020).

Besides the LysM domain, other fungal effectors like Avr4 of *C. fulvum* contain a chitin-binding domain (CBM14) and bind to chitin oligomers to shield them from plant chitinase degradation (Hurlburt et al., 2018; van den Burg et al., 2006). UvCBP1, secreted by *Ustilaginoidea virens*, competes with the rice chitin receptor OsCEBiP to suppress chitin-induced immunity (Li et al., 2021). Additionally, fungal proteases like Mep1 and Sep1 of *Fusarium oxysporum* and VdSSEP1 of *V. dahlia* cleave or hydrolyze chitinase-related proteins to reduce immune recognition (L. Han et al., 2019; Jashni et al., 2015). Furthermore, polysaccharide deacetylase PDA1 of *V. dahlia* and effectors with chitinase activity (EWCAs) of *Podosphaera xanthii* alter the host plant's perception of chitin (Gao et al., 2019; Martínez-Cruz et al., 2021).

2.2.2.2 Manipulating plant immunity through cell wall degrading enzymes

Plant pathogens often release cell wall degrading enzymes (CWDEs) to promote their pathogenicity. For example, *Phytophthora sojae* secretes XEG1, a glycoside hydrolase, during early infection, which triggers defense responses in plants (Ma et al., 2015). The

Introduction

plant protease inhibitor GIP1 binds to XEG1, inhibiting its hydrolase activity and activating the immune response (Ma et al., 2015). However, to evade plant recognition, *P. sojae* uses the XEG1-like protein 1 (XLP1), which serves as a ‘decoy effector’ and lacks enzymatic activity (Ma et al., 2015). Moreover, *P. sojae* protects XEG1 from degradation by modifying the plant extracellular aspartic acid protease GmAP5 (Xia et al., 2020). When XEG1 is recognized by different plants, it triggers immune responses through the RXEG1 receptor, which interacts with BAK1 and SOBIR1 to convey defense signals (Ma et al., 2015; L. Wang et al., 2022; Wang et al., 2018). XEG1 promotes heterodimerization of RXEG1 and BAK1 receptors, leading to plant resistance (Sun et al., 2022). Similarly, other fungal CWDEs such as *Fusarium oxysporum* secrete FoEG1, which causes plant cell death and increases disease resistance (Zhang et al., 2021). *V. dahlia* CWDEs, VdEG1 and VdEG3 trigger cell death and immunity in *N. benthamiana* by associating differently with BAK1 and SOBIR1 receptors, thereby manipulating plant immunity (Gui et al., 2017).

2.2.2.3 Reprogramming of plant transcriptome to evade immune response

Pathogens secrete effector proteins to reprogram the host transcriptome, which is a crucial mechanism to evade the immune response. These effectors can act as transcription factors, repressors, or modulators of host transcription factors, thereby interfering with the expression and regulation of host genes. Transcription activator-like effectors (TALEs) are one example of this strategy, secreted by pathogens such as *Xanthomonas* and *Ralstonia* (Boch et al., 2014; de Lange et al., 2013). TALEs have the capability to directly bind to the promoters of target genes in the host plant to activate their expression, thereby promoting pathogen proliferation (Boch et al., 2014; de Lange et al., 2013; Hutin et al., 2015). For example, ERF121 from *Brassica oleracea*, which belongs to the AP2/ERF family of transcription factors, was found as a gene of interest for the conserved TALEs in various strains of *Xanthomonas campestris* pv. *campestris* (Zlobin et al., 2021). The TALE activation of the ERF121 transcription factor leads to a weakened plant defense, increasing the susceptibility of the plant to *Xanthomonas* infection (Zlobin et al., 2021). *Xanthomonas* AvrBs3 localizes in the plant nucleus, inducing hypertrophy of mesophyll cells in the host

plant (Boch & Bonas, 2010; Marois et al., 2002). AvrBs3 induces the upregulation of the basic helix-loop-helix (bHLH) domain transcription factor *upa20*, thereby stimulating the developmental reprogramming of host cells (Boch & Bonas, 2010; Kay et al., 2007). The soybean-like heterochromatin protein 1-2 (GmLHP1-2) and plant homeodomain finger protein 6 (GmPHD6) complex binds to the G-rich elements found in immune-related gene promoters such as GmBAK1-3 and GmPR1, which prompts the transcription process (Qiu et al., 2023). The nuclear effector PsAvh110 of *P. sojae* binds to the GmLHP1-2/GmPHD6 complex, interfering with its formation and transcriptional activity, thereby suppressing plant immune responses to *Phytophthora* (Qiu et al., 2023). Two nuclear-localized effectors, HTR1 and HTR2, secreted by *M. oryzae* appear to act as transcriptional repressors and reprogram the transcription of genes associated with defense (Kim et al., 2020). Additionally, the *Rhizoctonia solani* effector AOS2 interacts with the rice transcription factors WRKY53 and GT1 to activate the hexose transporters SWEET2a and SWEET3a, thereby facilitating the transport of intracellular sugars to the extracellular environment for uptake by pathogens (Yang et al., 2022).

2.2.2.4 Manipulation the cytoskeleton to invade host cells

Another mechanism by which pathogen effector proteins manipulate host cells is through remodeling of the host cytoskeleton. This involves altering the network of protein fibers that provide structural support, facilitate cell movement and re-form new structures that are conducive to pathogen invasion (Li & Day, 2019). The cytoskeleton also has a significant impact on protein transport and information transmission (Li & Day, 2019). An instance of this is the *P. syringae* effector protein HopZ1a, which is an acetyltransferase that is activated by phytic acid (Lee et al., 2012). Once activated, HopZ1a acetylates both itself and tubulin, causing a decrease in the microtubule network. As a result, the secretory pathways of the plant are disrupted, and its cell wall-mediated defenses are suppressed (Lee et al., 2012). It has been discovered that the C-terminal domain of *P. syringae* effector HopW1 interacts directly with F-actin *in vitro*, interfering with the actin cytoskeleton and disrupting plant immunity (Kang et al., 2014). Similarly, the *P. syringae* effector HopG1

Introduction

reduces host actin filament structure and pathogen virulence (Shimono et al., 2016). The ROPIP protein of *Blumeria graminis* f.sp. *hordei* (Bgh) is responsible for targeting the barley ROP GTPase HvRACB, which it recruits to microtubules (Nottensteiner et al., 2018). This action destabilizes the organization of host cell microtubules and helps facilitate entry into the host (Nottensteiner et al., 2018).

In summary, the arm-race between plants and their pathogens has long been characterized by intense interactions. However, as the study of plant-pathogen interactions has advanced, a deeper appreciation for the importance of pathogens in plant infection has emerged. As a result, the investigation of the strategies and mechanisms employed by pathogens to infect plants has become increasingly important for enhancing our understanding of plant immunity and developing new therapeutic options.

3. The *Ustilago maydis*-maize interaction

U. maydis is a notable exception among smut fungi, which represents the second-largest group of plant pathogens after rusts and encompass over 1,500 known species (Zuo et al., 2019). Typically, smut fungi infect plants from the Poaceae family, including economically important crops like maize, wheat, barley, sorghum, and sugarcane, producing teliospores that affect the host reproductive organs (Zuo et al., 2019). However, *U. maydis*, the causal agent of common smut in maize, stands out for its distinct infection style. During its life cycle, *U. maydis* undergoes several distinct penetration steps, each of which involves the delivery of specific effector proteins that manipulate the host plant to create a favorable environment for fungal growth and development. This unique interaction between *U. maydis* and maize has made *U. maydis* an important model organism for studying fungal pathogenesis and plant immunity.

3.1 The Life cycle of *U. maydis*

U. maydis colonizes all the aerial parts of maize plants, resulting in the formation of conspicuous tumors (Banuett, 1992; Christensen, 1963). To complete its life cycle, *U. maydis* goes through several crucial stages (**Fig. 2**). The dissemination of dormant teliospores occurs through their dispersion in the air, followed by landing on the host

surface. Upon encountering a suitable environment with optimal temperature and humidity conditions, teliospores germinate and undergo meiosis, leading to the migration of four haploid nuclei into a promycelium, where cells are separated by septa (Banuett, 1992; Lanver et al., 2017). Subsequently, the yeast-like haploid cells bud off from the promycelium. Two compatible haploid cells engage in a process of conjugation tube recognition and mating under the regulation of the pheromone receptor *a* locus (Banuett & Herskowitz, 1989, 1994; Bölker et al., 1992, 1992; Hartmann et al., 1996). Next, the fused haploid cells undergo mitosis to form a pathogenic dikaryotic hypha. During the mating process, heterodimers with compatible bE and bW alleles of the *b* locus were formed (Gillissen et al., 1992; Kämper et al., 1995; Kronstad & Leong, 1989, 1990). These heterodimers initiate the transcriptional expression of pathogenicity-associated genes, which is primarily regulated by the downstream transcription factor Rbf1 (Heimel et al., 2010). Unlike other fungi, the mycelium of *U. maydis* produces appressoria without melanin deposition or the exertion of high mechanical pressure (Schirawski et al., 2005; Snetselaar & Mims, 1992, 1993). At 0.5-1 days post-infection(dpi), Rbf1 regulates the transcriptional induction and secretion of hydrolytic enzymes, and early effector proteins that are secreted upon the formation of penetration structures called appressoria (Heimel et al., 2010; Kämper et al., 2006; Lanver et al., 2017; Schmitz et al., 2018). The appressoria penetrate the cuticle of the plant surface, invade host epidermal cells, and are tightly wrapped by the host plasma membrane (Lanver et al., 2010; Snetselaar & Mims, 1992). During the biotrophic development phase (2-4 days after inoculation), the transcription factors Hdp2 and Biz1 are involved in the regulation of about 228 effector genes (Lanver et al., 2017; Schmitz et al., 2018). Several highly induced and characterized core effectors are in this stage. Invasive hyphae then induce proliferation in mesophyll cells and vascular bundles, resulting in hypertrophy and hyperplasia (Matei et al., 2018). Subsequently, the transcription factor Fox1 regulates possibly about 38 effectors to repress plant defense (Zahiri et al., 2010). Ultimately, a significant amount of teliospores is formed in the tumor, serving as a source of transmission that can germinate in a suitable environment and

Introduction

perpetuate the cycle of infection (Banuett & Herskowitz, 1996). During the teliospore formation stage, the transcription factor Ros1 differentially regulates 198 effector genes (Tollot et al., 2016). Among these, 45 effectors were inducible at this late stage, while some effectors that were important during early colonization were downregulated (Tollot et al., 2016). In addition, Nlt1 is an important transcription factor for late leaf tumor regulation (Lanver et al., 2018).

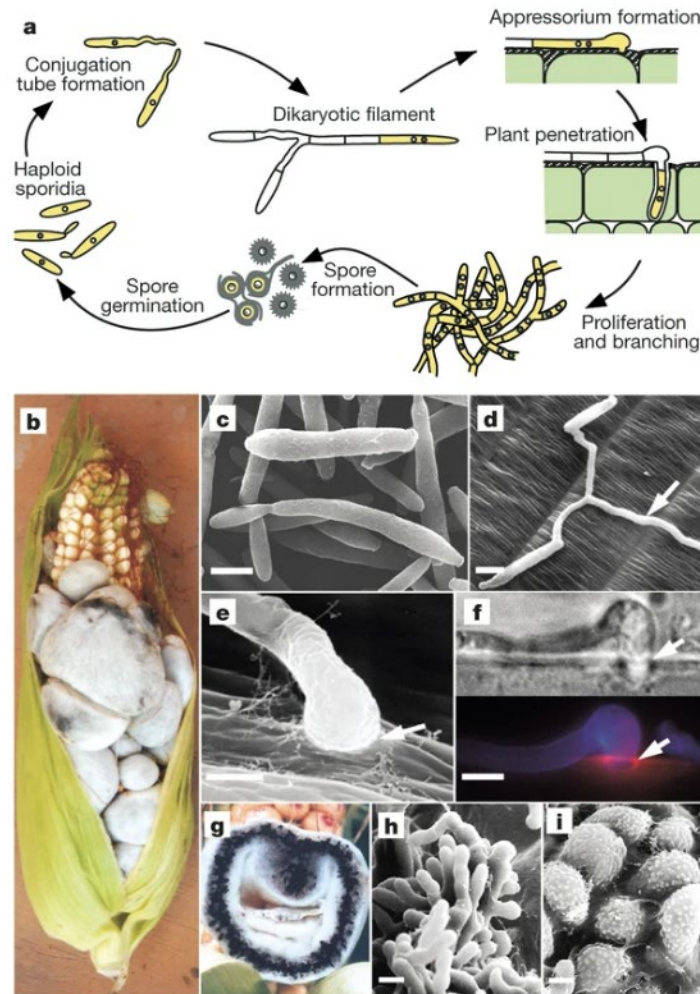


Fig. 2. Key stages and structures of *U. maydis* life cycle on the maize plant. (a) A diagram depicts the life cycle of *U. maydis*. (b) Symptoms of tumor formation in maize. (c) Scanning electron microscopy (SEM) images show haploid sporidia, (d) mated sporidia with a dikaryotic filament signified by an arrow, and (e) the appressorium with a penetrating site marked by an arrow. (f) The top image shows the appressorium, and the bottom image shows the fungal cell wall stained with calcofluor (blue) and endocytotic vesicles stained with FM4-64 (red), with the penetration point indicated by arrows. (g) Black teliospores are visible in tumor sections. (h) SEM images show sporogenous hyphae and (i) ornamented teliospores. Picture taken from Kämper et al., 2006.

3.2 *U. maydis* as model organism for fungal pathology

U. maydis has gained attention as a valuable model organism for investigating fungal effectors and plant interactions, due to its numerous effectors that are exclusively active during plant colonization (Brefort et al., 2009; Dean et al., 2012; Zuo et al., 2019). Its genome, which encodes around 6900 genes and is approximately 20.5 Mb in size, has been fully sequenced and annotated (Kämper et al., 2006). This revealed that many effector genes are clustered together in a manner similar to bacterial pathogenicity islands (Kämper et al., 2006; Lanver et al., 2017). Up to 19% of the effectors are distributed in 12 clusters that are upregulated upon infection, and five of these clusters significantly affect *U. maydis* pathogenicity (Kämper et al., 2006). Unlike obligate biotrophic fungi, *U. maydis* can be grown in the laboratory in haploid forms with synthetic medium (Holliday, 1961, 1974). Additionally, maize seedlings can be infected by mixing compatible hybrids or using the solopathogenic strain SG200, and disease symptoms typically appear within 2 days with observable disease symptoms evaluated within 2 weeks (Bölker et al., 1995; Dean et al., 2012; Kämper et al., 2006). Gene knockouts in *U. maydis* have been highly efficient, and the introduction of CRISPR technology has further improved the process (Kämper, 2004). With CRISPR, it is possible to perform parallel knockouts of multiple genes, making the process even faster and more versatile (Schuster et al., 2016; Zuo et al., 2020). In addition, standard immunoprecipitation techniques and mass spectrometry (MS) analysis have been used to identify host targets of *U. maydis* effectors (Han et al., 2019; Zuo et al., 2023). Recently, proximity labeling (PL) via TurboID-catalyzed intracellular biotinylation has been established for in-depth proteomics studies (Shi et al., 2023). These experiments have provided valuable support for the identification of effector-interacting proteins. Several transcriptomic studies have provided new insights into the interactions between *U. maydis* and maize. A detailed transcriptomic analysis revealed that the expression of effectors varies depending on the infection stages, with peak expression usually occurring at specific stages (Lanver et al., 2018). By comparing the transcriptional profiles of *U. maydis* infection in different maize organs, it has been observed that *U.*

Introduction

maydis employs organ-specific effectors to achieve a higher degree of specialization and adaptation to the host (Redkar et al., 2015; Schilling et al., 2014; Skibbe et al., 2010). The application of laser dissection confocal microscopy allowed separation and observation of hypertrophic mesophyll tumor cells and hyperplastic bundle sheath tumor cells in cells. This revealed specific spatial and cell type-specific regulation of effectors by transcriptomic profiles (Matei et al., 2018; Villajuana-Bonequi et al., 2019). In a study analyzing the transcriptome of six maize lines infected with *U. maydis*, varying levels of susceptibility and resistance were observed (Schurack et al., 2021). Furthermore, another study identified differential expression of effector orthologs between *U. maydis* and *Sporisorium reilianum*, highlighting the role of both transcriptional regulation and protein function in the diversification of effectors in these two closely related pathogens (Zuo et al., 2021).

Recent structural prediction studies have discovered that 22 out of the 24 genes located on chromosome 19 of *U. maydis*, initially believed to be unrelated with respect to sequences, actually possess a strikingly similar structure and are classified as Tin2-like effector proteins (Seong & Krasileva, 2023). Furthermore, the same approach identified a total of 31 Tin2-like effector proteins encoded in the *U. maydis* genome (Seong & Krasileva, 2023). All of these proteins contain folded structures exclusive to the secretory effector genome (Seong & Krasileva, 2023).

3.3 Understanding the molecular functions of *U. maydis* effectors

U. maydis employs a complex strategy during its infection process, characterized by the secretion of specific effector proteins at various stages, including appressorium formation, host colonization, and tumor formation, to evade plant defense responses and interfere with host cellular physiological functions (Lanver et al., 2017, 2018). The successfully identified *U. maydis* effectors have multiple roles, including inhibiting enzymes that are detrimental to *U. maydis*, suppressing ROS bursts, evading host plant recognition, degrading or inactivating host compounds, and interfering with host hormones (**Fig. 3**). Interestingly, unlike its close relative *Ustilago hordei*, *U. maydis* does not have any

identified Avr proteins that can be recognized by NLRs of maize (Lanver et al., 2017). The mechanism by which *U. maydis* avoids the activation of maize NLRs is currently unknown. Nevertheless, understanding the function of *U. maydis* effectors is still valuable in identifying key components of the plant immune system and developing strategies to enhance plant resistance to disease.

Despite characterizing an increasing number of effectors in recent years, the mechanism of their secretion remains poorly understood. Recent studies have suggested that the STP complex, which comprises five effector proteins (stp1-3, cce1 (stp4) and pep1) and two transmembrane proteins (stp5 and stp6) exposed on the cell surface, may be responsible for the secretion of effectors into host cells (Ludwig et al., 2021). The study found that the absence of any member of the STP complex resulted in a complete loss of *U. maydis* virulence, suggesting that any member of the complex is essential for *U. maydis* virulence, possibly because the secretion of effectors is compromised, leading to the inability to complete infection and colonization (Ludwig et al., 2021).

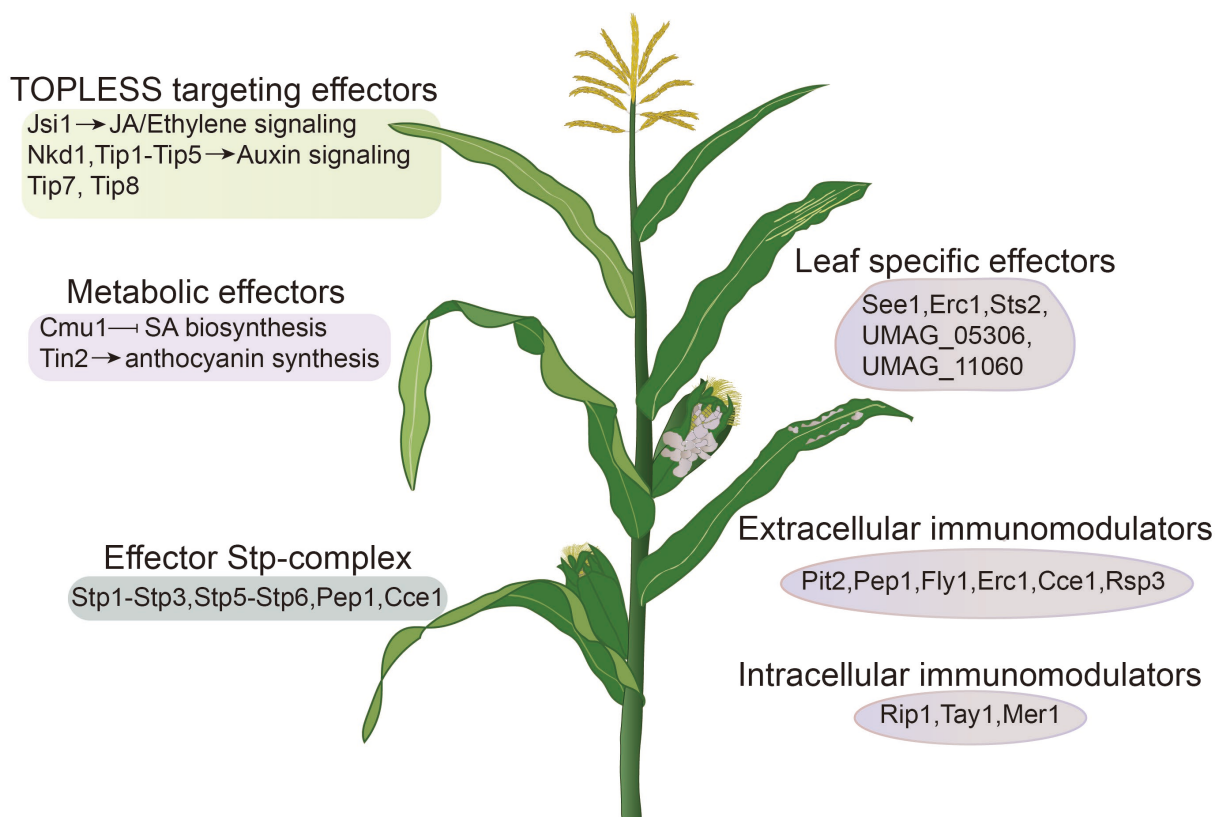


Fig. 3. Biological roles of the *U. maydis* effectors in their interaction with maize. The effectors facilitate effector protein secretion, modify plant cell walls, inhibit ROS burst, suppress proteases, regulate biosynthesis, suppress plant intracellular and extracellular immunity, and regulate plant

Introduction

hormones salicylic acid (SA), jasmonic acid (JA), and ethylene (ET). The image has been modified from Djamei et al. 2023.

3.3.1 Evasion of host target recognition

Pathogenic fungi often use physical isolation through surface modification to evade recognition by plant defense proteins. One such effector is *U. maydis* Rsp3, which is anchored to the fungal hyphal cell wall through its N-terminal domain (Ma et al., 2018). Rsp3 plays a crucial role in virulence and anthocyanin accumulation by interacting with maize anti-fungal proteins AFP1 and AFP2 during biotrophic stages (Ma et al., 2018). AFP1 interferes with the activity of chitin deacetylases by its mannose-binding activity, but Rsp3 blocks its antifungal activity, which is vital for the virulence of *U. maydis* (Ma et al., 2018, 2023). Moreover, Rsp3 is found in all sequenced smut fungi, and its ortholog from *S. reilianum* can restore the *U. maydis* *rsp3* mutant, suggesting a broad fungal defense mechanism (Ma et al., 2018). *U. maydis* also secretes UmFly1, a metalloprotease that cleaves chitinase ZmChiA and reduces its enzymatic activity by impairing its chitinase binding domain (Ökmen et al., 2018). Fly1 also activates fungal endogenous chitinase 1 (Cts1), which is essential for separating *U. maydis* yeast-like stage haploid sporidia (Ökmen et al., 2018).

Additionally, Cce1, a *U. maydis* apoplastic cysteine-rich core effector, and its constituent Stp4 within the STP complex are vital for infection (Ludwig et al., 2021; Seitner et al., 2018). Deleting the *cce1* gene triggers callose deposition and leads to early-stage infection blockage, highlighting the critical role of Cce1 in the pathogenicity of *U. maydis* (Seitner et al., 2018).

3.3.2 Inhibition of ROS burst

Upon microbial infection, plants rapidly produce ROS bursts as a defense mechanism. However, studies have shown that *U. maydis* possesses multiple effector proteins that allow it to suppress host oxidative stress during infection. For example, Pep1 reduces ROS production in maize during *U. maydis* infection by directly interacting with the maize peroxidase POX12, which exhibits oxidase activity to produce ROS (Hemetsberger et al.,

2012). Pep1 is a pathogenic core effector and a critical component of the STP effector complex (Doehlemann et al., 2009; Hemetsberger et al., 2012, 2015; Ludwig et al., 2021). The $\Delta pep1$ mutant is unable to infect the host and is severely blocked after the initial penetration (Doehlemann et al., 2009). This results in the accumulation of callose and hydrogen peroxide around the infection site and the induction of PR genes (Doehlemann et al., 2009). Pep1 is highly conserved in smut fungi, and the Pep1 orthologs from *Ustilago hordei*, *Ustilago avenae*, *Ustilago nuda*, and *Melanopsichium pennsylvanicum* can rescue the *U. maydis* $\Delta pep1$ mutant (Hemetsberger et al., 2015).

Additionally, Rip1 has been identified as an inhibitor of ROS burst, with Zmlox3 as its target (Saado et al., 2022). Zmlox3 is a defense susceptibility factor that encodes a lipoxygenase, which is responsible for catalyzing the oxidation of linoleic acid, a precursor to various defense metabolites (Gao et al., 2007; Pathi et al., 2020). Zmlox3 acts as a negative regulator of ROS production (Saado et al., 2022). Under normal conditions, Zmlox3 is primarily located in the cytoplasm, but co-localization with Rip causes it to relocate to the nucleus and inhibit ROS burst (Saado et al., 2022). The RIFL motif in the C-terminus of Rip1 is crucial for its inhibition of ROS, as Rip1 orthologs lacking this motif fail to suppress ROS burst, while adding it results in inhibitory activity (Saado et al., 2022). Furthermore, the gene cluster 10a in the *U. maydis* genome encodes a family of proteins called Pleiades, which contains 10 different effector proteins (Navarrete et al., 2021a). Among these proteins, Taygeta1 (Tay1) and Merope1 (Mer1) are shown to inhibit ROS production (Navarrete et al., 2021a). Interestingly, Tay1 and Mer1 are localized in distinct cellular regions, the cytoplasm and the nucleus, respectively (Navarrete et al., 2021a).

3.3.3 Targeting and inhibiting cysteine protease activity

The apoplastic space is the compartment where effectors and proteins from the plant are in close contact. The upregulation of maize corn cystatin 9 (CC9) genes upon infection was observed, and virus-induced gene silencing (VIGS) targeting CC9 prevented SA-dependent gene expression, indicating the requirement of CC9 for successful *U. maydis* infection (van der Linde et al., 2012). Papain-like cysteine proteases (PLCPs) in the apoplast trigger PR

Introduction

gene expression in maize in response to SA treatment (van der Linde et al., 2012). CC9 effectively inhibits five PLCPs, including CP1A, CP1B, CP2, XCP2 and CathB (van der Linde et al., 2012). The *U. maydis* effector protein Pit2 is a substrate mimic of maize apoplastic PLCPs and prevents the triggering of SA-mediated host immune resistance (Mueller et al., 2013). A conserved inhibitory core motif of 14 amino acids is present in Pit2, which is sufficient to inhibit PLCP activity (Misas Villamil et al., 2019). PLCPs CP1 and CP2 mediate the cleavage of the endogenous precursor small protein proZip, releasing the maize immune signal peptide Zip1 (Ziemann et al., 2018). Zip1 activates SA-related resistance pathways, including the expression of PR genes, the accumulation of SA, and the post-translational activation of PLCP (Ziemann et al., 2018). Therefore, PLCPs potentially promote immune responses by mediating the release of Zip1, which activates SA-related resistance pathways.

3.3.4 Metabolic reprogramming by *U. maydis* effectors

The effector proteins of *U. maydis* have been found to have the ability to reprogram the metabolic pathways of the host. For instance, Tin2 is a well-known example of host metabolic reprogramming by *U. maydis* effector proteins. It has been shown that Tin2 binds to ZmTTK1, a cytoplasmic serine/threonine protein kinase in maize (Tanaka et al., 2014). This binding of Tin2 to ZmTTK1 effectively prevents the recognition and degradation of the ZmTTK1 N-terminal DSGxS sequence by the plant ubiquitin-proteasome system, resulting in the stabilization of ZmTTK1 (Tanaka et al., 2014). In turn, this maintains its protein kinase activity and activates the maize transcription factor ZmR1, inducing up-regulated expression of genes related to anthocyanin synthesis (Tanaka et al., 2014). This leads to a significant depletion of coumaroyl coenzyme A (4-coumaroyl CoA), a shared precursor for both anthocyanins and lignin, ultimately resulting in the attenuation of lignification in plant tissues (Tanaka et al., 2014). It is worth noting that SrTin2, the *S. reilianum* ortholog of Tin2, targets ZmTTK2 and ZmTTK3, and failed to compensate for the lack of $\Delta tin2$ virulence (Tanaka et al., 2019). These findings imply that Tin2 has evolved novel functions for host adaptation.

Another example of *U. maydis* effector protein-mediated metabolic reprogramming is Cmu1, which acts as a chorismate mutase and reduces SA synthesis in maize. Chorismate mutases convert chorismate to prephenate, which is an essential precursor for the synthesis of tyrosine and phenylalanine (Djamei et al., 2011). Cmu1 interacts with maize chorismate mutase ZmCM2 in the cytoplasm, leading to a reduction in levels of SA synthesis (Djamei et al., 2011). Cmu1 has a unique structure compared to maize chorismate mutases ZmCM1 and ZmCM2, with an additional $\alpha 2a$ helix and a large loop region near the $\alpha 2$ helix that leads to sustained catalytic conversion of chorismate to prephenate, attenuating SA synthesis (Han et al., 2019). Additionally, the maize protein Kiwellin 1 (ZmKWL1) was identified by mass spectrometry followed by immunoprecipitation and was found to interact with Cmu1 (Han et al., 2019). It was found that two molecules of ZmKWL1 bind to one Cmu1 homodimer, blocking the substrate active site and thereby reducing its chorismate mutase activity (Han et al., 2019). In addition, ZmKWL1-b, a paralogous homolog of ZmKWL1, has also been shown to bind specifically to Cmu1 and inhibit the chorismate mutase activity (Altegoer et al., 2020). Furthermore, ZmKWL1 has also been shown to affect the translocation of Cmu1 to the cytoplasm (Han et al., 2019).

3.3.5 Effectors for tumorigenesis

The Ustilaginaceae fungi *U. hordei* and *S. reilianum* infect their host plants through the vascular system and gradually move towards the apical meristem (Zuo et al., 2019). However, *U. maydis* behaves differently as it colonizes various plant organs and forms tumors in all aerial parts. Approximately 45% of putative effectors are expressed as early as 3 dpi, with 28 exclusively expressed during seedling leaf infection and 9 contributing specifically to virulence (Schilling et al., 2014; Skibbe et al., 2010).

See1 is the first well-characterized effector that contributes to tumorigenesis by interacting with the maize SGT1 protein, resulting in DNA synthesis reactivation and enhanced cell division activity (Matei et al., 2018; Redkar et al., 2015). The $\Delta see1$ mutant reduces nuclear division in maize bundle sheath cells, resulting in reduced proliferation

Introduction

of hyperplastic tumor cells (Matei et al., 2018). Moreover, SGT1 primarily regulates plant immunity, and its phosphorylation of MAPK in immune responses is inhibited by See1 (Redkar et al., 2015).

Sts2 is another effector found to exhibit cell-specific expression within leaf hypertrophic tumors, and its ortholog in *S. reilianum* were found to be incapable of compensating for the loss of virulence resulting from the Δ Sts2 mutant in *U. maydis* (Matei et al., 2018; Zuo et al., 2021, 2023). Further investigation revealed that *Srst2* and *Umst2* are differentially regulated during the infection of seedlings by each respective pathogen, suggesting that the functions of these orthologs may be diverse (Zuo et al., 2021). Furthermore, Sts2 was found to be differentially expressed in different maize lines during *U. maydis* infection (Schurack et al., 2021). Recently, Sts2 has been characterized as a transcriptional activator that promotes tumor cell hyperplasia in the maize cell nucleus (Zuo et al., 2023). It interacts with ZmNECAP1, a plant transcriptional activator, to activate leaf developmental regulators and enhance tumor formation (Zuo et al., 2023). Inhibiting Sts2 results in a decrease in tumor formation, highlighting its crucial role in tumorigenesis (Zuo et al., 2023). These findings provide new insights into the diverse functions of Sts2 orthologs and the mechanisms underlying *U. maydis* induced tumor formation. Another *U. maydis* organ-specific effector Erc1, has been identified as exhibiting 1,3-glucanase activity and is crucial for cell-to-cell elongation in leaf bundle sheaths (Ökmen et al., 2022).

3.3.6 Targeting TOPLESS corepressors by *U. maydis* effectors

3.3.6.1 Overview of the maize TOPLESS repressor

TOPLESS (TPL) is a transcriptional co-repressor protein that plays a critical role in regulating gene expression during plant development (Causier et al., 2012; Liu et al., 2019). In *Arabidopsis thaliana*, TPL and TPL-related (TPR) co-repressor genes have been identified that function in plant immune regulation by controlling the activation or repression of gene expression (Long et al., 2002, 2006). DNA-binding transcription factors recruit TPL/TPRs to directly or indirectly suppress the expression of target genes (Causier et al., 2012; Liu et al., 2019). Transcription factors typically interact with TPL through

transcriptional repression motifs, such as the ERF-associated amphiphilic repression (EAR) motif, which features the LxLxLx or DLNxxP sequence and is often found to mediate interaction with TPL/TPR (Causier et al., 2012; Hiratsu et al., 2003; Kagale & Rozwadowski, 2011; Liu et al., 2019; Ohta et al., 2001). The TPL/TPR proteins are comprised of several highly conserved domains, including LisH, CTLH, and CRA domains in the N-terminal region and WD40 repeats in the C-terminal region (Ke et al., 2015; Ma et al., 2017; Martin-Arevalillo et al., 2017). The LisH-CTLH region interacts with the LxLxL motif, while the C-terminal WD40 domain interacts with the DLNxxP domain and the B3 repression domain (Collins et al., 2019; Ke et al., 2015; Liu et al., 2019; Martin-Arevalillo et al., 2017).

TPL/TPR repression mechanisms are linked to chromatin remodeling at transcriptional gene loci. For example, in *Arabidopsis*, TPL/TPRs interact with histone deacetylase 19 (HDA19) to suppress transcription and enable appropriate shoot differentiation during the embryogenesis transition, which is closely related to auxin (Long et al., 2006). During development, APETALA2 (AP2) recruits TPL and HDA19 to regulate floral gene expression (Krogan et al., 2012). GIR1 and GIR2, which regulate root hair development, interact with TPL to promote histone hypoacetylation at their repression sites (Wu & Citovsky, 2017). Transcription factor brassinazole-resistant 1 (BZR1) is a regulator of brassinosteroid (BR) signaling, which recruits the TPL to activate or repress target genes in various cellular processes (Oh et al., 2014). The regulation of TPL by BZR1 requires interaction with histone deacetylases (Oh et al., 2014).

During screening for five TPL/TPRs interactors in *Arabidopsis*, numerous transcriptional regulators were identified from the AP2/ERF (APETALA2/ethylene-responsive element binding factor), AUX/IAA, Zn finger, and MYB families (Causier et al., 2012). The AP2/ERF family of transcription factors, primarily found in plants is characterized by the AP2 DNA-binding domain, which interacts with *cis*-elements including ethylene response elements (ERE) and dehydration response elements (DRE), both of which are designated as GCC boxes (Büttner & Singh, 1997; Hao et al., 1998; Masaru & Hideaki, 1995; Okamuro et al.,

Introduction

1997). DRE elements are typically present in genes related to abiotic stress responses, while EREs are commonly found in genes induced by jasmonic acid, ethylene, and pathogen attacks (Brown et al., 2003; Büttner & Singh, 1997; Chakravarthy et al., 2003; Lorenzo et al., 2003; Ohme-Takagi & Shinshi, 1995; Pré et al., 2008; Sakuma et al., 2002, 2002; Sessa et al., 1995). Some AP2/ERF transcription factors can bind both elements and participate in both abiotic and biotic responses (De Boer et al., 2011). In conclusion, this family of transcription factors plays a critical role in plant growth, development, and response to various stresses, as well as hormone signaling and pathogen defense through its interactions with TPL family genes.

3.3.6.2 The role of TPL targeted by *U. maydis* effectors

The infection of maize by *U. maydis* results in hormonal imbalances that affect multiple signaling pathways, including the induction of JA signaling and the downregulation of SA signaling, as well as the strong induction of auxin signaling expression (Doehlemann et al., 2008; Turian & Hamilton, 1960). This indicates the importance of hormone regulation for the successful infection of *U. maydis*. Therefore, *U. maydis* employs a well-established strategy of disrupting host immunity through hormone and signaling pathways. To achieve this, *U. maydis* effectors target transcriptional TPL corepressors.

Naked1 (Nkd1) is one such effector that interacts with maize TPL through a C-terminal LxLxLx motif, leading to increased auxin signaling (Navarrete et al., 2022b). This process enhances plant immunity by inhibiting PAMP-induced ROS bursts (Navarrete et al., 2022b). Further research has revealed that the Nkd1-TPL interaction hinders the enlistment of the Aux/IAA repressor to TPL, resulting in the removal of repression on auxin signaling (Navarrete et al., 2022b). Another example of *U. maydis* effectors targeting hormone signaling is the cluster 6A genes, which encodes five effector proteins known as Tips that induce auxin signaling (Bindics et al., 2022). Tip1 and Tip4 compete with the Aux/IAA repressor for TPL binding, ultimately resulting in the induction of auxin-responsive gene expression (Bindics et al., 2022). The effector protein Jsi1 interacts with TPL differently from Nkd1, binding to the second WD40 domain of TPL/TPR proteins via

a DLNxxP motif (Darino et al., 2021). This interaction promotes the biotrophic sensitivity of *Pst DC3000* in *Arabidopsis* by upregulating genes associated with the JA/ET signaling pathway (Darino et al., 2021).

4. Aim of this thesis

The *U. maydis* genes *UMAG_11060* and *UMAG_05306* were shown to be effectors with seedling-specific virulence functions (Schilling et al., 2014). However, their molecular functions have not been clearly elucidated. The primary aim of this study is to functionally characterize *UMAG_11060* and *UMAG_05306* to gain a deeper understanding of their roles in *U. maydis* virulence. To achieve this aim of functionally characterizing *UMAG_11060* and *UMAG_05306*, the following objectives will be pursued:

- (1) Determine the subcellular localization of *UMAG_11060* and *UMAG_05306* to provide insight into their spatial context and target interactions;
- (2) Identify and investigate the specific targets of *UMAG_11060* and *UMAG_05306* in maize to comprehend their contribution to *U. maydis* virulence;
- (3) Explore and unravel the biological mechanisms of *UMAG_11060* and *UMAG_05306* to understand their functions.

Chapter 2. Functional characterization of U_{MAG_11060}

1. Functional characterization of U_{MAG_11060} (Tip6)

1.1 Tip6 is required for full virulence of *U. maydis*

The *U. maydis* gene *UMAG_11060* encodes for Topless interacting protein 6 (Tip6), which was initially deleted via homologous recombination and identified as an effector gene with an organ-specific virulence function in maize leaves (Schilling et al., 2014). To functionally characterize Tip6 described in this thesis, a new knockout strain (Δ Tip6) was generated using the CRISPR-Cas9 system in the solopathogenic strain SG200 (Kämper et al., 2006; Schuster et al., 2016, 2018). The resulting frame-shift mutation was confirmed by sequencing. To assess whether Δ Tip6 contributes to virulence, the maize infection assay with Δ Tip6 and the *U. maydis* reference strain SG200 were performed as previously described (Redkar & Dohlemann, 2016). The strain Δ Tip6 showed a significantly reduced pathogenic phenotype compared to SG200, which confirmed the previously described phenotypes (**Fig. 4**) (Schilling et al., 2014).

To confirm that the reduced virulence phenotype of the Δ Tip6 strain was specifically caused by the mutation of the *Tip6* gene, a full-length *Tip6* gene sequence driven by its native promoter (*pTip6*) was integrated into the *ip* locus of the Δ Tip6 strain. The *ip* locus encodes for the succinate dehydrogenase enzyme (*UMAG_00844*, *sdh2*) and can serve as a site for homologous recombination-based integration, which confers carboxin resistance (Keon et al., 1991). The single integration of the recombinant DNA strain was confirmed by Southern blot analysis and designated it as complementation strain Tip6C (**Appendix Fig. 1**). The resulting Tip6C completely restored the virulence of the Δ Tip6 strain, demonstrating that the reduced virulence phenotype was indeed caused by the mutation of the *Tip6* gene (**Fig. 4**).

To test whether the virulence reduction of Δ Tip6 was due to a growth defect, filamentation on charcoal-containing medium was tested for all the strains that were used for maize infection. The charcoal plate showed that neither Δ Tip6 nor Tip6 complementation strain Tip6C had defects in hyphal formation compared to SG200 (**Fig. 4**). These results suggest that Tip6 is required for full virulence of *U. maydis*.

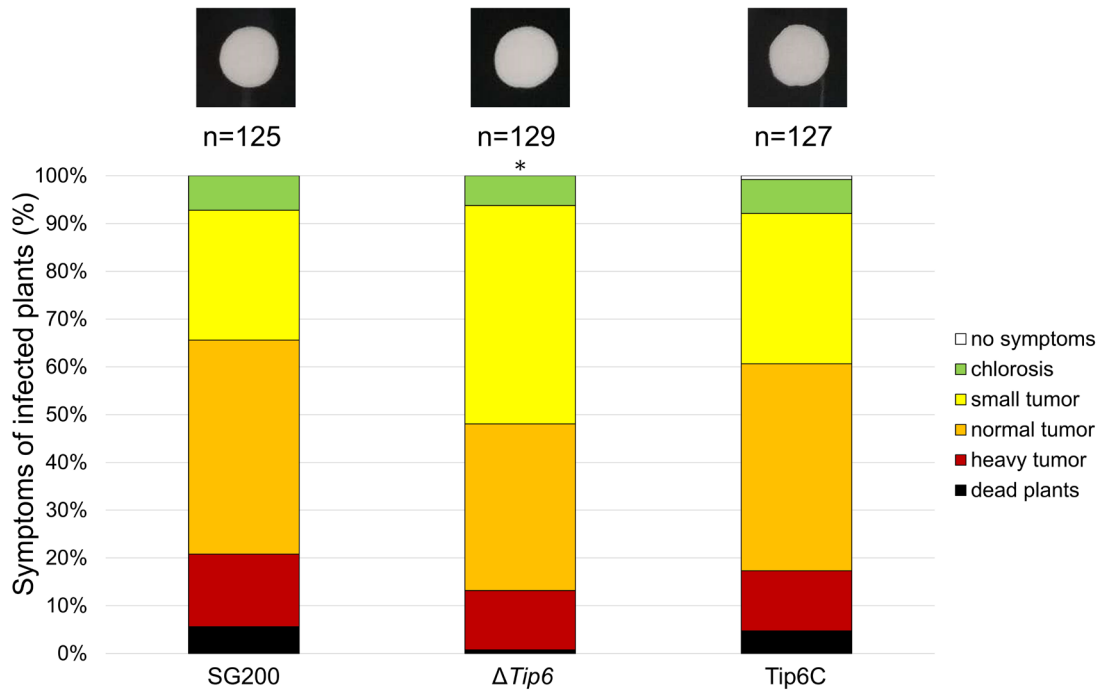


Fig. 4. Disease symptoms of $\Delta Tip6$ and its complementation strain in comparison to *U. maydis* SG200. For virulence analysis, maize seedlings were infected with SG200, $\Delta Tip6$ and the complementation strain Tip6C. Filament formation tests on charcoal-containing media of all the strains used for pathogenicity analysis were shown on top of the indicated strains. Disease symptom scoring was done at 12 dpi. The average disease index from three biological replications was used for significance testing with the Student's t-test. n = number of infected plants, *, p-value ≤ 0.05 .

1.2 Host target of Tip6 during *U. maydis* infection

1.2.1 Identification of host targets of Tip6

To identify the targets of Tip6 in the host plant maize, a co-immunoprecipitation (co-IP) assay coupled with mass spectrometry (MS) was performed. Therefore, maize seedlings were infected with *U. maydis* strain SG200 $\Delta Tip6$ expressing *Ppit2*-Tip6 fused to 2xHA, or SG200 expressing an effector signal peptide fused with mCherry and 3xHA (*Ppit2*-SP-mCherry-3xHA) as a negative control under the *pit2* promoter. This promoter was chosen, because it confers a constitutively high expression level during the biotrophic phase (Mueller et al., 2013). Maize leaves were collected 3 dpi after infection; total proteins were extracted and incubated with magnetic anti-HA beads to immunoprecipitate (IP) potential bound targets (**Fig. 5A**). To check whether both proteins were expressed in full length, a western blot of the total extracted lysate and HA beads IP protein was prepared. The blot indicated that both proteins were expressed (**Fig. 5B**). In collaboration with Dr.

Results

Hirofumi Nakagami (Max Planck Institute for Breeding, Cologne, Germany), the immunoprecipitated proteins were then analyzed and identified by mass spectrometry (**Fig. 5A**). Interestingly, the maize TOPLESS family proteins ZmTPL1, ZmTPL2, ZmTPL3, and ZmTPL4 were found to be highly enriched on Tip6-2xHA bound beads samples (**Fig. 5C**). Especially ZmTPL2 protein peptides were only present in the Tip6-2xHA samples, but not in the control samples. This indicates that ZmTPL2 might be a potential target of Tip6 in the plant.

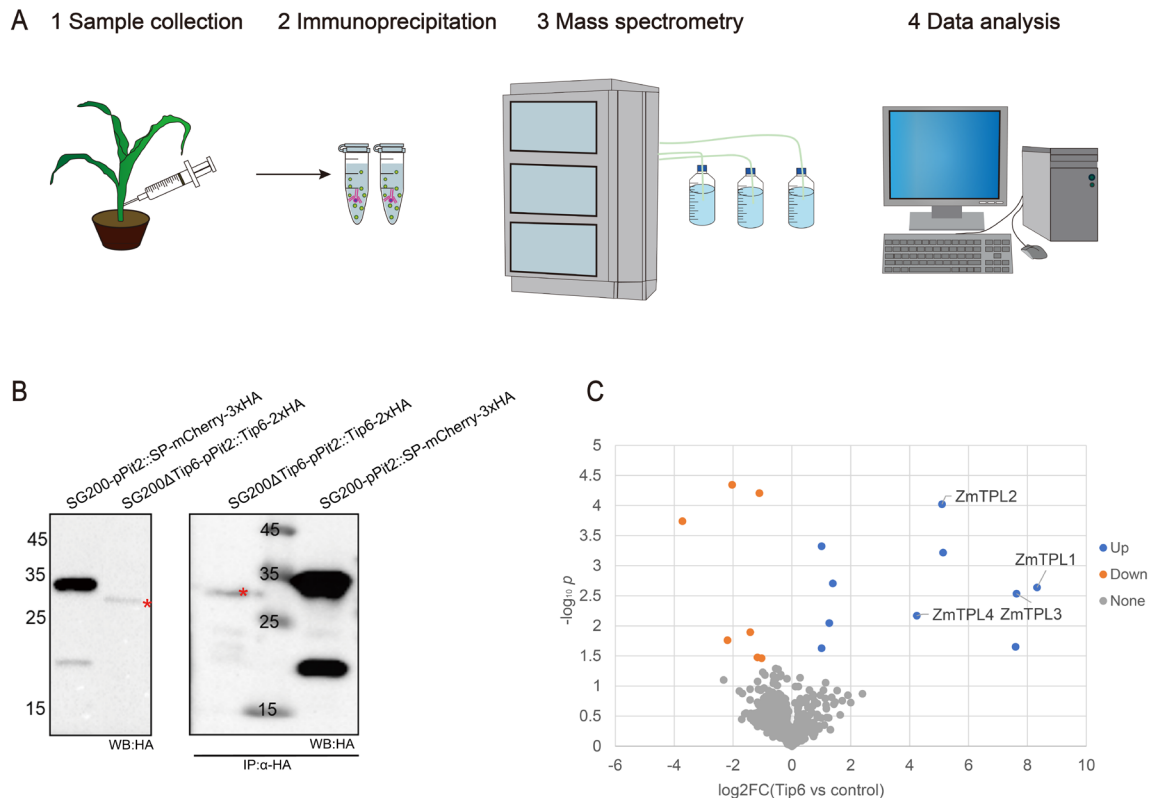


Fig. 5. Co-immunoprecipitation to identify host interaction targets. **A.** Workflow for finding host targets by mass spectrometry. (1) Maize leaves were collected at 3 dpi after infection with *U. maydis* SG200 strains expressing *Ppit2*-SP-mCherry-3xHA or SG200ΔTip6 strains expressing *Ppit2*-Tip6-2xHA. (2) Total proteins were extracted and immunoprecipitation was performed. (3) The bound proteins on the magnetic HA beads were identified by mass spectrometry. (4) Identified protein peptides were analyzed to search for possible interacting genes. **B.** Western blot analysis of SG200-*Ppit2*-SP-mCherry-3xHA or SG200ΔTip6-*Ppit2*-Tip6-2xHA in cell lysates and co-IP beads samples. Immunoblotting with the HA antibody. The molecular weight of fusion proteins is: SP-mCherry-3xHA: 30.45 kDa; Tip6-2xHA: 28.9 kDa. The asterisk labels the expected specific bands. **C.** Volcano plots showing the difference between Tip6 and control. The log2 FC fold change represents the difference in the average label-free quantitation (LFQ) intensity of identified protein peptides in Tip6 compared to control. The y-axis value represents the $-\log_{10}$ of the p-value. Each dot represents a detected protein. A fold change of >1.0 or -1 with $p < 0.05$ (Student's t-test) was considered significant. Gray dots represent no significant changes proteins, blue dots represent less abundant proteins, and red dots

represent more abundant proteins. Maize TPL family proteins were labeled. Control represents SP-mCherry-3xHA, and treatment represents Tip6-2xHA. The graph was generated in Excel.

1.2.2 Interactions of Tip6 with maize TPL proteins

To verify whether Tip6 interacts with proteins of the maize TPL family, a Y2H assay was performed. The maize TPL genes *ZmTPL1*, *ZmTPL2*, *ZmTPL3*, and *ZmTPL4* were fused into the Gal4 activation domain (Gal4AD). Tip6 lacking a signal peptide (Tip6₂₂₋₂₂₆) was inserted into the Gal4 DNA binding domain (Gal4BD). An empty vector was used as a negative control. If growth is observed on the high-stringency selection medium, it indicates an interaction. Tip6 with *ZmTPL2* or *ZmTPL3* grew well on high-stringency selection media, whereas Tip6 with *ZmTPL1* or *ZmTPL4* did not grow on selection media (**Fig. 6**). This indicates that Tip6 interacts with *ZmTPL2* and *ZmTPL3*, but does not interact with *ZmTPL1* or *ZmTPL4*. Despite the fact that *ZmTPL1* and *ZmTPL4* protein peptides were enriched in Tip6 expressing samples by MS analysis, this might be attributed to binding and precipitation by *ZmTPL2* or *ZmTPL3* proteins. Since the interaction was demonstrated among *ZmTPL2*, *ZmTPL3*, and *ZmTPL4*, all could interact with *ZmTPL1* (Liu et al., 2019). This might explain why four TPL proteins were identified in the MS.

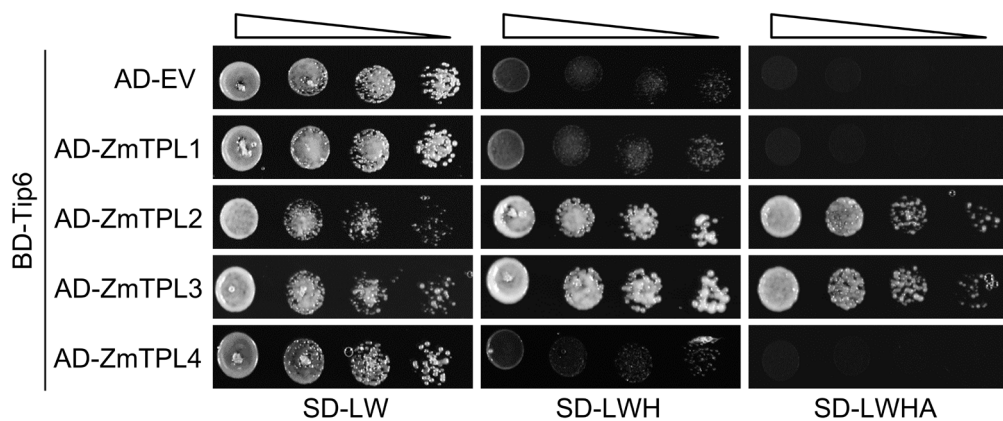


Fig. 6. Analysis of Tip6 interaction with maize TPL2 and TPL3 in Y2H assays. The interaction of Tip6 and maize TPLs was analyzed in Y2H assays. Plasmids containing pGADT7, pGADT7-ZmTPL1, pGADT7-ZmTPL2, pGADT7-ZmTPL3 and pGADT7-ZmTPL4 were individually co-transformed with pGBKT7-Tip6 into yeast cells. The obtained transformants were serially diluted ten times and plated onto nutrition-deficient synthetic defined (SD) media lacking Leucine and Tryptophan (SD/-Leu/-Trp), or lacking Leucine, Tryptophan and Histidine (SD/-Leu/-Trp/-His), or lacking Leucine, Tryptophan, Histidine and Adenine (SD/-Leu/-Trp/-His/-Ade). Growth on high-stringency selection media indicates an interaction. Pictures of the plates were taken after 3-4 days.

Results

1.2.3 Tip6 interacts with ZmTPL2 by Co-IP

ZmTPL2 was only detected in Tip6 expressing samples in the MS analysis and was found to interact with Tip6 in the Y2H assay. One of these reasons is that ZmTPL2 was considered as the most relevant host interaction partner of Tip6. To further confirm the interaction between Tip6 and ZmTPL2, Tip6 and ZmTPL2 were transiently co-expressed in *N. benthamiana* leaves for Co-IP. The co-infiltration of *Agrobacterium* strains carrying ZmTPL2-Myc and Tip6₂₂₋₂₂₆-6xHA was performed, while the negative control used *Agrobacterium* strains with GFP-4xMyc co-infiltrated with Tip6₂₂₋₂₂₆-6xHA. After 2 days, *N. benthamiana* leaves were collected for protein extraction, and the extracted protein supernatant was immunoprecipitated with α -Myc magnetic beads. The co-IP results showed that Tip6-6xHA was co-immunoprecipitated with ZmTPL2-4xMyc, but not with GFP-4xMyc (**Fig. 7**), suggesting that Tip6 interacts with ZmTPL2. This result further confirms that ZmTPL2 may serve as the host target of Tip6 during *U. maydis* infection.

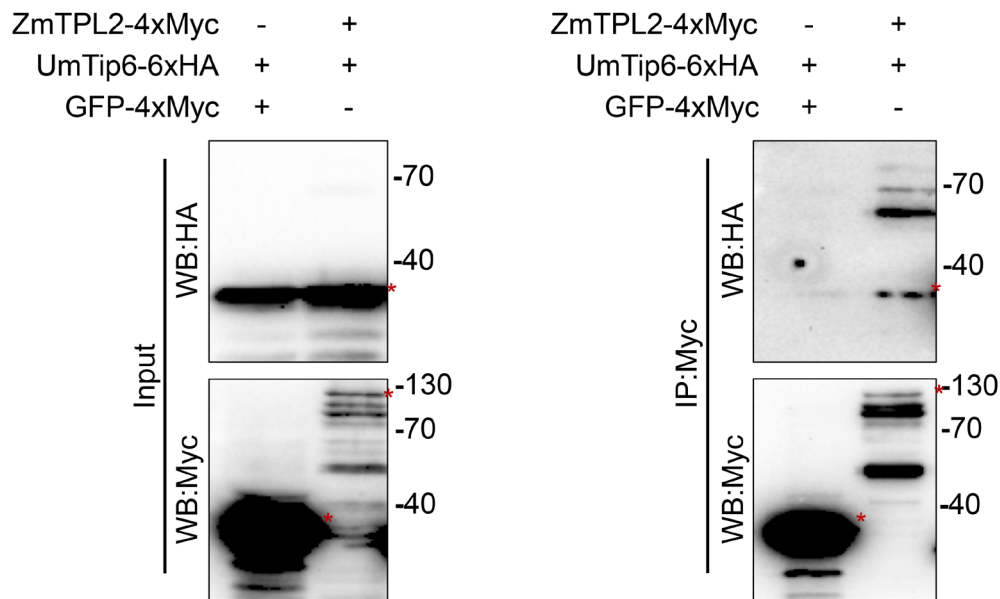


Fig. 7. Tip6 interacts with ZmTPL2. *p2x35S*-Tip6₂₂₋₂₂₆-6xHA was transiently co-expressed with *p2x35S*-ZmTPL2-4xMyc or *p35S*-GFP-4xMyc in *N. benthamiana*. Magnetic Myc-trap beads were used for co-immunoprecipitation (Co-IP) assays. Input (left blot) and immunoprecipitated proteins (right blot) were detected with anti-HA or anti-Myc antibodies, respectively. The expected molecular weight of fusion proteins is: ZmTPL2-4xMyc: 130.6 kDa; GFP-4xMyc: 31.8 kDa; Tip6₂₂₋₂₂₆-6xHA: 30.7 kDa. Red asterisks * indicate expected bands.

1.2.4 Tip6 binds to the N-terminal of ZmTPL2

1.2.4.1 Tip6 interacts with N-terminal of ZmTPL2 in Yeast two hybrid assays

The TPL/TPR proteins have several highly conserved domains; the N-terminal region consists of LisH, CTLH, and CRA domains, and the C-terminal region is made up of two WD40 repeats (**Fig. 8A**) (Ke et al., 2015; Ma et al., 2017; Martin-Arevalillo et al., 2017). Notably, sequence alignment of *A. thaliana* and *O. sativa* TPL genes showed that the N-terminal of ZmTPL2 has LisH, CTLH, and CRA domain that are conserved in the maize TPL family (**Fig. 8B**).

To determine which domain of ZmTPL2 contributes to the interaction with Tip6, a Y2H assay using various truncated versions of ZmTPL2 was performed. The ZmTPL2 truncated versions included ZmTPL2 consisting only of the N-terminal of ZmTPL2 (ZmTPL2^N), the C-terminal of ZmTPL2 (ZmTPL2^C), the N-terminal lacking the CRA domain (ZmTPL2^{ΔCRA}) and the N-terminal CRA domain alone (ZmTPL2^{CRA}) (**Fig. 8C**). Tip6 with ZmTPL2 or ZmTPL2^N showed thriving growth on high-stringency selection media, but Tip6 with other truncated variants of ZmTPL2 (ZmTPL2^{ΔCRA} and ZmTPL2^{CRA}) did not grow well on high stringency selection media (**Fig. 8D**). These results reveal that the N-terminal of ZmTPL2 interacts strongly with Tip6, indicating that ZmTPL2^N is responsible for interaction with Tip6, but not the WD40 repeat domain.

Results

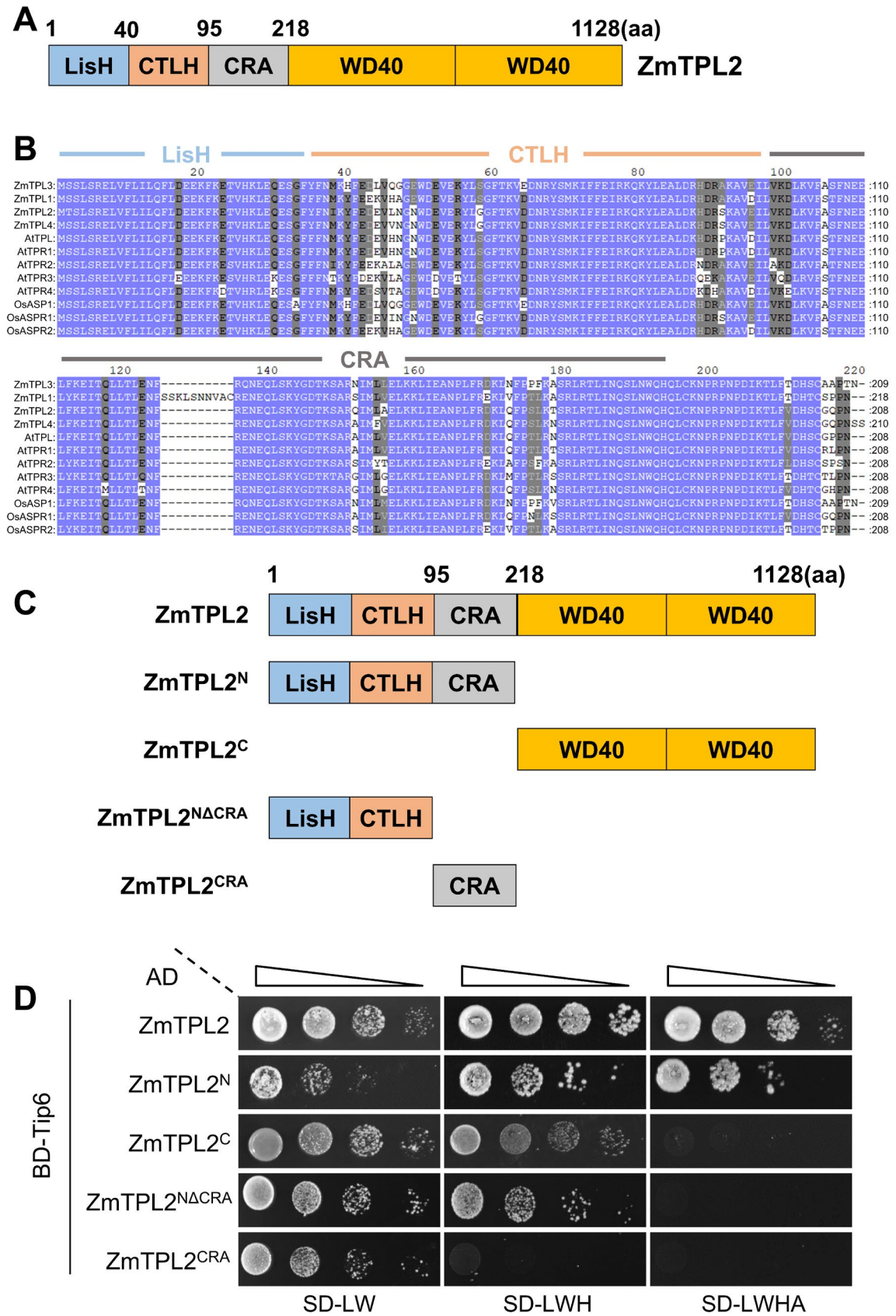


Fig. 8. Tip6 interacts with the N-terminal of ZmTPL2. **A.** Schematic diagram of the ZmTPL2 protein domains. ZmTPL2 is composed of the LIS1 homology domain (LisH), the C-terminal LisH motif domain (CTLH), the CT11-RanBPM domain (CRA), and the WD40 repeat domain (WD40). **B.** Sequence

alignment of the N termini of TPLs from *Zea mays* (Zm); *Arabidopsis thaliana* (At); and *Oryza sativa* (Os). The protein sequences were obtained from the maize genome database (<https://www.maizegdb.org/>) and NCBI (<https://www.ncbi.nlm.nih.gov/>). For alignment, Clustal X and Genedoc software were used. **C.** Schematic representation of ZmTPL2 and the prepared truncated variants. ZmTPL2 truncation variants ZmTPL2^N (1-218 aa of ZmTPL2 N-terminal), ZmTPL2^C (216-1128 aa of ZmTPL2 C-terminal), ZmTPL2^{NACRA} (1-95 aa of ZmTPL2 N-terminal with Lish and CTLH domains), and ZmTPL2^{CRA} (90-218 aa of ZmTPL2 N-terminal, CRA domain) were shown. **D.** Yeast two-hybrid shows the interaction between Tip6 and ZmTPL2^N. Plasmids carrying pGADT7-ZmTPL2, pGADT7-ZmTPL2^N, pGADT7-ZmTPL2^C, pGADT7-ZmTPL2^{NACRA}, pGADT7-ZmTPL2^{CRA} were individually co-transformed with pGBKT7-Tip6 into yeast cells. The obtained transformants were serially diluted ten times and plated onto nutrition-deficient synthetic defined (SD) media lacking Leucine and Tryptophan (SD/-Leu/-Trp), or lacking Leucine, Tryptophan and Histidine (SD/-Leu/-Trp/-His), or lacking Leucine, Tryptophan, Histidine and Adenine (SD/-Leu/-Trp/-His/-Ade). Pictures of the plates were taken after 3-4 days.

1.2.4.2 Tip6 interacts with ZmTPL2^N by *in vitro* pull-down assays

In addition, an *in vitro* pull-down assay was performed to test if ZmTPL2^N and Tip6 interact directly. The proteins His-ZmTPL2^N-His (hexahistidine-His6), GST-Tip6-mCherry, and GST-mCherry were expressed in *Escherichia coli* and purified. The recombinant proteins GST-mCherry or GST-Tip6-mCherry were purified using GST glutathione sepharose and then subjected to cleavage of the GST tag using PreScission Pierce HRV 3C protease. The proteins were then subjected to size exclusion chromatography (SEC) for their size verification, and SDS-PAGE coupled with coomassie staining and the western blot were performed to confirm their correct molecular weight (**Fig. 9A&B**). His6-tagged ZmTPL2^N was purified using Ni-NTA (Nickel-Nitrilotriacetic acid) agarose and SEC, and its correct molecular weight was also confirmed by SDS-PAGE (**Fig. 9C**).

The purified His-ZmTPL2^N-His was mixed with either Tip6-mCherry or mCherry, then incubated with magnetic mCherry-trap beads for pull-down. The results of the western blot showed that ZmTPL2^N was specifically pulled down by the magnetic beads when co-expressed with Tip6-mCherry, but not with mCherry alone, indicating that the interaction between ZmTPL2^N and Tip6 is direct (**Fig. 9D**), which is consistent with the previously shown results. Taken together, these results strongly suggest that Tip6 interacts with the N-terminal of ZmTPL2.

Results

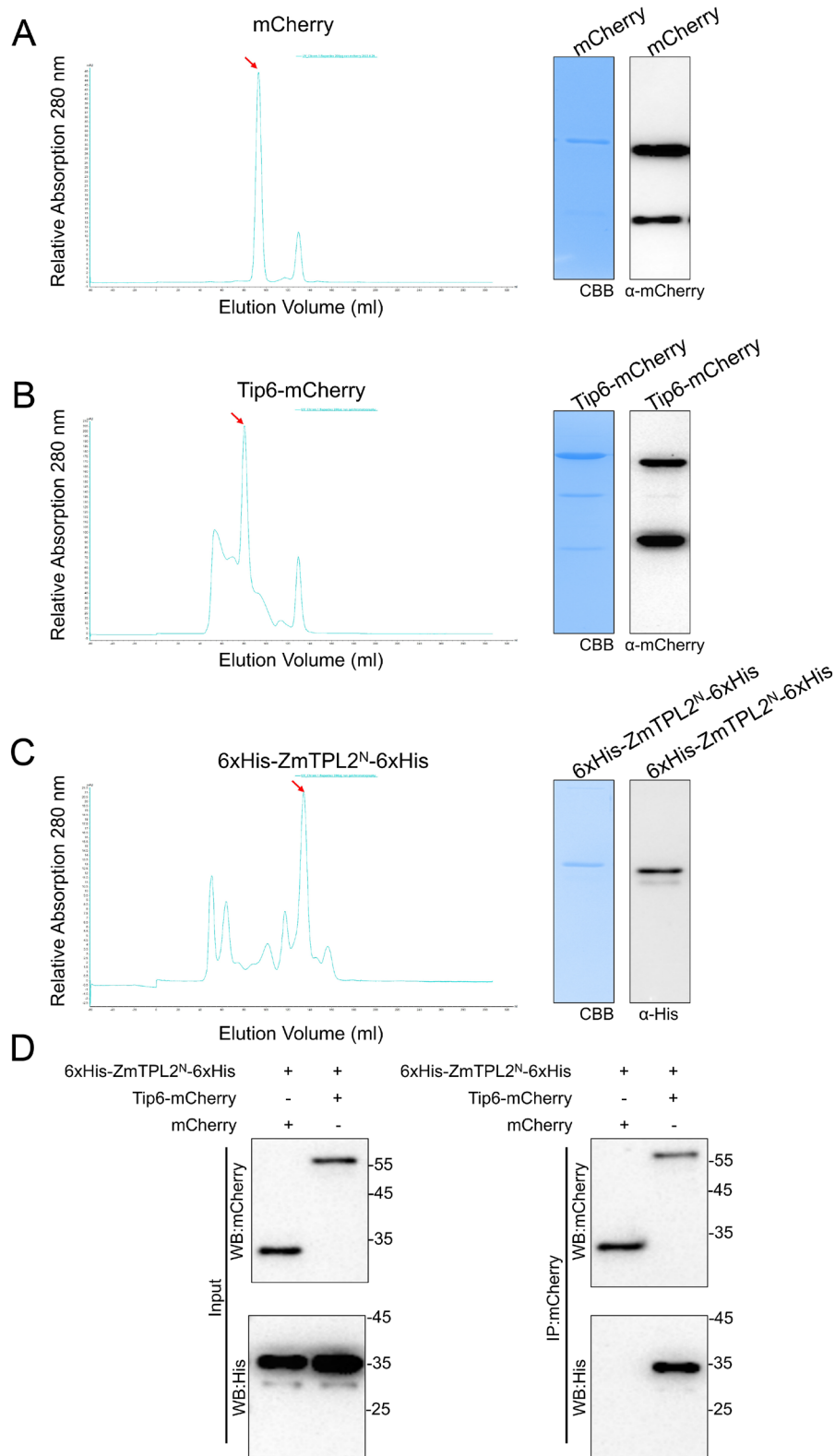


Fig. 9. Tip6 interacts with the N-terminal of ZmTPL2 in an *in vitro* pull-down assay. A, B. Purification of recombinant proteins mCherry and Tip6-mCherry. Elution profile from the SEC run with recombinant proteins either mCherry or Tip6-mCherry. The peak with the red asterisk presents the corresponding size (left). The SDS-PAGE of the peak elution was stained by coomassie brilliant blue (CBB) staining and detected by western blotting with mCherry antibodies. C. Purification of the

recombinant protein 6xHis-ZmTPL2^N-6xHis. The protein migration profile in the SEC was labeled with a red asterisk (left). The SDS-PAGE of the peak fraction was stained by CBB staining and detected by western blotting with His6 antibodies. **D.** The interaction of purified Tip6 protein with ZmTPL2^N. Purified recombinant proteins mCherry or Tip6-mCherry were mixed with recombinant 6xHis-ZmTPL2^N-6xHis proteins, and magnetic mCherry-trap beads were used for protein immunoprecipitation. The immunoprecipitated proteins were detected with anti-His and anti-mCherry antibodies. The expected sizes of fusion proteins are: 6xHis-ZmTPL2^N-6xHis: 33.8 kDa; mCherry: 26.6 kDa; Tip6₂₂₋₂₂₆-mCherry: 49.9 kDa.

1.2.4.3 Tip6 interacts with ZmTPL2^N in co-immunoprecipitation

To confirm the interaction between ZmTPL2^N and Tip6 in *planta*, co-IP assays were performed in *N. benthamiana*. The *Agrobacterium* strain carrying Tip6-6xHA was co-infiltrated with the strain carrying ZmTPL2^N-4xMyc in *N. benthamiana* leaves. As negative controls, the *Agrobacterium* strain carrying GFP-4xMyc and ZmTPL2^N-4xMyc were co-expressed. Magnetic Myc-Trap beads were used for immunoprecipitation. The Western blot results showed that Tip6-6xHA was detected in the ZmTPL2^N-4xMyc bound beads but not in the GFP-4xMyc bound beads (**Fig. 10**), thus confirming the interaction between the ZmTPL2^N and Tip6.

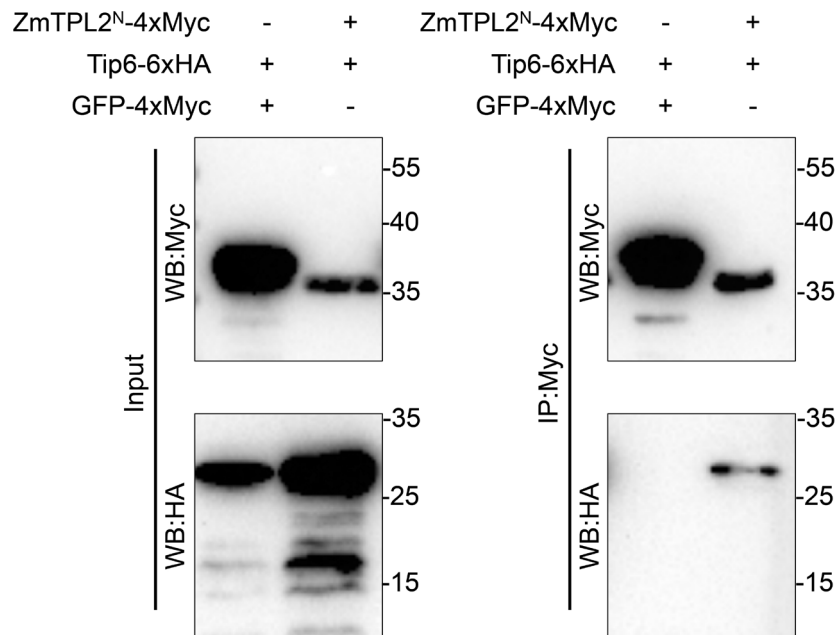


Fig. 10. Tip6 interacts with the N-terminal of ZmTPL2 in co-IP assay. p2x35S-Tip6₂₂₋₂₁₆-6xHA with either p2x35S-ZmTPL2^N-4xMyc or p2x35S-GFP-4xMyc were transiently co-expressed in *N. benthamiana* for 2 days, respectively. Input (left blot) and Myc-Trap beads immunoprecipitation proteins (right blot) were detected with anti-HA or anti-Myc antibodies, respectively. The expected sizes of the fusion proteins are: ZmTPL2^N-4xMyc: 31.7 kDa; GFP-4xMyc: 31.8 kDa; Tip6₂₂₋₂₂₆-6xHA: 30.7 kDa.

Results

1.3 Tip6 interacts with ZmTPL2 through EAR motifs

The TPL/TPR family has been found to interact with numerous transcription factors that contain the EAR domain with the LxLxLx sequence (Causier et al., 2012; Hiratsu et al., 2003; Kagale & Rozwadowski, 2011; Liu et al., 2019; Masaru & Hideaki, 1995; Ohta et al., 2001). In this context, I found that the *U. maydis* effector Tip6 contains an intact LxLxLx type EAR motif (amino acid sequence LGLSLG), even though it was not predicted by Pfam (<http://pfam.xfam.org/ncbiseq>). To investigate whether the putative LxLxLx type EAR motif of Tip6 is functional and important for interaction with ZmTPL2, an EAR motif truncated version of Tip6 (Tip6 Δ EAR1) was generated and tested for interaction with ZmTPL2 in a Y2H assay (**Fig. 11A&B**). In line with previous results, the full-length Tip6 with ZmTPL2 grew on all selection plates, suggesting that it interacts with ZmTPL2. Tip6 Δ EAR1 with ZmTPL2 grew normally on the intermediate stringency medium but only weakly on the high stringency medium (**Fig. 11B**). This result indicates that the EAR1 motif is required for the interaction between Tip6 and ZmTPL2, and it is likely that other parts of Tip6 may also be necessary for this interaction.

Tip6 has an additional LxLx pattern ('TELSLGG'; 56-62 aa), which could potentially serve as an additional EAR motif. To confirm this hypothesis, a mutant version of Tip6 (designated as Tip6 Δ EAR2) was created to test whether this sequence motif (indicated as 'EAR2') functions as an EAR motif. The interaction between Tip6 and the putative EAR motif was determined using a Y2H assay (**Fig. 11A&B**). Tip6 Δ EAR2 exhibited insufficient growth on the intermediate stringency medium and almost no growth on the high stringency medium (**Fig. 11B**), suggesting that the EAR2 motif is essential for binding to ZmTPL2. Therefore, we defined the 'TELSLGG' sequence in Tip6 as a functional EAR motif. In addition, a double EAR motifs truncated version Tip6 Δ 2EAR was generated (**Fig. 11A**). Tip6 Δ 2EAR showed no growth on both the intermediate and high stringency medium, indicating that Tip6 Δ 2EAR had completely lost the ability to interact with ZmTPL2 (**Fig. 11B**). Moreover, using the AlphaFold protein structure prediction method, the structure of Tip6 Δ 2EAR was generated and found to be structurally similar to Tip6 (**Appendix Fig. 2**) (Jumper et al., 2021). In conclusion, these results suggest that both EAR motifs in Tip6

are important for binding to ZmTPL2.

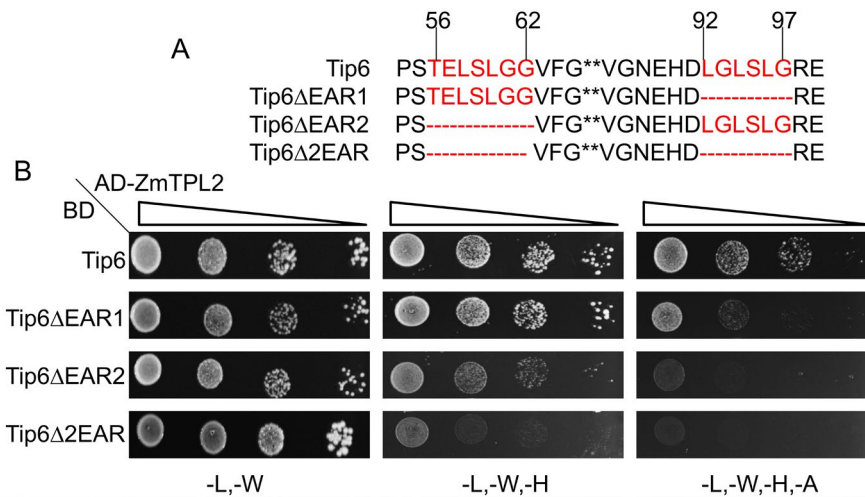


Fig. 11. Interaction between Tip6 and ZmTPL2 through EAR motifs. **A.** Schematic diagram illustrating the EAR motifs of Tip6. Tip6 contains two EAR repression domains, with the positions of the EAR motifs indicated in red and the corresponding numbers. **B.** The Y2H assay shows the difference in interaction of Tip6 EAR motifs with ZmTPL2. Yeast cells were co-transformed with plasmids carrying pGBKT7-Tip6, pGBKT7-Tip6ΔEAR1, pGBKT7-Tip6ΔEAR2, and pGBKT7-Tip6Δ2EAR, along with pGADT7-ZmTPL2. The resulting transformants were serially diluted ten times and plated onto nutrition-deficient synthetic defined (SD) media, SD/-Leu/-Trp, SD/-Leu/-Trp/-His, or SD/-Leu/-Trp/-His/-Ade. The plates were incubated for 3-4 days, and images were captured.

1.4 EAR motifs are essential for the virulence function of Tip6

To investigate whether the EAR motifs of Tip6 affect the virulence of *U. maydis*, a complementation strain of Δ Tip6 with mutations in the EAR motifs of Tip6 was generated and designated as the Tip6EARM strain. Therefore, the EAR1 and EAR2 motifs were replaced by alanine residues (**Fig. 12A**). The resulting strain was confirmed by southern blot to ensure successful insertion of a single copy of *Tip6EARM* into *ip* locus of Δ Tip6 strain (**Appendix Fig. 3**). While the insertion of the full length of Tip6 into Δ Tip6 was designated as Tip6C. The pathogenicity of the obtained Tip6EARM strain was assessed in comparison to SG200, Δ Tip6 and Tip6C (complementation strain) by infecting maize seedlings. All strains used for infection were tested for filamentation on charcoal-containing media (**Fig. 12B**). The charcoal plates showed that none of the strains had defects in hyphal formation compared to SG200. Tip6C restored Δ Tip6 virulence deficiency to the level of SG200. However, Tip6EARM was unable to restore the reduced virulence of Δ Tip6 (**Fig. 12B**). These results suggest that the EAR motifs of Tip6 are

Results

indispensable for the full virulence of *U. maydis*.

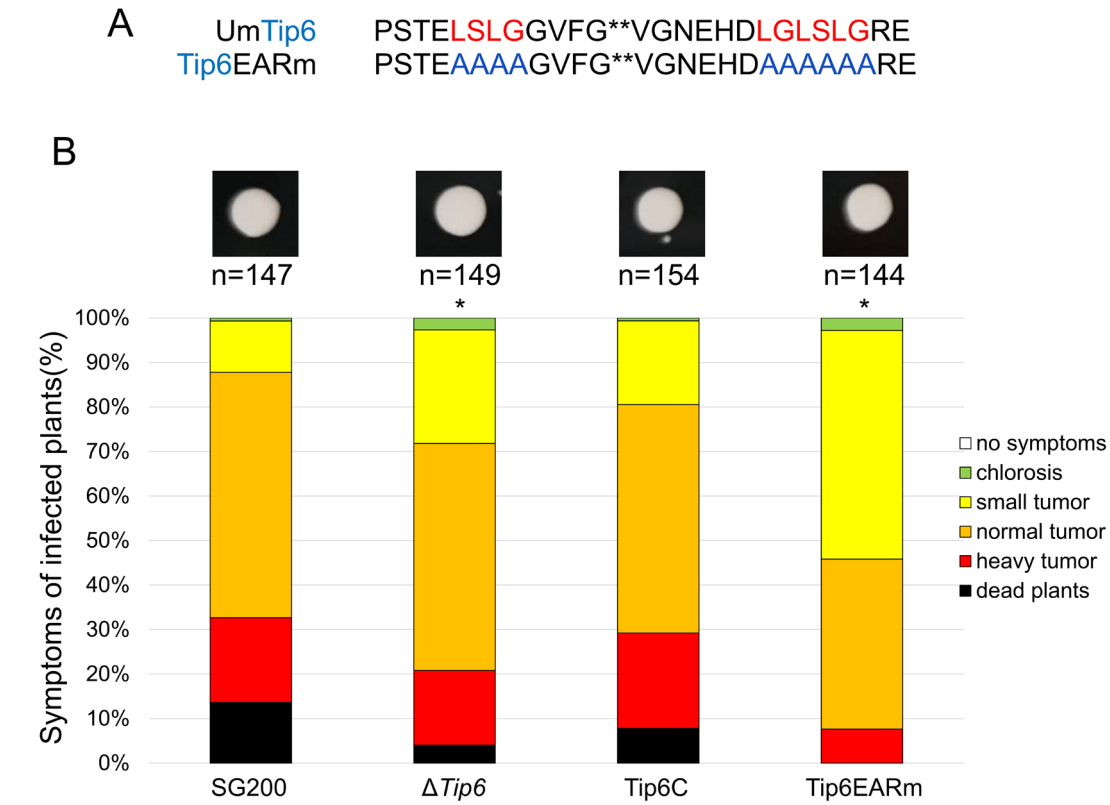


Fig. 12. EAR motifs mutation version Tip6 cannot restore Δ Tip6 virulence deficiency. **A.** Schematic diagram of Tip6 EAR motifs mutation sites. Protein sequences marked in red represent the mutated positions of the EAR motifs in Tip6, in which all EAR motifs sequences were replaced with alanine and marked in blue. **B.** Virulence activity of SG200 and Tip6 variant strains. Seven-day-old maize seedlings were infected with the SG200, Δ Tip6, Tip6C, and Tip6EARm *U. maydis* strains, respectively. The filamentation formation was tested for all indicated strains and disease symptoms were scored at 12 dpi. An asterisk indicates significant differences ($p < 0.05$; Student's t-test). The experiments were performed with three biological replicates.

1.5 Impact of Tip6 on maize gene expression

To understand the mechanism of the Tip6 virulence function and to assess the effects of EAR motifs of Tip6 in infection, transcriptome analysis using RNA-sequencing (RNA-seq) was performed on maize seedling leaves individually infected with *U. maydis* strains SG200, Δ Tip6 or Tip6EARm. Tip6EARm is a complementation form of Δ Tip6 in which the amino acid within the EAR motifs is replaced with alanine. As Tip6 expression peaks between 2 and 4 dpi during early biotrophic development (Lanver et al., 2018; Zuo et al., 2021). RNA-seq analysis was done on samples collected at 3 dpi.

Differentially expressed genes (DEGs) analysis was conducted using DESeq2 (Love et al.,

2014) and edgeR (Robinson et al., 2010) on gene counts. The criteria for identifying significant DEGs were based on fold-change ≥ 1 or ≤ -1 and p-value < 0.05 between different comparisons. The numbers of DEGs identified using DESeq2 and edgeR were different for each comparison, with 257, 300, and 419 DEGs identified using DESeq2 and 168, 203, and 313 DEGs identified using edgeR for the comparisons of $\Delta Tip6$ with SG200, $\Delta Tip6$ with Tip6EArm and Tip6EArm with SG200, respectively. To obtain a consensus set of DEGs, the overlap of DEGs identified by both DESeq2 and edgeR were used for further analysis. The resulting set of DEGs consisted of 162, 193, and 306 genes for the comparisons of $\Delta Tip6$ with SG200, $\Delta Tip6$ with Tip6EArm, and Tip6EArm with SG200, respectively (**Fig. 13A**). In response to the $\Delta Tip6$ and Tip6EArm mutants, a remarkable shift in gene expression was observed. Specifically, 91 genes were up-regulated and 71 genes were down-regulated in $\Delta Tip6$ compared to SG200, while 60 genes were up-regulated and 133 genes were down-regulated in $\Delta Tip6$ compared to Tip6EArm. Furthermore, Tip6EArm compared to SG200 had 191 up-regulated genes and 115 down-regulated genes (**Fig. 13B**).

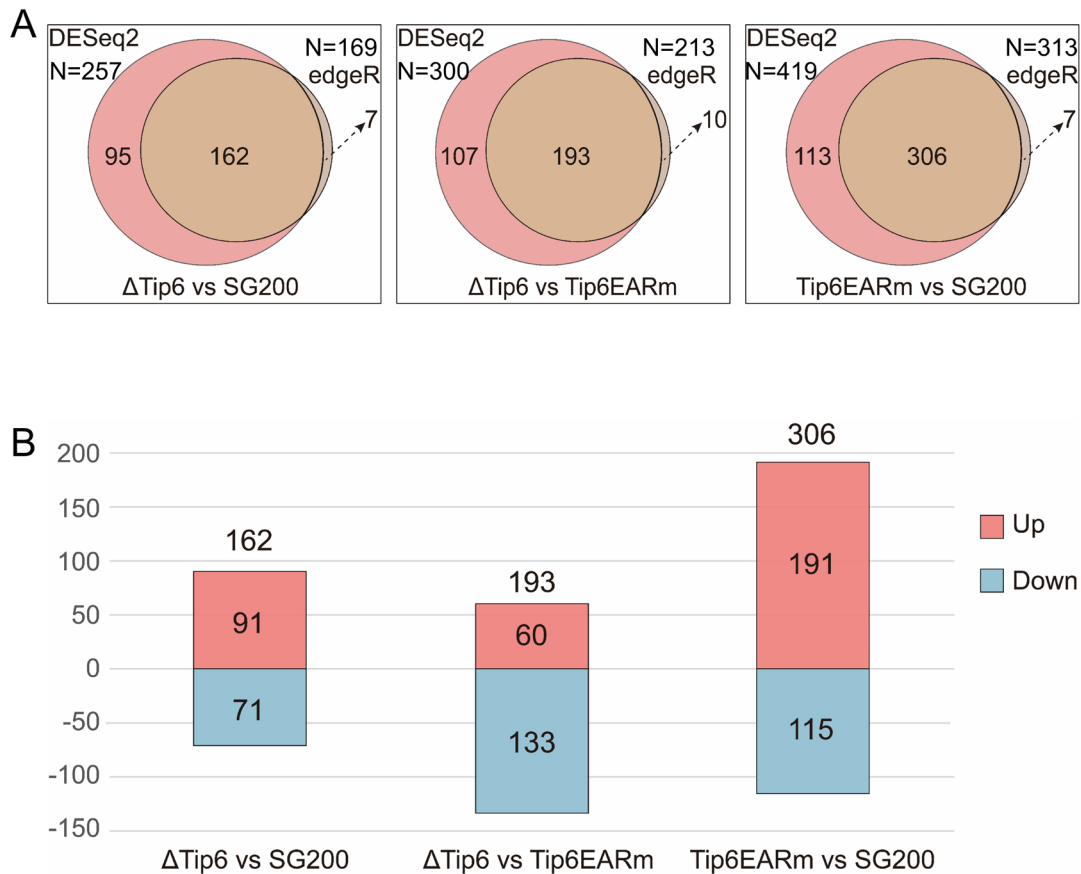


Fig. 13. The number of significant differentially expressed genes in different comparisons. A.

Results

Venn diagrams depict the overlap of DESeq2 and edgeR identified differentially expressed genes (DEGs). Left, the number of DEGs in $\Delta Tip6$ and SG200 comparison; middle, the number of DEGs in $\Delta Tip6$ and Tip6EArm comparison. right, the number of DEGs in Tip6EArm and SG200 comparison. DEGs were classified as significant when Foldchange ≥ 1 or ≤ -1 and p-value < 0.05 . **B.** A bar graph shows the number of up- and down-regulated differentially expressed genes in three comparisons.

To assess in which biological processes Tip6 is involved, gene ontology (GO) enrichment analysis was performed with ShinyGO v0.66 (Ge et al., 2020). In the $\Delta Tip6$ vs. SG200 comparison, 109 annotated DEGs out of 162 DEGs were used for GO enrichment analysis. The results revealed that DEGs are related to ‘cellular biosynthetic’, ‘transcription’, and ‘gene expression’ (**Fig. 14A**). In addition, in the Tip6EArm vs. SG200 comparison, 223 annotated DEGs out of 306 DEGs were used for GO enrichment analysis. The result showed that DEGs were also related to ‘cellular biosynthetic’, ‘transcription’, and ‘gene expression’ (**Fig. 14B**). These results suggest that Tip6 is involved in many transcriptional regulation pathways.

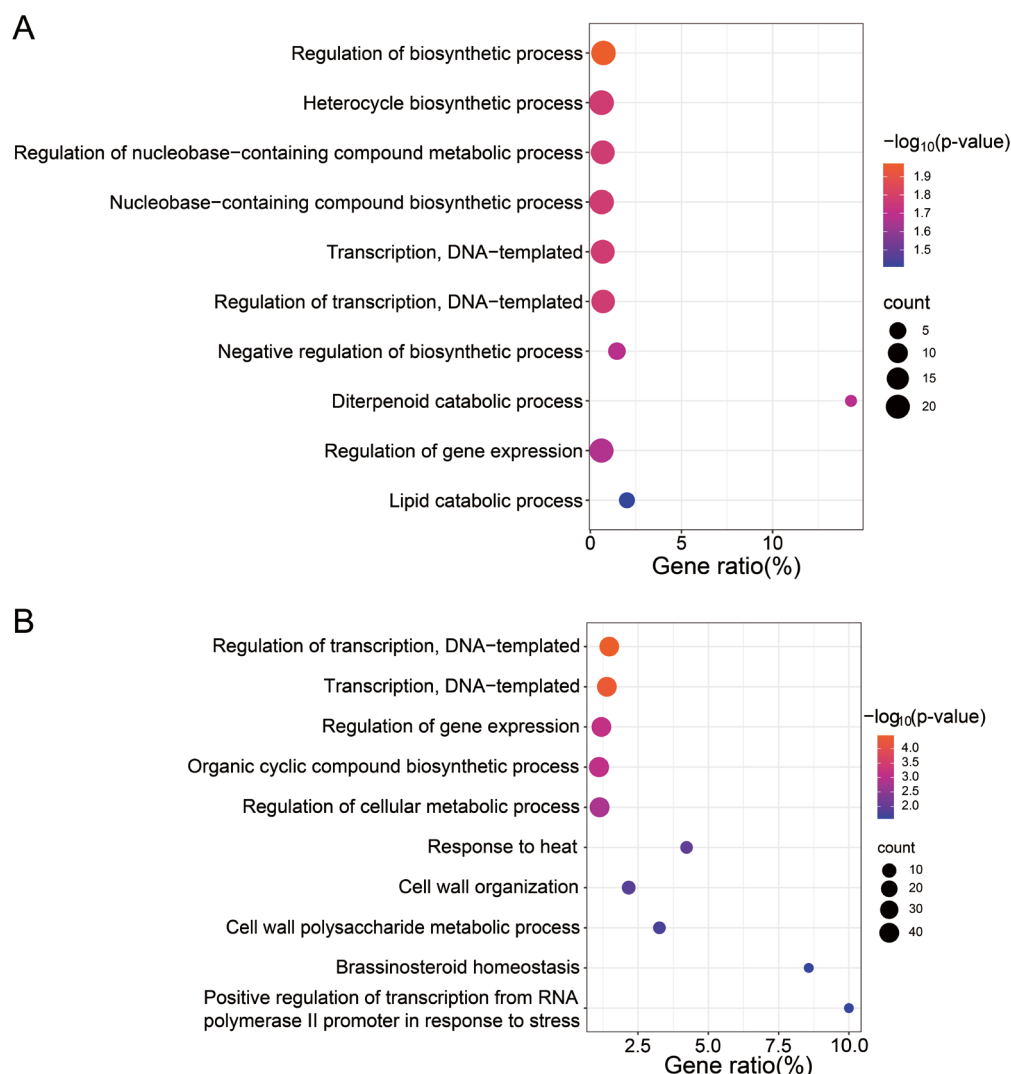


Fig. 14. Gene ontology (GO) analysis reveals Tip6 involvement in cellular biosynthesis and transcriptional regulation pathways. **A.** GO analysis of DEGs in $\Delta Tip6$ and SG200 comparison. The size of the dots represents the number of analyzed genes in the corresponding term. The gene ratio represents the ratio of the number of DEGs to the total number of genes in each term. Only 10 significant terms were shown. $-\log_{10}(P\text{-value})$ values are color-coded from red to blue. **B.** GO analysis of DEGs in Tip6EARm and SG200 comparison. The size of the dots represents the number of analyzed genes in the corresponding term. The gene ratio represents the ratio of the number of DEGs to the total number of genes in each term. Only 10 significant terms were shown. $-\log_{10}(P\text{-value})$ values are color-coded from red to blue.

To further test a role of Tip6 in transcriptional regulation, I checked whether DEGs include transcription factors (TFs). In the $\Delta Tip6$ vs. SG200 comparison, DEGs include 18 TFs (**Fig. 15A**) (**Appendix Tab. 1**). Interestingly, 9 of the 18 TFs belong to AP2-EREB family members, which were frequently found in the screening of interactors of five *Arabidopsis* TPL/TPRs. Among the 9 AP2/ERF TFs, 7 genes were up-regulated and 2 genes were down-

Results

regulated. The down-regulated genes are the TFs branched silkless 1 (*bd1*) and the AP2 subfamily TF gene *ereb26*. The TFs that were upregulated include *ereb13*, *ereb23*, *ereb36*, *ereb125*, *dbp4*, *erf014* and *CBF3*-like gene. Others, such as *OVATE11* and SHI/STY transcription factor 2 (*SRS2*), were down-regulated in $\Delta Tip6$ infected maize, while *NAC73* and *WRKY80* were up-regulated.

Tip6EARM regulated genes were also highly enriched in transcriptional regulation processes. To further investigate this, the differentially expressed TFs in the DEGs of Tip6EARM vs. SG200 were examined. This revealed that 47 TFs were differentially expressed. 20 of those TFs are AP2-EREB family members, of which 19 were up-regulated **(Fig. 15B) (Appendix Tab. 2)**. As in $\Delta Tip6$ infected samples, the TF *bd1* is down-regulated. $\Delta Tip6$ and Tip6EARM were compared to SG200 to identify generally Tip6-regulated DEGs. The 9 common DEGs identified from these two comparisons were then analyzed to gain insight into genes most likely related to the function of Tip6 **(Fig. 15C)**. Among these, seven were members of the AP2/ERF family, with six up-regulated and only one, *bd1*, down-regulated **(Fig. 15D)**. All these data suggest that Tip6 regulates various host TFs. It seems likely that several AP2/ERF family TFs are suppressed by Tip6, as they are up-regulated in the absence of Tip6.

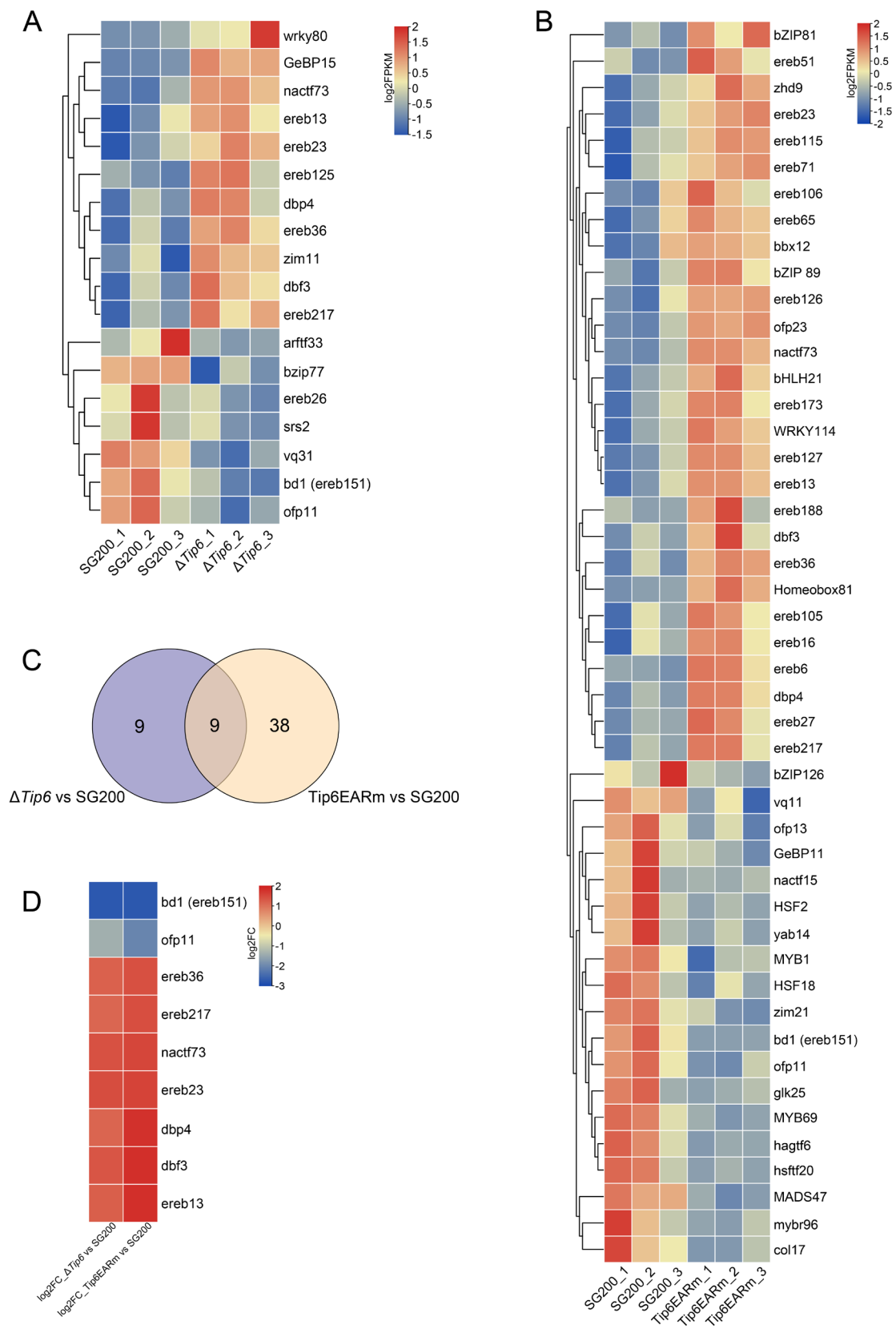


Fig. 15. Tip6 interferes with the expression of a group of transcription factors. **A.** Heatmap showing differentially expressed TFs in the comparison of $\Delta Tip6$ vs. SG200 infected maize. The original FPKM values were adjusted to log2 FPKM values. TBtools used the Euclidean distance method and the

Results

complete linkage method to cluster rows and columns (Chen et al., 2020). Gene expression ranges from red (high expression) to blue (low expression). **B.** Heatmap representation of differentially expressed TFs in Tip6EARM infected and SG200 infected maize. The heat map was generated as stated in **Fig. 15A**. **C.** Venn diagram illustrates the differentially expressed TFs shared by $\Delta Tip6$ or Tip6EARM samples in comparison with SG200 samples. The common DEGs were obtained from the comparison of $\Delta Tip6$ vs. SG200 and Tip6EARM vs. SG200. **D.** Heatmap representation of differentially expressed TFs shared by $\Delta Tip6$ or Tip6EARM samples in comparison with SG200 samples. The heatmap shows log2 (fold change in expression) values of $\Delta Tip6$ vs. SG200 and Tip6EARM vs. SG200. The heat map was generated as stated for **Fig. 15A**.

ZmTPL2, along with other TPL genes, is hypothesized to be recruited by host TFs to suppress gene expression (Causier et al., 2012; Liu et al., 2019). Given that Tip6 recruits ZmTPL2, it is possible that the recruitment of ZmTPL2 by host TFs could be affected by the effector. To identify potential TF regulators involved in the recruitment of ZmTPL2, DEGs were examined for TF binding motifs and the resulting TFs were enriched using the PlantTFDB database (<http://planttfdb.cbi.pku.edu.cn>), which is a comprehensive database of TFs in plants (Guo et al., 2008; Tian et al., 2020).

By comparing $\Delta Tip6$ vs. SG200 DEGs, 11 enriched TFs were identified using Fisher's exact test ($p < 0.05$) (**Fig. 16A**). Notably, the up-regulated TF *ereb125* was enriched for binding to 31 genes out of 134 input DEGs. *Ereb125* is also the putative regulator of *dbp4*, *zim11*, *NAC73*, and *wrky80* TFs, which were all up-regulated in $\Delta Tip6$. Additionally, several other TFs were found to be enriched in the input 277 DEGs of Tip6EARM, e. g. *ramosa2*, *ereb147*, *ereb125* and *ereb146* (**Fig. 16B**). *Ramosa2* is the putative regulator of 66 DEGs, *ereb147* regulates 63 DEGs, and *ereb125* regulates 61 DEGs. These results suggest that Tip6 affects host TFs regulation potentially through ZmTPL2, especially for AP2/ERF family TFs.

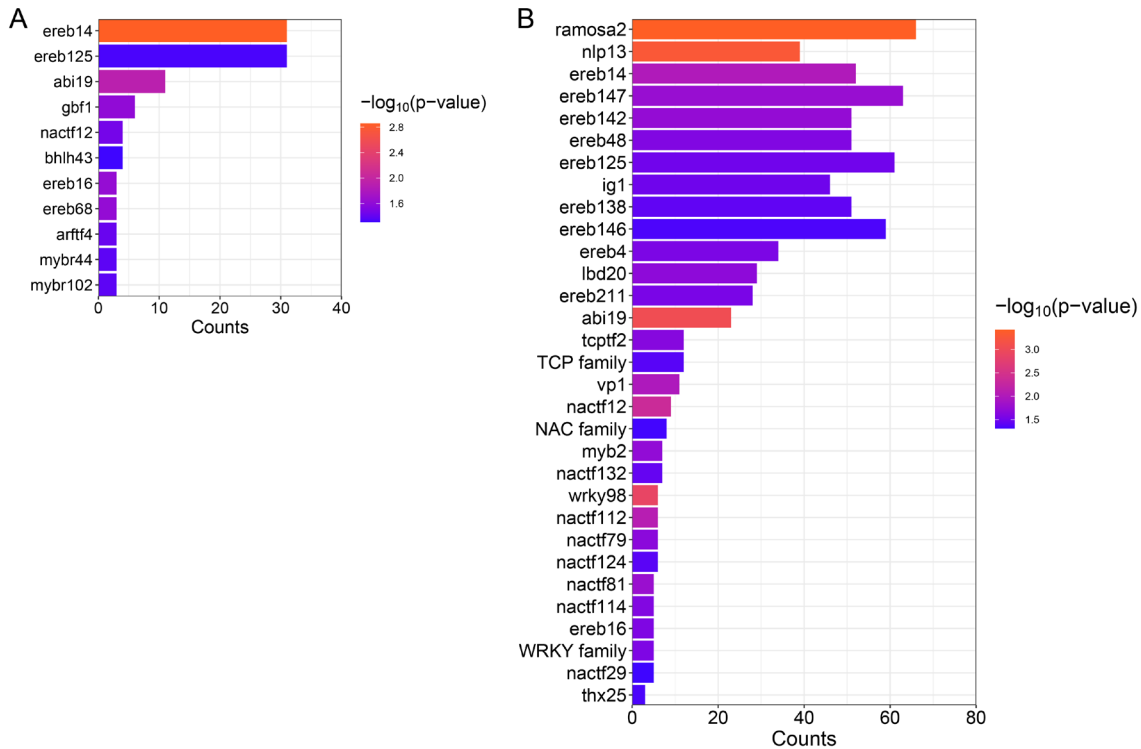


Fig. 16. Identification of putative transcription factors regulators potentially involved in ZmTPL2 recruitment by Tip6. **A.** The bar diagram shows potential TFs that regulate the DEGs obtained in the comparison of $\Delta Tip6$ vs. SG200. Counts represent the number of DEGs containing putative binding sites for the corresponding TF. $-\log_{10}(P\text{-value})$ is colored from blue to red. **B.** The bar diagram shows the potential transcription factors that regulate the DEGs obtained in the comparison of Tip6EARm vs. SG200. Counts represent the number of DEGs containing putative binding sites for the corresponding TF. $-\log_{10}(P\text{-value})$ is colored from blue to red.

1.6 Co-localization of Tip6 and ZmTPL2 in plant cells

1.6.1 Tip6 is localized in the nucleus and cytoplasm

To investigate the subcellular localization of Tip6, transient expression of Tip6₂₂₋₂₂₆-mCherry fusion protein was performed in *N. benthamiana* leaves via *Agrobacterium* mediated transformation. The protein encoded by Tip6₂₂₋₂₂₆-mCherry lacks the N-terminal signal peptide of Tip6, which was predicted with SignalP 4.0 (Petersen et al., 2011). Confocal laser scanning microscopy (CLSM) showed that Tip6₂₂₋₂₂₆-mCherry is primarily localized in the nucleus and cytoplasm of infiltrated *N. benthamiana* leaves (**Fig. 17A**).

To further verify the localization of Tip6 in the natural host plant, the localization of Tip6₂₂₋₂₂₆-mCherry was examined in maize epidermal cells by biolistic bombardment. A

Results

nuclear localization signal (NLS) fused with mCherry was used as a nuclear marker. Confocal microscopy revealed that Tip6₂₂₋₂₂₆-mCherry localized to the maize nucleus, which is consistent with the Tip6₂₂₋₂₂₆-mCherry localization in *N. benthamiana* (**Fig. 17B**). Taken together, these results indicate that Tip6 may be translocated into the host nucleus and cytoplasm during the *U. maydis* infection.

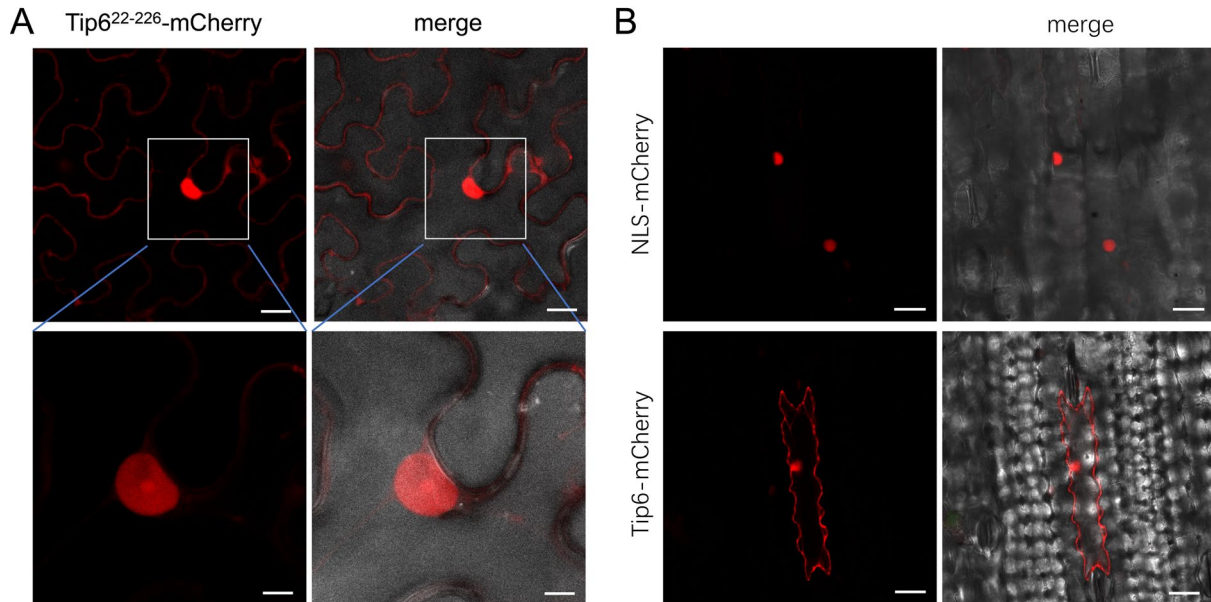


Fig. 17. Tip6 is localized in the host nucleus and cytoplasm. **A.** Subcellular localization of Tip6 without a signal peptide in *N. benthamiana*. *p2x35S*-Tip6₂₂₋₂₂₆-mCherry fusion protein was transiently expressed in *N. benthamiana* using *A. tumefaciens* for delivery. Images were taken at 2 dpi. The white box marks the magnified nuclear region. Scale bar, 20 μ m. **B.** Subcellular localization of Tip6 or a nuclear marker (NLS-mCherry) in maize. *p2x35S*-NLS-mCherry or *p2x35S*-Tip6₂₂₋₂₂₆-mCherry was expressed in maize epidermal cells. NLS-mCherry was used as a nuclear protein marker. Images were taken at 16-24h after transformation. The yellow line marks the maize cell wall. Scale bar, 25 μ m.

1.6.2 Subcellular localization of ZmTPL2

To examine the subcellular localization of ZmTPL2, ZmTPL2 tagged N-terminally with GFP was transiently expressed in *N. benthamiana* leaves using *Agrobacterium* mediated delivery. Confocal imaging revealed that ZmTPL2-GFP aggregated in the nucleus and formed speckles (**Fig. 18A**). To further investigate the nuclear localization of ZmTPL2-GFP, ZmTPL2-GFP was transiently expressed in maize epidermal cells by biolistic bombardment. 24 hours after bombardment, samples were detected for fluorescent signal by confocal microscopy. ZmTPL2-GFP was located in the nucleus and formed speckles (**Fig. 18B**), which was consistent with the localization of ZmTPL2-GFP observed in *N.*

benthamiana (**Fig. 18A**). Collectively, these results suggest that ZmTPL2 accumulates in nuclear speckles.

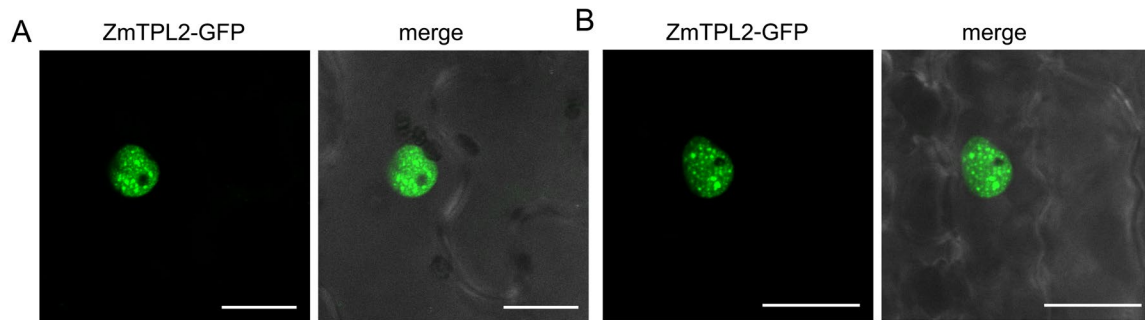


Fig. 18. ZmTPL2 localizes in the nucleus and forms a distribution pattern. **A.** Subcellular localization of ZmTPL2 in *N. benthamiana*. *p2x35S-ZmTPL2-GFP* was expressed in the epidermal cells of *N. benthamiana* by *Agrobacterium*-mediated transformation. Confocal imaging was performed at 2 dpi. Scale bar, 20 μm. **B.** Subcellular localization of ZmTPL2 in maize. *p2x35S-ZmTPL2-GFP* was expressed in the maize epidermal cells by biolistic bombardment. Images were taken 16-24h after transformation. Scale bar, 20 μm.

1.6.3 Tip6 alters the localization of ZmTPL2

To investigate whether Tip6 has an influence on the localization of ZmTPL2, Tip6-mCherry was co-expressed with ZmTPL2-GFP in *N. benthamiana*. As a negative control, mCherry was co-expressed with ZmTPL2-GFP. The nuclear speckles of ZmTPL2-GFP showed no change in the presence of mCherry alone (**Fig. 19**). Remarkably, in the presence of Tip6, the nuclear speckle pattern of ZmTPL2-GFP was significantly reduced. Moreover, the strict nuclear localization of ZmTPL2-GFP was abolished, as the fluorescence signal expanded to the cytoplasm in the presence of Tip6 (**Fig. 19**).

Results

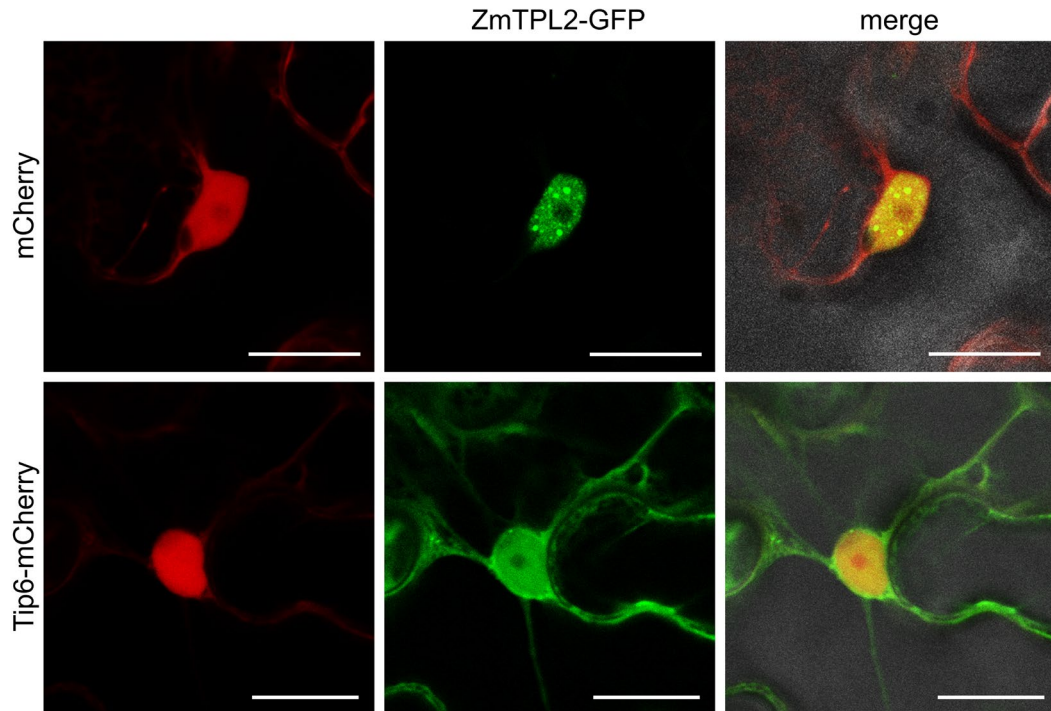


Fig. 19. Tip6 changes the nuclear distribution pattern of ZmTPL2. Subcellular localization of ZmTPL2 in the presence of mCherry or Tip6₂₂₋₂₂₆-mCherry. *p2x35S*-ZmTPL2-GFP was co-expressed with *p2x35S*-mCherry or *p2x35S*-Tip6₂₂₋₂₂₆-mCherry in *N. benthamiana* by *Agrobacterium*-mediated transformation. Pictures were taken at 2 dpi using a confocal microscope. Scale bar, 20 μ m.

Previous results have shown that both EAR motifs of Tip6 are essential for Tip6 to bind to ZmTPL2. To test whether the EAR motifs affect ZmTPL2 nuclear speckle formation, the Tip6 mutant lacking both EAR motifs (Tip6 Δ 2EAR-mCherry) was co-expressed with ZmTPL2-GFP in *N. benthamiana* leaves. As a negative control, ZmTPL2-GFP was co-expressed with mCherry alone. Interestingly, confocal imaging revealed that ZmTPL2-GFP localized to nuclear speckles when co-expressed with mCherry alone or Tip6 Δ 2EAR-mCherry (**Fig. 20A**). These results show that the Tip6 Δ 2EAR mutant was unable to alter the nuclear distribution pattern of ZmTPL2 in *N. benthamiana* plants. Therefore, the EAR motifs of Tip6 are necessary for Tip6 to alter the localization of ZmTPL2.

To further verify that Tip6 affects the formation of ZmTPL2 nuclear speckles, the number of ZmTPL2 nuclear speckles in different co-expressing cells of *N. benthamiana* was counted (**Fig. 20B**). The quantification of speckles showed that ZmTPL2 speckles were drastically reduced in Tip6-expressing cells. However, in Tip6 Δ 2EAR-expressing cells in which Tip6 does not contain EAR motifs, the number of ZmTPL2 speckles was similar to

that in mCherry-expressing cells.

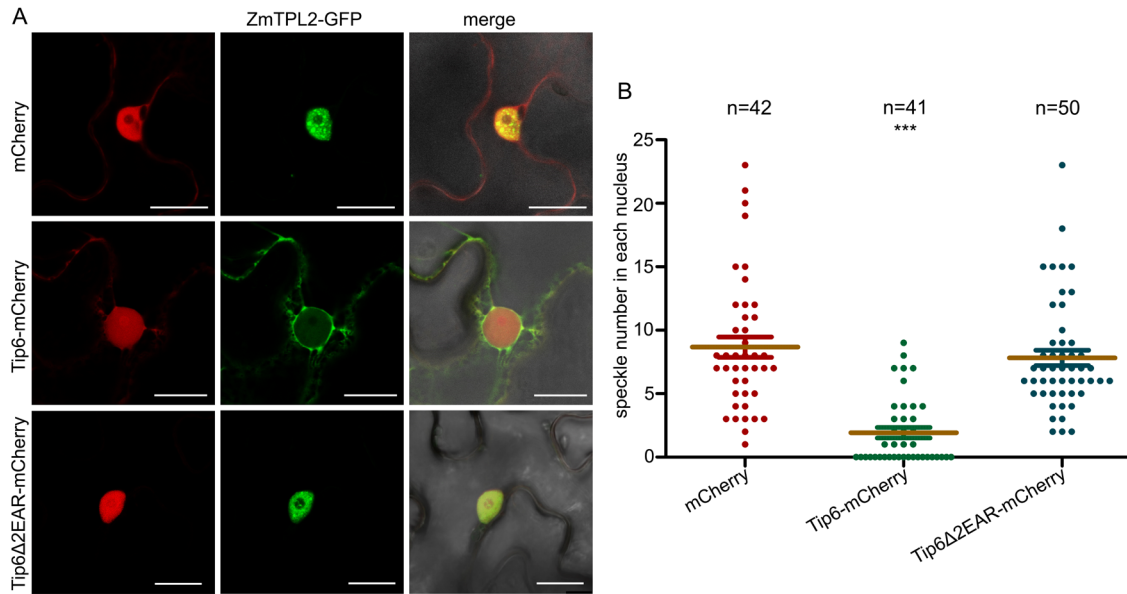


Fig. 20. Effect of EAR motifs in Tip6 on ZmTPL2 nuclear speckle formation in *N. benthamiana*. **A.** *p2x35S-ZmTPL2-GFP* was co-expressed with *p2x35S-mCherry*, *p2x35S-Tip6₂₂₋₂₂₆-mCherry* or *p2x35S-Tip6Δ2EAR₂₂₋₂₂₆-mCherry* in *N. benthamiana*, respectively. Pictures were taken 2 days after infiltration using a confocal microscope. Scale bar, 20 μm. **B.** Tip6 changes the nuclear speckle number of ZmTPL2. The number of ZmTPL2 nuclear speckles per cell in the presence of mCherry, Tip6₂₂₋₂₂₆-mCherry, or Tip6₂₂₋₂₂₆ Δ2EAR-mCherry. Nuclear speckles in **Fig. 20A** observed cells were counted. Results were obtained from three independent experiments. Each dot represents a speckle number in each nucleus. N represents the total number of counted nuclei. ($p < 0.001$, ANOVA, Tukey's).

To verify the localization of ZmTPL2-GFP in maize, ZmTPL2-GFP was transiently co-expressed with Tip6-mCherry or NLS-mCherry in maize epidermal cells by biolistic bombardment. ZmTPL2-GFP co-localized with the nuclear marker NLS-mCherry in the nucleus and formed speckles in the nucleus (**Fig. 21A**), indicating that NLS-mCherry may have no effect on ZmTPL2-GFP. However, when co-expressed with Tip6-mCherry, ZmTPL2-GFP localized in the nucleus, forming a few speckles, as well as at the cell periphery (**Fig. 21B**). These results provide further evidence to support the observation in *N. benthamiana*.

Taken together, these results suggest that Tip6 has the ability to change the nuclear distribution pattern of ZmTPL2 in plants. Particularly, the EAR motifs of Tip6 are critical for altering the localization of ZmTPL2.

Results

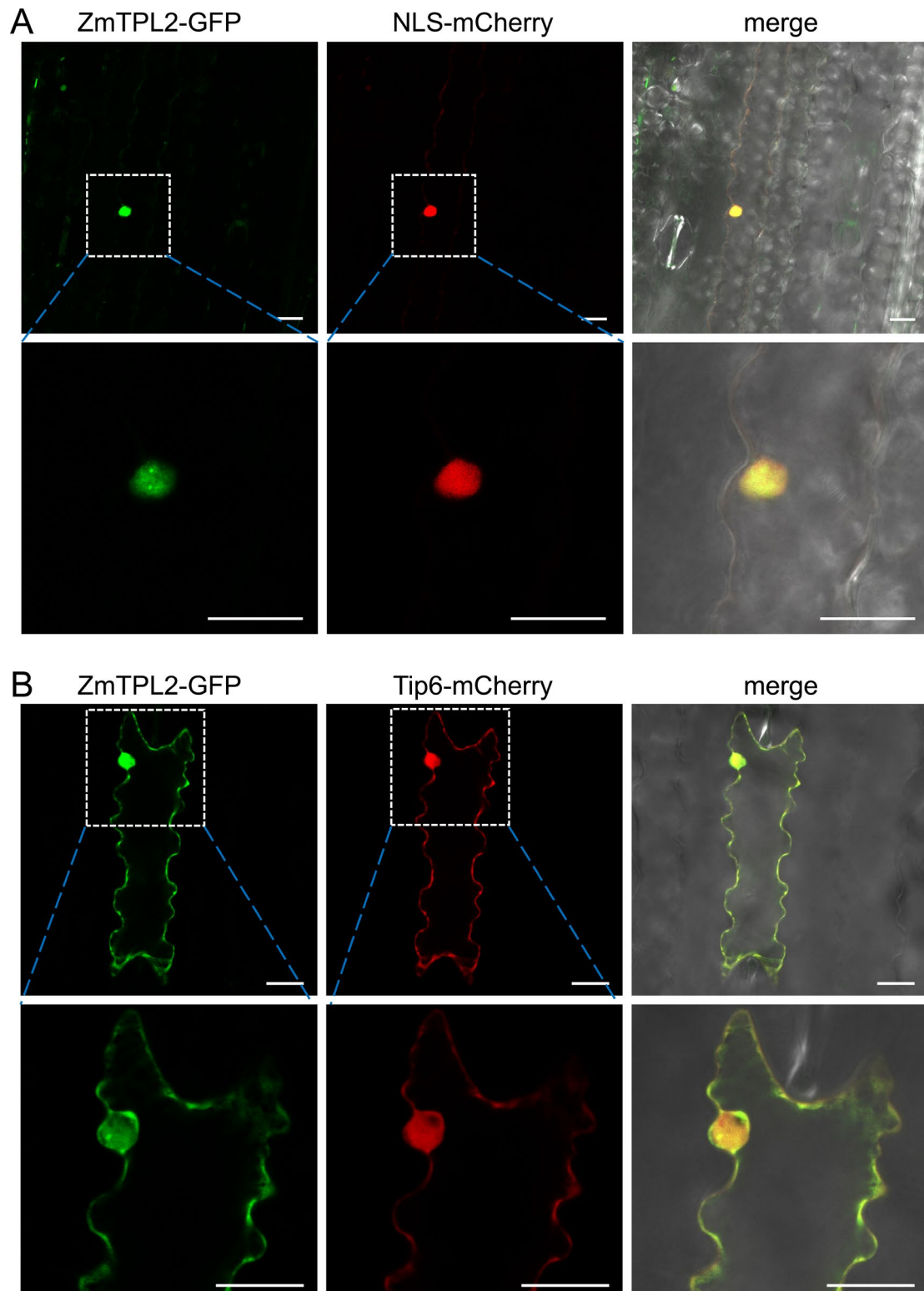


Fig. 21. Tip6 alters the nuclear distribution pattern of ZmTPL2 in maize. **A.** Co-localization of ZmTPL2 in the presence of NLS-mCherry. Maize epidermal cells were co-bombarded with *p2x35S*-ZmTPL2-GFP and the negative control *p2x35S*-NLS-mCherry. The lower panel shows a magnified view of the white square in the upper panel. Images were taken 16-24h after the bombardment. Scale bar, 20 μ m. **B.** Co-localization of ZmTPL2 in the presence of Tip6₂₂₋₂₂₆-mCherry. Maize epidermal cells were co-bombarded with *p2x35S*-ZmTPL2-GFP and *p2x35S*-Tip6₂₂₋₂₂₆-mCherry. The lower panel shows an

enlarged view of the white square in the upper image. Images were taken 16-24h after the bombardment. Scale bar, 20 μ m.

1.6.4 Tetramer formation of ZmTPL2 is required for its nuclear localization

The crystal structure of the N-terminal region of AtTPL, which consists of 202 amino acids (AtTPL202), was solved, revealing that four specific amino acid sites are crucial for tetramer formation (Martin-Arevalillo et al., 2017). The resulting mutated version with these four sites disrupted was designated AtTPL202m. The molecular weight of AtTPL202m was determined to be only half that of AtTPL202, indicating that disrupting these four sites led to the formation of dimers instead of tetramers (Martin-Arevalillo et al., 2017).

To investigate the conservation of these four specific amino acid sites in ZmTPL2, the protein sequences of the N-terminus of five *Arabidopsis* TPL proteins and ZmTPL2 were aligned (**Fig. 22**). The alignment revealed that these four sites are present in ZmTPL2^N, suggesting their conservation and potential role in ZmTPL2 tetramer formation.

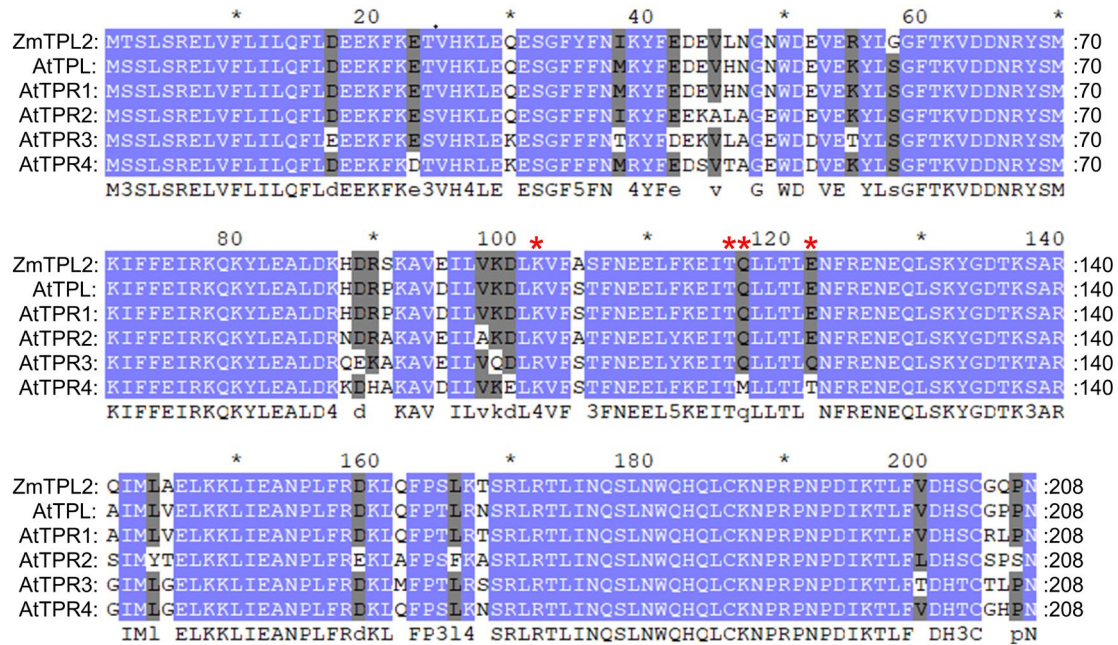


Fig. 22. Conservation of crucial amino acid sites for tetramer formation in *A. thaliana* TPL/TPRs and ZmTPL2^N. Protein sequences were obtained from the maize genome database (<https://www.maizegdb.org/>) and NCBI (<https://www.ncbi.nlm.nih.gov/>) for alignment using the Clustal X and Genedoc software. Zm, *Zea mays*; At, *Arabidopsis thaliana*. The conserved site for tetramer formation was indicated by red asterisks.

Results

To test the functionality of the tetramer-forming sites and their effects on ZmTPL2 localization, site-directed mutagenesis was performed on ZmTPL2-GFP. The mutated version of ZmTPL2-GFP, ZmTPL2m-GFP, was generated using the mutagenesis strategy of the AtTPL202 mutated version, which replaced Lys102, Thr116, Gln117, and Glu122 with Ser, Ala, Ser, and Ser, respectively (Martin-Arevalillo et al., 2017). The subcellular localization of ZmTPL2m-GFP was then examined in *N. benthamiana* by *Agrobacterium*-mediated transient expression. ZmTPL2m-GFP was observed to accumulate in the nucleus, but with fewer or less obvious nuclear speckles compared to ZmTPL2-GFP (**Fig. 23A**). These results suggest that Lys102, Thr116, Gln117, and Glu122 are functional in the localization of ZmTPL2, and that the nuclear speckles may represent a homotetramer of ZmTPL2. Thus, the identified amino acid sites are significant in ZmTPL2 tetramer formation and subcellular localization.

Furthermore, to assess whether Tip6 can alter ZmTPL2m localization, Tip6-mCherry was co-expressed with ZmTPL2m-GFP in *N. benthamiana* leaves. Interestingly, in the presence of Tip6-mCherry, ZmTPL2m-GFP was localized in both the nucleus and cytoplasm (**Fig. 23B**), as observed for the co-expression of Tip6-mCherry and ZmTPL2-GFP. These results suggest that Tip6 is able to alter the translocation of ZmTPL2m from the nucleus to the cytoplasm, indicating that Tip6 might be able to modify the localization of both dimeric and tetrameric forms of ZmTPL2 in plants.

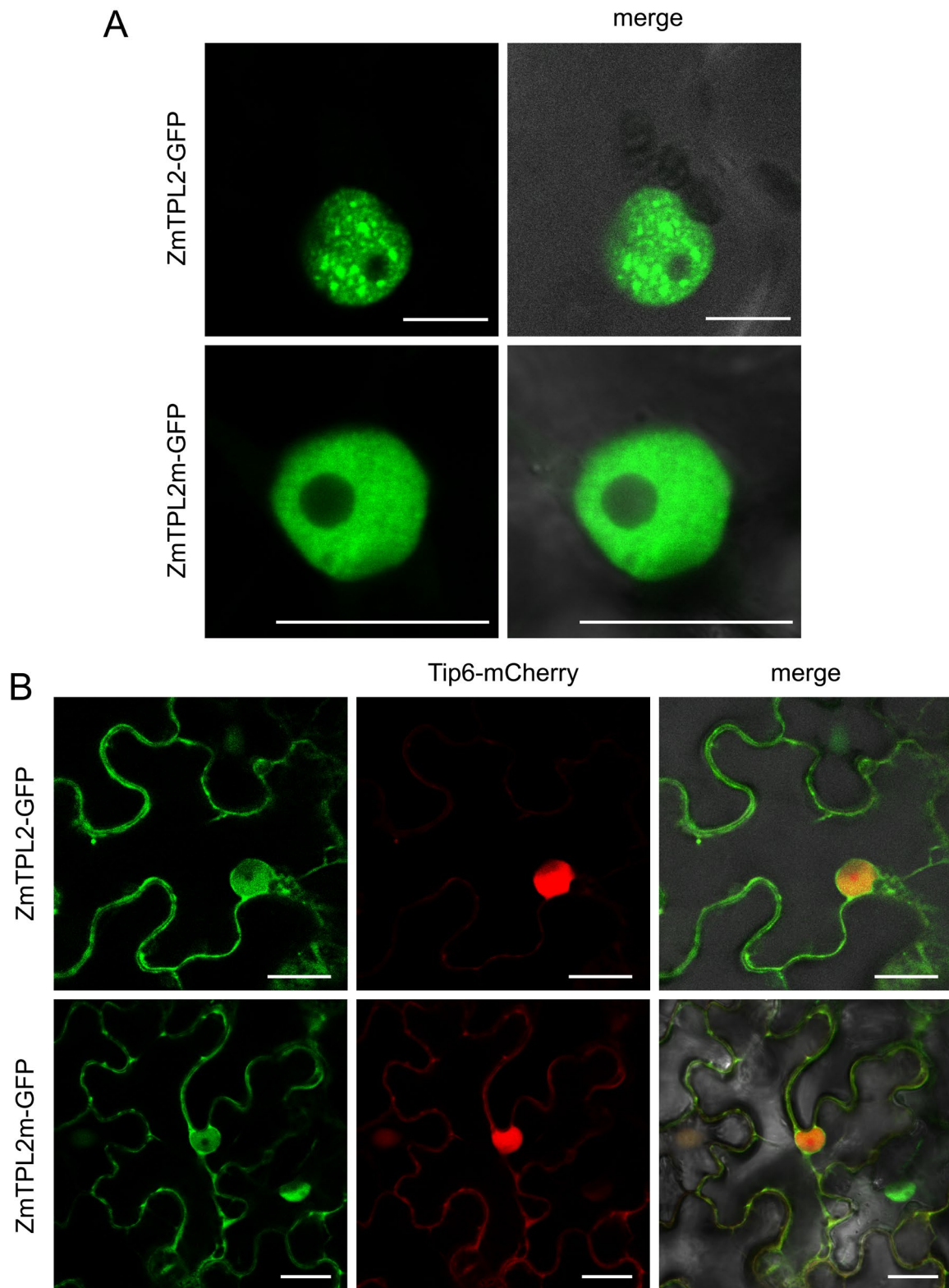


Fig. 23. Mutagenesis of ZmTPL2 tetramer-forming sites reveals their role in subcellular localization and Tip6-mediated translocation in plants. **A.** ZmTPL2m localizes in the nucleus of *N. benthamiana*. *p2x35S*-ZmTPL2-GFP or *p2x35S*-ZmTPL2m-GFP were individually expressed in *N. benthamiana* leaves. Confocal images were taken 2 days after *Agrobacterium* infiltration. Scale bar, 20 μ m. **B.** Tip6 alters the nuclear localization of ZmTPL2m. ZmTPL2-GFP and ZmTPL2m-GFP localization in the presence of Tip6-mCherry in *N. benthamiana* plants. Scale bar, 20 μ m.

Results

1.6.5 Tip6 co-localization with ZmTPL1 and ZmTPL3

Maize has four TPL proteins, namely ZmTPL1, ZmTPL2, ZmTPL3, and ZmTPL4. To investigate whether the other maize TPL proteins also exhibit speckled localization in the nucleus, the subcellular localization of ZmTPL1 and ZmTPL3 was determined. Empty GFP as a control or ZmTPL1-GFP and ZmTPL3-GFP were individually expressed in *N. benthamiana* leaves. Surprisingly, it was observed that ZmTPL1-GFP and ZmTPL3-GFP localized in the nucleus but did not form speckles (**Fig. 24**). This suggests that the speckled accumulation of ZmTPL2 may be unique among the TPL family proteins in maize.

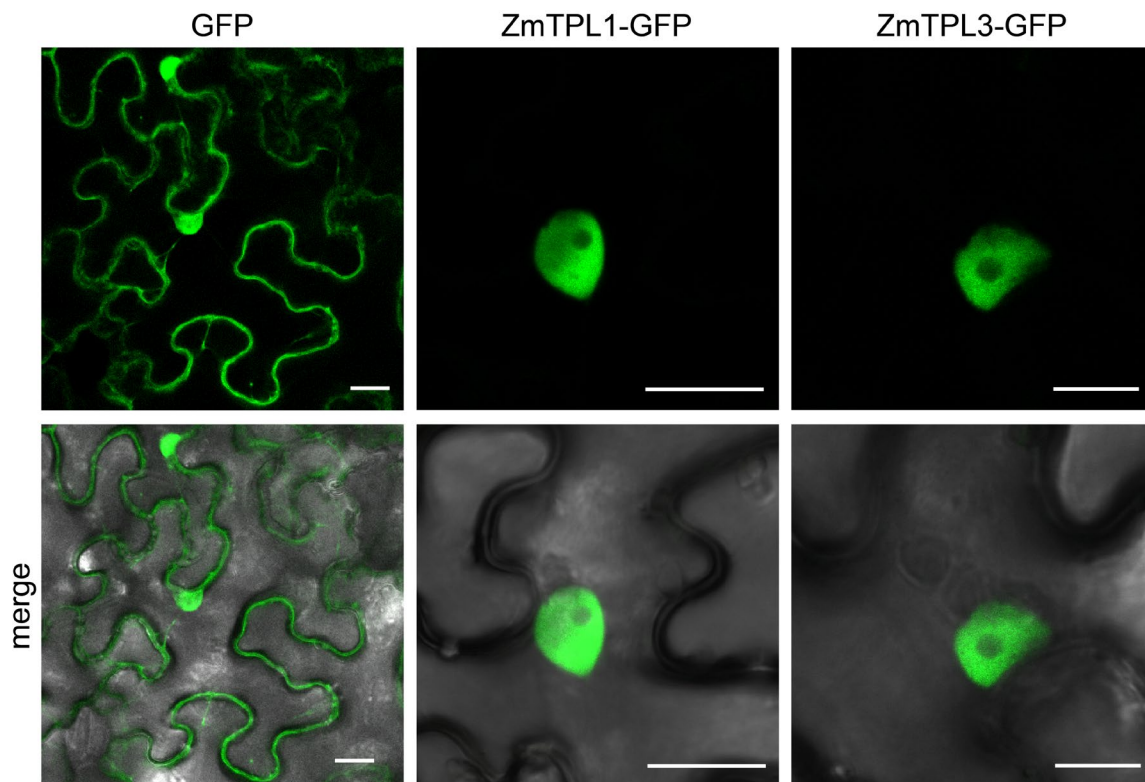


Fig. 24. Subcellular localization of ZmTPL1 and ZmTPL3. In *N. benthamiana* leaves, either *p2x35S-ZmTPL1-GFP* or *p2x35S-ZmTPL3-GFP* were expressed. Confocal images were taken 2 days after *Agrobacterium* infiltration. Scale bar, 20 μ m.

To demonstrate whether Tip6 specifically alters the localization of ZmTPL2 or also other maize ZmTPL proteins, Tip6-mCherry was expressed together with either ZmTPL1-GFP, ZmTPL3-GFP or GFP alone in *N. benthamiana* leaves. Confocal imaging showed that GFP, ZmTPL1-GFP and ZmTPL3-GFP as well as Tip6-mCherry localized to the nucleus (**Fig. 25**). This indicates that Tip6 was unable to alter the localization of ZmTPL1 or ZmTPL3.

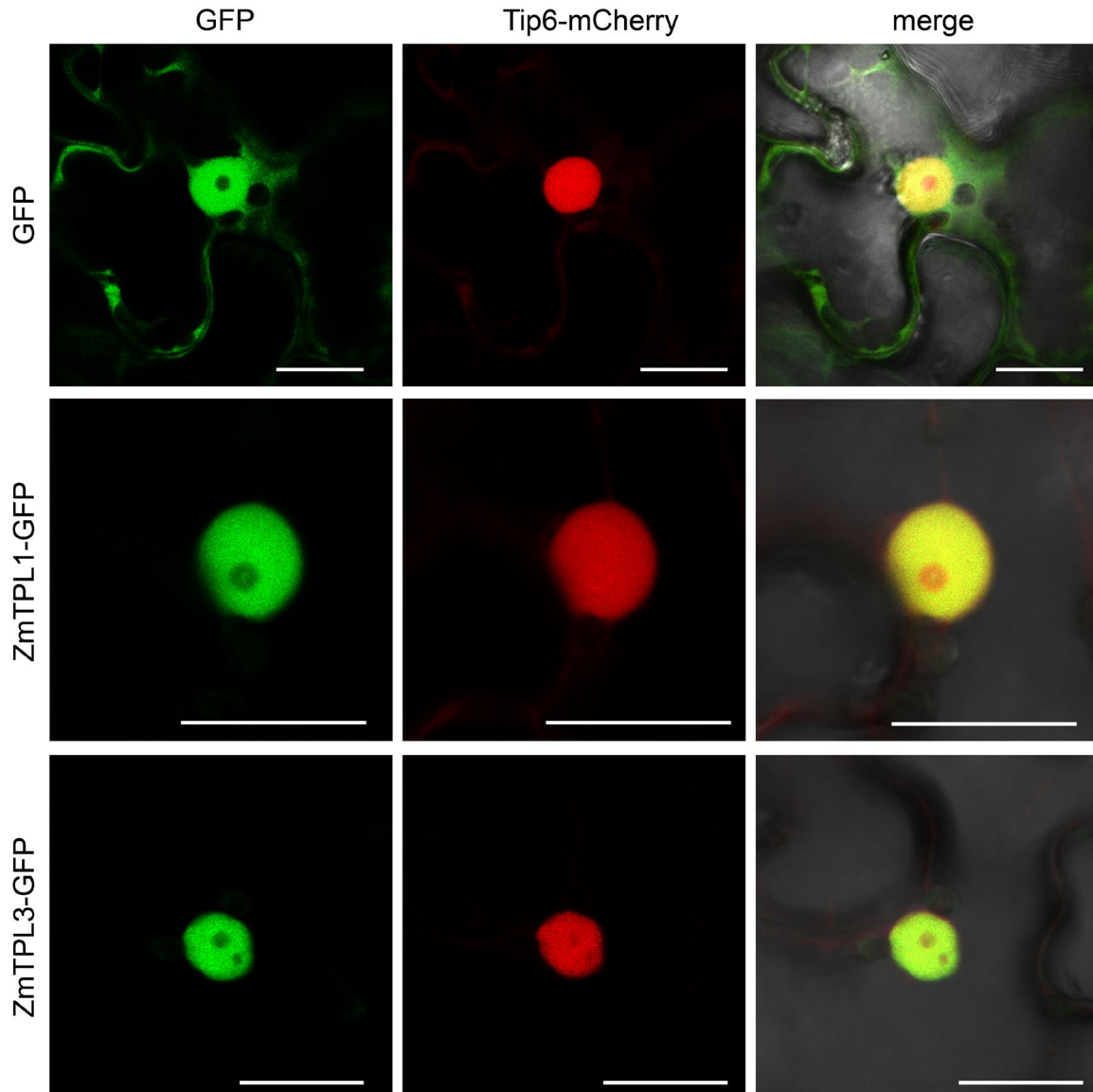


Fig. 25. Tip6 does not alter the nuclear localization of ZmTPL1 and ZmTPL3. Tip6-mCherry was co-expressed with either GFP, ZmTPL1-GFP, or ZmTPL3-GFP in *N. benthamiana* plants as indicated. Scale bar, 20 μ m.

1.7 Tip6 has a functional ortholog in *S. reilianum*

The smut fungus *S. reilianum* is closely related to *U. maydis*, but it causes systemic infections and produces a large number of teliospores in inflorescence structures (Schirawski et al., 2010). To investigate the functional conservation of the effector protein Tip6 between these two species, *UmTip6* was converted to its *S. reilianum* ortholog *SrTip6* using CRISPR-Cas9-mediated genome editing in SG200 (Zuo et al., 2021). Despite *SrTip6* sharing only 25.65% sequence identity with *UmTip6*, the resulting mutants showed that *SrTip6* has a similar phenotype to *UmTip6*, suggesting that these proteins may be

Results

functionally conserved (Zuo et al., 2021). Furthermore, the amino acid alignment showed that both EAR motifs are highly conserved in SrTip6 (**Fig. 26A**). These findings suggest that UmTip6 and SrTip6 might be functionally conserved proteins.

To investigate whether SrTip6 interacts with maize TPL genes as observed for UmTip6, the coding sequence of SrTip6 lacking a signal peptide was generated and tested for interaction with TPL family proteins in the Y2H assay. An empty vector is used as a negative control. SrTip6 with ZmTPL2 or ZmTPL3 showed growth on strict high stringency medium, but SrTip6 with ZmTPL1 or ZmTPL4 did not grow on selection medium (**Fig. 26B**). This suggests that SrTip6 interacts with ZmTPL2 and ZmTPL3, but not ZmTPL1 or ZmTPL4. This result is consistent with UmTip6 interacting with the maize TPL family proteins.

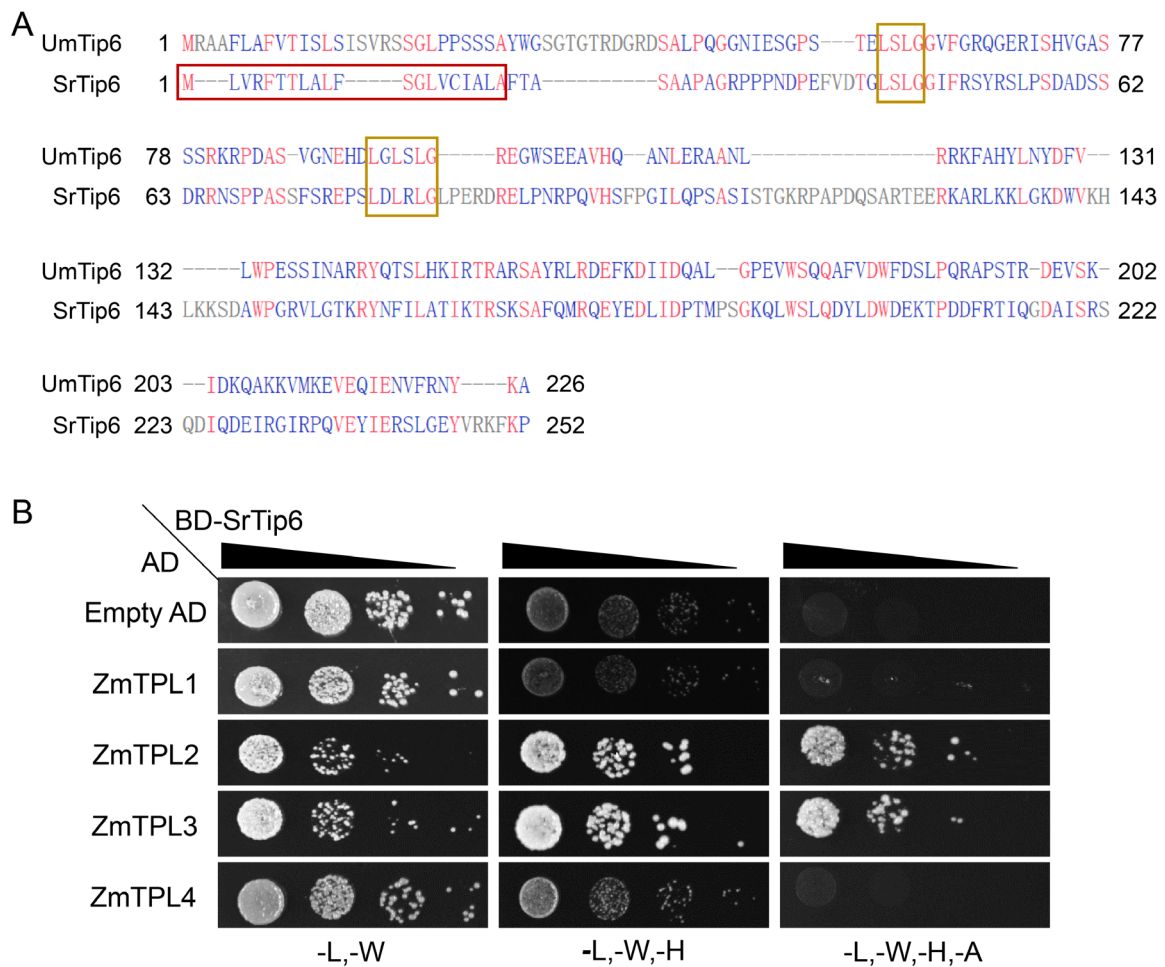


Fig. 26. Conservation of EAR motifs in UmTip6 and SrTip6 and interaction between SrTip6 and maize TPL family proteins. A. Amino acid sequence comparison of UmTip6 and SrTip6. The amino acid sequences of *U. maydis* Tip6 (UMAG_11060) and the Tip6 ortholog from *S. reilianum* (Sr14941) were aligned using the NCBI multiple alignment tool (https://www.ncbi.nlm.nih.gov/tools/cobalt/re_

cobalt.cgi). The red-framed area represents predicted signal peptides by SignalP 4.0, while the yellow-framed area represents conserved EAR motif sequences. Amino acids marked in red are conserved, those marked in blue are paired, and those marked in gray are completely unpaired. **B.** Interaction among SrTip6 and the maize TPL family in the Y2H assay. Yeast cells were co-transformed with SrTip6 and either ZmTPL1, ZmTPL2, ZmTPL3, ZmTPL4, or an empty control plasmid. The transformed cells were then plated onto nutrition-deficient synthetic defined (SD) media plates: SD/-Leu/-Trp, SD/-Leu/-Trp/-His/-Ade, or SD/-Leu/-Trp/-His/-Ade to check for protein-protein interactions. Plates were incubated for 3-4 days and pictures were taken.

To investigate the subcellular localization of SrTip6, SrTip6 lacking the signal peptide and fused to mCherry (SrTip6₂₁₋₂₅₂-mCherry) was transiently expressed in *N. benthamiana* via *Agrobacterium*-mediated transformation. SrTip6₂₁₋₂₅₂-mCherry primarily localizes in the cytoplasm and nucleus (**Fig. 27A**). This result reveals that SrTip6 and UmTip6 have very similar subcellular localizations.

To examine if SrTip6 could alter the localization of ZmTPL2 as UmTip6, SrTip6-mCherry was co-expressed with ZmTPL2-GFP in *N. benthamiana*. The co-expression of mCherry with ZmTPL2-GFP served as a negative control. ZmTPL2-GFP is localized as speckles in the nucleus in the presence of mCherry (**Fig. 27B**). In the presence of SrTip6-mCherry, however, ZmTPL2-GFP translocated to the cytoplasm, but still aggregated into speckles in the nucleus. Conversely, ZmTPL2-GFP altered the localization of SrTip6-mCherry to form speckles in the nucleus, whereas speckles were not observed when SrTip6-mCherry localized alone (**Fig. 27B**). These results suggest that SrTip6-mCherry and ZmTPL2-GFP can mutually influence their subcellular localization.

Results

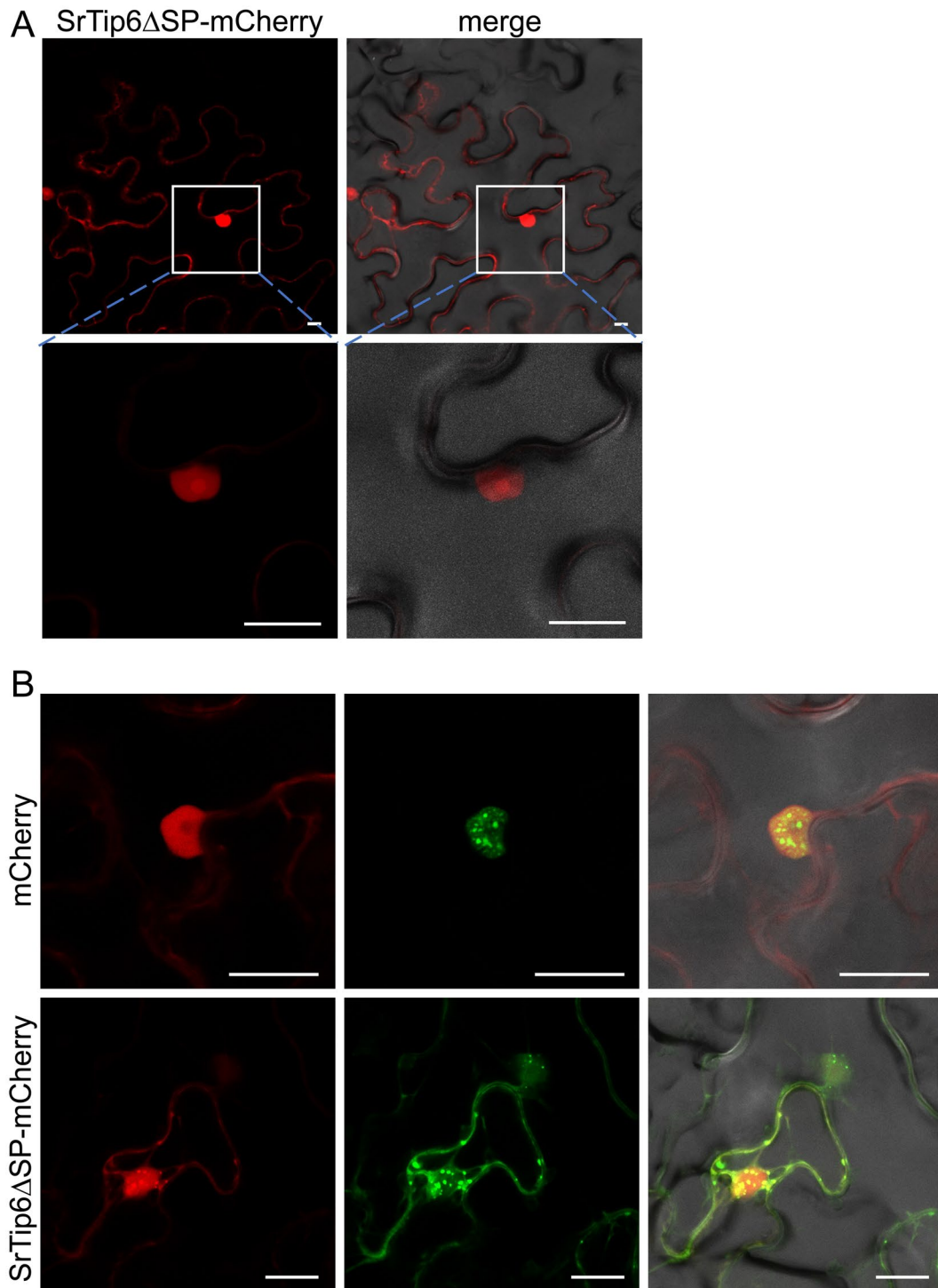


Fig. 27. Subcellular localization and co-localization of SrTip6-mCherry and ZmTPL2-GFP in *N. benthamiana*. **A.** Subcellular localization of SrTip6 in *N. benthamiana*. The p2x35S-SrTip6₂₁₋₂₅₂-mCherry fusion protein lacking the signal peptide was transiently expressed in *N. benthamiana* using *A. tumefaciens* for transformation. Confocal images were taken at 2 dpi. The magnified white square area shows localization in the cytoplasm and nucleus. Scale bar, 20 μ m. **B.** Co-localization of SrTip6₂₁₋₂₅₂-mCherry and ZmTPL2 in *N. benthamiana*. p2x35S-ZmTPL2-GFP was co-expressed with p2x35S-mCherry or p2x35S-SrTip6₂₁₋₂₅₂-mCherry in *N. benthamiana* epidermal cells using *Agrobacterium*-mediated transformation. Confocal images were taken at 2 dpi. Scale bar, 20 μ m.

2. Discussion

The manipulation of host transcription by effector proteins is a key mechanism of plant pathogens, which can regulate the plant extracellular environment more suitable for their colonization. This study investigates how the effector protein Tip6, secreted by *U. maydis* during colonization, disrupts the transcriptional regulation of maize plants. Tip6 interacts with ZmTPL2, a plant protein involved in transcriptional regulation. This interaction leads to an altered nuclear distribution of ZmTPL2, mis-regulation of host transcription factors, and ultimately a reprogramming of transcriptional networks in the host.

2.1 Tip6 uses EAR motifs to recruit ZmTPL2

This study provides evidence that the effector protein Tip6 of *U. maydis* mimics plant mechanisms to recruit maize corepressor ZmTPL2 by using the LxLxLx type (sequence with LSLG or LGLSLG) of EAR repression motifs. Tip6 contains two EAR motifs, which are responsible for interacting with ZmTPL2. Plant transcriptional repressors recruit the TPL/TPR family of proteins via their EAR repression motif to target genes for transcriptional repression, and this mechanism is highly conserved in plants (Ke et. al, 2015; Liu et. al, 2019; Ma et. al, 2017). It is interesting to note that in *Arabidopsis* approximately 48% of the TPL/TPR interactors have the LxLxLx motif (Causier et al., 2012). Similarly, in maize, a screen of REL2 (ZmTPL3) interactors revealed that 44% contained LxLxL-type repression motifs and 13% had a DLNxxP-type repression motif (Liu et al., 2019). The specificity of the Tip6-ZmTPL2 interaction relies on the presence of EAR motifs, as demonstrated by the abolition of the interaction when the individual EAR motifs are deleted. Furthermore, it has been observed that the first EAR motif plays a more crucial role in mediating the Tip6-ZmTPL2 interaction in the Y2H assay, as deletion of this motif completely abolishes the interaction. While deletion of the second EAR motif leads to a weaker interaction between Tip6-ZmTPL2. These findings suggest that while both EAR motifs are involved in mediating the Tip6-ZmTPL2 interaction, their individual contributions to this process are not equal. It is worth noting that the rhizogenic *Agrobacterium* effector protein RolB contains both N- and C-terminal EAR motifs. However, studies have shown that only the C-terminal EAR motif is required for the recruitment of

TPL and the development of hairy roots (Gryffroy et al., 2023). In *Arabidopsis*, the biological and molecular functions of the two EAR motifs of IAA7, an Aux/IAA repressor 7 were analyzed, using substitution mutant forms. This showed that the first EAR motif is essential for interacting with all TPL/TPR members, while the second EAR motif plays a minor role in interaction with TPL and is specifically needed for interacting with TPR1 (Lee et al., 2016). Additionally, the second EAR motif plays a minor repressive role in auxin-related developmental processes and gene expression (Lee et al., 2016). These findings suggest that the two EAR motifs of IAA7 play specific and different repressive roles in auxin responses by interacting with TPL/TPRs. As suggested for the EAR motifs in IAA7, it is unclear whether the two EAR motifs in Tip6 have similar or different roles in transcriptional repression and protein-protein interactions. Further exploration is needed to determine the precise roles of each EAR motif in Tip6.

The identification of Tip6 as an additional effector containing the LxLxLx-type EAR motif that interacts with ZmTPL2 in *U. maydis*, together with previous findings of Nkd1, suggests that the use of LxLxLx-type EAR motifs for TPL-mediated interactions is a common mechanism among diverse plant pathogens. This mechanism has also been observed in the oomycete *Hyaloperonospora arabidopsidis* (Hpa), where the effector HaRxL21 interacts with TPL/TPR through its EAR motif (with the sequence LMLTL) and contributes to virulence (Harvey et al., 2020).

2.2 LxLxLx-type EAR motifs of Tip6 are required for virulence

The EAR motifs present in Tip6 are crucial for the full virulence of *U. maydis*. However, the role of EAR motifs in *U. maydis* effector proteins can vary depending on the specific effector and its mode of action during infection. For example, the LxLxLx type EAR motif located at the C-terminus of Nkd1 is important for its interaction with ZmTPL2. Deletion or mutation of this motif affects the ability of Nkd1 to interact with ZmTPL2, but does not affect its ability to restore virulence in *U. maydis* infection (Navarrete et al., 2022b). This suggests that the EAR motif in Nkd1 is not necessary for its full virulence. However, proper binding of Nkd1 to TPL is crucial for its function, as demonstrated by the reduction in virulence in *U. maydis* when Nkd1SRDX mutants are generated to increase binding to TPL

(Navarrete et al., 2022b).

In the Y2H assay, the deletion of one EAR motif (sequence with LSLG or LGLSLG) in Tip6 reduces its binding to ZmTPL2, suggesting that the binding capacity of Tip6 to ZmTPL2 is increased due to the presence of two EAR motifs within the protein itself. Moreover, our collaborator Dr. Mamoon Khan (University of Bonn) confirmed the results by testing the interaction of site mutations in two EAR motifs of Tip6 with ZmTPL2 (personal communication). The Y2H assays revealed that site mutations in either EAR motif led to a reduction in binding to ZmTPL2, indicating that both EAR motifs in Tip6 are essential for binding to ZmTPL2. In conclusion, these findings suggest that the binding capacity of Tip6 to ZmTPL2 is increased due to the presence of both EAR motifs. Although this study did not investigate the specific contribution of each EAR motif in Tip6 to virulence, the Tip6EARm mutation, was unable to complement the deficiency caused by $\Delta Tip6$ and showed reduced virulence. This suggests that the EAR motifs in Tip6 play an important role in its virulence.

Interestingly, an Nkd1SRDX mutant showed increased binding capacity to TPL2, reduced virulence and it was unable to complement the Nkd1 phenotype (Navarrete et al., 2022b). In contrast, Tip6 possesses two EAR motifs to enhance its binding capacity to ZmTPL2, suggesting that these two effectors bind to ZmTPL2 by different mechanisms. These findings emphasize the crucial role of proper binding to TPL2 for the function of both Tip6 and Nkd1 in *U. maydis* virulence. It is worth noting that although further research is needed to determine the specific contribution of each EAR motif in Tip6 to virulence, the results highlight the importance of proper binding to TPL2 for *U. maydis* virulence.

2.3 Tip6 perturbs ZmTPL2 and changes its distribution in cells

This study shows that ZmTPL2 localizes in the nucleus and forms speckles, while Tip6 localizes in both the nucleus and cytoplasm. However, Tip6 alters the localization of ZmTPL2, causing it to form fewer speckles in the nucleus and shift towards cytoplasmic localization. This effect is mediated by the EAR motifs of Tip6, as the Tip6 Δ EARs mutant did not change ZmTPL2 localization. Interestingly, TPR1 in *Arabidopsis* is rarely detected in the nucleus; instead, it is mostly excluded from the nucleus, as indicated by its detection

in total protein extraction or the cytosolic fraction (Xu et al., 2021). But its nuclear localization is associated with increased plant immunity by repressing the negative regulators of plant immunity (Xu et al., 2021; Zhu et al., 2010). This suggests that maintaining a proper level of TPR1 localized in the nucleus is crucial for plants as continuous activation of immunity can have detrimental effects (Xu et al., 2021). These findings suggest that Tip6 may interfere with the transcriptional regulation of ZmTPL2, potentially leading to inhibition of plant defense. However, TPL/TPRs functions for plant immunity are rather complex in *Arabidopsis*. TPR2 and TPR3 are involved in both suppressing positive regulators of the immune response and impeding the repression of negative regulators by TPR1.

Given that the repressive capacity of the TPL family has been linked to their ability to recruit histone deacetylases, mediators, and nucleosomes to compact chromatin structures (Ito et al., 2016; Leydon et al., 2021; Long et al., 2006; Ma et al., 2017; Oh et al., 2014). The expression of Tip6 in infected maize was found to lead to more abundant Histone H2B.1 and Histone H1 in mass spectrometry data. This suggests that chromatin remodeling might be more active in the presence of Tip6, which could potentially be related to the observed changes in ZmTPL2 localization. The RNA-seq data showed that two Histone 2A genes (Zm00001eb319670, Zm00001eb266530) were down-regulated in the $\Delta Tip6$ infections, indicating a role of Tip6 in regulating histone expression. Although mass spectrometry and RNAseq are not showing the same Histone genes, these results indicate a role of Tip6 in regulating histone expression. Further studies are needed to elucidate the mechanism by which Tip6 induces the mis-localization of ZmTPL2 and how this relates to chromatin remodeling and gene expression.

2.4 Tip6 binds to the N-terminus of ZmTPL2

The EAR motifs in Tip6 interact with the EAR binding groove of ZmTPL2, potentially resulting in structural changes that affect the nuclear localization and speckle formation of ZmTPL2. The N-terminal domain of ZmTPL2 is composed of three domains: the LisH, CTLH, and CRA domains. The monomeric structure of the N-terminus of AtTPL (AtTPL184) contains three hydrophobic grooves (G1-G3), with G3 being the EAR motif binding site,

which comprises a part of the LisH-CTLH domain and the CRA domain (Martin-Arevalillo et al., 2017). Tip6 interacts with the N-terminal of ZmTPL2, but when the N-terminus is further divided into either the LisH-CTLH or CRA domain alone, Tip6 has a weak interaction with LisH-CTLH, while no interaction is observed with the CRA domain. This may be due to the incomplete composition of the G3 groove, as the EAR motifs of Tip6 are unable to efficiently bind to LisH-CTLH or CRA.

Mutations of the four tetramerization-binding site amino acids of ZmTPL2 (ZmTPL2m) resulted in reduced nuclear speckles formation, despite ZmTPL2m localizing in the nucleus. This indicates that disruption of ZmTPL2 tetramerization may impact nuclear speckle formation. Therefore, it is possible that Tip6's interaction with ZmTPL2 affects its tetramerization, resulting in the observed reduction in nuclear speckles. The G3 mutants F74Q, L130A, and Y133A of AtTPL202 were found to form dimers due to the high overlap of the EAR motif binding site and the TPL tetramerization interface (Martin-Arevalillo et al., 2017). Interestingly, the binding of IAA12 EAR motif peptides to AtTPL202 did not affect its tetramerization (Martin-Arevalillo et al., 2017). These results suggest that modification of the EAR binding site can impact AtTPL202 tetramerization, but the binding of the EAR motif peptides to AtTPL202 does not affect its oligomerization (Martin-Arevalillo et al., 2017). The precise mechanism by which Tip6's interaction with ZmTPL2 affects its tetramer formation remains unclear and may involve additional factors beyond the EAR motif binding.

Notably, the EAR motifs in Tip6 bind to the EAR binding site of ZmTPL2, potentially inducing structural changes that affect its multimerization and repression effect. In protoplasts, the G3 groove site mutants and tetramerization formation site mutants abolished their repression activity in *planta* (Martin-Arevalillo et al., 2017). While in yeast, AtTPL188's repression effect was minimally impacted by its multimerization (Leydon et al., 2021). Further investigations are required to elucidate the underlying mechanisms.

2.5 Tip6 regulates expression of various host transcription factors

The RNA-seq analysis revealed that 59 maize transcription factors were mis-regulated in

Discussion

the absence of Tip6 ($\Delta Tip6$) or with a mutation in Tip6 (Tip6EARM) compared to SG200. GO analysis of the DEGs in $\Delta Tip6$ vs. SG200 DEGs and Tip6EARM vs. SG200 showed that these genes were primarily related to transcriptional pathways. This finding is not surprising, as it reflects the impact of Tip6 in the host through its targeting of ZmTPL2. ZmTPL2 acts as a transcriptional corepressor and is likely involved in multiple pathways through its interaction with various transcription factors. A previous Y2H screen of Rel2 (ZmTPL3) interacting proteins identified 36 transcription factors belonging to 18 families (Liu et al., 2019). Similar studies in *Arabidopsis* have shown that transcription factors account for 51%-88% of the total interactor proteins in the five TPL/TPR genes (Causier et al., 2012). The *rel2-ref* (Y527 STOP) mutant of ZmTPL3 only retained the N-terminus due to premature termination in its WD domain (Liu et al., 2019). RNA-seq analysis of *rel2-ref* and wild-type maize revealed significant enrichment of DEGs in the transcriptional regulatory pathway, including negative regulatory factors such as AP2/ERF and Aux/IAA transcription factors (Liu et al., 2019).

In this study, the DEGs were predicted for TF binding motifs and the resulting TFs were enriched using the PlantTFDB database. For the DEGs obtained from the comparison between $\Delta Tip6$ and SG200, *ereb125* was predicted to target 31 DEGs, including *dbp4*, *NAC73*, *zim11*, and *wrky80* transcription factors. Similarly, *ereb14* was predicted to target 31 DEGs, including *dbp4*, *NAC73*, and *wrky80* TFs, while *abi19* was predicted to target 11 DEGs, including *ofp11* and *ereb13*. These results suggest that these TFs may be involved in the recruitment of ZmTPL2 and contribute to the virulence of *U. maydis*.

In the comparison between Tip6EARM and SG200, *ereb125* was predicted to target 61 DEGs, including *dbp4*, *NAC73*, *ereb51*, Homeobox transcription factor 81, *bHLH21*, *ereb127*, and bZIP transcription factor-like TFs. Some of the DEGs in both comparisons are hypothetical targets for *ereb125*, with the involvement of several different DEG TFs. The prediction findings suggest that the interaction of Tip6 and ZmTPL2 may interfere with the recruitment of ZmTPL2 by indeterminate maize TFs, which may regulate other host TFs. Specifically, AP2/ERF family TFs may be involved. Furthermore, it is worth noting that *ereb125* expression was up-regulated in $\Delta Tip6$, while it was not differentially expressed in Tip6EARM. These findings suggest that Tip6 may play a role in regulating the expression

of *ereb125*, which in turn, may contribute to the virulence of *U. maydis*.

Although some of these genes have not been previously reported in maize, their orthologs in other species have been identified and explored. For example, *OVATE11* and *SHI/STY* transcription factor 2 (*SRS2*) were found to be down-regulated in maize infected with $\Delta Tip6$, whereas *NAC73* and *wrky80* showed up-regulation. Ovate transcription factors, such as *Arabidopsis* ovate family protein 1 (*AtOFP1*) and rice ovate family protein 6 (*OsOFP6*), have been demonstrated to act as repressor regulators that inhibit cell elongation, regulate lateral root growth, leaf inclination, and responses to abiotic stimuli (Ma et al., 2017; Sun et al., 2020; Wang et al., 2007). *SHI/STY* transcription factors are related to organ development and hormone regulation (Fang et al., 2023; He et al., 2020; Zhang et al., 2015). The *Arabidopsis* homologue of *ZmNAC73*, *JUNGBRUNNEN1* (*JUB1*), acts as a negative regulator that regulates leaf senescence (Wu et al., 2012). Additionally, *NAC* TFs and *WRKY* TFs were found to play roles in disease resistance and abiotic stress response (Hu et al., 2021; Rushton et al., 2010; G. Wang et al., 2020). Taken together, these genes play roles in various biological processes, including meristem maintenance, floral organ morphogenesis, disease resistance, and abiotic stress response.

Furthermore, the RNA-seq analysis in this study also revealed the mis-regulation of several individual DEGs involved in hormone and plant development in $\Delta Tip6$. Specifically, *ZmGA2ox6*, *ZmGA2ox8*, and *ZmGA2ox12*, which belong to the gibberellin 2-oxidase family of genes, were found to be misregulated. This family of genes plays a critical role in the gibberellic acid (GA) catabolic pathway, which helps to regulate plant growth and development (Rieu et al., 2008). Previous studies have shown that *ZmGA2ox10* is up-regulated in the leaf sheath under GA treatment, and *ZmGA2ox12* may regulate GA balance *in planta* (Ci et al., 2021). Moreover, studies have shown that overexpression of *Arabidopsis* *AtGA2ox7* and *AtGA2ox8* in tobacco causes dwarf plants, while *Arabidopsis* plants lacking *AtGA2ox7* and *AtGA2ox8* show increased GA levels (Schomburg et al., 2003). Similarly, overexpression of either *GA2ox9* or *GA2oxs* in rice caused semi-dwarfism and an increase in tiller numbers (Lo et al., 2008).

In addition, this study found that *ZmARGOS8*, a negative regulator of the ethylene response, was down-regulated in $\Delta Tip6$. *ZmARGOS8* plays a crucial role in enhancing drought

tolerance and improving grain yield by increasing the sensitivity to ethylene (Shi et al., 2015, 2016). Additionally, overexpression of ARGOS genes in *Arabidopsis* has been found to cause an increase in cell number and size during plant organ growth (Hu et al., 2003). Besides, the *yabby14* transcription factor was found to be downregulated in TipEARm. This gene is thought to regulate the lateral outgrowth of leaves, and its expression is limited to the adaxial side of the leaf primordia and the central layer of ground tissue (Juarez et al., 2004).

2.6 Tip6 regulates AP2/ERF B1 family of transcription factors

ERF transcription factors normally interact with the cis-regulatory element known as the GCC box, which comprises the DRE/CRT element and the ERE element (Büttner & Singh, 1997; Fujimoto et al., 2000; Hao et al., 1998; Masaru & Hideaki, 1995; Sessa et al., 1995). These factors are commonly found in the promoters of genes that respond to abiotic stress, jasmonate- and ethylene-inducible genes, and genes related to pathogenesis (Büttner & Singh, 1997; Chakravarthy et al., 2003; Lorenzo et al., 2003; Maruyama et al., 2013; Masaru & Hideaki, 1995; Pré et al., 2008). The ERF family is divided into six subgroups, labeled B1 to B6, with the B3 family regulating multiple disease resistance pathway genes (McGrath et al., 2005; Moffat et al., 2012). For example, when the ERF-B3 gene *AtERF1* was overexpressed, Plant Defensin1.2 (PDF1.2) and chitinases were upregulated (Lorenzo et al., 2003; Solano et al., 1998). Similarly, when the tomato ERF-B3 gene *Pti4* was overexpressed, the expression of *PR1* and *PR2* was stimulated, leading to increased resistance against fungal and bacterial pathogens (Gu et al., 2002). In *A. thaliana*, *U. maydis* Jsi1 expression was induced within 6 hours of β -estradiol induction using the estradiol-inducible XVE system (Darino et al., 2021). Jsi1 expression is capable of inducing the upregulation of 14 transcription factors from the AP2/ERF family, out of which seven belong to the B3 family (Darino et al., 2021). These include ERFs such as ERF2, ERF5, ERF6, and ERF107, which are linked to the defense responses of plants against necrotrophic infections. In addition, Jsi1 expression in *Arabidopsis* resulted in the upregulation of genes that were previously found to be induced by B3 group ERF1 and ORA59 (Darino et al., 2021). There was a 20% overlap with genes such as *PR5* being upregulated and a 30%

overlap with genes such as PDF1.2 being upregulated (Darino et al., 2021). As a result, *Arabidopsis* plants expressing Jsi1 are more susceptible to *Pst DC3000* infections, with the ERF branch of the JA/ET defense signaling pathway being activated (Darino et al., 2021). In maize, the expression of Jsi1-mCherry under the 35S promoter was induced via bombardment, and the expression of genes such as ZmERF1, ZmERF1a, and ZmPR5 was found to be induced after 10 hours (Darino et al., 2021). Similarly, the rhizogenic *Agrobacterium* protein RolB induces upregulation of eight AP2/ERF B3 family genes in the hairy roots of tomato (*Solanum lycopersicum*) (Gryffroy et al., 2023). The ERF B3 subfamily has been shown to act as the positive transcriptional regulator, activating the JA/ET hormone signaling pathways. Both Jsi1 and RolB activate the ERF branch of the JA/ET signaling pathway by recruiting TPL (Darino et al., 2020; Gryffroy et al., 2023).

When the $\Delta Tip6$ and Tip6EARM mutants were compared to SG200, it was observed that the absence or EAR mutation of Tip6 resulted in the upregulation of 20 out of 22 DEGs from the AP2/ERF family, with 13 belonging to the B1 family, while two DEGs were downregulated. Notably, no DEGs belonging to the B3 group were identified in this study. The B1 family of transcription factors typically functions as a transcriptional repressor and plays roles in various plant developmental processes (Chandler, 2018). For example, overexpression of the B1 groups *Enhancer of Shoot Regeneration* (ESR) 1 and ESR2 can induce callus regeneration (Banno et al., 2001; Chandler et al., 2007; Ikeda et al., 2006). The B1 group *Arabidopsis* protein PUCHI contributes to lateral root cell division and floral meristem identity (Bellande et al., 2022; Hirota et al., 2007; Karim et al., 2009). Homologs of PUCHI in other species, such as *bd1* in maize and FRIZZY PANICLE (FZP)/BRANCHED FLORETLESS1 (BFL1) in rice, have also been found to play important roles in floral meristem development (Chuck et al., 2002; Komatsu et al., 2003). Interestingly, the expression of *bd1* was found to be down-regulated in both the $\Delta Tip6$ and Tip6EARM mutants compared to SG200.

In this study, it was revealed that *ereb125* is up-regulated in $\Delta Tip6$, but there is no difference in Tip6EARM. Although the exact function of *ereb125* in maize is yet to be determined, its homolog in *Arabidopsis*, the LEAFY PETIOLE (LPE) (AT5G13910.1) was initially discovered in mutant screens for leaf development (van der Graaff et al., 2000).

Discussion

The LEP mutant produces petiole-less curled leaves, abnormal branching, and an altered silique shape (van der Graaff et al., 2000). In wild-type *Arabidopsis*, the expression of the *LPE* gene is very low and is strongest in young leaves, with weaker expression as leaves become older and have certain tissue specificities (van der Graaff et al., 2000). These findings suggest that *ereb125* may play a role in leaf development.

The present study suggests that the DEGs from the ERF-B1 branch exhibit the presence of three pairs of paralogs, namely *cbf3/ereb36*, *ereb105/ereb16*, and *ereb13/ereb217*, which are presumed to belong to the same subfamily of ERF and may potentially share similar functions (Chandler, 2018; Cheng et al., 2023). *dbp4* and *cbf3*, which are highly activated by cold and play a regulatory role in the abiotic stress responses of plants, were down-regulated in the presence of *Tip6* (Han et al., 2020; Wang et al., 2011). This indicates that *ereb36* may have a similar function to *dbp4* and *cbf3*. The paralogous genes, *ereb13* and *ereb217*, have *Arabidopsis* homologs known as *DREB26*, which act as trans-activators (Krishnaswamy et al., 2011). *DREB26* is strongly expressed in the cotyledonary leaves of 7-day-old seedlings, as well as in ovules and immature siliques, with weak expression in 14-day-old seedlings (Krishnaswamy et al., 2011). Overexpression of *DREB26* in transgenic plants resulted in abnormal morphology, including dwarfism, reduced leaf number, and fewer secondary branches (Krishnaswamy et al., 2011). As a result, the T1 generation of *DREB26* transgenic plants perished prematurely during the vegetative phase (Krishnaswamy et al., 2011). Furthermore, *DREB26* exhibited a relatively weak response to stress and stress hormones, indicating that its primary function may be in promoting growth and development, rather than in defense response (Krishnaswamy et al., 2011). Overall, these findings provide insights into the potential functions of the *ereb13* and *ereb217* genes in maize. Additionally, *ereb26*, a member of the AP2 subfamily involved in floral formation, was found to be down-regulated in $\Delta Tip6$ (Kunst et al., 1989).

ZmERF4 was identified as an interactor of ZmTPL3 (Rel2) through Y2H, and *U. maydis* Jsi1 may interfere with the destabilization of ZmTPL2 by ZmERF4 (Darino et al., 2020; Liu et al., 2019). Interestingly, 63 DEGs in maize infected with *Tip6EArm* appear to have a putative target site for ZmERF4. Although interference with the ZmTPL2-ZmERF4 interaction may similarly cause a large number of DEGs, the GO analysis of *Tip6*-regulated

DEGs does not show enrichment in the JA/ET or SA signaling pathways, suggesting that different branches of the ERF pathway are affected. Specifically, the B3 and B1 branches of the ERF pathway genes were found to be differentially affected.

RolB has a dual role in plant biology. In addition to repressing the immune response, it also plays a crucial role in hair root development by affecting the AP2/ERF transcription factor and the NINJA adaptor. This suggests that RolB may have the potential to connect JA and ET signaling with auxin signaling (Gryffroy et al., 2023). Collectively, the proposition is that the ERF B1 branch impacted by Tip6 has a strong association with plant growth and development, which may affect the formation of leaf tumors by *U. maydis*.

2.7 *U. maydis* uses different strategies to target ZmTPL2

U. maydis uses a variety of effectors to target ZmTPL2 proteins via repression domains or other mechanisms, resulting in changes in host genes. These effectors display highly distinct stage-specific expression patterns during maize infection, suggesting differences in their functions and host adaptation. For example, Tip6 expression peaks at 2 dpi during early biotrophic development, indicating a potential role in interfering with ZmTPL2 during this phase (Lanver et al., 2018). Jsi1 expression peaks at 4 dpi, and Nkd1 expression peaks at 6-8 dpi during tumor formation, suggesting that they may have specific functions during later stages of infection (Darino et al., 2021; Lanver et al., 2018; Navarrete et al., 2022b). Among Tip1-Tip5, all except for Tip3 peak at 2 dpi (Bindics et al., 2022). These ZmTPL2 targeting effectors have staggered expression patterns during the *U. maydis* infection process, suggesting potential ways to prevent competitive ZmTPL2 recruitment and indicating functional differences among these effectors.

Jsi1, Nkd1, and Tip1-Tip5 activate genes in hormone signaling pathways, including JA/ET, auxin, and SA, by relieving ZmTPL2-mediated repression and promoting plant defense responses (Bindics et al., 2022; Darino et al., 2021; Navarrete et al., 2022b). These effects ultimately increase susceptibility to *U. maydis* infection. However, these effects were not observed in the regulation of Tip6, which is more likely to affect plant development during leaf tumor formation by interfering with ZmTPL2.

Nkd1 and Jsi1 use their repression domains to target the host TPL protein and disrupt

Discussion

hormone-related gene expression, which appears to be similar to the canonical mechanism that regulates hormone responses in plants. Under normal conditions, TPL corepressors repress inappropriate gene expression by being recruited to transcription factors bound to the promoters of hormone-responsive genes through an adaptor protein (Plant et al., 2021). When intracellular hormone levels increase, the hormone binds to a specific E3 ubiquitin ligase complex, which targets the adaptor protein for degradation via the 26S proteasome (Plant et al., 2021). The TPL corepressor then dissociates from the target gene, promoting its expression (Plant et al., 2021).

Nkd1 and Jsi1 disrupt this mechanism by binding to the TPL protein and interfering with its recruitment to specific target genes, leading to target gene de-repression. Their repression domain mimics the activity of host transcription factors and interacts with the TPL protein, forming an effector-TPL complex that disrupts TPL-specific target genes, altering host hormone signaling and promoting fungal growth. Nkd1 possesses an LxLxLx type EAR motif that recruits maize ZmTPL2, hindering its interaction with ZmIAA5, a transcriptional repressor of auxin signaling pathways (Navarrete et al., 2022b). This disruption causes an increase in the expression levels of genes involved in auxin signaling transduction. Jsi1 has a DLNxxP motif that interacts with TPL2 (Darino et al., 2021). ZmERF4 and ZmTPL2 also interact, but ZmERF4 destabilizes ZmTPL2 (Darino et al., 2021). ZmERF4 mutants showed increased susceptibility to *F. graminearum* infection and down-regulation of all defense-associated ZmPRs, except ZmPR4 (Cao et al., 2023). In the presence of Jsi1, ZmERF4 and ZmTPL2 become more stable and they do not compete for binding to ZmTPL2, leading to the upregulation of ERF branch genes and activation of JA/ET signaling pathways (Darino et al., 2021).

Tip1-Tip5 target maize TPL protein. They do not have a repression domain but bind to EAR motif binding sites in ZmTPL2. When these binding sites mutate, it affects the interaction of Tip1-Tip4 with ZmTPL2 in different ways, indicating that Tip1-Tip4 do not have EAR motifs but instead bind to the EAR binding groove in ZmTPL2 (Bindics et al., 2022). The exact mechanism of Tip1-Tip4 targeting TPL is still unknown. Moreover, in a Y3H assay, Tip1 and Tip4 compete with ZmIAA3 and ZmIAA8 for ZmTPL2, which may interfere with IAA interaction with ZmTPL2 in the host, leading to the increased

expression of auxin-related genes (Bindics et al., 2022).

This study identified Tip6 as another effector that targets ZmTPL2, which contains two LxLxL type EAR repression domains. However, Tip6 appears to downregulate genes in the AP2/ERF family by binding to ZmTPL2 and altering ZmTPL2 spatial localization from the nucleus towards the cytoplasm. This suggests a different mechanism by which Tip6 impacts host gene expression through ZmTPL2. Tip6 affects DEGs that are not involved highly in hormone signaling, with a greater number of downregulated genes than upregulated genes. Tip6 alters the speckle formation of ZmTPL2, which was expected to release repressed gene expression but surprisingly does not have this effect.

Overall, *U. maydis* seems to use multiple mechanisms to target the host TPL proteins and modulate hormone signaling pathways, allowing it to establish infection and promote its growth. The effectors employ diverse strategies to target and impact the activity of TPL, emphasizing the critical role of TPL proteins as a central hub of plant transcriptional regulation during *U. maydis* invasion. The identification of these mechanisms provides insights into the complex interplay between plant hosts and their pathogenic fungal counterparts, and may contribute to the development of novel strategies for controlling plant diseases.

2.8 Working model and future plans

In conclusion, this study presents an in-depth investigation into the molecular mechanisms underlying the *U. maydis* effector protein Tip6 and its interaction with the plant protein ZmTPL2. Tip6 manipulates host transcriptional regulation by altering the nuclear distribution pattern of ZmTPL2 and interfering with the proteins involved in its repression. Tip6 has a significant impact on the regulation of host transcription factors, mainly the 22 AP2/ERF family transcription factors. The findings propose a model in which Tip6 interacts with ZmTPL2, utilizing EAR repressive motifs to alter its nuclear speckles formation and causing the reprogramming of transcriptional networks in the host plant (**Fig. 28**).

Future studies could focus on investigating the transcriptional regulation of the AP2/ERF family transcription factors and the downstream effects of their mis-regulation by Tip6. It

Discussion

would be valuable to explore the potential interaction between Tip6/ZmTPL2 and the transcription factors, specifically, the putative candidate ereb125, to better understand their roles in *U. maydis* infection. Reports indicate that ZmERF105 serves as an activator of transcription and increases several PR genes, which in turn enhances maize resistance to *Exserohilum turcicum* (Zang et al., 2020). Thus, exploring the role of transcription factors in the AP2/ERF family, including ereb125, in response to *U. maydis* infection could lead to new insights on plant resistance mechanisms.

One approach to investigating the interactions between Tip6, ZmTPL2, and ereb125 is to perform a yeast three-hybrid assay. The bait construct Gal4-BD-ZmTPL2 can be expressed together with either Gal4AD-Zmereb125 or other candidate transcription factors as prey constructs in the presence of Tip6. Alternatively, a co-IP assay could confirm the interaction. For example, ZmTPL2 and Zmereb125 can be expressed as fusion proteins with HA and FLAG tags, respectively, in *N. benthamiana* or maize protoplasts. In the presence or absence of Tip6 with a GFP tag, the lysate can be immunoprecipitated with anti-HA, anti-FLAG or anti-GFP trap beads. The precipitates can then be analyzed by western blotting. These two approaches can provide valuable information on the protein-protein interactions between *U. maydis* effectors and plant proteins, allowing for a better understanding of the molecular mechanisms underlying *U. maydis* infection.

If ereb125 is the transcription factor interfered with by Tip6 and ZmTPL2 interaction, a transcriptional reporter assay can be performed to test the regulatory effect of ZmTPL2 and Tip6 on the expression of ereb125. For example, ereb125 can be cloned upstream of a reporter gene, such as β -glucuronidase (GUS) or luciferase. The construct is then introduced into the cells or tissues of interest (*N. benthamiana* or maize protoplasts) with ZmTPL2, and in the presence of Tip6, the activity of the reporter gene is measured using spectrophotometry (in the case of GUS) or a luminometer (in the case of luciferase) (Jefferson et al., 1987; Solberg & Krauss, 2013). This could determine whether there is a regulatory effect on the expression of ereb125 by ZmTPL2 and Tip6, as well as gain insights into the potential role of Tip6 in this interaction. This approach can provide valuable information on the regulatory interactions between ZmTPL2 and transcription factors, allowing for a better understanding of the molecular mechanisms underlying *U.*

maydis effector Tip6 expression in plants. If it is possible to identify specific promoters in response to altered expression of the AP2/ERF family of transcription factors, this assay can also be used to test the activity effect of expression, which could help identify specific genes and pathways regulated by these transcription factors and provide insight into their downstream effects.

Additionally, a recent publication introduced a novel approach for maize transformation that involves using Wuschel2 (Wus2) and Babyboom (Bbm) to significantly enhance leaf transformation efficiency (N. Wang et al., 2023). This approach also enables the retrieval of plants with targeted gene insertions and Cas9-mediated gene dropouts (N. Wang et al., 2023). Given its success, this approach could be used to study the potential interactions between Tip6, ZmTPL2 and Zmreb125 and their effects on plant-pathogen interactions. Transgenic plants with altered levels of ZmTPL2 or Zmreb125 expression could be generated to examine their effects on *U. maydis* pathogenesis. Furthermore, this method could also be used to express the effector Tip6 and investigate its role in maize. The enhanced transformation efficiency provided by the Wus2/Bbm method would facilitate the generation and study of these transgenic plants.

It is worth noting that the effects of a ZmTPL2 mutation may not be restricted to the interaction with Tip6, as ZmTPL2 is targeted by several *U. maydis* effectors and involved in various biological processes. Although Tip6EARm lost its interaction with ZmTPL2, it showed a deficiency in *U. maydis* virulence. Therefore, additional experiments may be necessary to fully understand the specific role of ZmTPL2 in the interaction with Tip6. While the Wus2/Bbm method provides a promising tool for studying the role of ZmTPL2 and Zmreb125 in *U. maydis* infection, further experiments will be needed to fully elucidate their specific interactions with Tip6 and their broader functions in maize physiology and pathogenesis.

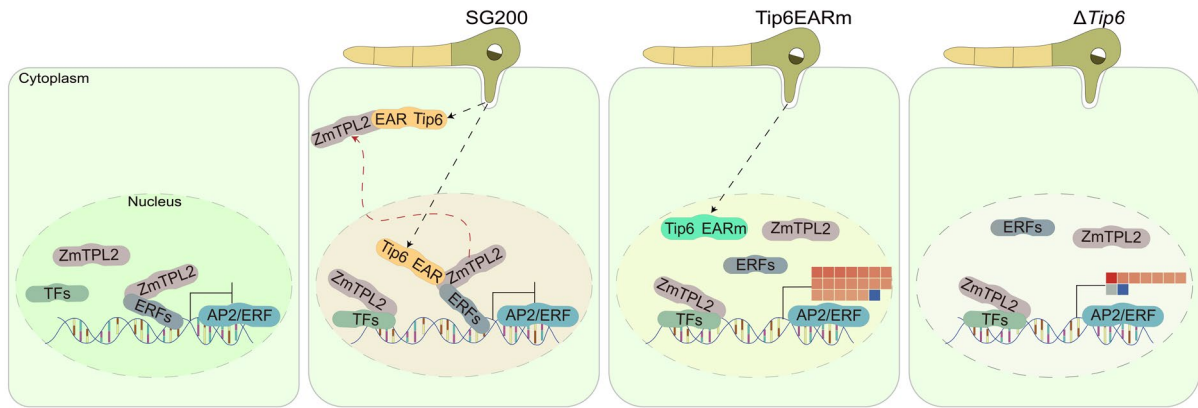


Fig. 28. Tip6 impacts host gene regulation by interacting with the ZmTPL2 corepressor. The figure consists of four panels illustrating the role of Tip6 in *U. maydis* pathogenesis. The first panel depicts a healthy plant cell where ERF family transcription factors recruit ZmTPL2 and repress AP2/ERF family transcription factors. While some unknown transcription factors (TFs) present, they do not recruit ZmTPL2 yet. The second panel presents the SG200 strain infected cell, where Tip6 is expressed and secreted into the plant host. Tip6 interacts with ZmTPL2 utilizing EAR repressive motifs, leading to a change in the localization of ZmTPL2 from the nucleus to the cytoplasm and interfering with its repressor proteins. The third panel shows Tip6 with the EAR motif mutated into Alanine, which loses the ability to interact with ZmTPL2. This loss of interaction causes an unknown impact that leads to the mis-regulation of AP2/ERF family transcription factors. The fourth panel represents the knockout mutant, which lacks Tip6 and its interaction with ZmTPL2, suggesting that Tip6 plays a crucial role in the pathogenesis of *U. maydis*. The heatmap indicates differentially expressed AP2/ERF transcription factors.

Chapter 3. Functional characterization of UMAG_05306

1. The effector gene *UMAG_05306*

UMAG_05306 is an effector gene in *U. maydis* that was initially identified as being associated with virulence function in maize leaf tumor formation (Schilling et al., 2014). This effector exhibits a seedling-specific expression pattern, with its highest expression peak observed at 4 days post-infection (Lanver et al., 2018; Skibbe et al., 2010).

1.1 *UMAG_05306* is required for virulence of *U. maydis*

To confirm the role of *UMAG_05306* in pathogenicity, a *UMAG_05306* coding sequence frame-shift mutant (Δ *UMAG_05306*) was generated in the solopathogenic strain SG200 using CRISPR/Cas9. In addition, a complementation strain designated as *UMAG_05306C* was obtained and confirmed to have a single copy insertion through Southern blot analysis (**Appendix Fig. 4**). Infection assays were performed using Δ *UMAG_05306*, *UMAG_05306C*, and SG200 strains to assess virulence. Results from three independent biological replicates showed that the complementation *UMAG_05306C* strain was not different from SG200 (**Fig. 29**), indicating that the reduced virulence was restored. Contrary, the Δ *UMAG_05306* mutant had a reduced virulence compared to SG200, confirming the previous result that *UMAG_05306* is necessary for full virulence of *U. maydis* in seedling infection (**Fig. 29**) (Schilling et al., 2014).

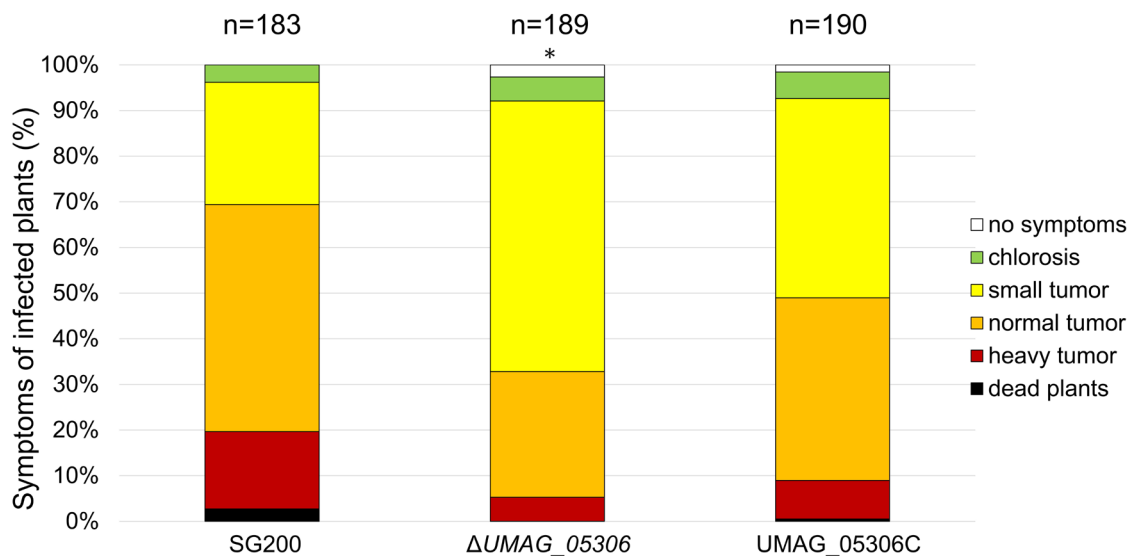


Fig. 29. *UMAG_05306* is required for *U. maydis* virulence. The disease symptoms of maize seedlings infected with the SG200, Δ *UMAG_05306*, and *UMAG_05306C* strains were scored 12 days after infection. Results were generated from three independent biological replicates. *, p-value 0.05 with Student's t-

Results

test, n = number of infected plants.

1.2 Subcellular localization of UMAG_05306

1.2.1 UMAG_05306 localization in *N. benthamiana*

To determine the cellular localization of UMAG_05306, it was fused to GFP without its N-terminal signal peptide (UMAG_05306 Δ SP-GFP) (predicted by SingalP 4.0) and expressed in *N. benthamiana* leaves via *Agrobacterium* infiltration. In addition, GFP alone was expressed as a negative control. Confocal microscopy showed that the UMAG_05306 Δ SP-GFP signal mainly aggregated into twisted filaments in the cytoplasm, with a few filaments located close to the plasma membrane and a few small puncta (**Fig. 30A**). Punctate structures were observed very rarely. To further confirm the specificity of the subcellular localization of UMAG_05306, UMAG_05306 without the signal peptide fused to mCherry (UMAG_05306 Δ SP-mCherry) was also prepared and expressed in *N. benthamiana*, then observed via confocal microscopy. Consistent with UMAG_05306 Δ SP-GFP localization, UMAG_05306 Δ SP-mCherry localized as twisted filaments in the cytoplasm, but punctate localization was never observed (**Fig. 30B**). This suggests that UMAG_05306 is uniquely localized as twisted filaments in the cytoplasm.

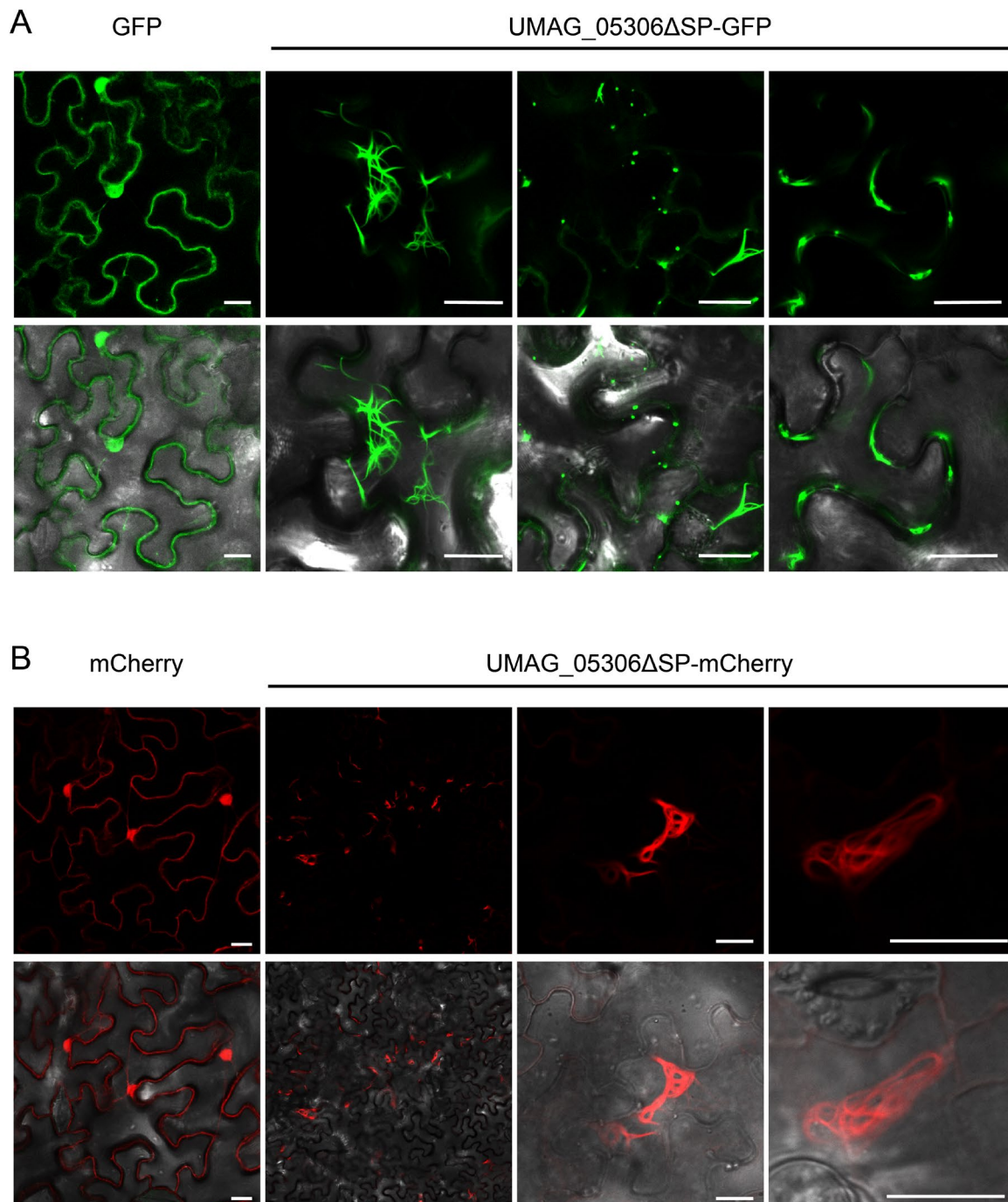


Fig. 30. Subcellular localization of UMAC_05306 as twisted filaments in the cytoplasm of *N. benthamiana*. **A.** Comparison of UMAC_05306ΔSP-GFP localization with GFP alone. **B.** Comparison of UMAC_05306ΔSP-mCherry localization with mCherry alone. UMAC_05306ΔSP-GFP (**A**) and UMAC_05306ΔSP-mCherry (**B**) were expressed in *N. benthamiana* leaves via *Agrobacterium* infiltration, and compared to GFP alone and mCherry alone, respectively. Confocal microscopy was performed two days after infiltration. Scale bar = 20 μm.

1.2.2 UMAC_05306 localization in *Z. mays*

To gain further insight into the localization of UMAC_05306, the expression of

Results

UMAG_05306ΔSP-GFP and UMAG_05306ΔSP-mCherry was individually examined in maize epidermal cells by biolistic bombardment. GFP and mCherry were expressed as controls. The images revealed that UMAG_05306ΔSP-GFP and UMAG_05306ΔSP-mCherry localized in the maize cytoplasm and aggregated into knotted filaments (**Fig. 31 A&B**). This is in line with the location of UMAG 05306 fused to either GFP or mCherry in *N. benthamiana*. The fluorescent proteins GFP or mCherry were found in the nucleus and cytoplasm of maize (**Fig. 31A&B**). Collectively, these results suggest that UMAG_05306 may translocate into the host cytoplasm during *U. maydis* infection, resulting in this specific localization.

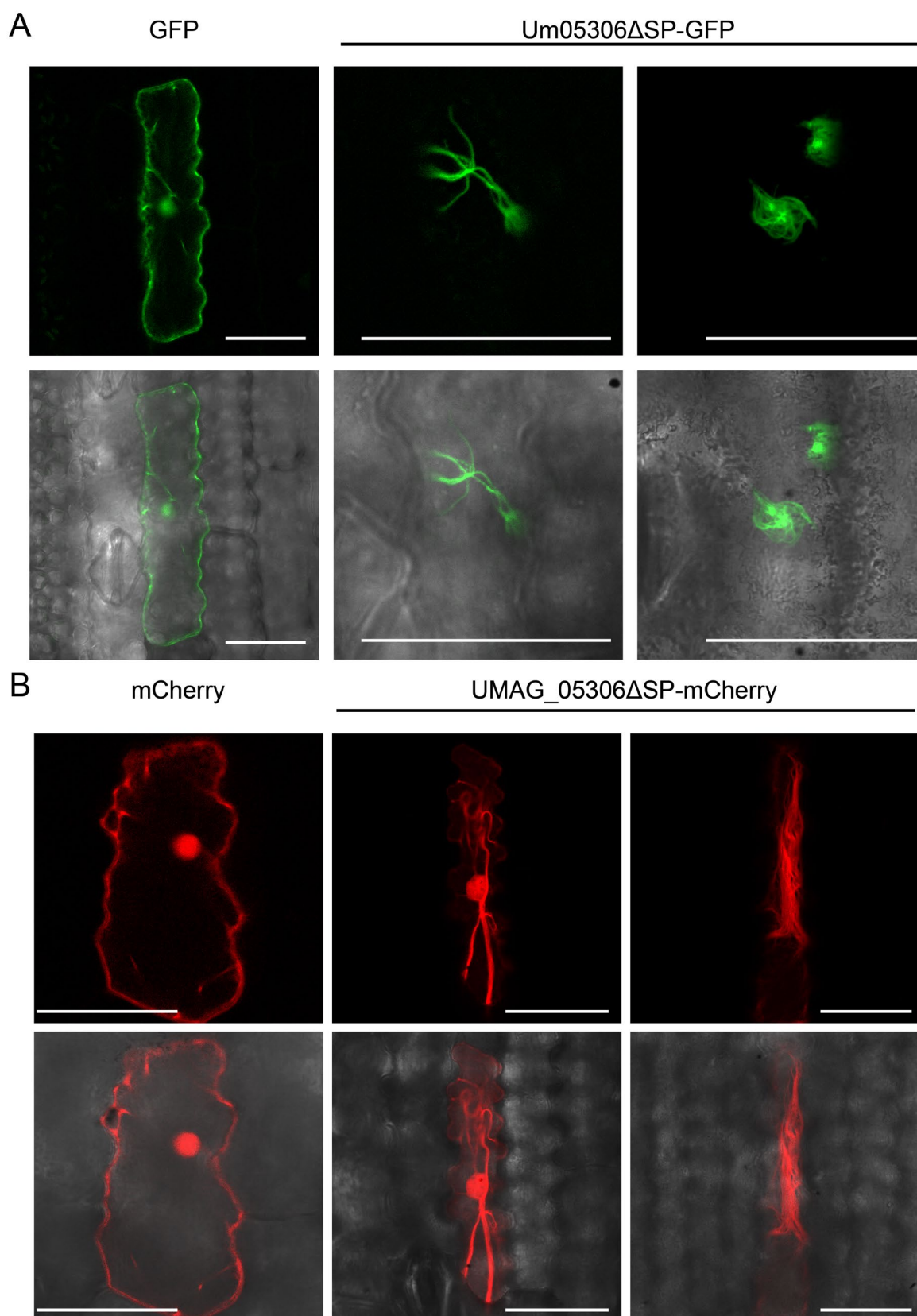


Fig. 31. UMAG_05306 trans-locates into the host cytoplasm and forms a knotted thick filament structure. A. Subcellular localization of UMAG_05306-GFP in *Z. may*. **B.** Subcellular localization of UMAG_05306-mCherry in *Z. may*s. UMAG_05306 Δ SP-GFP (**A**) and UMAG_05306 Δ SP-mCherry (**B**) were

Results

expressed in *Z. mays* epidermal cells by biolistic bombardment and compared to GFP alone and mCherry alone, respectively. Confocal microscopy was performed 16-24h after bombardment. Scale bar, 50 μ m.

1.2.3 Co-localization of UMAG_05306 with the actin marker Lifeact

Since UMAG_05306 localizes as thick and twisted filamentous structures, we asked whether these structures interact with or are dependent on the cytoskeleton of the host cell. To determine whether UMAG_05306 filamentous structures co-localize with actin, it was tested whether UMAG_05306 co-localizes with the actin marker Lifeact-mCherry (Riedl et al., 2008). Before conducting the experiments, the localization of Lifeact as an actin marker was initially confirmed by expressing Lifeact-mCherry in *N. benthamiana* and maize. Confocal imaging revealed that Lifeact-mCherry localized to filamentous actin in both plants, indicating that it can be used as an actin marker (**Appendix Fig. 5A&B**). Next, Lifeact-mCherry was co-expressed with UMAG_05306 Δ SP-GFP in *N. benthamiana*. Confocal imaging shows that UMAG_05306 localized with Lifeact. Interestingly, the twisty and super bundle filamentous structure of UMAG_05306 Δ SP-GFP was dissociated into long and thin strings when co-expressed with Lifeact (**Fig. 32**). The results of the co-expression experiments suggest that Lifeact may have an unintended impact on the localization of UMAG_05306 Δ SP-GFP.

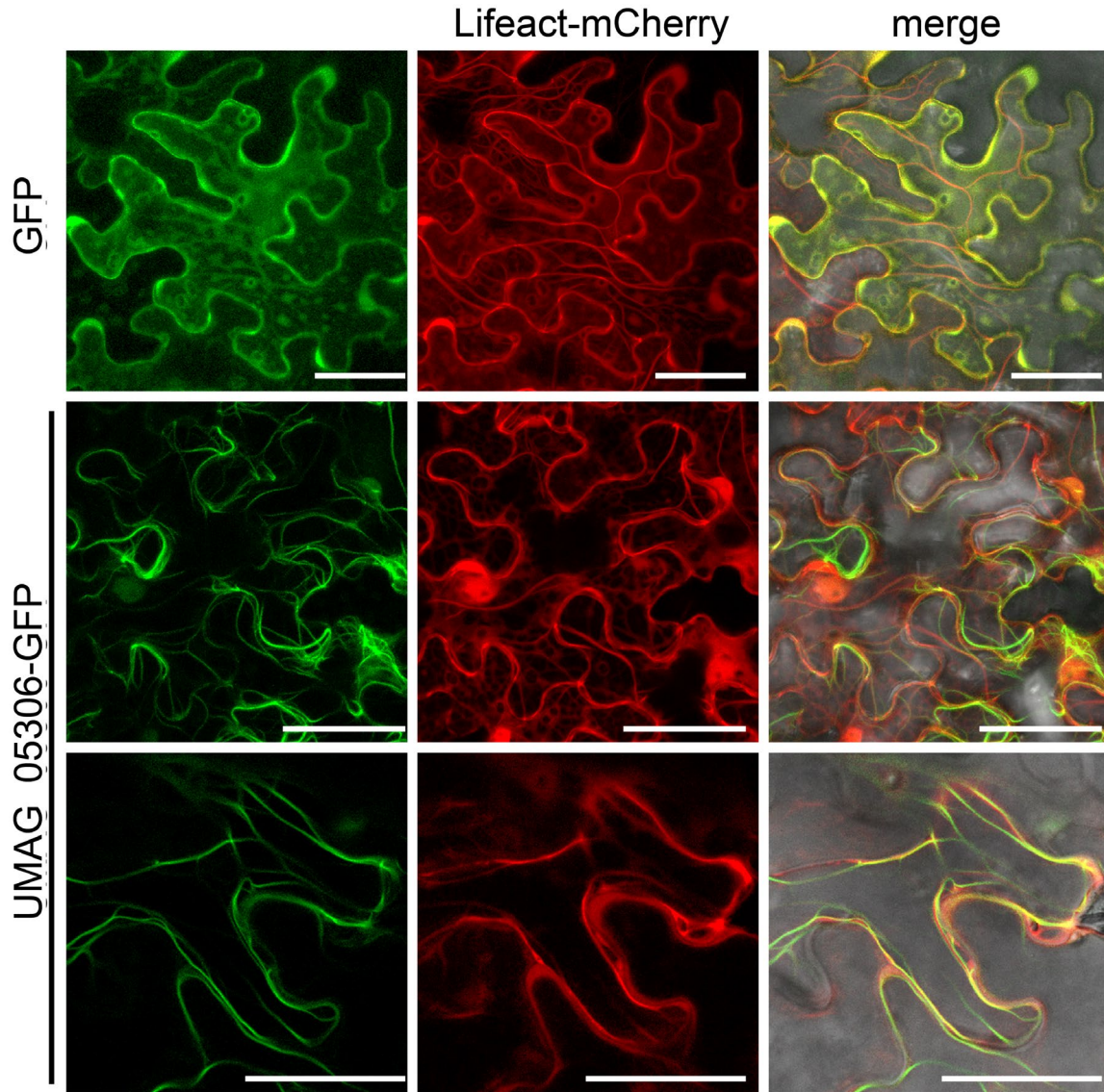


Fig. 32. Impact of Lifeact on the localization of UMAC_05306 in *N. benthamiana*. UMAC_05306 Δ SP-GFP or GFP was co-expressed with Lifeact-mCherry in *N. benthamiana* using *Agrobacterium*-mediated transformation. Confocal microscopy was performed 2 days after infiltration. Scale bar, 50 μ m.

1.2.4 UMAC_05306 localization in maize by transmission electron microscopy

The co-localization assay using Lifeact was found to be insufficient in determining the localization of UMAC_05306. Therefore, an alternative approach was employed, which involved performing immunogold labeling to directly observe the signal of UMAC_05306 localization and secretion in maize seedlings via transmission electron microscopy (TEM). 7-day-old maize plants were infected with a strain expressing UMAC_05306-2xHA under

Results

the strong transcriptional *pit2* promoter in the knockout strain Δ UMAG_05306, and infected leaves were collected at 3 dpi for further section and analysis. As a negative control, the strain (p*Pit2*-SP-mCherry-HA) expressing SP-mCherry-HA under the *pit2* promoter was used. The UMAG_05306-2xHA and SP-mCherry-HA expressing strains were confirmed to be gene single insertion strains by Southern blot. To detect the UMAG_05306-2xHA signal for immunogold labeling, an immunoprecipitation assay using HA magnetic beads was conducted. The resulting Western blot and SDS PAGE analysis with Sypro ruby dye confirmed the expression of UMAG_05306-2xHA in infected maize seedlings, further validating the use of the HA-tag immunogold labeling approach for TEM localization assays (**Appendix Fig. 6**). TEM was performed in collaboration with Dr. Ulla Neumann (Central Microscopy (CeMic), Max Planck Institute for Plant Breeding Research, Köln). The UMAG_05306-2xHA signals were mainly observed in the periphery of the fungal cell wall and the host cytoplasm, with very few signals detected in the fungal cells (**Fig. 33**). The SP-mCherry-2xHA signal was observed in the fungal cell wall and inside the fungal cell wall (**Fig. 33**). This indicates that UMAG_05306 was secreted during the *U. maydis* infection, but our experiment could not show targeting of specific plant organelles.

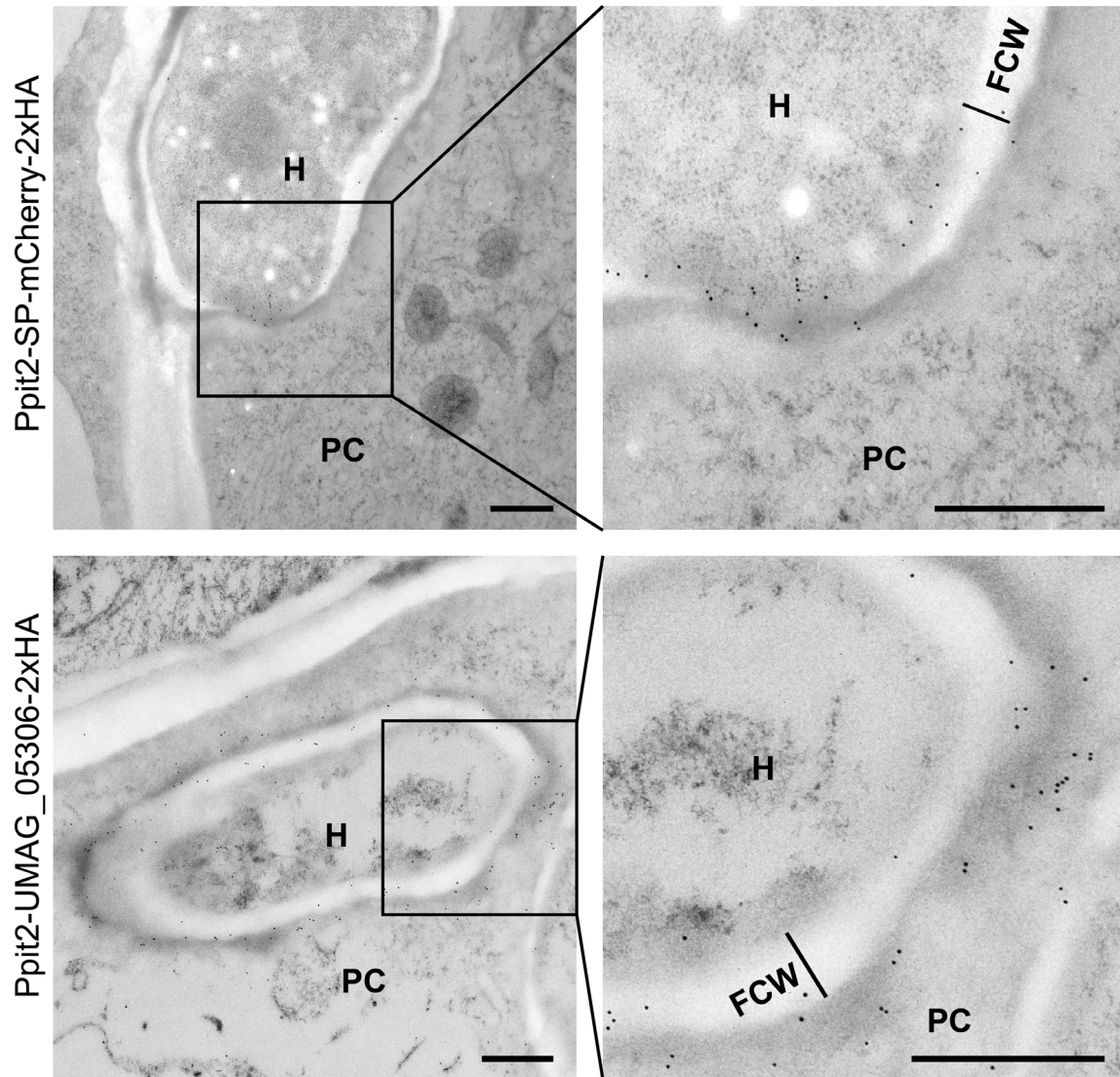


Fig. 33. Localization and secretion of UMAC_05306-2xHA in maize seedlings during *U. maydis* infection. Transmission electron microscopy images showing immunogold labeling of UMAC_05306-2xHA and SP-mCherry-2xHA in maize seedlings infected with *U. maydis*. UMAC_05306-2xHA signals were mainly localized in the fungal cell wall and periphery (FCW), while the SP-mCherry-2xHA signal was observed in the fungal cell wall and inside the fungal cell wall. The image on the right is a magnified view of the black frame on the left. **FCW**: fungal cell wall; **H**: hyphae; **PC**: plant cell cytoplasm. Scale bar, 500 nm.

1.3 UMAC_05306 targets dynamin related protein in the maize

1.3.1 UMAC_05306 interacts with four maize DRPs by CoIP

To identify potential host targets of UMAC_05306, UMAC_05306 Δ SP-GFP was expressed in *N. benthamiana* and a co-IP assay with GFP-trap beads coupled with MS analysis was conducted (experiment performed by lab members Daniel Hilbig and Dr. Bilal Ökmen).

Results

GFP was expressed as a negative control. MS analysis (performed by Dr. Sara Christina Stolze and Anne Harzen, Max-Planck Institute for Plant Breeding Research, Cologne, Germany) yielded a series of putative targets, and candidates were chosen for further investigation based on their distinctive appearance in the IP-bound beads. Among UMAG_05306ΔSP-GFP bound proteins, dynamin 2 was identified, while it was not found among the control GFP-bound proteins. Therefore, dynamin 2 was postulated as a potential host target candidate.

There are five dynamin 2 isoforms and five dynamin related proteins (DRPs) in maize. To assess whether UMAG_05306 interacts with maize DRPs, namely ZmDRP1C, ZmDRP3A, ZmDRP4C, and ZmDRP5A, a co-IP assay was performed. It should be noted that these four DRPs were successfully cloned and up-expressed in maize during *U. maydis* infection (Lanver et al., 2018). Therefore, UMAG_05306 was fused to GFP, while the maize DRPs were fused to HA and expressed in *N. benthamiana*. Western blot results showed that all four tested DRP proteins were detected individually upon pull-down with GFP beads with UMAG_05306ΔSP-GFP but not in GFP controls (**Fig. 34**). These results suggest that ZmDRP1C, ZmDRP3A, ZmDRP4C, and ZmDRP5A interact with UMAG_05306.

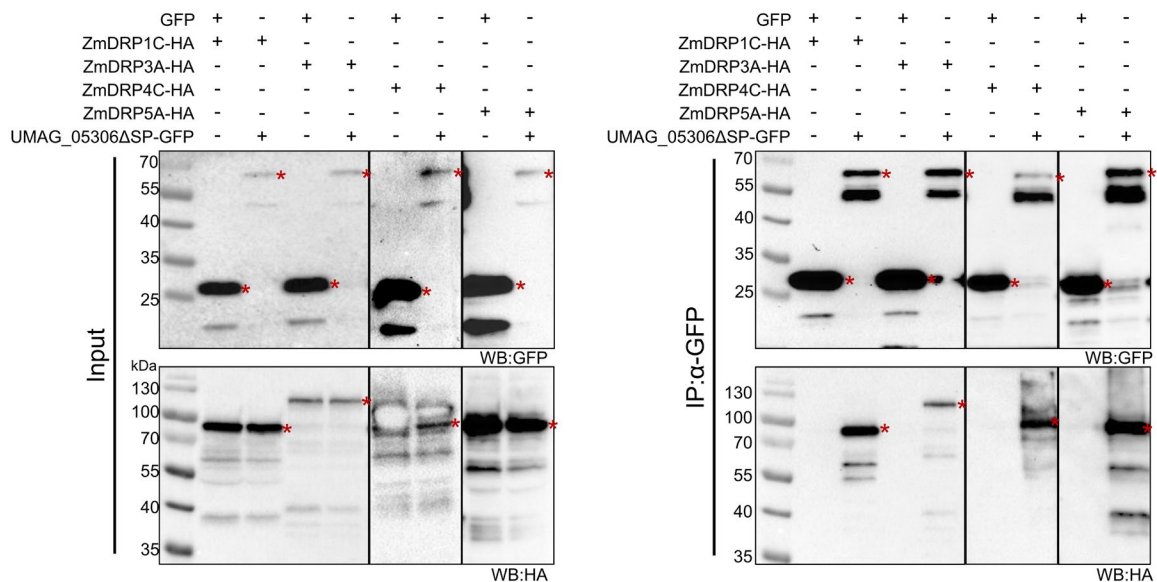


Fig. 34. UMAG_05306 interacts with ZmDRP1C, ZmDRP3A, ZmDRP4C, and ZmDRP5A. UMAG_05306ΔSP-GFP or an empty cytoplasmic GFP with indicated DRPs were co-expressed in *N. benthamiana* via *Agrobacterium*-mediated transformation. Anti-GFP and anti-HA antibodies were used to detect the input and IP proteins by Western blot. Expected sizes: GFP: 26.8 kDa, UMAG_05306ΔSP-GFP: 57.4 kDa, ZmDRP1C-HA: 75.5 kDa, ZmDRP3A-HA: 97.7 kDa, ZmDRP4C-HA: 82.2 kDa, ZmDRP5A-

HA:80.4 kDa. The asterisks indicate the expected band.

1.3.2 UMAG_05306 interacts with N- and C-termini of ZmDRP5

Although maize dynamin or dynamin-related protein sequences are very diverse, they share a conserved GTPase domain at the N-terminus. Thus, dynamin proteins have GTPase activity (Chappie et al., 2010; Ferguson & De Camilli, 2012). To investigate which region of the DRP protein mediates the interaction with UMAG_05306, two truncated versions of ZmDRP5 were generated. One version contains only the N-terminal GTPase domain part (ZmDRP5^N) and the second version contains the rest of the part (ZmDRP5^C). Both were tested for interaction with UMAG_05306 by a co-IP assay (**Fig. 35A**). Therefore, the UMAG_05306-GFP fusion protein was co-expressed with ZmDRP5^N-HA or ZmDRP5^C-HA in *N. benthamiana*. GFP alone was expressed as a control. The co-IP assay indicates that ZmDRP5^N-HA or ZmDRP5^C-HA are both able to co-immunoprecipitate with UMAG_05306, but not with GFP alone, indicating that either ZmDRP5^N or ZmDRP5^C are both important for interaction with UMAG_05306 (**Fig. 35B**).

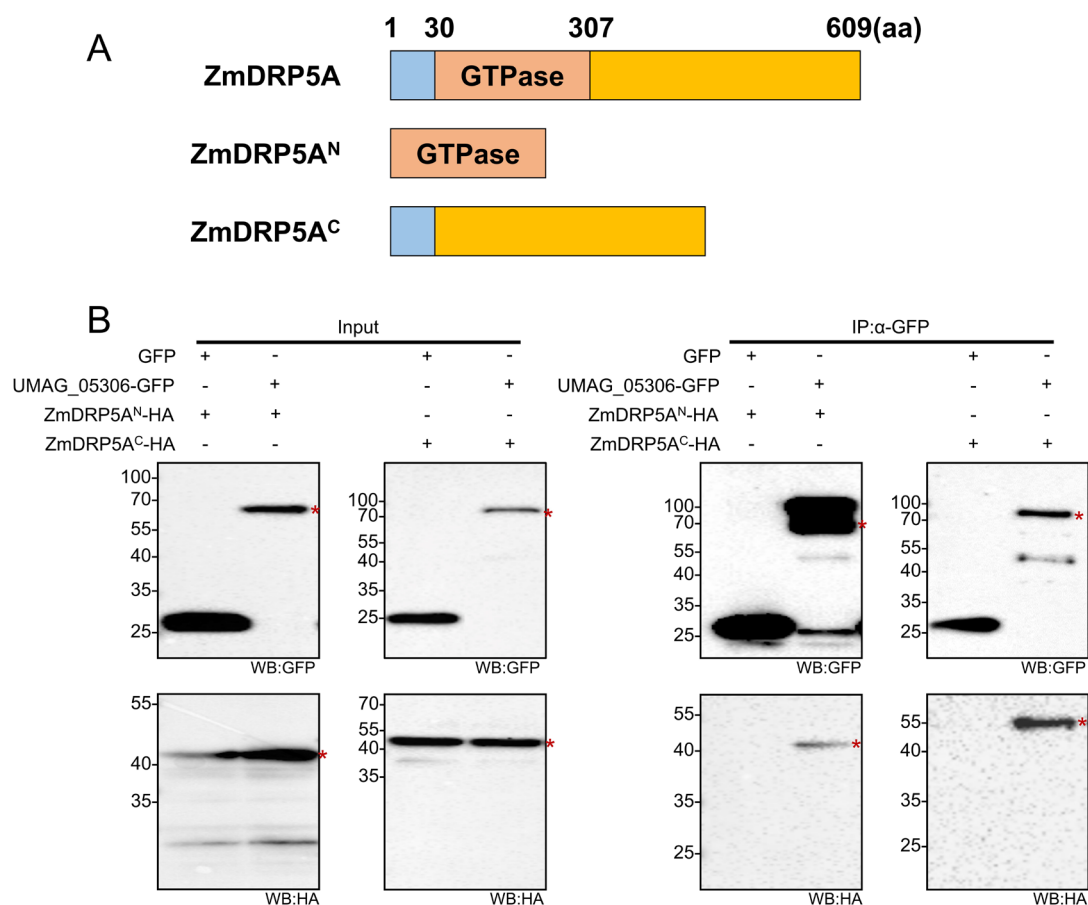


Fig. 35. Interactions between UMAG_05306 and truncated variants of ZmDRP5 in *N.*

Results

benthamiana. **A.** Schematic diagram of ZmDRP5 and its truncated variants. ZmDRP5^N (from the N-terminus 30-307aa of ZmDRP5), ZmDRP5^C (1-29aa combined with the C-terminal 308-609aa of ZmDRP5). **B.** UMG_05306 interacts with ZmTPL2^N and ZmTPL2^C in the co-IP assay. *Agrobacterium* strains carrying UMG_05306-GFP or GFP were co-expressed in *N. benthamiana* leaves with truncated variants of the N- or C-terminus of ZmDRP5, respectively. GFP trap beads were used for protein precipitation, and HA and GFP antibodies were used for Western blotting. The expected molecular weight of the proteins is as follows: GFP: 26.8 kDa; UMG_05306-GFP: 57.4 kDa; ZmDRP5^N-HA: 38.7 kDa; ZmDRP5^C-HA: 45.4 kDa. The asterisks indicate the expected band.

1.4 Maize DRPs and UMG_05306 both interact with maize

Tubulin

α β -tubulin heterodimers form microtubules, which are essential components of the cytoskeleton structure in cells (Nogales et al., 1998). Dynamins, which were initially isolated from microtubules and categorized as microtubule-associated proteins, are known to play important roles in membrane remodeling and trafficking (Collins, 1991; Maeda et al., 1992). Therefore, it was hypothesized that DRPs interact with microtubules. Maize possesses different forms of tubulin that exhibit different expression patterns. ZmTubulin α 6 is prevalent in leaves and anthers, while ZmTubulin β 3 and ZmTubulin β 4 exhibit similar expression patterns and abundant transcripts in the shoots of seedlings (Wang et al., 2004). As UMG_05306 is required for leaf tumor formation, ZmTubulin α 6 was chosen for further investigation. To investigate whether maize DRPs interact with ZmTubulin α 6, co-IP assays were performed by co-expressing either ZmTubulin α 6-GFP or GFP alone with four DRPs (ZmDRP1C-HA, ZmDRP3A-HA, ZmDRP4C-HA, and ZmDRP5A-HA) in *N. benthamiana* leaves. The results showed that ZmDRP1C-HA, ZmDRP4C-HA, and ZmDRP5A-HA were pulled down with ZmTubulin α 6-GFP using GFP beads, indicating that ZmTubulin α 6 interacts with ZmDRP1C, ZmDRP4C, and ZmDRP5A, but not with ZmDRP3 (Fig. 36A).

To determine if maize DRPs interact with another tubulin, co-IP assays were also performed with ZmTubulin β 3 and ZmDRP1C, ZmDRP4C, and ZmDRP5A. ZmDRP1-GFP, ZmDRP5-GFP or GFP alone were co-expressed with ZmTubulin β 3-HA in *N. benthamiana*, and ZmDRP4-HA was co-expressed with GFP or ZmTubulin β 3-GFP. The results showed that ZmTubulin β 3 interacts with ZmDRP1C, ZmDRP3C, and ZmDRP5A as ZmTubulin β 3-

HA was pulled down with ZmDRP1C-GFP and ZmDRP5A-GFP, while ZmDRP4C-HA was pulled down with ZmTubulin β 3-GFP (**Fig. 36B**).

To test if UMAG_05306 directly interacts with Tubulin, co-IP assays were performed for UMAG_05306 and ZmTubulin β 3. GFP was used as a control. GFP or UMAG_05306-GFP was co-expressed with ZmTubulin β 3-HA in *N. benthamiana* leaves. The results showed that UMAG_05306 interacts with ZmTubulin β 3 (**Fig. 36B**). Tubulin exists as paired α and β subunits, so the interaction between UMAG_05306 and ZmTubulin α 3 was evaluated. The results imply that UMAG_05306 interacts with ZmTubulin α 3, suggesting that UMAG_05306 may be directly associated with Tubulin or indirectly associated with Tubulin by DRPs (**Fig. 36C**).

Results

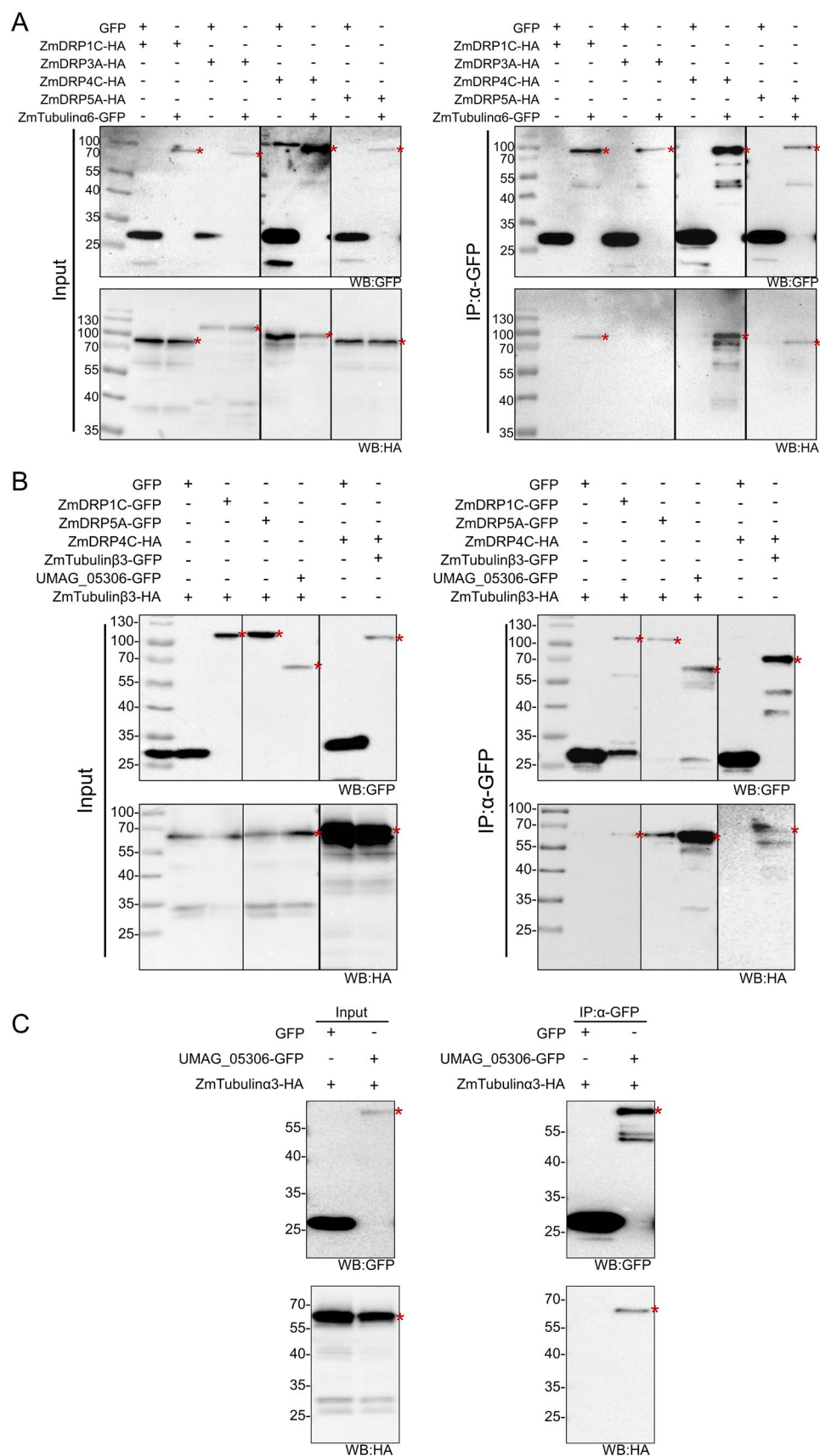


Fig. 36. Interactions between maize DRPs and different forms of tubulins, including ZmTubulin α 6 and ZmTubulin β 3, and the potential interaction of UMAG_05306 with tubulins. A.

ZmTubulin α 6 interacts with ZmDRP1C, ZmDRP4C, and ZmDRP5A. ZmTubulin α 6-GFP or GFP was co-expressed with the indicated HA-tagged DRP protein in *N. benthamiana*. GFP-trap magnetic beads were used for pull-down. Anti-GFP and anti-HA antibodies were used to detect the input and IP proteins. The expected sizes of the recombinant proteins were GFP: 26.8 kDa, ZmTubulin α 6-GFP: 76.6 kDa, ZmDRP1C-HA: 75.5 kDa, ZmDRP3A-HA: 97.7 kDa, ZmDRP4C-HA: 82.2 kDa, and ZmDRP5A-HA: 80.4 kDa. **B.** ZmTubulin β 3 interacts with ZmDRP1C, ZmDRP4C and ZmDRP5A. Co-expression of ZmDRP1C-GFP, ZmDRP5A-GFP or GFP alone with ZmTubulin β 3-HA, and either GFP or ZmTubulin β 3-GFP with ZmDRP4-HA in *N. benthamiana*, and the interaction was detected using GFP-trap magnetic beads. Western blot analysis was performed using anti-GFP and anti-HA antibodies to detect the recombinant proteins with the expected sizes indicated: GFP: 26.8 kDa, UMAG_05306 Δ SP-GFP: 57.4 kDa, ZmTubulin β 3-HA: 57 kDa, ZmTubulin β 3-GFP: 76.5 kDa, ZmDRP1C-GFP: 95 kDa, and ZmDRP5A-GFP: 96 kDa. **C.** UMAG_05306 interacts with ZmTubulin α 3. GFP or UMAG_05306-GFP was co-expressed with ZmTubulin α 3-HA in *N. benthamiana*. GFP-trap magnetic beads were used for pull-down. Anti-GFP and anti-HA antibodies were used for the detection of recombinant proteins. The expected sizes were GFP: 26.8 kDa, UMAG_05306 Δ SP-GFP: 57.4 kDa, ZmTubulin α 3-HA: 57 kDa. The asterisk indicates the expected band.

1.5 UMAG_05306 interacts with ZmDRP1C and ZmTubulin β 3 in split luciferase assays

To further confirm the interaction of UMAG_05306 with maize DRP and tubulin, a split-luciferase complementation imaging assay was performed. The assay fuses the amino- and carboxyl-terminal halves of the luciferase enzyme to two proteins of interest, and the resulting interaction reconstitutes the luciferase protein, leading to detectable activity that can be visualized using low-light imaging (Chen et al., 2008). UMAG_05306 Δ SP was fused to the amino-terminal half of luciferase (nLuc), and ZmDRP1C and ZmTubulin β 3 were fused to the carboxyl-terminal half of luciferase (cLuc). Empty nLuc and cLuc vectors were used as controls. The four paired proteins, nLuc and cLuc, UMAG_05306 Δ SP-nLuc and cLuc, nLuc and ZmDRP1C-cLuc, UMAG_05306 Δ SP-nLuc and ZmDRP1C-cLuc, were co-expressed in *N. benthamiana*. Similarly, ZmDRP1C was replaced with ZmTubulin β 3. Luminescence signals were detected only in leaf areas co-expressing UMAG_05306 and ZmDRP1C, but not in leaf areas co-expressing UMAG_05306 and cLuc, or ZmDRP1C and nLuc. This indicates that UMAG_05306 interacts with ZmDRP1C (**Fig. 37A**). Similarly, luminescence was only detected upon the co-expression of UMAG_05306 and ZmTubulin β 3, indicating that UMAG_05306 also interacts with ZmTubulin β 3 (**Fig. 37B**).

Results

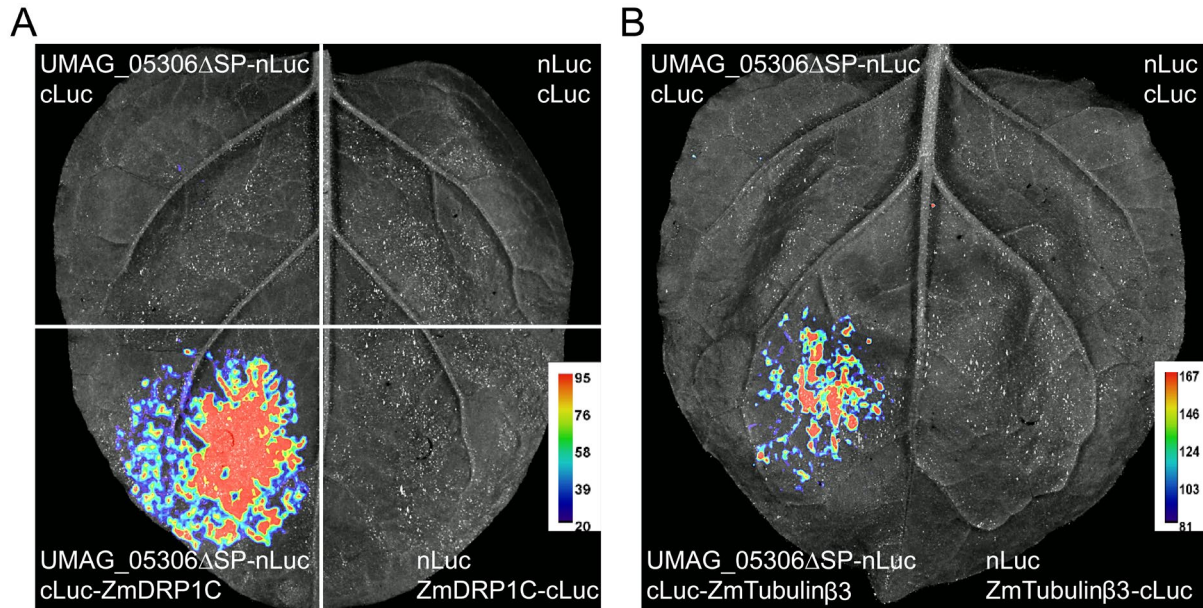


Fig. 37. Split-luciferase assay of UMAC_05306 with ZmDRP1 and ZmTubulin β 3. **A.** Split-luciferase assay of UMAC_05306 with ZmDRP1C. *Agrobacterium* carrying constructs with UMAC_05306 Δ SP-nLuc, cLuc-ZmDRP1C, empty nLuc or empty cLuc combined as indicated were transiently co-expressed in *N. benthamiana*. Luminescence signal was detected by a CCD imaging system using Bio-Rad ChemiDoc. **B.** Split-luciferase assay of UMAC_05306 with ZmTubulin β 3. *Agrobacterium* strains were transiently co-expressed in *N. benthamiana* as indicated. The images show representative pictures from three independent biological replicates. Pseudo-fluorescence was added in ImageJ.

1.6 Subcellular localization of maize DRPs

To understand the functional role of DRPs, the subcellular localization of ZmDRP1C-GFP, ZmDRP3A-GFP, and ZmDRP5A-GFP were examined in *N. benthamiana* by confocal microscopy. ZmDRP1C-GFP is localized in punctate dots and is distributed in the plasma membrane or cytoplasm (**Fig. 38A**). ZmDRP3A-GFP, and ZmDRP5A-GFP were found to have similar localization as ZmDRP1C-GFP (**Fig. 38A**). DRPs localization in maize was also assessed. ZmDRP5A was expressed in the epidermal cells of maize via biolistic bombardment. The confocal image shows that ZmDRP5A-GFP is localized in punctate structures. Furthermore, the Z-stack image shows that the punctate structures are localized on filaments (**Fig. 38B**).

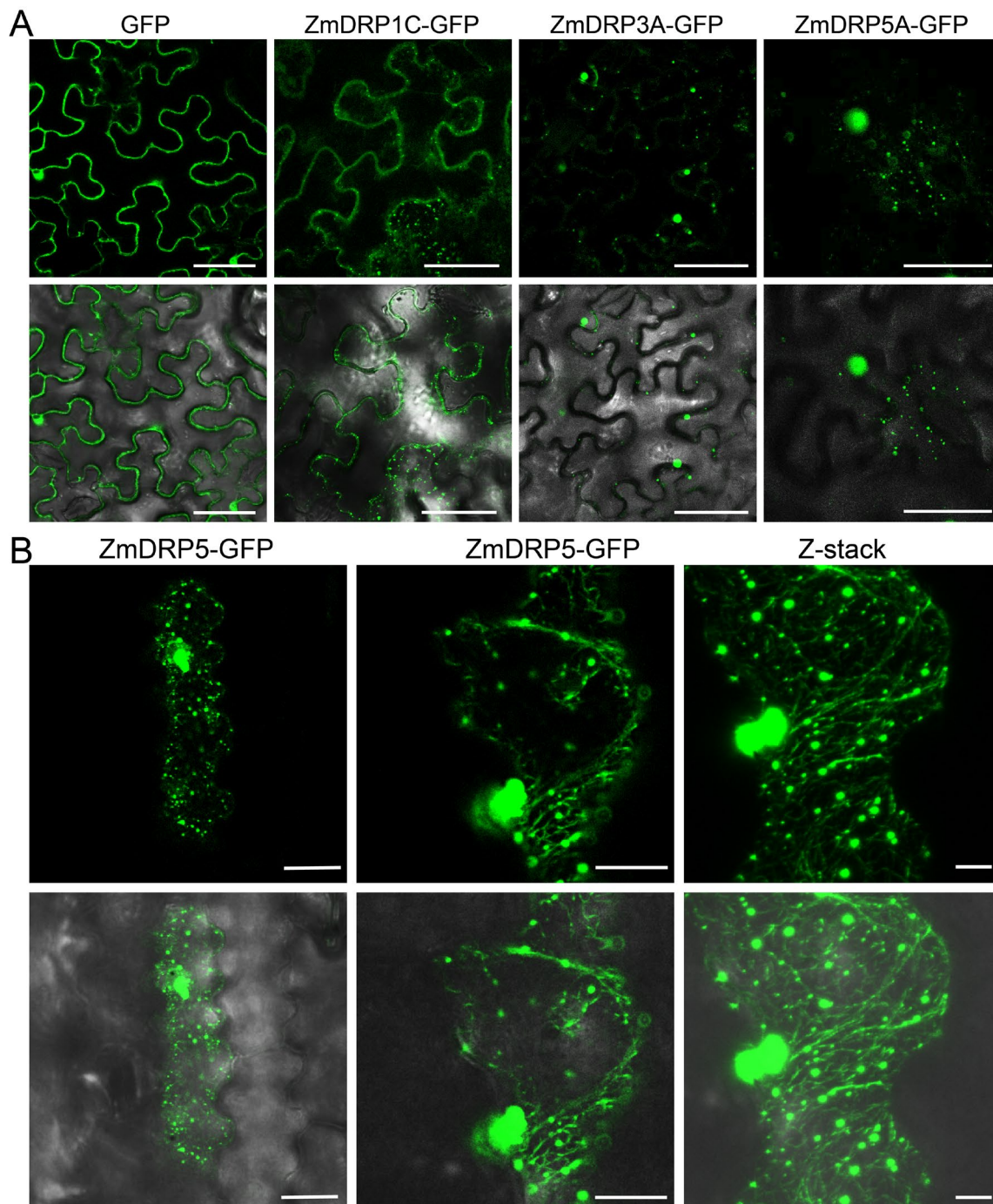


Fig. 38. Subcellular localization of ZmDRP1C-GFP, ZmDRP3A-GFP, and ZmDRP5A-GFP in *N. benthamiana* and maize epidermal cells. **A.** Maize dynamin-related proteins form punctate structures in *N. benthamiana* cells. GFP, ZmDRP1C-GFP, ZmDRP4C-GFP, or ZmDRP5A-GFP were expressed in *N. benthamiana* leaves for 2 days and visualized using confocal microscopy. Scale bar, 50 μm . **B.** Subcellular localization of ZmDRP5A in maize. ZmDRP5-GFP was transiently expressed in maize via biolistic bombardment. The middle panel shows a zoomed-in picture, and the right panel shows a Z-stack projection. Scale bar, 25 μm .

Moreover, to determine the co-localization of UMAG_05306 with the ZmDRP5A protein, co-expression assays were performed. ZmDRP5A-GFP was co-expressed with

Results

UMAG_05306 Δ SP-mCherry in *N. benthamiana*, and the resulting expression was compared with the co-expression of ZmDRP5A-GFP and mCherry. The co-expressed proteins were observed under a confocal microscope to analyze their localization. Interestingly, the punctate structures of ZmDRP5A were found to accumulate at the filamentous localization of UMAG_05306. On the other hand, in the presence of mCherry, the punctate structures of ZmDRP5A showed a more random distribution. These results suggest that UMAG_05306 may play a role in the localization of ZmDRP5A (**Fig. 39**).

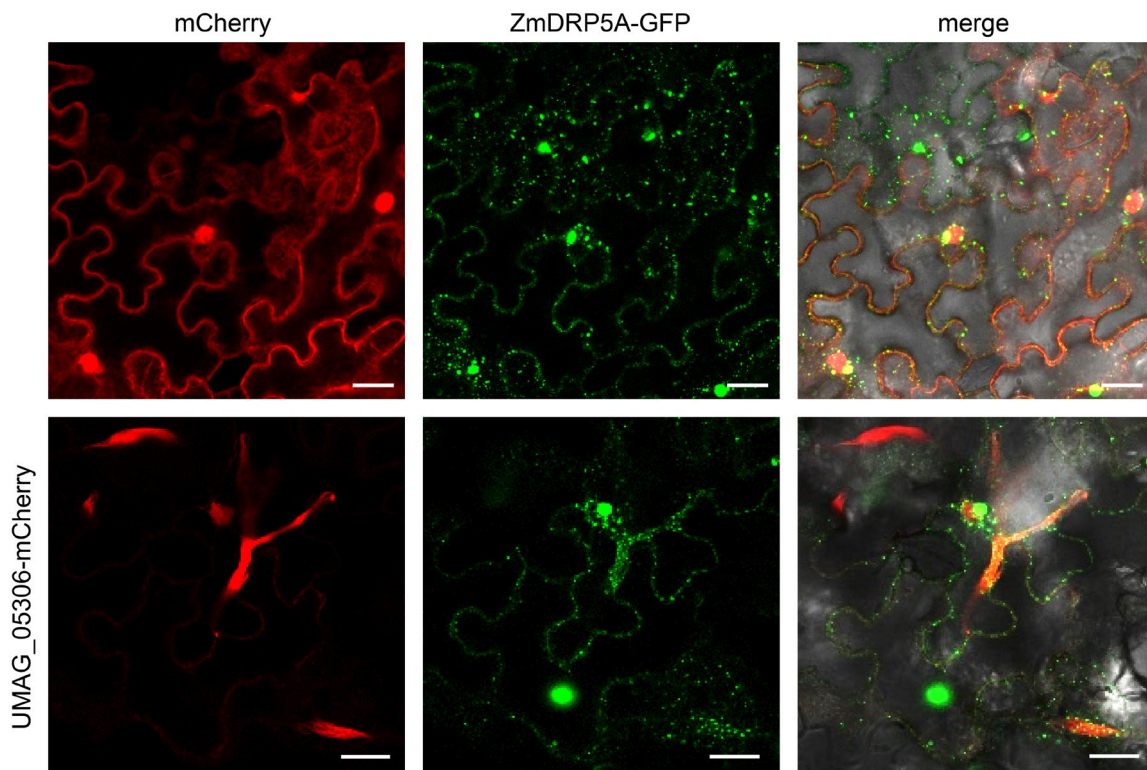


Fig. 39. Impact of UMAG_05306 on ZmDRP5A localization in *N. benthamiana*. ZmDRP5A-GFP fusion proteins were co-expressed with either UMAG_05306 Δ SP-mCherry or mCherry in *N. benthamiana* through *Agrobacterium*-mediated transformation. Confocal imaging was taken at 2 dpi. Scale bar, 25 μ m.

2. Discussion

U. maydis infects maize plants and utilizes effector proteins to manipulate host cellular processes to promote its own propagation. However, the pathogen also displays host adaptation specificity and is capable of secreting organ-specific effectors (Skibbe et al., 2010). Understanding the role of these effectors in tumor formation and their host targeting is crucial to comprehending the interaction between *U. maydis* and maize plants. Therefore, this study aims to elucidate the mechanistic basis of the interaction between the organ-specific effector UMAG_05306 and its host targets in the *U. maydis*/maize system. UMAG_05306 has been shown to be important for *U. maydis* leaf tumor formation (Schilling et al., 2014). This study found a complex interaction network between UMAG_05306, dynamin related proteins, and tubulin that may contribute to *U. maydis* pathogenesis.

2.1 UMAG_05306 is a virulence factor for *U. maydis* infection

UMAG_05306 has been identified as a virulence factor required for full pathogenicity of *U. maydis* in seedling infection (Schilling et al., 2014). In this study, the role of UMAG_05306 in *U. maydis* pathogenicity was confirmed through the use of CRISPR/Cas9 mutants, which showed reduced virulence. Also, its complementation restored virulence to levels seen in the SG200 strain. The effector protein See1 has also been characterized as an organ-specific virulence factor that promotes tumor formation in vegetative maize tissues (Redkar et al., 2015). The expression profile of See1 is highly specific to seedling leaves, supporting its essential role in tumor formation in maize leaves but not in floral tissues (Redkar et al., 2015). Similarly, UMAG_05306 appears to contribute specifically to leaf tumor formation but not tassel formation (Schilling et al., 2014). *UMAG_05306* expression peaks at 4 dpi during seedling infection (Lanver et al., 2018). Its expression in the tassel is lower than in seedling leaves and does not increase over the serial stages of tumor expansion from 3 dpi to 9 dpi, indicating consistently low expression levels in non-target organs (Schilling et al., 2014; Skibbe et al., 2010). These findings indicate a specific role for *UMAG_05306* in the virulence of *U. maydis* in maize leaves.

The *UMAG_05306* knockout mutant exhibited reduced virulence compared to the SG200

Discussion

strain, but was still able to infect maize plants. In contrast, *U. maydis* mutants of the 'core effectors' Pep1 and Pit2 showed increased callose deposition and were unable to infect and induce macroscopic host cell death responses (Doehlemann et al., 2009, 2011). Wheat germ agglutinin (WGA) staining for fungal cell walls and propidium iodide (PI) staining for plant cell walls did not reveal any noticeable differences between the UMAG_05306 mutant and SG200 during the early stages of biotrophy (MSc thesis of Daniel Hilbig, 2017). Similarly, the *U. maydis* Sts2 mutant showed reduced leaf tumor formation but did not exhibit any defects in penetration or colonization compared to SG200 when analyzed using WGA and PI co-staining at 2 dpi (Zuo et al., 2023). Pep1 and Pit2 are crucial virulence factors for successful colonization of plants as they both target critical elements of the plant's immune system, and their inhibition is essential for the establishment and maintenance of biotrophic interactions (Doehlemann et al., 2009, 2011; Hemetsberger et al., 2012, 2015; Misas Villamil et al., 2019; Mueller et al., 2013). The findings suggest that the defect in leaf tumor formation observed in the UMAG_05306 is not caused by compromised biotrophic growth of the mutant, and that UMAG_05306 may not play a direct role in suppressing host defenses or promoting fungal growth during the biotrophic phase. Nonetheless, this study confirms the virulence function of UMAG_05306 in seedling infection and highlights the diversity of effector functions in *U. maydis*, as well as the importance of understanding their specific roles in promoting pathogenesis.

2.2 UMAG_05306 has specific localization *in planta*

Understanding the localization of effectors within the plant during infection is crucial for elucidating their function. For example, previous studies using the rice blast fungus *M. oryzae* have utilized live-cell imaging to observe fluorescently labeled effectors secreted by invasive hyphae. This revealed that the effector proteins PWL2 and BAS1 are translocated into the rice cytoplasm and moved into uninvaded neighboring cells, which may indicate the preparation of host cells prior to invasion (Khang et al., 2010). However, determining effector trafficking in *U. maydis* has proven technically challenging and relies mainly on proxy experiments conducted independently of the pathogen in a transient assay (Djamei et al., 2011). To determine the localization of UMAG_05306, a combination

of genetic manipulation and confocal microscopy was employed, revealing that UMAG_05306 localizes as twisted filaments in the cytoplasm of both *N. benthamiana* and maize epidermal cells. In *situ* translocation assays using biolistic bombardment and live cell imaging of fluorescent reporter proteins have also been used to study the localization of other fungal *U. maydis* effectors, such as Cmu1 and See1, which have been found to localize to the cytoplasm or nucleus and have been observed in neighboring cells, possibly due to effectors translocation (Djamei et al., 2011; Redkar et al., 2015).

Besides heterologous expression in *N. benthamiana* and biolistic bombardment in maize, transmission electron microscopy (TEM) in combination with immunogold labeling has been commonly used to explore the secretion and localization of *U. maydis* effectors, including Cmu1, See1, Erc1, Rsp3, and the Stp complex (Djamei et al., 2011; Ludwig et al., 2021; Ma et al., 2018; Ökmen et al., 2022; Redkar et al., 2015). To observe the localization of UMAG_05306 by TEM, it was tagged with HA and expressed in *U. maydis*. The integration of UAMG_05306-2xHA in the *U. maydis* strain was checked by western blot analysis of infected maize tissue, it was detectable the full length, which indicates the UAMG_05306-2xHA is intact and does not cleave. The results were in line with the biolistic bombardment, as the HA tag linked to UMAG_05306 was found to be secreted as the signal was detected in the host cells. These findings provide valuable insights into the localization of UMAG_05306, although its specific function in *U. maydis* infection remains unclear from this study. Nevertheless, its unique cytoplasmic localization may suggest a role in the infection process.

2.3 UMAG_05306 interacts with multiple maize DRPs

Mass spectrometry and a co-IP assay, indicated that UMAG_05306 interacts with multiple maize DRPs, specifically ZmDRP1C, ZmDRP3A, ZmDRP4C, and ZmDRP5A, which were up-regulated during *U. maydis* infection in maize (Lanver et al., 2018). This suggests that UMAG_05306 may target a conserved cellular process involving these proteins. DRPs are large GTPases that play critical roles in endocytosis, vesicle trafficking, peroxisomes and mitochondrial fission (Praefcke & McMahon, 2004). In *Arabidopsis*, 16 DRPs have been identified and classified into 6 functional subfamilies (DRP1–6) based on their

Discussion

phylogenetic relationships and the presence of functional motifs (Hong et al., 2003a). Specifically, DRP1 proteins consist of five members designated as DRP1A-E (Hong et al., 2003a). Although DRPs share a similar domain structure with dynamin and are involved in similar processes, they have distinct functions and specificities (Hong et al., 2003a).

DRPs from maize have not been extensively studied to date, so, to gain further insight into their potential functions, the *Arabidopsis* DRPs that showed high amino acid sequence identity to the maize DRPs were checked. The maize DRPs identified in this study show varying degrees of amino acid sequence identity to their *Arabidopsis* counterparts. ZmDRP5A shares 83.9% amino acid sequence identity with AtDRP1B, while ZmDRP1C, ZmDRP3A, and ZmDRP4C share 81%, 59%, and 57% sequence identity with AtDRP1C, AtDRP3A, and AtDRP4C, respectively. AtDRP1C plays crucial roles in plant development, including the formation and maintenance of the pollen cell surface, cell plate formation in somatic cells, and plasma membrane dynamics in root hairs (Kang et al., 2003). It also participates in clathrin-mediated membrane dynamics at the cell cortex in tip growing root hairs and expanding epidermal cells (Konopka et al., 2008). In the G1 phase of the cell cycle, AtDRP1C associates with the cytoskeleton and in mitotic cells, it localizes with the mitotic spindle and forms punctate structures throughout the cell (Hong et al., 2003b). During cytokinesis, DRP1C is mostly targeted to the forming cell plate edges (Hong et al., 2003b). AtDRP3A is involved in the division of peroxisomes and mitochondria in plants, and mutations in AtDRP3A lead to aberrant morphology of both organelles, resulting in reduced metabolic efficiency (Mano et al., 2004). The roles of AtDRP1B and AtDRP4C have not been fully characterized yet.

All members of the dynamin and DRP protein families share a conserved domain organization consisting of an N-terminal GTP-binding domain (GD) that regulates GTPase activity, a middle domain for dimerization during self-assembly, and a GTPase effector domain (GED) that is distinct from other GTPases (Chappie et al., 2010; Praefcke & McMahon, 2004). Classical dynamin proteins also possess a pleckstrin homology (PH) domain and a C-terminal proline-rich domain (PRD), which interact with Src homology 3 (SH3) domain-containing proteins critical for dynamin recruitment to clathrin-coated pits (CCPs) (Praefcke & McMahon, 2004). The absence of a PH domain and PRD is the defining

feature that sets DRPs apart from classical dynamins (Kar et al., 2021). Both the N-terminal GTPase domain and the C-terminal part of ZmDRP5 are crucial for interaction with UMG_05306, as demonstrated by co-IP assays, indicating that this interaction may involve multiple regions of DRPs. The complexity of these interactions implies that UMG_05306 may have diverse effects on DRP-mediated cellular processes in maize.

Other effectors have been shown to target DRPs to modulate host cellular processes. The MoCDIP4 effector of *M. oryzae* has been found to target the rice OsDjA9-OsDRP1E protein complex, resulting in perturbation of mitochondrial dynamics and inhibition of plant immunity (Xu et al., 2020). In addition, *P. infestans* AVR3a suppresses immunity through multiple pathways by associating with NtDRP2 and reducing the internalization of activated FLS2, involving key cellular trafficking and membrane-remodeling complexes (Chaparro-Garcia et al., 2015). Similarly, UMG_05306 may interact with multiple maize DRPs and potentially play a role in regulating endocytosis, peroxisomal division, and mitochondrial division in maize cells.

Moreover, the sequence similarities and differences between maize and *Arabidopsis* DRPs highlight the need for further investigation into the functional conservation and divergence of DRPs across plant species. Understanding the functional roles of DRPs in maize and other plant species can provide insights into the mechanisms of intracellular trafficking, organelle division, and other essential cellular processes in plants. However, the exact mechanisms by which UMG_05306 interacts with these DRPs and regulates these processes in maize cells remain to be elucidated.

2.4 DRPs interact with Tubulin

The results of this study show that DRPs interact with different forms of tubulin in maize. Specifically, co-IP assays showed that ZmDRP1C, ZmDRP4C, and ZmDRP5A interact with both ZmTubulin α 6 and ZmTubulin β 3. Microtubules are dynamic structures composed of tubulin subunits and are involved in many cellular processes, including cell division, intracellular transport, and cell morphology (Goodson & Jonasson, 2018; Hashimoto, 2015). Previously, AtDRP3A was also found to associate with microtubules during xylem tracheary element formation in *Arabidopsis* (Derbyshire et al., 2015). Propyzamid is an

Discussion

herbicide that disrupts microtubules, while cytochalasin D is a fungal toxin that disrupts actin filaments (S. Brown & Spudich, 1979; Nakamura et al., 2004). The sensitivity of the distribution pattern of AtDRP1A to propyzamid and its insensitivity to cytochalasin D suggest that AtDRP1A is linked with microtubules rather than actin filaments, and the association of AtDRP1A with microtubules was also confirmed by *in vitro* spin-down assays (Hong et al., 2003b). As *Arabidopsis* DRPs are linked to microtubules, it might be possible that DRPs play important roles in regulating microtubule dynamics, as they are involved in membrane remodeling and trafficking. By interacting with different forms of tubulin, DRPs may control the stability and organization of microtubules in different cellular contexts. Furthermore, the expression patterns of different tubulin isoforms in maize suggest that they may have distinct functions in different tissues and developmental stages (Hussey et al., 1990; Uribe et al., 1998). It would be interesting to investigate whether the interactions between DRPs and tubulins are also tissue-specific, and whether they play a role in regulating plant growth and development.

The identification of specific DRPs that interact with ZmTubulin α 6 and ZmTubulin β 3 could provide insights into the regulation of microtubule-associated processes in maize. These DRPs may play distinct roles in microtubule-based processes such as cell division, cell expansion, and organelle transport, which could be investigated in future studies. Overall, these results provide a starting point for further investigation into the role of DRPs and different forms of tubulin in plant development and cellular function.

2.5 UMAG_05306 interacts with Tubulin

Co-IP assays demonstrated that UMAG_05306 interacts directly with both ZmTubulin α 3 and ZmTubulin β 3, and UMAG_05306 interacts with ZmTubulin β 3 in luciferase split assays. These findings suggest that UMAG_05306 may play a role in microtubule dynamics and organization, which are critical for proper cell division and differentiation as microtubules are composed of tubulin subunits (Martinez et al., 2020; Uribe et al., 1998). Microtubules are critical for many cellular processes, and alterations in their dynamics can have profound effects on these processes, such as cell division, intracellular transport, cell polarity, signaling pathways, and morphogenesis (Hashimoto, 2015). In particular,

perturbation of tubulin function has been implicated in a variety of pathogen effectors, indicating the importance of proper tubulin function for plant health and defense. An example is the *P. syringae* effector HopE1, which uses its host calmodulin as a cofactor to target the microtubule-associated protein 65 (MAP65), leading to the dissociation of MAP65-GFP from microtubules and impairing cell wall-based extracellular immunity (Guo et al., 2016). Another example is ROPIP1, a retroelement-derived transcript produced by the powdery mildew fungus *Blumeria graminis* f.sp. *hordei*, which targets HvRACB to manipulate host cell microtubule organization for facilitated host cell entry (Nottensteiner et al., 2018). Alpha and beta tubulin are two different subunits that make up the microtubule (Nogales et al., 1998). Both alpha and beta tubulin can bind to the nucleotide GTP, but the role of GTP binding is different for each subunit. Nucleotide binding to alpha-tubulin is mainly structural, while the assembly and disassembly of microtubules is driven by the binding and subsequent hydrolysis of GTP bound to beta-tubulin (Bera & Gupta, 2022; Nogales, 2000). The interaction between UMAG_05306 and both alpha and beta tubulin isoforms suggests that it may have a broad range of effects on microtubule dynamics within the cell. The interaction between UMAG_05306 and tubulin may affect various cellular processes, such as cell division, cell migration, and intracellular transport, depending on the specific isoforms of tubulin involved and the timing and localization of the interaction. Further research is necessary to determine the precise nature of the interaction between UMAG_05306 and tubulin and to identify the downstream effects of this interaction on cellular processes.

2.6 Perspectives

This study showed that UMAG_05306 contributes to the induction of leaf tumors in *U. maydis*. Its localization in plants and interaction with multiple DRPs and microtubule tubulin proteins suggest that it may be involved with the phragmoplast, a microtubule-based structure critical for plant cell plate formation (Smertenko et al., 2018). In land plants, the phragmoplast forms during the telophase of the cell cycle and is responsible for the formation of the cell plate and the completion of cytokinesis (Otegui et al., 2005). Proper organization of microtubule networks during mitosis is crucial for growth and

Discussion

development at both the cell and organismal levels, including the formation of the phragmoplast that directs the deposition of new cell walls during cell division (Ehrhardt & Shaw, 2006; Elliott & Shaw, 2018). Microtubule organization is modulated by interactions between microtubules themselves and other proteins. Furthermore, plant cytokinesis requires DRPs, which mediate the formation of membranous tubular structures from fusing vesicles, leading to the stabilization of the membranous tubules that assemble in the growing edge of the cell plate (Kang et al., 2003; Otegui et al., 2001). One possible scenario is that UMAG_05306 links DRPs and microtubules to promote leaf tumor formation. The interaction between UMAG_05306, maize DRPs and microtubules supports the idea that UMAG_05306 may play a role in plant cell division and cytokinesis. DRPs localize at the plant cell plate and are involved in membrane trafficking and vesicle transport, while microtubules provide the structural framework for the formation of the cell plate during cytokinesis. The interaction between UMAG_05306, DRPs and microtubules suggests that UMAG_05306 may play a role in facilitating membrane trafficking and vesicle transport during cytokinesis and regulating microtubule dynamics. In conclusion, the interaction between UMAG_05306, maize DRPs and microtubules is a fascinating area of research in the field of plant cell biology. Further studies are needed to explore the precise role of UMAG_05306 in leaf tumor formation and to determine the mechanisms by which UMAG_05306 interacts with DRPs and microtubules to promote this process.

Chapter 4. Material and methods

4.1 Material and methods

4.1.1 Chemicals

All chemicals used in this study were purchased from Biozym (Hessisch Oldendorf, Germany), Difco (Augsburg, Germany), GE Healthcare (Freiburg, Germany), Invitrogen (Darmstadt, Germany), Merck (Darmstadt, Germany), Roche (Mannheim, Germany), Roth (Karlsruhe, Germany), and Sigma-Aldrich (Darmstadt, Germany).

4.1.2 Buffers and solutions

Standard buffers and solutions were prepared following protocols described in laboratory manuals (Frederick M et al., 2001; Sambrook et al., 1989). Special buffers and solutions were supplied with the respective techniques. Autoclaving was carried out for 5 min at 121°C for all buffers, media and solutions. Heat-sensitive solutions were sterilized using a 0.2 µm filter (GE Health Care Life Science, Freiburg, Germany) to maintain integrity.

4.1.3 Enzymes, antibodies and IP trap beads

The majority of restriction enzymes used in this study were obtained from New England Biolabs (NEB, Frankfurt, Germany), with a small quantity sourced from Thermo Fisher Scientific (Duesseldorf, Germany). DNA polymerases used in the study included Phusion® High Fidelity DNA Polymerase, Q5® High Fidelity DNA Polymerase (NEB, Frankfurt, Germany), and GoTaq® Green Master Mix (Promega, Heidelberg, Germany). DNA ligation was performed using T4 DNA ligase (NEB, Frankfurt, Germany). Gibson assembly cloning was carried out with the use of NEBuilder® HiFi DNA Assembly Master Mix (NEB, Frankfurt, Germany). Enzymatic degradation of *U. maydis* cell walls were achieved using Novozyme 234 (Novo Nordisk, Copenhagen, Denmark). Antibodies were purchased from Sigma-Aldrich (Darmstadt, Germany) and Cell Signaling Technology (Danvers, USA). Immunoprecipitation trap beads were obtained from GE Healthcare (Freiburg, Germany) and ChromoTek GmbH (München, Germany). A comprehensive list of the protein trap beads and antibodies used can be found in the corresponding method sections.

4.1.4 Commercial kits

Material and methods

The NucleoSpin® Gel and PCR Clean-up Kit (Macherey-Nagel, Düren, Germany) was used to clean up PCR products. Plasmid DNA extraction was conducted using the NucleoSpin® Plasmid Kit (Macherey-Nagel, Düren, Germany). Enzymatic degradation of DNA in RNA extracted with TRIzol (Thermo Fisher Scientific, Duesseldorf, Germany) was achieved using the TURBO DNA-free™ Kit (Ambion®/Thermo Fisher Scientific, Duesseldorf, Germany). cDNA synthesis was performed using the RevertAid H Minus First Strand cDNA Synthesis Kit (Thermo Fisher Scientific, Duesseldorf, Germany). Site-directed mutagenesis of amino acids in plasmids was conducted with the QuikChange II Site-Directed Mutagenesis Kit (Agilent, Waldbronn, Germany). Chemiluminescence detection in a western blot was performed using SuperSignal™ West Pico PLUS Chemiluminescent Substrate and SuperSignal™ West Femto Maximum Sensitivity Substrate (Thermo Fisher Scientific, Duesseldorf, Germany). For ethidium bromide electrophoresis gel size standards, Thermo Scientific™ GeneRuler™ 1 kb DNA ladder (Thermo Fisher Scientific, Duesseldorf, Germany) was used, and for SDS-polyacrylamide gel electrophoresis, PageRuler™ Prestained Protein Ladder, 10 to 180 kDa (Thermo Scientific, Duesseldorf, Germany) was utilized (**Fig. 40**). Further materials are listed in the corresponding method sections.

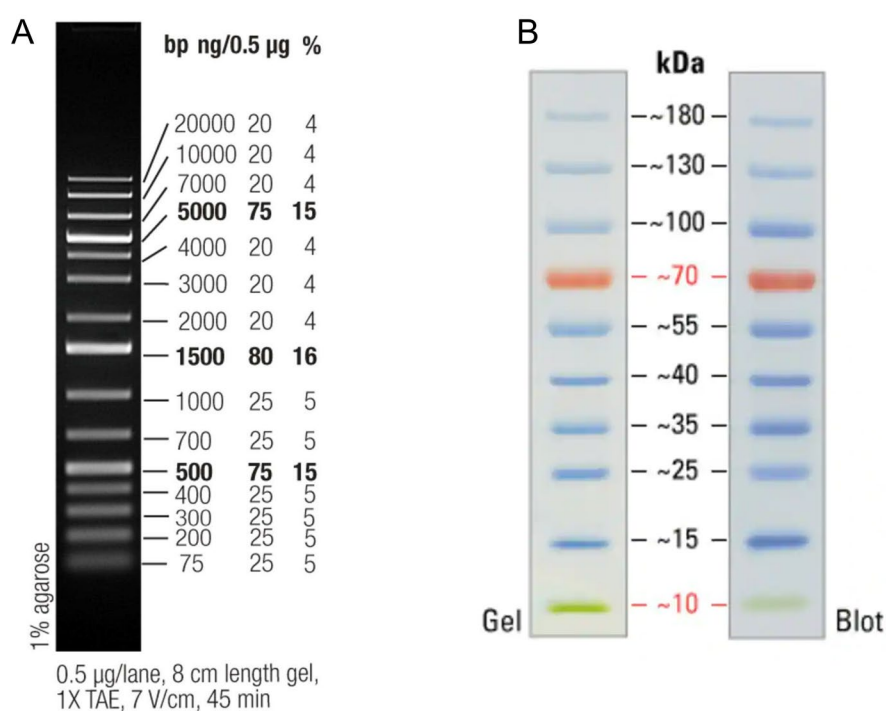


Fig. 40. The standard markers used in this study. **A.** Thermo Scientific™ GeneRuler™ 1 kb DNA

Ladder (Thermo Fisher Scientific, Duesseldorf, Germany) for determining the size of DNA fragments on agarose gels. **B.** PageRuler™ Prestained Protein Ladder, 10 to 180 kDa, for SDS-PAGE electrophoresis (Thermo Scientific, Duesseldorf, Germany). Photos were obtained from the product website.

4.2 Media and cultivation

4.2.1 Media for microbes

The media listed in **Tab. 3** were used for cultivating microorganisms. All media were autoclaved at 121°C for 5 min prior to use, except when specified otherwise.

Tab. 3. Composition of culture media

Name	Ingredients	Note
dYT (Sambrook et al., 1989)	1.6% (w/v) Tryptone 1.0% (w/v) Yeast extract 0.5% (w/v) NaCl	dYT Agar addition of 1.5% (w/v) Bacto Agar
Lysogeny Broth (LB) (Bertani, 1951)	1.0% (w/v) Tryptone 0.5% (w/v) Yeast-Extract 1.0% (w/v) NaCl	LB Agar addition of 2% (w/v) Bacto Agar
YEPSlight (modified from Tsukada et al., 1988)	1 % (w/v) Yeast extract 1% (w/v) Peptone 1% (w/v) Saccharose	
Potato-Dextrose-Agar (PD)	2.4% (w/v) Potato-Dextrose Broth 2% (w/v) Bacto Agar	PD-Charcoal Agar addition of 1.0% (w/v)
Regeneration Agar (Schulz et al., 1990)	1.5 % (w/v) Bacto Agar 1M Sorbitol 1 % (w/v) Yeast extract 1% (w/v) Peptone 1% (w/v) Saccharose	
YPDA (-Agar)	2% (w/v) Peptone 1 % (w/v) Yeast extract 0.003% (w/v) Adenine-Hemisulfate 2% (w/v) Bacto Agar	Adjust the pH to 6.5 and after autoclaving add 2% (w/v) filtered glucose

Material and methods

SD (-Agar)	0.67% (w/v) Yeast nitrogen base	
Synthetic Defined	Without amino acids	Adjust the pH to 5.8 and after autoclaving add
	0.06% (w/v) Dropout Solution [(-Ade, -His, -Leu, -Trp) or (-His, -Leu, -Trp, -Ura)]	2% (w/v) filtered glucose
	2% (w/v) Bacto Agar	

4.2.2 Cultivation of *E. coli* and *A. tumefaciens*

E. coli and *A. tumefaciens* strains were cultured in dYT liquid medium or YT solid medium with the corresponding antibiotics, as specified in Frederick M et al. (2001) and Sambrook et al. (1989). The final antibiotic concentrations are detailed in **Tab. 4**. Liquid cultures were incubated at either 37°C or 28°C with constant shaking at 200 rpm. Solid media cultures were incubated at either 37°C or 28°C. For long-term preservation, overnight liquid cultures were preserved with a final concentration of 25% (v/v) glycerol and stored at -80°C.

Tab. 4. Antibiotics concentration for selective growth

Antibiotic	Selective concentration
Carbenicillin (Carb)	100 µg/mL
Kanamycin (Kan)	40 µg/mL
Spectinomycin (Spec)	50 µg/mL
Rifampicin (Rif)	50µg/mL
Chloramphenicol (Chl)	34 µg/mL
Gentamicin (Gent)	25 µg/mL)

4.2.3 Cultivation of *U. maydis*

The solid cultures of *U. maydis* SG200 and its derivatives were grown on Potato Dextrose Agar (PDA) at 28°C. The *U. maydis* was cultivated in a YEPsLight liquid medium at 28°C with shaking at 200 rpm, reaching an optical density (OD₆₀₀) of 0.6-0.8. Transformants were selected by adding either carboxin (Cbx) antibiotic at 2 µg/mL or hygromycin B (Hyg) antibiotic at 200 µg/mL to PD solid medium or Regeneration agar medium. Overnight cultures with an OD₆₀₀ of 0.6-1.0 were preserved by adding glycerol at a final

concentration of 25% (v/v) and stored at -80°C for long-term preservation.

4.2.4 Cultivation of *S. cerevisiae*

The *S. cerevisiae* strain AH109 was grown in either YPD or SD liquid medium, and cultivated on either YPD or SD solid medium. SD media supplemented with or without adenine, histidine, leucine, and tryptophan were used to select transformants. Liquid cultures were incubated at 28°C with continuous shaking at 200 rpm, while solid media were incubated under aerobic conditions at the same temperature. Overnight cultures were preserved by adding 50% (v/v) glycerol and stored at -80°C for long-term storage.

4.2.5 Measurement of cell density

The cell density was measured using an absorption reading at 600 nm (OD₆₀₀) on a Genesis 10S VIS spectrophotometer (Thermo Fisher Scientific, Duesseldorf, Germany). The readings were taken using the respective sterilized medium as a reference and the cultures were diluted 1:10 or 1:20. An OD₆₀₀ reading of 1 corresponded to 1.5×10^7 cells for *U. maydis*, while for *E. coli* and *A. tumefaciens*, it represented 1×10^9 cells.

4.3 Strains, oligonucleotides and plasmids

4.3.1 *E. coli* strains

E. coli strains Top10 and DH5 α were used for plasmid vector cloning. The *E. coli* BL21 (DE3) strain was used for heterologous *in vitro* protein expression.

E. coli K-12 Top10: [FmcrA Δ (mrr-hsd RMS-mcrBC) Φ 80lacZ Δ M15 Δ lacO74 recA1 ara Δ 139 Δ (ara98leu) 7697galU galK rpsL (StrR) endA1 nupG] (Invitrogen, Carlsbad, USA) (Grant et al., 1990)

E. coli K-12 DH5 α : F- Φ 80d lacZ Δ M15 Δ (lacZYA-argF) U169 deoR recA1 endA1 hsdR17(rK-, mK+) phoA supE44 λ - thi-lgyr A96 relA1] (GibcoBRL, Eggenstein, Germany) (Hanahan, 1983)

BL21(DE3) pLys: [F- ompT gal dcm lon hsdSB (rB -mB -) A(DE3) pLysS(cmR)] (Novagen, Merck (Darmstadt))

4.3.2 *A. tumefaciens* strains

The *A. tumefaciens* GV3101 strain was employed for transient expression of heterologous

Material and methods

proteins and observation of their subcellular localization in *N. benthamina* (Koncz & Schell, 1986).

4.3.3 *S. cerevisiae* strains

The yeast two-hybrid assay was performed using the *Saccharomyces cerevisiae* AH109 strain. AH109 is derived from the PJ69-2A strain, which contains the selectable markers ADE2 and HIS3 (James et al., 1996). MEL1 is an endogenous gene responsive to GAL4. The AH109 strain was constructed by introducing the lacZ reporter gene into PJ69-2A (Holtz, unpublished).

AH109 (Clontech, Saint-Germain-en-Laye, France): (MATa, trp1-901, leu2-3, 112, ura3-52, his3-200, gal4Δ, gal80Δ, LYS2:GAL1_{UAS}-GAL1_{TATA}-HIS3, GAL2_{UAS}-GAL2_{TATA}-ADE2, URA3:MEL1_{UAS}-MEL1_{TATA}-lacZ)

4.3.4 *U. maydis* strains

The solopathogenic strain SG200, which was engineered, was used as a reference for the wild type (Kämper et al., 2006). The other strains mentioned and generated in this study are listed in **Tab. 5** below.

Tab. 5. *U. maydis* strains used in this study

Strain	Resistance	Reference
SG200	Phleo	Kämper et al., 2006
SG200ΔUMAG_11060 (Δ <i>Tip6</i>)	Phleo, Hyg	Schilling et al., 2014
SG200ΔUMAG_05306	Phleo, Hyg	Schilling et al., 2014
SG200ΔUMAG_11060_UMAG_11060-3xHA	Phleo, Hyg, Cbx	This study
SG200ΔUMAG_05306_UMAG_05306-2xHA	Phleo, Hyg, Cbx	This study
SG200ΔUMAG_05306_Ppit2-UMAG_05306-2xHA	Phleo, Hyg, Cbx	This study
SG200ΔUMAG_011060_Ppit2-UMAG_11060-2xHA	Phleo, Hyg, Cbx	This study
SG200ΔUMAG_11060_UMAG_11060EARm-2xHA	Phleo, Hyg, Cbx	This study

phleomycin (Phleo), hygromycin (Hyg), carboxin (Cbx)

4.3.5 Oligonucleotides

All the oligonucleotides utilized in this study were purchased from Sigma-Aldrich (Darmstadt, Germany). The names, sequences, and respective applications of the oligonucleotides are listed in **Tab. 6** in the appendix.

4.3.6 Plasmids

4.3.6.1 Plasmids for *E. coli* protein expression

The plasmids pRSET-GST-PP-mCherry and pRSET-GST-PP-Um11060-mCherry were generated in this study. The original plasmid backbone, pRSET-GST-PP, contains a GST (glutathione-S-transferase) tag linked to the PreScission Pierce HRV 3C protease recognition sequence (Leu-Glu-Val-Leu-Phe-Gln-Gly-Pro) and can be cleaved after glutamine residues (Schreiner et al., 2008). The mCherry or Um11060-mCherry fragments were inserted into the pRSET-GST-PP backbone via Gibson assembly using the SacI and HindIII sites, respectively. For pHAT2_6xHis-ZmTPL2_1-218aa-6xHis plasmid construction, the ZmTPL2_1-218aa was amplified and inserted into pHAT2 via Gibson assembly using the NruI and SpeI sites.

4.3.6.2 Plasmids for transient protein expression via bombardment or *A. tumefaciens*

The plasmid used in this study is listed below in **Tab. 7**.

Tab. 7. Plasmids used for transient expression in this study

Name	Purpose and remark information
pL1M-p2×35s-ZmTPL2-myc	
pL1M-p2×35s-ZmTPL2_mutation-GFP-myc	ZmTPL2_K102S_T116Q_Q117S_ E122S mutation
pL1M-p2×35s-ZmTPL2_216-1130aa-GFP-myc	
pL1M-p2×35s-ZmTPL2_1-218aa-myc	
pL1M-p2×35s-ZmTPL2_1-218aa mutation-myc	ZmTPL2_K102S_T116Q_Q117S_ E122S mutation
pL1M-p2×35s-ZmTPL2_1-218aa mutation-GFP-myc	ZmTPL2_K102S_T116Q_Q117S_ E122S mutation
pL1M-p2×35s-ZmTPL2_mutation-myc	ZmTPL2_K102S_T116Q_Q117S_

Material and methods

	E122S mutation
pL1M-p2×35s-ZmTPL3-myc	
pL1M-p2×35s-UMAG_11060_Δ2EAR-6HA	2 LxLx motif both deleted
pL1M-F1-2x35s-UMAG011060-GFP-35ster	
pL1M-35S-ZmTPL4-6xHA-35ster	
pL1-F1-p2×35s::ZmTPL2-myc::35ster	
pL1-F1-p2×35s::ZmTPL2-mcherry::35ster	
pL1-F1-p2×35s::ZmTPL2-HA::35ster	
pL1-F1-p2×35s::ZmTPL2-GFP::35ster	
pL1-F1-p2×35s::ZmTPL1-HA::35ster	
pL1-F1-p2×35s::ZmTPL1-GFP::35ster	
pL1-F1-p2×35s::ZmTPL4-GFP::35ster	
pL1-F1-p2×35s::UMAG_11060ΔEAR-HA::35ster	intact LxLxLx motif deleted
pL1-F1-p2×35s::UMAG_11060ΔEAR-GFP::35ster	intact LxLxLx motif deleted
pL1-F1-p2×35s::UMAG_11060mEAR-HA::35ster	LxLxLx motif mutated
pL1-F1-p2×35s::UMAG_11060mEAR-GFP::35ster	LxLxLx motif mutated
pL1B-F1-p2×35s-ZmTPL2-mCherry-6xHA	
pL1B-F1-p2×35s-ZmTPL2_T116Q_Q117S-mCherry-6xHA	ZmTPL2_T116Q_Q117S mutation
pL1B-F1-p2×35s-ZmTPL2_T116Q_Q117S-GFP-myc	ZmTPL2_T116Q_Q117S mutation
pL1B-F1-p2×35s-ZmTPL2_Lish_CTLH-GFP-4myc	
pL1B-F1-p2×35s-ZmTPL2_CAR-GFP-4myc	
pL1B-F1-p2×35s-ZmTPL2_1-218aa-GFP-4myc	ZmTPL2 N-terminal
pL1B-F1-p2×35s-ZmTPL3-mcherry-6HA	
pL1B-F1-p2×35s-ZmTPL3-GFP-4myc	
pL0M-SC-UMAG_11060ΔEAR_2	
pL0M-SC-UMAG_11060mEAR	
pL0M-SC1-UMAG_11060	Level 0 modular for level1

4.3.6.3 Plasmids for *S. cerevisiae* AH109 transformation and yeast two-hybrid analysis

In the Y2H assay, the genes of interest are integrated into the designed backbones of pGBKT7 and pGADT7. The pGBKT7 plasmid contains a DNA-binding domain (BD), while the pGADT7 plasmid contains an activation domain (AD). The plasmids used for Y2H are

listed in **Tab. 8**.

Tab. 8. Plasmids used for Y2H in this study

Plasmid name	Purpose and remark information
pGBKT7-UMAG_11060	Protein-protein interaction
pGBKT7-UMAG_11060ΔEAR	EAR motifs deleted
pGBKT7-Sr14941	
pGADT7-ZmTPL2 ^C	216-1130aa
pGADT7-ZmTPL2 ^N	1-218aa
pGADT7-ZmTPL1	
pGADT7-ZmTPL2	
pGADT7-ZmTPL3	
pGADT7-ZmTPL4	
pGADT7M-ZmTPL2_Lish_CTLH	1-95aa
pGADT7M-ZmTPL2_CRA	

4.3.6.4 Plasmids for generation of stable *U. maydis* mutants

p123 (Aichinger et al., 2003)

This plasmid serves as a backbone vector for integrating the gene of interest into the *U. maydis ip* locus. The *ip* locus, which encodes the succinate dehydrogenase enzyme (*UMAG_00844*, *sdh2*), is known to confer carboxin resistance and provides a site for homologous recombination-based integration (Keon et al., 1991).

pMS73 (Schuster et al., 2016)

The plasmid comprises a codon-optimized Cas9 regulated by the *hsp70* promoter of *U. maydis* and the U6 promoter of *U. maydis* for sgRNA expression. It is Cbx-resistant, allowing for the selection of transformed *U. maydis*. The plasmid serves as a backbone for introducing frame-shift mutations in the target gene locus.

Tab. 9. Plasmids used for the transformation of *U. maydis*

Construct	Purpose
pMS73-Cas9_pU6::sgRNA_UMAG_11060	Knockout UMAG_11060
pMS73-Cas9_pU6::sgRNA_UMAG_05306	Knockout UMAG_05306
p123-np-UMAG_11060-3xHA	Complementation ΔUMAG_11060
p123-np-UMAG_11060EARm-3xHA	Complementation ΔUMAG_11060
p123-np-UMAG_05306-2xHA	Complementation ΔUMAG_05306
p123-Ppit2-UMAG_11060-3xHA	Complementation ΔUMAG_11060

Material and methods

p123-Ppit2-UMAG_05306-2xHA	Complementation Δ UMAG_05306
np: native promoter	

4.4 Microbiological standard experiment methods

4.4.1 Competent cell preparation and transformation of *E. coli*

A single colony of *E. coli* (Top10 or DH5 α) cells was grown in 100 ml of dYT medium containing 10 mM MgCl₂ and MgSO₄ at 37 °C with shaking at 200 rpm until an approximate OD₆₀₀ of 0.6. The cells were then cooled on ice for 30 min, collected by centrifugation at 3,000 rpm at 4 °C for 15 min, and resuspended in 33 ml of ice-cold RF1 solution. After 30 min incubation at 4°C, the cells were collected again by centrifugation at 3,000 rpm and 4 °C for 15 min, and the supernatant was discarded. The cells were then resuspended in 5 ml of RF2 and incubated at 4°C for at least 30 min. Finally, 50 μ l of the cells were aliquoted into pre-chilled 1.5-ml Eppendorf tubes, snap-frozen in liquid nitrogen, and stored at -80 °C until further use.

RF1 solution	100 mM RbCl
	50 mM MnCl ₂ ·4H ₂ O
	30 mM Potassium acetate ¹
	10 mM CaCl ₂ ·2H ₂ O
	15% (w/v) Glycerol
	pH 5.8 (adjusted with glacial acetic acid), sterile-filtered
RF2 solution	10 mM MOPS ²
	10 mM RbCl
	75 mM CaCl ₂ x 2 H ₂ O
	15% (w/v) Glycerol
	pH 5.8 (adjusted with NaOH), sterile-filtered

1: Prepare a 1 M potassium acetate solution with pH 7.5 using glacial acetic acid.

2: Prepare a 0.5 M MOPS solution with pH 6.8 using NaOH.

Approximately 1-5 ng of plasmid DNA or the Gibson assembly ligation product was added to 50 μ l of the competent cells prepared in the previous step and incubated on ice for 30 min. The reaction tubes were then subjected to a heat treatment at 42 °C for 1 min, followed by cooling on ice for 3 min. The cells were then incubated for 1h at 37°C with 200

rpm shaking in 200 µl of dYT. Finally, the cells were plated on YT solid plates containing the appropriate antibiotics for selection and incubated overnight at 37°C for growth.

4.4.2 Protoplast preparation and transformation of *U. maydis*

U. maydis cells were grown in 10 ml of YEPSlight medium for 8–10 hours at 28 °C with shaking at 200 rpm. The next day, the overnight culture was diluted to an OD600 of 0.2 in 55 ml YEPSlight and incubated at 28°C until an OD600 of 0.6-0.8 was reached. The culture was then centrifuged at 3,500 rpm for 10 min. The pellet was resuspended in 10 ml SCS and centrifuged again for 5 min at 3,500 rpm. The pellet was then lysed by resuspension in 2 ml of SCS containing 7 mg/ml of Novozyme 234 (Novo Nordisk, Copenhagen, Denmark) and filtered to become sterile. The cells were incubated at room temperature for 5-10 min, and 40-50% of the cells were observed under a microscope to form protoplasts. The cells were then added to 10 ml of ice-cold SCS and centrifuged at 2,500 rpm for 10 min at 4 °C. The pellet was carefully resuspended in 10 ml of ice-cold SCS and the cells were centrifuged at 2,500 rpm for 10 min at 4 °C twice. The pellet was then resuspended in 10 ml of ice-cold STC and the cells were centrifuged again at 2,500 rpm for 10 min at 4°C. Finally, the pellets were resuspended in 500 µl of ice-cold STC and divided into 50 µl portions in pre-chilled reaction tubes, then stored at -80°C.

SCS solution	20 mM Na-Citrate, pH 5.8 1 M Sorbitol sterile filtered
STC solution	10 mM Tris-HCl, pH 7.5 100 mM CaCl ₂ 1 M Sorbitol sterile filtered
STC/PEG solution	15 ml STC 10 g PEG4000

For *U. maydis* protoplast transformation, the protoplasts prepared in the previous step were thawed on ice and a maximum volume of 10 µl of 1.5–5 µg of linearized plasmid DNA (with *SSpI* site digestion, for homologous recombination, such as gene complementation) or non-linear plasmid DNA (for CRISPR/Cas9-mediated gene editing) was added. Additionally, 1 µl of heparin solution (1 mg/ml) was added and incubated on ice for 10

Material and methods

min. The protoplasts were then mixed with 500 µl of STC/PEG solution and incubated on ice for 15 min. Finally, the mixed protoplast was gently spread on freshly prepared regeneration agar plates with a 10 ml bottom layer containing the 2x selection resistance marker and a 10 ml top layer without the selection marker. The plates were incubated at 28°C for 3-7 days until colonies showed up. The transformants were then picked onto PD plates containing selective markers. For stringent selection, individual colonies were transferred again to PD plates with the selectable marker and finally to plates without the resistance marker. The DNA from the colonies could then be extracted for gene sequencing or Southern blot analysis.

4.4.3 Competent cell preparation and transformation of *A. tumefaciens*

The preparation and transformation of *Agrobacterium* were performed according to the protocol by Höfgen and Willmitzer with slight modifications, using dYT liquid medium instead of YEB liquid medium (Höfgen & Willmitzer, 1988).

The transformation was carried out through electroporation by mixing 1 µL of the target plasmid with 50 µL of competent *Agrobacterium* cells, which were then transferred to a pre-chilled 1 mm electroporation cuvette. The cuvette was placed into the *E. coli* Pulser apparatus (Eppendorf, Hamburg, Germany) and subjected to 1440 volts for 5 seconds. Afterwards, 1 mL of dYT medium without antibiotics was added to the cuvette to suspend the cells. The cell suspension was then transferred to a 1.5 mL microcentrifuge tube and recovered at 28 °C with continuous shaking for 1 h. Finally, around 30 µL of the cell suspension was spread on YT agar plates containing the appropriate antibiotics.

4.4.4 Competent cell preparation and transformation of *S. cerevisiae*

The procedure of this assay followed the Clotech yeast two hybrid protocols. Several single colonies of *S. cerevisiae* AH109 cells, each 2-3 mm in size, were selected and inoculated in 5 mL of YPD medium. The colonies were vigorously shaken by a vortex for five min to disperse them, and then grown overnight at 28 °C with 200 rpm shaking. The following day, the overnight culture was diluted to an OD600 of 0.2 in 50 ml of YPD and grown to an OD of 0.4-0.6 after being shaken for 3-4 hours at 28°C. The cells were then collected by centrifugation at 4000 rpm for 5 min and washed once with sterile water or 1x TE solution.

The yeast cells were centrifuged again and the supernatant was discarded. The pellet was resuspended in 1.5 ml of freshly prepared 1x TE/1x LiAc solution. In a new 2 mL reaction tube, 100 μ l of the prepared cell suspension was gently mixed with 1 μ g of plasmid (or 0.5 μ g each for the interaction test) and 0.1 mg of carrier DNA (denatured herring testes carrier DNA, 10 mg/mL), followed by 600 μ l of sterilized PEG/LiAc, and thoroughly mixed. The cells were recovered by shaking at 200 rpm for 30 min at 30°C. Afterwards, 70 μ l of DMSO was added to each tube and gently mixed, then incubated at 42°C for 30 min. The cells were then centrifuged at maximum speed for 15 seconds to remove the supernatant. Next, the cells were resuspended in 100 μ l of 0.9% NaCl solution, and 50 μ l were spread on the appropriate selective medium and incubated at 28°C for 3-5 days. Finally, the yeast colonies grown on the screening plate were transferred to plates containing the selective markers and further used for the assay.

PEG/LiAc solution	40% (w/v) PEG3350
(Polyethylene glycol/	1x LiAc
lithium acetate)	1x TE
Stock solutions	50% PEG 3350
	100% DMSO (Dimethyl sulfoxide)
	10x TE buffer: 0.1 M Tris-HCl, 10 mM EDTA, pH 7.5, autoclave.
	10x LiAc: 1 M lithium acetate Adjust to pH 7.5, with dilute acetic acid and autoclave.

4.4.5 Dropout assay for *S. cerevisiae*

The yeast two-hybrid assay was performed according to the manufacturer's instructions (Clontech, Saint-Germain-en-Laye, France). Yeast cells were grown overnight at 28°C with continuous shaking at 200 rpm in 5 mL of SD-Leu-Trp medium. The next day, the cell density was adjusted to an OD₆₀₀ of 0.2 using the same medium, and the cultures were incubated until they reached an OD₆₀₀ of 1.0. Then, the culture was collected by centrifugation at 4000 rpm for 5 min and the pellet was washed twice with sterile distilled water. Finally, the pellet was resuspended in sterile ddH₂O to an OD₆₀₀ of 1, and four sequential dilutions (1:10, 1:100, 1:1000, and 1:10,000) were performed. 5 μ L of the suspension for each dilution was dropped onto low stringency (SD-Leu-Trp), medium

Material and methods

stringency (SD-Leu-Trp-His), and high stringency (SD-Leu-Trp-Ade-His) medium plates, respectively. The plates were incubated for 4-5 days at 28 °C.

4.4.6 Filamentous growth test for *U. maydis*

The *U. maydis* strain was grown in YEPs liquid medium at 28°C with 200 rpm shaking until the OD_{600 nm} reached approximately 0.8. The cells were then collected by centrifugation at 3500 rpm for 10 min, and the resulting pellet was resuspended in sterile water and washed once. The OD_{600 nm} of the culture was adjusted to 1.0 in sterile water. Approximately 5 µL of the suspension culture was then dropped onto a PD plate containing charcoal, and the plates were incubated at 28 °C for 2-3 days. The formation of white mycelium indicated successful filamentous growth.

4.5 Molecular microbiological methods

4.5.1 Isolation of nucleic acids

4.5.1.1 Isolation of plasmid DNA from *E. coli*

The NucleoSpin® Plasmid Kit (Macherey-Nagel, Düren, Germany) was used to isolate plasmids from *E. coli* following the manufacturer's recommendations.

4.5.1.2 Isolation of genomic DNA from *U. maydis*

To extract *U. maydis* genomic DNA, overnight cultures of *U. maydis* were centrifuged at 1,2000 rpm for 2 min in 2 ml Eppendorf tubes. The supernatant was discarded, and 200 µl of glass beads, 400 µl of *Ustilago* lysate buffer, and 500 µl of phenol/chloroform were added to the pellets. The mixture was then shaken at 2,500 rpm for 15-20 min on a Vibra-VXR shaker (IKA, Staufen, Germany), followed by centrifugation at 1,2000 rpm for 15-20 min. The extracted DNA was transferred to a new 1.5 ml tube along with 400 µl of the upper aqueous phase. 1 ml of 100% EtOH was added and well mixed by turning the tube up and down. The DNA pellets were obtained after 10 min of centrifugation at 12,000 rpm, and the supernatant was discarded. The precipitate was resuspended in 400 µl of 70% ethanol and centrifuged at 12,000 rpm for 5 min. The supernatant was discarded, and the pellets were dried at room temperature for 10 min until the ethanol completely evaporated. Finally, 100 µl of H₂O was added to the pellet and incubated in a thermomixer (Eppendorf, Hamburg, Germany) at 55 °C for 30 min to promote dissolution. The extracted

DNA was stored at -20 °C until use.

<i>Ustilago</i> lysis buffer	50 mM Tris-HCl, pH 7.5
	50 mM Na ₂ -EDTA
	1% (w/v) SDS
Phenol / Chloroform	50% (v/v) Phenol (equilibrated in TE buffer)
	50% (v/v) Chloroform

4.5.1.3 Isolation of total RNA from infected maize tissue

To isolate total RNA, maize seedling samples were pulverized with liquid nitrogen. 1 mL of TRIzol reagent (Invitrogen, Darmstadt, Germany) was added to approximately 400 µl of powdered tissue in a 1.5 mL microcentrifuge tube. The mixture was vortexed and incubated at room temperature for 10 min. After centrifugation at 13,000 rpm at 4°C for 10 min, the supernatant was transferred to a new 1.5 mL centrifuge tube, which included 0.2 mL chloroform. The samples were mixed by inverting the tube and incubated for 3 min at room temperature. The samples were then centrifuged at 13,000 rpm for 15 min at 4°C. To precipitate RNA, the upper aqueous phase was transferred to an additional 1.5 mL microcentrifuge tube and combined with 0.5 mL isopropanol. After 10 min of incubation at room temperature, the samples were centrifuged at 13,000 rpm for 10 min at 4°C. After removing the supernatant, the pellet was washed with 1 mL of 70% ethanol and dried at room temperature. The dried RNA pellet was dissolved in 50 µL of RNase-free ddH₂O for 10 min at 55 °C. Finally, the RNA concentration was measured and evaluated with a NanoDrop ND_1000 spectrophotometer (Thermo Fisher Scientific, Duesseldorf, Germany), and the RNA quality was evaluated on a 1% TBE gel. Total RNA was stored at -20°C until use.

4.5.1.4 Purification PCR fragments product

DNA fragment amplification was performed using a polymerase chain reaction (PCR) thermocycler from Bio-Rad Laboratories (Hercules, USA). The appropriate polymerase was selected based on the intended use of amplification. To confirm clonal transformation, GoTaq® Green Master Mix from Promega (Heidelberg, Germany) was used. Long fragment amplification or coding sequence amplification for vector construction was carried out using either Phusion® High-Fidelity DNA Polymerase or Q5® High-Fidelity DNA Polymerase from New England Biolabs (NEB, Frankfurt, Germany). Reagents were added

Material and methods

following the manufacturer's instructions.

4.5.2 Nucleic acid modification

4.5.2.1 Restriction of nucleic acid

The restriction of DNA was carried out using type II restriction endonucleases for 1-16 hours at the required temperatures for active enzyme in the reaction buffer (NEB, Frankfurt, Germany). The digestion was carried out according to the instructions provided by the NEBcloner (<https://nebcloner.neb.com>).

4.5.2.2 Ligation of DNA fragments

The DNA fragments were ligated using T4 DNA ligase (NEB, Frankfurt, Germany). A 3:1 to 5:1 molar ratio of insert to vector was used in the ligation reaction, with the ratio being dependent on the size of the DNA indicated. For sticky ends, the ligation was carried out overnight at 16 °C or for 10 min at room temperature. For blunt ends or single-base overhangs, the ligation was carried out overnight at 16 °C or for at least 2 hours at room temperature. Finally, the enzyme was inactivated at 65 °C for 10 min to prepare it for subsequent transformation.

4.5.2.3 Gibson assembly

The Gibson assembly was performed using NEBuilder® HiFi DNA Assembly Master Mix (NEB, Frankfurt, Germany) according to the manufacturer's instructions. A molar ratio of 2-3 times the amount of each insert to 50-100 ng of backbone vector was used. In the case of 4-6 fragment assemblies, the molar ratio per insert to vector was 1:1. The samples were incubated in a thermocycler at 50 °C for 15 min for 2 or 3 fragment assemblies and for 60 min for 4-6 fragment assemblies. After incubation, the samples were stored either on ice or at -20 °C for subsequent transformations.

4.5.2.4 DNase-treatment of total RNA

After RNA isolation, contaminating DNA was removed using the Turbo DNFree™ kit from Ambion Life technologies™ (Thermo Fisher Scientific, Duesseldorf, Germany), following the manufacturer's instructions. To remove the DNA, 10 µg total RNA was mixed with 5 µl of 10x TURBO DNase buffer and 1 µl of TURBO DNase in a 50 µl reaction, and the mixture was incubated at 37 °C for 30 min. The DNase activity was then inactivated by

adding 5 μ l of DNase Inactivation Reagent and incubating the mixture at room temperature with occasional agitation for 5 min. The samples were centrifuged at 10,000 rpm for 2 min, and 40 μ l of the supernatant was transferred to a new reaction tube. Finally, the RNA concentration and quality were measured using a NanoDrop ND_1000 spectrophotometer (Thermo Fisher Scientific, Duesseldorf, Germany), and evaluated on a 1% TBE gel.

4.5.2.5 cDNA synthesis

After treating RNA with DNase, cDNA synthesis was performed using the Thermo Scientific RevertAid H Minus First Strand cDNA synthesis kit according to the manufacturer's instructions (Thermo Fisher Scientific, Duesseldorf, Germany).

A mixture of 1-5 μ g RNA and 1 μ l oligo(dT)₁₈ primer was combined with nuclease-free water to a total volume of 12 μ l and incubated at 65 °C for 5 min. Next, a mixture of 4 μ l of 5x Reaction Buffer, 1 μ l of RiboLock RNase Inhibitor (20U/ μ l), 2 μ l of 10 mM dNTP Mix, and 1 μ l of RevertAid H Minus M-MuLV Reverse Transcriptase (200U/ μ l), with a total volume of 20 μ l, was incubated at 42 °C for 60 min. Finally, the reaction was stopped by heating at 70 °C for 5 min. The synthesized cDNA was stored at -80 °C until further use.

4.5.2.6 Quantitative real-time PCR (qRT-PCR)

For the quantitative real-time PCR (qRT-PCR), a 1:20 dilution of the synthesized cDNA (described in Chapter 4.5.2.5) was used. The qRT-PCR reactions were performed using GoTaq® qPCR Mastermix (Promega, Heidelberg, Germany) as directed by the manufacturer's instructions. A total of 5 μ l of diluted cDNA was added to each reaction to achieve a total volume of 15 μ l. All qRT-PCRs were carried out on an iCycler system (Bio-Rad, Hercules, USA) using the following program: 95 °C/2 min, followed by 45 cycles of (95 °C/30 s, 62 °C/30 s, 72 °C/30 s). A melting curve analysis was generated after the qPCR run to confirm the specificity of the reaction. The threshold cycles were determined using the Bio Rad software, and the relative expression values were calculated using the $2^{-\Delta\Delta C_t}$ method.

4.5.2.7 Site-directed mutagenesis

Site-directed mutagenesis was conducted using the QuikChange Lightning Multi Site-Directed Mutagenesis Kit (Agilent, Waldbronn, Germany) for the insertion of single or

Material and methods

multiple site-specific mutations into double-stranded plasmids. The procedure was according to the manufacturer's instructions.

4.5.3 Separation and detection of nucleic acids

4.5.3.1 Agarose gel electrophoresis

Agarose gel electrophoresis is mainly used for the separation of nucleic acid fragments. Depending on the size of the fragments to be separated, agarose gel concentrations of 0.8% and 2% (w/v) can be prepared. The agarose was boiled and dissolved in 1x TAE buffer solution, and after cooling, ethidium bromide (0.25 µg/ml) was added. The prepared gel was poured into a gel casting tray and a suitable comb was inserted. After solidification, the comb was removed, and the gel was transferred to an electrophoresis running chamber filled with 1x TAE buffer. The samples were mixed with 6x DNA loading dye and added to the comb spotting site. Electrophoresis was performed at a constant voltage of 90-120 V for 30-60 min. The separated DNA fragments were visualized under ultraviolet radiation (Peqlab/VWR, Radnor, USA). The desired band could be excised, and the DNA fragments could be purified and recycled using NucleoSpin® Gel and PCR Clean-up Kit (Macherey Nagel, Düren, Germany) for further experiments.

50x TAE-buffer	2 M Tris-Base 2 M Acetic acid 50 mM EDTA, pH 8.0 dissolve in ddH ₂ O
6x DNA loading dye	50% (w/v) Sucrose 0.1% (v/v) Bromophenol blue dissolve in 1x TE
1x TE buffer	10 mM Tris-Base mM Na ₂ -EDTA 2H ₂ O dissolve in ddH ₂ O, adjust pH to 8.0 with HCl and autoclave

4.5.3.2 Southern blot analysis

The detection of specific DNA fragments in intact genomic DNA was performed using the Southern blot method, as described by Southern (Southern, 1975). The DNA extracted in the previous step (Chapter 4.5.1.2) was digested overnight with an appropriate endonuclease. To the reaction mixture, 1/10 volume of 3 M sodium acetate and 2 volumes

of 100% EtOH were added, and the mixture was incubated at -20 °C for 1 hour. It was then centrifuged at 4 °C with 12,000 rpm for 30 min to collect the DNA precipitation. The pellet was dissolved in 20 µl of 1x DNA loading dye, and the DNA fragments were separated using gel electrophoresis on a 0.8% agarose gel at 110 V for 2 hours. The agarose gel was then depurinated with 0.25 M HCl for 15 min and neutralized in a transfer buffer containing 0.4 M NaOH for 30 min. The DNA was transferred from the gel to a nylon membrane (GE Health Care Life Sciences, Freiburg, Germany) using transfer solution for capillary blotting. The DNA fragments were fixed to the membrane using UV crosslinking (Amersham Biosciences, Little Chalfont, UK). The membrane was pre-hybridized in a hybridization oven (UVP HB-1000 Hybridizer, Ultra-violet Products Ltd., Cambridge, UK) at 65°C for 30 min with 20 mL of Southern hybridization buffer. The DNA was detected using DIG-labeled probes, created by labeling DNA fragments with PCR DIG labeling mix (Roche, Mannheim, Germany).

The probe preparation was carried out according to the manufacturer's experimental manual. The probes were boiled for 10 min to denature, added to the hybridization buffer, and incubated at 65°C with rotation for at least 6 hours. The membrane was washed three times with a Southern wash buffer for 15 min each at 65°C. The following processes were all carried out at room temperature. The membrane was then incubated with DIG wash buffer for 5 min, blocked with DIG buffer 2 for 30 min, and incubated with DIG antibody solution for 1 hour. The membrane was washed three times for 15 min each with DIG wash buffer to remove antibodies. Then equilibrated in DIG buffer 3 for 5 min and incubated with 2.5 ml of CDP-star solution in a small autoclave bag for 10 min at 37°C. Finally, the membrane was visualized using ChemiDoc™ MP (Bio-Rad, Hercules, USA) to detect the DIG-labeled DNA fragments.

Depurination solution	0.25 M HCl
Transfer buffer	0.5 M NaOH 1.5 M NaCl
Southern hybridization buffer	0.5 M Na-phosphate buffer, pH 7 7% (w/v) SDS
Southern wash buffer	0.1 M 1M Na-phosphate buffer, pH 7 0.2 1% (w/v) SDS

Material and methods

DIG buffer 1	0.1 M maleic acid 0.2 0.15 M NaOH 0.3 set pH to 7.5 with NaOH autoclave
DIG buffer 2	1% (w/v) skimmed milk powder in DIG1
DIG buffer 3	0.1 M Tris-HCl (pH 9.5) 0.2 0.1 M NaCl 0.3 0.05 M MgCl ₂
DIG wash buffer	0.3% (v/v) Tween-20 in DIG1
Southern antibody solution	Anti-Dioxigenin-AP antibody 1:10,000 in DIG2 (Roche, Mannheim, Germany)
CDP-star solution	CDP-Star 1:200 in DIG3 (Roche, Mannheim, Germany)
Na-phosphate buffer, 1 M (pH 7.0)	1 M Na ₂ HPO ₄ 1 M NaH ₂ PO ₄ ·H ₂ O Add NaH ₂ PO ₄ ·H ₂ O to Na ₂ HPO ₄ until pH reaches 7.0 in ddH ₂ O

4.5.3.3 DNA sequencing and RNA sequencing

DNA sequencing reactions were supplied by Eurofins (formerly GATC, Luxembourg). Before sequencing plasmids or PCR fragments, the plasmid was isolated using the plasmid kit, and PCR fragments were purified using Nucleospin® Gel and PCR Clean-up Kit (Macherey-Nagel, Düren, Germany) as previously described in Chapter 4.5.1. The DNA sequencing results were compared and analyzed using Clone Manager 9 (Sci-Ed, Denver, USA) software. Novogene (Beijing, China) conducted Illumina sequencing of mRNA using the Illumina NovaSeq 6000 (Illumina, San Diego, USA)

4.6 Protein methods and biochemical assays

4.6.1 Protein heterologous protein expression in *N. benthamiana*

To transiently express heterologous proteins in *N. benthamiana*, *A. tumefaciens* GV3101 strains carrying the relevant plasmids of interest were infiltrated into the leaves. The GV3101 with the desired plasmid was first grown to an OD₆₀₀ of 1.0 in dYT medium containing the necessary antibiotics. The culture was then centrifuged at 4000 rpm for 10 min and washed twice with distilled water to remove the medium. The cell pellet was suspended in MES buffer (10 mM MES, 10 mM MgCl₂, 100 μM acetosyringone) to an OD₆₀₀ of 0.5. The GV3101 cell suspension was mixed according to the experimental

design and infiltrated into the underside of the leaf using a 1 mL needle-free syringe. After 2-3 days, the infiltrated leaves were collected and protein was extracted.

4.6.2 Protein overexpression in *E. coli* and purification

For overexpressing the recombinant proteins GST-Tip6 Δ SP-mcherry, GST-mcherry, and 6xHis-ZmTPL2^N-6xHis, the plasmids were transformed into the *E. coli* BL21 Star (DE3) strain (Thermo Fisher Scientific, Duesseldorf, Germany).

A single colony of verified *E. coli* cells was inoculated into 10 ml of dYT medium and grown overnight at 37°C with constant shaking. The next day, the culture was diluted to an OD₆₀₀ of 0.2 for the desired induction volume and grown in dYT medium containing 50 mg/mL Kan at 37°C until the OD₆₀₀ reached 0.6. Then, 1 mM isopropyl-B-D-thiogalactopyranoside (IPTG) was added. The culture was incubated for 16 hours at 18°C with constant shaking. The cells were harvested by centrifugation at 4000 rpm for 20 min at 4°C, and the resulting cell pellets were stored at -20°C. The cell pellets were suspended in protein lysis buffer and extracted proteins were obtained by sonication for further study.

4.6.2.1 GST-tag fusion proteins purification

The GST-mCherry and GST-Tip6 Δ SP-mCherry recombinant proteins contain a glutathione-S-transferase (GST) tag, which allows for affinity purification using glutathione conjugated to Sepharose. A PreScission protease cleavage site is inserted between the GST tag and the target protein, enabling the removal of the GST tag after purification. The previously collected cell pellet (Chapter 4.6.2) was thawed on ice, resuspended in 20 ml lysis buffer and incubated at room temperature for 20 min. The suspension was then subjected to five rounds of sonication for 30 seconds on ice, followed by centrifugation at 4°C and 10,000 rpm for 30 min. Gravity-flow columns were loaded with 1 ml to 2 ml of Glutathione Sepharose 4B (GE Healthcare, Freiburg, Germany) and equilibrated with 10 ml of 1xPBS buffer. The supernatant from the centrifuged lysate was added to the column and incubated on a rotary shaker (Kisker Biotech, Steinfurt, Germany) at 4°C for 1 hour. The column was then placed vertically, the cap was removed, and a small amount of the protein flow was taken as a later test sample. The remaining unbound protein flow was discarded. The column was then washed three times with 10 ml of 1xPBS buffer and once with 10 ml

Material and methods

of PreScission®-cleavage buffer. The GST tag was subsequently removed using PreScission® protease (GE Healthcare, Freiburg, Germany) by adding 80 µl of PreScission® Protease and 920 µl of PreScission® cleavage buffer to the column and incubating at 4 °C for 16 hours. The column was then opened, and the protein flow was collected. The mCherry tag in these two recombinant proteins can be visualized in pink. The remaining protein was washed with 2 ml of PreScission® elution buffer several times until the eluted protein became lighter in color, typically 3 to 5 times. Since the recombinant protein size is greater than 25 kDa, all flow-through fractions were concentrated using an Amicon Ultra-15 column (Millipore/Merck, Darmstadt, Germany) to exclude proteins smaller than 15 kDa, resulting in a protein solution with a volume of approximately 6 ml in size exclusive chromatography (SEC) buffer. The eluted proteins were then analyzed using Coomassie Brilliant Blue (CBB)-stained SDS-PAGE gels and Western blotting.

The protein concentration was roughly measured using a Nanodrop spectrophotometer (Thermo Fisher Scientific, Duesseldorf, Germany). The protein solutions were stored at 4 °C for short-term storage or were mixed with glycerol to a final concentration of 10% (v/v) and stored at -80 °C for long-term storage.

Lysis buffer	0.2 M NaH ₂ PO ₄ /0.2M Na ₂ HPO ₄ , pH 6.4 150 mM NaCl Lysozyme 100 µg/ml Protease inhibitor (Roche, Mannheim, Germany)
PreScission cleavage buffer	50 mM Tris-HCl, pH 7.0 150 mM NaCl 1 mM EDTA 1 mM DTT
PreScission elution buffer	50 mM Tris-HCl, pH 8.0 10 mM reduced glutathione
SEC buffer	0.2 M NaH ₂ PO ₄ /0.2M Na ₂ HPO ₄ , pH 6.4 150 mM NaCl dissolve in ddH ₂ O and filter-sterilize

4.6.2.2 His-tag fusion proteins purification

The collected His-tagged homologous recombinant protein was suspended in lysate and subjected to sonication five times, each for 30 seconds on ice. Afterward, the suspension was centrifuged at 4°C and 10,000 rpm for 30 min. A 2 ml Ni-NTA agarose resin was loaded

into a gravity flow column, and equilibrated with 10 ml His tag lysis buffer. The lysate supernatant was then passed through the column. Non-specifically bound protein was eluted using imidazole concentrations of 50 mM, 100 mM and 200 mM at pH 6.5, and then resin-bound protein was finally eluted using 300 mM and 500 mM imidazole. The eluted proteins were analyzed using SDS-PAGE gels stained with CBB and Western blotting. The flow-through fractions were concentrated using an Amicon Ultra-15 column (Millipore/Merck, Darmstadt, Germany), and high-concentration imidazole was replaced with phosphate buffer (pH 6.5). A protein solution with a volume of about 6 ml was collected, and its protein concentration was roughly determined using Nanodrop. The protein solution was stored at 4°C for short-term storage and at -80°C for long-term storage after adding glycerol to a final concentration of 10% (v/v).

Lysis buffer	0.2 M NaH ₂ PO ₄ /0.2 M Na ₂ HPO ₄ , pH 6.4
	150 mM NaCl
	10 mM imidazole, pH 6.4
	Lysozyme 100 ug/ml
	Protease inhibitor tablets
Elution buffer	0.2 M NaH ₂ PO ₄ /0.2 M Na ₂ HPO ₄ , pH 6.4
	150 mM NaCl
	300 mM imidazole, pH 6.4
	Protease inhibitor tablets

4.6.2.3 Proteins purification by size exclusion chromatography

The purified recombinant proteins were subjected to size exclusion chromatography (SEC), using a HiLoad 16/600 Superdex 200 pg column in an Äkta system (GE Healthcare, Freiburg, Germany) and a buffer consisting of 0.2 M NaH₂PO₄/0.2 M Na₂HPO₄ pH 6.4 and 150 mM NaCl. The eluted protein solutions of corresponding sizes were collected. The eluted proteins were analyzed using SDS-PAGE gels stained with CBB and Western blotting.

4.6.3 Protein extraction from *S. cerevisiae*

The proteins from yeast strains in Y2H assays were prepared as previously described (Kushnirov, 2000). A single colony of yeast strains was grown overnight in YPD medium, and 1 mL of the culture was centrifuged for 1 min at 10,000 rpm. The resulting pellets

Material and methods

were resuspended in 100 μ L of distilled water and 100 μ L of 0.2 M NaOH, centrifuged for 5 min at 4,000 rpm, and incubated at room temperature for 10 min. The pellets were then resuspended in 50 μ L of 1x sample buffer, heated for 10 min, and centrifuged. The supernatant was stored at -20°C or used for further experiments by loading onto an SDS-PAGE gel.

4.6.4 Protein extraction from maize or tobacco

To extract proteins from plant material, maize leaves infected with *U. maydis* or *N. benthamiana* leaves infiltrated with *Agrobacterium* containing the plasmid of interest were harvested based on the experimental design and promptly frozen in liquid nitrogen. The frozen plant material was then finely ground using liquid nitrogen. 300 mg of each ground plant powder was transferred to a 2 mL Eppendorf tube and mixed with 1.5 mL of protein extraction buffer (EWB). The samples were incubated on ice for 30 min, with shaking every 10 min to ensure proper mixing. The samples were then centrifuged at 13,000 rpm for 20 min at 4°C to remove debris, and the supernatant was transferred to a fresh 1.5 mL Eppendorf tube for re-centrifugation at 13,000 rpm for 20 min to completely remove any remaining debris. The resulting supernatant represented the total extracted protein and was used for subsequent experiments.

Extraction/Washing Buffer (EWB)

	Stock	100 ml
50mM Tris pH 7.5	1M	5 ml
150mM NaCl	5M	3 ml
10% Glycerol	Glycerol 80%	12,5 ml
2mM EDTA	0,5M	400 μ l
Water		79,1 ml

Keep at RT

Add fresh to	Stock	10ml of EWB
5mM DTT	1M	50 μ l
1% Triton		100 μ l
Protease inhibitor tablets	1 tablet in 1 ml EWB	100 μ l

4.6.5 Co-immunoprecipitation assay in plant

The co-immunoprecipitation assays utilized antibody-conjugated magnetic beads to

capture proteins of interest. Depending on the label fused with the target protein, different antibody-bound magnetic beads were selected. Firstly, 5-10 ul of trap beads were added to 300 ul of EWB and incubated on ice for 1 min. The beads were collected with a magnetic stand, and this process was repeated twice to equilibrate the beads. 1 ml of the total extracted plant protein obtained previously (Chapter 4.6.4) was then added and incubated at 4°C with constant rotation for 1-2 hours. 50 ul of total extracted protein was used as input without incubating the beads to check for protein expression. The beads were collected with the magnetic stand and then washed three times with an extraction buffer and three times with a wash buffer. The beads were added to 50-80 µL 1x loading buffer and boiled at 95°C for 5-10 min. Samples were detected by Western blot and immunoblotting was performed with the respective antibodies.

4.6.5.1 Co-immunoprecipitation of HA-tagged protein in maize and followed by mass spectrometry

Total proteins were extracted from maize seedling leaves infected with *U. maydis* expressing SG200Δ*Tip6::Propit2*-Tip6-2xHA or SG200::Propit2-SP-mCherry-3xHA according to the protocol described in chapter 4.6.4. The HA magnetic beads (Thermo Fisher Scientific, Duesseldorf, Germany) were equilibrated and incubated with total extracted protein at 4 °C for 1-2 hours as described in Chapter 4.6.5. The magnetic beads were collected using a magnetic holder and washed three times with 700 µL of washing buffer. The protein-bound beads were then sent for mass spectrometry analysis.

4.6.5.2 *In vitro* pull-down assay

To verify the interaction between Tip6 and ZmTPL2^N, mCherry, Tip6ΔSP-mCherry, and His-ZmTPL2^N-His recombinant proteins were expressed (Chapter 4.6.2), extracted (Chapters 4.6.2.1 and 4.6.2.2), and purified (Chapters 4.6.2.1, 4.6.2.2 and 4.6.2.3) according to previously described methods. 200 ul of purified recombinant mCherry or Tip6ΔSP-mCherry protein were mixed with 200 ul of His-ZmTPL2^N-His protein, respectively. 10 µL of the mixture was taken out, 10 µL of 2x loading buffer was added, and the sample was boiled for 10 min. The remaining mixture was incubated with pre-washed magnetic mCherry-Trap beads (ChromoTek, Martinsried, Germany) at 4°C for 1 hour with constant rotation. The beads were collected using a magnetic stand and washed five to

Material and methods

seven times with a wash buffer. Then 100 μ L of 1x loading buffer was added, and the samples were boiled for 10 min. The supernatant from the boiled protein samples was detected by SDS-PAGE and Western blot. Immunoblotting was performed using an anti-His antibody (Thermo Fisher Scientific, Duesseldorf, Germany) at a dilution of 1:10,000 and an anti-mCherry antibody (Cell Signaling Technology, Frankfurt am Main, Germany) at a dilution of 1:3,000. A second antibody, anti-mouse IgG HRP (Cell Signaling Technology, Frankfurt am Main, Germany) was used at a dilution of 1:3,000.

4.6.6 SDS polyacrylamide gel electrophoresis (SDS PAGE)

Sodium dodecyl sulfate-polyacrylamide gel electrophoresis (SDS-PAGE) was utilized according to Laemmli (1970) to separate proteins in a sample based on their molecular weight (Laemmli, 1970). The polyacrylamide gel and the SDS reagent linearize the proteins. A reducing agent, such as dithiothreitol (DTT), is typically added to the sample to open disulfide bonds of folded proteins, while SDS negatively charges all proteins and linearizes them into peptides. The electrophoretic separation of peptides occurs in the polyacrylamide medium. The peptide runs toward the anode under the action of the electric field. Peptides with smaller molecular weights move faster in electrophoresis due to encountering less resistance. Peptides with higher molecular weights move slower due to encountering more resistance. Thus, proteins are separated entirely based on differences in molecular weight.

The protein gel is divided into two parts: the stacking gel and the resolving gel. The purpose of the stacking gel is to gather the protein mixture for separation at the dividing line between the stacking gel and the resolving gel. All proteins are then compacted and accumulated at the demarcation line before entering the resolving gel at the same time. The proteins in the sample are separated in the resolving gel. The percentage of resolving gel varies depending on the desired size of protein separation, typically ranging from 7 to 15%. The amount of sample loaded into each well should be consistent. Carefully adding the samples will ensure that the well is not damaged or that the sample does not overflow the well. At this stage, the protein samples appear blue due to the electrophoresis indicator dye, bromophenol blue, used in sample preparation. A protein marker with a

known molecular weight is used to reference protein size, with the PageRuler Prestained Protein Ladder (Thermo Fisher Scientific, Duesseldorf, Germany) serving as a scale.

4× Sample buffer	10 mL 1.5 M Tris-HCl pH 6.8 30 mL glycerin 6 mL 20 % SDS 5 mg bromophenol blue 3 g DTT (f. c. 400 mM) Fill up to 50 mL with ddH ₂ O
Stacking gel (5%)	0.5 mL 0.5 M Tris-HCl pH 6.8 0.333 mL 30 % Polyacrylamide (PAA) 20 µL 10 % SDS 20 µL 10 % Ammonium persulfate (APS) 2 µL Tetramethylethylenediamine (TEMED) 1.125 mL ddH ₂ O
Stacking gel (15 %)	1.25 mL 1.5 M Tris-HCl pH 8.8 2.49 mL 30 % Polyacrylamide (PAA) 50 µL 10 % SDS 50 µL 10 % Ammonium persulfate (APS) 5 µL Tetramethylethylenediamine (TEMED) 1.17 mL ddH ₂ O
SDS running buffer	25 mM Tris-HCl, pH 8.0 192 mM glycine 4 mM SDS dissolves in ddH ₂ O

4.6.7 Western blot

Using the semi-dry Trans-Blot Turbo transfer system from Bio-Rad (Munich, Germany), proteins separated by SDS-PAGE were transferred to PVDF nitrocellulose membranes. For the transfer procedure, a 6 cm x 8 cm nitrocellulose membrane was first wetted in MeOH for 15 s, followed by placing two pieces of 6.5 cm x 8.5 cm Whatman paper in the transfer buffer. The assembly order was arranged in the following order: Whatman paper, PVDF nitrocellulose membrane, SDS-PAGE gel, Whatman paper, and gently rolling on Whatman paper to eliminate air bubbles. The "Mixed MW (Turbo)" pre-program from Bio-Rad was used for proteins with a molecular weight between 5-150 kDa. The gels were transferred for 20-30 min at 1.3 A and 25 V (for one mini gel) or 2.5 A and 25 V (for two mini gels), depending on the size of the transferred protein. The membrane was then incubated in a

Material and methods

blocking solution at RT for 1 hour, followed by replacing the blocking solution with a primary antibody-containing antibody solution and incubating the mixture at 4°C for approximately 16 hours (usually overnight).

The membrane was washed three times with TBST buffer for 10 min each, followed by incubation in TBST buffer containing the secondary antibody for 1 hour at room temperature. It was then washed with TBST buffer three times for 10 min each. Finally, the membrane was subjected to signal detection using either SuperSignal™ West Pico PLUS Chemiluminescent Substrate or SuperSignal™ West Femto Maximum Sensitivity Substrate (Thermo Fisher Scientific, Duesseldorf, Germany) on a ChemiDoc™ MP (Bio-Rad, Hercules, USA). Antibodies used in this study were listed in **Tab. 10**.

Western transfer buffer	25 mM Tris-HCl, pH 10.4 192 mM glycine 15%(v/v) methanol
TBST	50 Mm Tris-HCl, pH 7.5 150 mM NaCl 0.1 % (v/v) Tween 20 dissolve in ddH2O
Blocking solution	5 % (v/v) skim milk powder in TBST
Antibody solution	Antibody dilute in blocking solution

Tab. 10. Antibodies used in this study

Name	Organism	Supplier	Working ratio
GFP	mouse	Roche	1:3000
RFP	mouse	ChromoTek	1:3000
HA	mouse	Sigma-Aldrich	1:30000
His	mouse	Thermo Fischer	1:3000
c-myc	mouse	Sigma-Aldrich	1:5000
GST	rabbit	Cell signaling technology	1:1000
His-HRP		QIAGEN	1:2000
GFP-HRP		Invitrogen	1:1000
HA-HRP		Roche	1:2000
rabbit IgG	goat	Cell signaling technology	1:3000
mouse IgG	goat	Cell signaling technology	1:3000

4.6.8 Coomassie staining of proteins

The SDS-PAGE gel was visualized by staining with CBB dye. The staining process was

performed for 15-30 min, followed by washing with either sterile H₂O or CBB destaining solution to remove excess dye.

Coomassie Brilliant Blue R-250	0.1% (W/V) Coomassie Brilliant Blue R250 25% (V/V) Isopropanol 10% (V/V) Glacial Acetic Acid
Coomassie Brilliant Blue Stain Destaining Solution	10% (V/V) Glacial Acetic Acid 5% (V/V) Ethanol

4.7 Plant assays

4.7.1 *Zea mays* material

The primary variety of maize used for *U. maydis* pathogenicity tests was *Zea mays* cv. Golden Bantam (Demeter International, Germany).

4.7.2 Cultivation of *Z. mays*

All maize plants were grown in a temperature-controlled greenhouse with a light-dark cycle of 16 hours at 28 °C and 8 hours at 22 °C. The same growing conditions were maintained in a walk-in plant chamber for the RNA-seq experiments.

4.7.3 *U. maydis* infection of *Z. mays*

The pathogenicity of *U. maydis* strains was evaluated using the method described by Kämper et al., 2006. The strains were grown according to the protocol in Chapter 4.2.3, until the OD₆₀₀ reached 1. A syringe was used to inoculate 1 mL of the cell suspension into 7-day-old maize seedlings. At 12 days post-inoculation (dpi), the severity of disease symptoms was rated in **Tab. 11**.

Tab. 11. Categorization of symptoms in infected maize seedlings

Symptoms	Description
No symptoms	No infections were visible in the plant
Chlorosis	Yellow discoloration was played on infected maize leaves
Small tumors	Only small tumors < 1 mm, a few numbers of tumors larger than 1 mm
Normal tumors	Most tumors were visible > 1 mm
Heavy tumors	Altered growth axes or formed large tumors at the base of the stem
Dead	The plant died from the infection with <i>U. maydis</i>

Material and methods

The disease index was assigned as 9 for dead plants, 7 for heavy tumors, 5 for normal tumors, 3 for small tumors, 1 for chlorosis, and 0 for plants without symptoms. The average disease index was calculated by multiplying the number of diseased plants by the corresponding disease index and dividing the resulting sum by the total number of plants used in the infection. The average disease index from three biological replicates was used for statistical significance testing via a Student's t-test.

4.7.4 Cultivation of *N. benthamiana*

All *N. benthamiana* plants were grown in a greenhouse with a 16-hour light and 8-hour dark cycle at a temperature of 22 °C. Six-week-old plants were used for the infiltration with *A. bacterium*.

4.7.5 Infiltration of *N. benthamiana* with *A. tumefaciens*

The cell suspension of *A. tumefaciens* GV3101 strains carrying the relevant plasmids of interest was mixed according to the experimental design and then infiltrated into the underside of the *N. benthamiana* leaves using a 1 mL needle-free syringe.

4.7.6 Biolistic transformation of maize leave cells

For transient protein expression in maize cells, 1.6 µm gold particles (Bio-rad, Muenich, Germany) were used for biolistic transformation. 60 mg of gold particles were suspended in 1 mL of 100% ethanol, vortexed for 9 min, and then centrifuged at maximum speed for 1 min to remove ethanol. The gold particles were suspended and washed twice with 1 mL of sterile distilled water. Next, gold particles were suspended in 250 µl of sterile 50% glycerol by vortexing for 3 min. The suspension was then divided into 40 µl aliquots and stored in 1.5 ml reaction tubes at -80 C for long-term use.

To mark the gold particles with plasmid DNA, 10 µL of gold suspension was mixed with 4-5 µg of plasmid and vortexed at maximum speed for 1 min. The mixture was then combined with 20 µL of 2.5 M CaCl₂ and vortexed for 3 min, followed by the addition of 10 µL of 0.1 M spermidine and vortexing for 1 min. The gold particles were then washed with 1 mL of 70% ethanol and 1 mL of 100% ethanol, respectively. Finally, the DNA-coated gold particles were resuspended in 40 µL of 100% ethanol.

For biolistic bombardment transformation, 10-day-old maize leaves were cut and placed

upside down on three layers of wet paper towels in a 9 cm Petri dish. The gold particle suspension was loaded on the carrier disk and the ethanol was allowed to evaporate for a few minutes. The pDS/1000 HeTM Biolistic Particle Delivery System (Bio-rad, USA) guide instructions were followed when assembling the delivery cartridges. The leaves were subjected to 900 psi of pressure in a vacuum at 27 inches of mercury. To allow for expression of the corresponding proteins, the bombarded leaves were placed at room temperature for 16–48 hours. Finally, the expression signals of the fusion proteins were monitored using a confocal laser scanning microscope (TCS-SP8, Leica, Germany).

4.7.7 Split-luciferase complementation assay

The split-luciferase assay was performed as described by (Zhou et al., 2018). The test gene was cloned into either the nLuc or cLuc vector, and *Agrobacterium* carrying the gene of interest was mixed and infiltrated into the leaves of *N. benthamiana* as described above. Two days after post-infiltration, the leaves were harvested and analyzed for luciferase activity. The backside of the leaves was sprayed with 1 mM D-luciferin solution, and then they were incubated in the dark for 10 min. Luminescence signals were then detected using a CCD imaging system (ChemiDoc, Bio-RAD) from at least three independent plants.

4.8 Confocal laser scanning microscopy

All live cell imaging was performed using a TCS SP8 confocal laser scanning microscope (Leica, Bensheim, Germany). The excitation wavelength of eGFP is 488 nm and the detection wavelength ranges between 490–540 nm. The excitation wavelength of mCherry is 561 nm, and the detection wavelength is collected between 580–660 nm. Image analysis was conducted using Leica's LASX software (Leica, Bensheim, Germany).

4.9 Bioinformatics methods

4.9.1 RNA-Seq analysis

Maize seedlings infected by *U. maydis* SG200, Δ Tip6, or Tip6EARm-2xHA at 3 dpi were harvested for total RNA extraction. RNA was prepared as described in Chapters 4.5.1.3 and 4.5.2.4. Each sample was collected in three independent replicates and sent to Novogene (Cambridge, UK) for library construction using an Illumina NovaSeq 6000

Material and methods

(Illumina). Low quality RNA-seq sequences and adaptors were removed using trim galore (Martin, 2011). The remaining clean reads were then mapped to the *Zea mays* B73 reference genome version 5 (V5) (Hufford et al., 2021) using STAR, version 2.7.0e (Dobin et al., 2013). Gene expression was quantified using Feature Counts (Liao et al., 2014) and 39756 genes were mapped. Genes with total counts below 25 in 9 samples were removed, leaving 29537 genes for further analysis. Differentially expressed genes (DEGs) were identified using the DESeq2 (Love et al., 2014) and edgeR (Robinson et al., 2010) packages in R (version 4.2.1). The cutoff criteria for significant DEGs were an absolute value of log2 fold-change ≥ 1 and p-value < 0.05 . The DEGs identified by both DESeq2 and edgeR were used for further analysis.

4.9.2 GO enrichment analysis

Maize gene ontology (GO) terms were annotated to the B73.v5 reference genome using ShinyGO v.0.06 (<http://bioinformatics.sdstate.edu/go65/>) (Ge et al., 2020). Significant enrichment of GO terms (FDR <0.05) was calculated for all gene subsets.

4.9.3 Gene accession

Tab.12. Gene IDs of TPL proteins for sequence alignment

Protein Name	Gene ID
ZmTPL1	Zm00001eb127680
ZmTPL2	Zm00001eb011010
ZmTPL3	Zm00001eb415530
ZmTPL4	Zm00001eb398420
AtTPL	AT1G15750.1
AtTPR1	AT1G80490.2
AtTPR2	AT3G16830.1
AtTPR3	AT5G27030.2
AtTPR4	AT3G15880.2
OsTPR2/ASP1	Os08g0162100
OsTPR3/ASPR1	Os03g14980
OsTPR1/ASPR2	Os01g0254100

5 Bibliography

- Ahuja, I., Kissen, R., & Bones, A. M. (2012). Phytoalexins in defense against pathogens. *Trends in Plant Science*, 17(2), 73–90. <https://doi.org/10.1016/j.tplants.2011.11.002>
- Aichinger, C., Hansson, K., Eichhorn, H., Lessing, F., Mannhaupt, G., Mewes, W., & Kahmann, R. (2003). Identification of plant-regulated genes in *Ustilago maydis* by enhancer-trapping mutagenesis. *Molecular Genetics and Genomics: MGG*, 270(4), 303–314. <https://doi.org/10.1007/s00438-003-0926-z>
- Albert, I., Hua, C., Nürnberger, T., Pruitt, R. N., & Zhang, L. (2020). Surface Sensor Systems in Plant Immunity. *Plant Physiology*, 182(4), 1582–1596. <https://doi.org/10.1104/pp.19.01299>
- Ali, S., Ganai, B. A., Kamili, A. N., Bhat, A. A., Mir, Z. A., Bhat, J. A., Tyagi, A., Islam, S. T., Mushtaq, M., Yadav, P., Rawat, S., & Grover, A. (2018). Pathogenesis-related proteins and peptides as promising tools for engineering plants with multiple stress tolerance. *Microbiological Research*, 212–213, 29–37. <https://doi.org/10.1016/j.micres.2018.04.008>
- Almagro Armenteros, J. J., Tsirigos, K. D., Sønderby, C. K., Petersen, T. N., Winther, O., Brunak, S., von Heijne, G., & Nielsen, H. (2019). SignalP 5.0 improves signal peptide predictions using deep neural networks. *Nature Biotechnology*, 37(4), Article 4. <https://doi.org/10.1038/s41587-019-0036-z>
- Altegoer, F., Weiland, P., Giammarinaro, P. I., Freibert, S.-A., Binnebesel, L., Han, X., Lepak, A., Kahmann, R., Lechner, M., & Bange, G. (2020). The two paralogous kiwellin proteins KWL1 and KWL1-b from maize are structurally related and have overlapping functions in plant defense. *Journal of Biological Chemistry*, 295(23), 7816–7825. <https://doi.org/10.1074/jbc.RA119.012207>
- Arnold, R., Brandmaier, S., Kleine, F., Tischler, P., Heinz, E., Behrens, S., Niinikoski, A., Mewes, H.-W., Horn, M., & Rattei, T. (2009). Sequence-Based Prediction of Type III Secreted Proteins. *PLOS Pathogens*, 5(4), e1000376. <https://doi.org/10.1371/journal.ppat.1000376>
- Banno, H., Ikeda, Y., Niu, Q.-W., & Chua, N.-H. (2001). Overexpression of Arabidopsis ESR1 Induces Initiation of Shoot Regeneration. *The Plant Cell*, 13(12), 2609–2618. <https://doi.org/10.1105/tpc.010234>
- Banuett, F. (1992). *Ustilago maydis*, the delightful blight. *Trends in Genetics: TIG*, 8(5), 174–180. [https://doi.org/10.1016/0168-9525\(92\)90220-x](https://doi.org/10.1016/0168-9525(92)90220-x)
- Banuett, F., & Herskowitz, I. (1989). Different a alleles of *Ustilago maydis* are necessary for maintenance of filamentous growth but not for meiosis. *Proceedings of the National Academy of Sciences of the United States of America*, 86(15), 5878–5882. <https://doi.org/10.1073/pnas.86.15.5878>
- Banuett, F., & Herskowitz, I. (1994). Morphological Transitions in the Life Cycle of *Ustilago maydis* and Their Genetic Control by the a and b Loci. *Experimental Mycology*, 18(3), 247–266. <https://doi.org/10.1006/emyc.1994.1024>
- Banuett, F., & Herskowitz, I. (1996). Discrete developmental stages during teliospore formation in the corn smut fungus, *Ustilago maydis*. *Development (Cambridge, England)*, 122(10), 2965–2976. <https://doi.org/10.1242/dev.122.10.2965>

Bibliography

- Bellande, K., Trinh, D., Gonzalez, A., Dubois, E., Petitot, A., Lucas, M., Champion, A., Gantet, P., Laplaze, L., & Guyomarc'h, S. (2022). PUCHI represses early meristem formation in developing lateral roots of *Arabidopsis thaliana*. *Journal of Experimental Botany*, 73(11), 3496–3510. <https://doi.org/10.1093/jxb/erac079>
- Bera, A., & Gupta, M. L. (2022). Microtubules in Microorganisms: How Tubulin Isotypes Contribute to Diverse Cytoskeletal Functions. *Frontiers in Cell and Developmental Biology*, 10. <https://doi.org/10.3389/fcell.2022.913809>
- Bindics, J., Khan, M., Uhse, S., Kogelmann, B., Baggely, L., Reumann, D., Ingole, K. D., Stirnberg, A., Rybecky, A., Darino, M., Navarrete, F., Doehlemann, G., & Djamei, A. (2022). Many ways to TOPLESS – manipulation of plant auxin signalling by a cluster of fungal effectors. *New Phytologist*, 236(4), 1455–1470. <https://doi.org/10.1111/nph.18315>
- Boch, J., & Bonas, U. (2010). Xanthomonas AvrBs3 Family-Type III Effectors: Discovery and Function. *Annual Review of Phytopathology*, 48(1), 419–436. <https://doi.org/10.1146/annurev-phyto-080508-081936>
- Boch, J., Bonas, U., & Lahaye, T. (2014). TAL effectors – pathogen strategies and plant resistance engineering. *New Phytologist*, 204(4), 823–832. <https://doi.org/10.1111/nph.13015>
- Bölker, M., Genin, S., Lehmler, C., & Kahmann, R. (1995). Genetic regulation of mating and dimorphism in *Ustilago maydis*. *Canadian Journal of Botany*, 73(S1), 320–325. <https://doi.org/10.1139/b95-262>
- Bölker, M., Urban, M., & Kahmann, R. (1992). The a mating type locus of *U. maydis* specifies cell signaling components. *Cell*, 68(3), 441–450. [https://doi.org/10.1016/0092-8674\(92\)90182-c](https://doi.org/10.1016/0092-8674(92)90182-c)
- Boller, T., & Felix, G. (2009). A renaissance of elicitors: Perception of microbe-associated molecular patterns and danger signals by pattern-recognition receptors. *Annual Review of Plant Biology*, 60, 379–406. <https://doi.org/10.1146/annurev.arplant.57.032905.105346>
- Bolton, M. D., van Esse, H. P., Vossen, J. H., de Jonge, R., Stergiopoulos, I., Stulemeijer, I. J. E., van den Berg, G. C. M., Borrás-Hidalgo, O., Dekker, H. L., de Koster, C. G., de Wit, P. J. G. M., Joosten, M. H. A. J., & Thomma, B. P. H. J. (2008). The novel *Cladosporium fulvum* lysin motif effector Ecp6 is a virulence factor with orthologues in other fungal species. *Molecular Microbiology*, 69(1), 119–136. <https://doi.org/10.1111/j.1365-2958.2008.06270.x>
- Boutrot, F., & Zipfel, C. (2017). Function, Discovery, and Exploitation of Plant Pattern Recognition Receptors for Broad-Spectrum Disease Resistance. *Annual Review of Phytopathology*, 55(1), 257–286. <https://doi.org/10.1146/annurev-phyto-080614-120106>
- Brefort, T., Doehlemann, G., Mendoza-Mendoza, A., Reissmann, S., Djamei, A., & Kahmann, R. (2009). *Ustilago maydis* as a Pathogen. *Annual Review of Phytopathology*, 47, 423–445. <https://doi.org/10.1146/annurev-phyto-080508-081923>
- Briesemeister, S., Rahnenführer, J., & Kohlbacher, O. (2010). YLoc—An interpretable web server for predicting subcellular localization. *Nucleic Acids Research*, 38(Web

- Server issue), W497-502. <https://doi.org/10.1093/nar/gkq477>
- Brown, R. L., Kazan, K., McGrath, K. C., Maclean, D. J., & Manners, J. M. (2003). A Role for the GCC-Box in Jasmonate-Mediated Activation of the PDF1.2 Gene of Arabidopsis. *Plant Physiology*, 132(2), 1020–1032. <https://doi.org/10.1104/pp.102.017814>
- Brown, S., & Spudich, J. (1979). Cytochalasin inhibits the rate of elongation of actin filament fragments. *The Journal of Cell Biology*, 83(3), 657–662. <https://doi.org/10.1083/jcb.83.3.657>
- Brutus, A., Sicilia, F., Maccone, A., Cervone, F., & De Lorenzo, G. (2010). A domain swap approach reveals a role of the plant wall-associated kinase 1 (WAK1) as a receptor of oligogalacturonides. *Proceedings of the National Academy of Sciences*, 107(20), 9452–9457. <https://doi.org/10.1073/pnas.1000675107>
- Büttner, M., & Singh, K. B. (1997). Arabidopsis thaliana ethylene-responsive element binding protein (AtEBP), an ethylene-inducible, GCC box DNA-binding protein interacts with an ocs element binding protein. *Proceedings of the National Academy of Sciences*, 94(11), 5961–5966. <https://doi.org/10.1073/pnas.94.11.5961>
- Cai, R., Lewis, J., Yan, S., Liu, H., Clarke, C. R., Campanile, F., Almeida, N. F., Studholme, D. J., Lindeberg, M., Schneider, D., Zaccardelli, M., Setubal, J. C., Morales-Lizcano, N. P., Bernal, A., Coaker, G., Baker, C., Bender, C. L., Leman, S., & Vinatzer, B. A. (2011). The Plant Pathogen Pseudomonas syringae pv. Tomato Is Genetically Monomorphic and under Strong Selection to Evade Tomato Immunity. *PLOS Pathogens*, 7(8), e1002130. <https://doi.org/10.1371/journal.ppat.1002130>
- Cao, H., Zhang, K., Li, W., Pang, X., Liu, P., Si, H., Zang, J., Xing, J., & Dong, J. (2023). ZmMYC7 directly regulates ZmERF147 to increase maize resistance to Fusarium graminearum. *The Crop Journal*, 11(1), 79–88. <https://doi.org/10.1016/j.cj.2022.05.006>
- Cao, Y., Liang, Y., Tanaka, K., Nguyen, C. T., Jedrzejczak, R. P., Joachimiak, A., & Stacey, G. (2014). The kinase LYK5 is a major chitin receptor in Arabidopsis and forms a chitin-induced complex with related kinase CERK1. *ELife*, 3, e03766. <https://doi.org/10.7554/eLife.03766>
- Carreón-Anguiano, K. G., Islas-Flores, I., Vega-Arreguín, J., Sáenz-Carbonell, L., & Canto-Canché, B. (2020). EffHunter: A Tool for Prediction of Effector Protein Candidates in Fungal Proteomic Databases. *Biomolecules*, 10(5), 712. <https://doi.org/10.3390/biom10050712>
- Causier, B., Ashworth, M., Guo, W., & Davies, B. (2012). The TOPLESS Interactome: A Framework for Gene Repression in Arabidopsis. *Plant Physiology*, 158(1), 423–438. <https://doi.org/10.1104/pp.111.186999>
- Chakravarthy, S., Tuori, R. P., D'Ascenzo, M. D., Fobert, P. R., Despres, C., & Martin, G. B. (2003). The tomato transcription factor Pti4 regulates defense-related gene expression via GCC box and non-GCC box cis elements. *The Plant Cell*, 15(12), 3033–3050. <https://doi.org/10.1105/tpc.017574>
- Chandler, J. W. (2018). Class VIIIb APETALA2 Ethylene Response Factors in Plant Development. *Trends in Plant Science*, 23(2), 151–162. <https://doi.org/10.1016/j.tplants.2017.09.016>

Bibliography

- Chandler, J. W., Cole, M., Flier, A., Grewe, B., & Werr, W. (2007). The AP2 transcription factors DORNROSCHEN and DORNROSCHEN-LIKE redundantly control Arabidopsis embryo patterning via interaction with PHAVOLUTA. *Development*, 134(9), 1653–1662. <https://doi.org/10.1242/dev.001016>
- Chaparro-Garcia, A., Schwizer, S., Sklenar, J., Yoshida, K., Petre, B., Bos, J. I. B., Schornack, S., Jones, A. M. E., Bozkurt, T. O., & Kamoun, S. (2015). Phytophthora infestans RXLR-WY Effector AVR3a Associates with Dynamin-Related Protein 2 Required for Endocytosis of the Plant Pattern Recognition Receptor FLS2. *PLOS ONE*, 10(9), e0137071. <https://doi.org/10.1371/journal.pone.0137071>
- Chappie, J. S., Acharya, S., Leonard, M., Schmid, S. L., & Dyda, F. (2010). G domain dimerization controls dynamin's assembly-stimulated GTPase activity. *Nature*, 465(7297), 435–440. <https://doi.org/10.1038/nature09032>
- Chen, C., Chen, H., Zhang, Y., Thomas, H. R., Frank, M. H., He, Y., & Xia, R. (2020). TBtools: An Integrative Toolkit Developed for Interactive Analyses of Big Biological Data. *Molecular Plant*, 13(8), 1194–1202. <https://doi.org/10.1016/j.molp.2020.06.009>
- Chen, H., Zou, Y., Shang, Y., Lin, H., Wang, Y., Cai, R., Tang, X., & Zhou, J.-M. (2008). Firefly Luciferase Complementation Imaging Assay for Protein-Protein Interactions in Plants. *Plant Physiology*, 146(2), 368–376. <https://doi.org/10.1104/pp.107.111740>
- Cheng, C., An, L., Li, F., Ahmad, W., Aslam, M., Ul Haq, M. Z., Yan, Y., & Ahmad, R. M. (2023). Wide-Range Portrayal of AP2/ERF Transcription Factor Family in Maize (Zea mays L.) Development and Stress Responses. *Genes*, 14(1), Article 1. <https://doi.org/10.3390/genes14010194>
- Chinchilla, D., Zipfel, C., Robatzek, S., Kemmerling, B., Nürnberger, T., Jones, J. D. G., Felix, G., & Boller, T. (2007). A flagellin-induced complex of the receptor FLS2 and BAK1 initiates plant defence. *Nature*, 448(7152), Article 7152. <https://doi.org/10.1038/nature05999>
- Christensen, J. J. (1963). Corn smut caused by Ustilago maydis. *Monographs. American Phytopathology Society*, 2. <https://doi.org/10.5962/bhl.title.62035>
- Chuck, G., Muszynski, M., Kellogg, E., Hake, S., & Schmidt, R. J. (2002). The Control of Spikelet Meristem Identity by the branched silkless1 Gene in Maize. *Science*, 298(5596), 1238–1241. <https://doi.org/10.1126/science.1076920>
- Ci, J., Wang, X., Wang, Q., Zhao, F., Yang, W., Cui, X., Jiang, L., Ren, X., & Yang, W. (2021). Genome-wide analysis of gibberellin-dioxygenases gene family and their responses to GA applications in maize. *PLoS ONE*, 16(5), e0250349. <https://doi.org/10.1371/journal.pone.0250349>
- Clarke, C. R., Chinchilla, D., Hind, S. R., Taguchi, F., Miki, R., Ichinose, Y., Martin, G. B., Leman, S., Felix, G., & Vinatzer, B. A. (2013). Allelic variation in two distinct Pseudomonas syringae flagellin epitopes modulates the strength of plant immune responses but not bacterial motility. *New Phytologist*, 200(3), 847–860. <https://doi.org/10.1111/nph.12408>
- Collemare, J., O'Connell, R., & Lebrun, M.-H. (2019). Nonproteinaceous effectors: The terra incognita of plant-fungal interactions. *New Phytologist*, 223(2), 590–596. <https://doi.org/10.1111/nph.15785>

- Collins, C. A. (1991). Dynamin: A novel microtubule-associated GTPase. *Trends in Cell Biology*, 1(2), 57–60. [https://doi.org/10.1016/0962-8924\(91\)90090-V](https://doi.org/10.1016/0962-8924(91)90090-V)
- Collins, J., O'Grady, K., Chen, S., & Gurley, W. (2019). The C-terminal WD40 repeats on the TOPLESS co-repressor function as a protein–protein interaction surface. *Plant Molecular Biology*, 100(1), 47–58. <https://doi.org/10.1007/s11103-019-00842-w>
- Couto, D., & Zipfel, C. (2016). Regulation of pattern recognition receptor signalling in plants. *Nature Reviews. Immunology*, 16(9), 537–552. <https://doi.org/10.1038/nri.2016.77>
- Darino, M., Chia, K. S., Marques, J., Aleksza, D., Soto-Jiménez, L. M., Saado, I., Uhse, S., Borg, M., Betz, R., Bindics, J., Zienkiewicz, K., Feussner, I., Petit-Houdenot, Y., & Djamei, A. (2020). Ustilago maydis effector Jsi1 interacts with Topless corepressor, hijacking plant jasmonate/ethylene signaling. *New Phytologist*, 229(6), 3393–3407. <https://doi.org/10.1111/nph.17116>
- Darino, M., Chia, K.-S., Marques, J., Aleksza, D., Soto-Jiménez, L. M., Saado, I., Uhse, S., Borg, M., Betz, R., Bindics, J., Zienkiewicz, K., Feussner, I., Petit-Houdenot, Y., & Djamei, A. (2021). Ustilago maydis effector Jsi1 interacts with Topless corepressor, hijacking plant jasmonate/ethylene signaling. *New Phytologist*, 229(6), 3393–3407. <https://doi.org/10.1111/nph.17116>
- De Boer, K., Tilleman, S., Pauwels, L., Vanden Bossche, R., De Sutter, V., Vanderhaeghen, R., Hilson, P., Hamill, J. D., & Goossens, A. (2011). APETALA2/ETHYLENE RESPONSE FACTOR and basic helix–loop–helix tobacco transcription factors cooperatively mediate jasmonate-elicited nicotine biosynthesis. *The Plant Journal*, 66(6), 1053–1065. <https://doi.org/10.1111/j.1365-313X.2011.04566.x>
- de Jonge, R., Peter van Esse, H., Kombrink, A., Shinya, T., Desaki, Y., Bours, R., van der Krol, S., Shibuya, N., Joosten, M. H. A. J., & Thomma, B. P. H. J. (2010). Conserved Fungal LysM Effector Ecp6 Prevents Chitin-Triggered Immunity in Plants. *Science*, 329(5994), 953–955. <https://doi.org/10.1126/science.1190859>
- de Lange, O., Schreiber, T., Schandry, N., Radeck, J., Braun, K. H., Koszinowski, J., Heuer, H., Strauß, A., & Lahaye, T. (2013). Breaking the DNA-binding code of Ralstonia solanacearum TAL effectors provides new possibilities to generate plant resistance genes against bacterial wilt disease. *New Phytologist*, 199(3), 773–786. <https://doi.org/10.1111/nph.12324>
- Dean, R., Van Kan, J. a. L., Pretorius, Z. A., Hammond-Kosack, K. E., Di Pietro, A., Spanu, P. D., Rudd, J. J., Dickman, M., Kahmann, R., Ellis, J., & Foster, G. D. (2012). The Top 10 fungal pathogens in molecular plant pathology. *Molecular Plant Pathology*, 13(4), 414–430. <https://doi.org/10.1111/j.1364-3703.2011.00783.x>
- Derbyshire, P., Ménard, D., Green, P., Saalbach, G., Buschmann, H., Lloyd, C. W., & Pesquet, E. (2015). Proteomic Analysis of Microtubule Interacting Proteins over the Course of Xylem Tracheary Element Formation in Arabidopsis. *The Plant Cell*, 27(10), 2709–2726. <https://doi.org/10.1105/tpc.15.00314>
- Ding, Y., Wang, J., Wang, J., Stierhof, Y.-D., Robinson, D. G., & Jiang, L. (2012). Unconventional protein secretion. *Trends in Plant Science*, 17(10), 606–615. <https://doi.org/10.1016/j.tplants.2012.06.004>
- Djamei, A., Schipper, K., Rabe, F., Ghosh, A., Vincon, V., Kahnt, J., Osorio, S., Tohge, T.,

Bibliography

- Fernie, A. R., Feussner, I., Feussner, K., Meinicke, P., Stierhof, Y.-D., Schwarz, H., Macek, B., Mann, M., & Kahmann, R. (2011). Metabolic priming by a secreted fungal effector. *Nature*, 478(7369), Article 7369. <https://doi.org/10.1038/nature10454>
- Dobin, A., Davis, C. A., Schlesinger, F., Drenkow, J., Zaleski, C., Jha, S., Batut, P., Chaisson, M., & Gingeras, T. R. (2013). STAR: Ultrafast universal RNA-seq aligner. *Bioinformatics* (Oxford, England), 29(1), 15–21. <https://doi.org/10.1093/bioinformatics/bts635>
- Doehlemann, G., Linde, K. van der, Aßmann, D., Schwammbach, D., Hof, A., Mohanty, A., Jackson, D., & Kahmann, R. (2009). Pep1, a Secreted Effector Protein of *Ustilago maydis*, Is Required for Successful Invasion of Plant Cells. *PLOS Pathogens*, 5(2), e1000290. <https://doi.org/10.1371/journal.ppat.1000290>
- Doehlemann, G., Reissmann, S., Assmann, D., Fleckenstein, M., & Kahmann, R. (2011). Two linked genes encoding a secreted effector and a membrane protein are essential for *Ustilago maydis*-induced tumour formation. *Molecular Microbiology*, 81(3), 751–766. <https://doi.org/10.1111/j.1365-2958.2011.07728.x>
- Doehlemann, G., Wahl, R., Horst, R. J., Voll, L. M., Usadel, B., Poree, F., Stitt, M., Pons-Kühnemann, J., Sonnewald, U., Kahmann, R., & Kämper, J. (2008). Reprogramming a maize plant: Transcriptional and metabolic changes induced by the fungal biotroph *Ustilago maydis*. *The Plant Journal*, 56(2), 181–195. <https://doi.org/10.1111/j.1365-313X.2008.03590.x>
- Dörfors, F., Holmquist, L., Dixelius, C., & Tzelepis, G. (2019). A LysM effector protein from the basidiomycete *Rhizoctonia solani* contributes to virulence through suppression of chitin-triggered immunity. *Molecular Genetics and Genomics*, 294(5), 1211–1218. <https://doi.org/10.1007/s00438-019-01573-9>
- Dutheil, J. Y., Mannhaupt, G., Schweizer, G., M.K. Sieber, C., Münsterkötter, M., Güldener, U., Schirawski, J., & Kahmann, R. (2016). A Tale of Genome Compartmentalization: The Evolution of Virulence Clusters in Smut Fungi. *Genome Biology and Evolution*, 8(3), 681–704. <https://doi.org/10.1093/gbe/evw026>
- Ehrhardt, D. W., & Shaw, S. L. (2006). Microtubule Dynamics and Organization in the Plant Cortical Array. *Annual Review of Plant Biology*, 57(1), 859–875. <https://doi.org/10.1146/annurev.arplant.57.032905.105329>
- Elliott, A., & Shaw, S. L. (2018). Update: Plant Cortical Microtubule Arrays. *Plant Physiology*, 176(1), 94–105. <https://doi.org/10.1104/pp.17.01329>
- Fang, D., Zhang, W., Ye, Z., Hu, F., Cheng, X., & Cao, J. (2023). The plant specific SHORT INTERNODES/STYLISH (SHI/STY) proteins: Structure and functions. *Plant Physiology and Biochemistry*, 194, 685–695. <https://doi.org/10.1016/j.plaphy.2022.12.018>
- FAO - News Article: New standards to curb the global spread of plant pests and diseases. (n.d.). Retrieved March 5, 2023, from <https://www.fao.org/news/story/en/item/1187738/icode/>
- Ferguson, S. M., & De Camilli, P. (2012). Dynamin, a membrane remodelling GTPase. *Nature Reviews. Molecular Cell Biology*, 13(2), 75–88. <https://doi.org/10.1038/nrm3266>
- Ficke, A., Cowger, C., Bergstrom, G., & Brodal, G. (2018). Understanding Yield Loss and

- Pathogen Biology to Improve Disease Management: Septoria Nodorum Blotch - A Case Study in Wheat. *Plant Disease*, 102(4), 696–707. <https://doi.org/10.1094/PDIS-09-17-1375-FE>
- Frederick M, A., Brent, R., E.Kingston, R., D. Moore, D., Seidman, J. G., A. Smith, J., & Struhl, K. (2001). *Current protocols in molecular biology*. <https://doi.org/10.1002/0471142727>
- Fujimoto, S. Y., Ohta, M., Usui, A., Shinshi, H., & Ohme-Takagi, M. (2000). Arabidopsis Ethylene-Responsive Element Binding Factors Act as Transcriptional Activators or Repressors of GCC Box-Mediated Gene Expression. *The Plant Cell*, 12(3), 393–405. <https://doi.org/10.2307/3870944>
- Gan, P., Ikeda, K., Irieda, H., Narusaka, M., O'Connell, R. J., Narusaka, Y., Takano, Y., Kubo, Y., & Shirasu, K. (2013). Comparative genomic and transcriptomic analyses reveal the hemibiotrophic stage shift of Colletotrichum fungi. *New Phytologist*, 197(4), 1236–1249. <https://doi.org/10.1111/nph.12085>
- Gao, F., Zhang, B.-S., Zhao, J.-H., Huang, J.-F., Jia, P.-S., Wang, S., Zhang, J., Zhou, J.-M., & Guo, H.-S. (2019). Deacetylation of chitin oligomers increases virulence in soil-borne fungal pathogens. *Nature Plants*, 5(11), Article 11. <https://doi.org/10.1038/s41477-019-0527-4>
- Gao, X., Shim, W.-B., Göbel, C., Kunze, S., Feussner, I., Meeley, R., Balint-Kurti, P., & Kolomiets, M. (2007). Disruption of a Maize 9-Lipoxygenase Results in Increased Resistance to Fungal Pathogens and Reduced Levels of Contamination with Mycotoxin Fumonisin. *Molecular Plant-Microbe Interactions®*, 20(8), 922–933. <https://doi.org/10.1094/MPMI-20-8-0922>
- Ge, S. X., Jung, D., & Yao, R. (2020). ShinyGO: A graphical gene-set enrichment tool for animals and plants. *Bioinformatics*, 36(8), 2628–2629. <https://doi.org/10.1093/bioinformatics/btz931>
- Gillissen, B., Bergemann, J., Sandmann, C., Schroeer, B., Bölker, M., & Kahmann, R. (1992). A two-component regulatory system for self/non-self recognition in Ustilago maydis. *Cell*, 68(4), 647–657. [https://doi.org/10.1016/0092-8674\(92\)90141-x](https://doi.org/10.1016/0092-8674(92)90141-x)
- Giraldo, M. C., Dagdas, Y. F., Gupta, Y. K., Mentlak, T. A., Yi, M., Martinez-Rocha, A. L., Saitoh, H., Terauchi, R., Talbot, N. J., & Valent, B. (2013). Two distinct secretion systems facilitate tissue invasion by the rice blast fungus Magnaporthe oryzae. *Nature Communications*, 4, 1996. <https://doi.org/10.1038/ncomms2996>
- Godfrey, D., Böhlenius, H., Pedersen, C., Zhang, Z., Emmersen, J., & Thordal-Christensen, H. (2010). Powdery mildew fungal effector candidates share N-terminal Y/F/WxC-motif. *BMC Genomics*, 11(1), 317. <https://doi.org/10.1186/1471-2164-11-317>
- Gómez-Gómez, L., & Boller, T. (2000). FLS2: An LRR Receptor-like Kinase Involved in the Perception of the Bacterial Elicitor Flagellin in Arabidopsis. *Molecular Cell*, 5(6), 1003–1011. [https://doi.org/10.1016/S1097-2765\(00\)80265-8](https://doi.org/10.1016/S1097-2765(00)80265-8)
- Goodson, H. V., & Jonasson, E. M. (2018). Microtubules and Microtubule-Associated Proteins. *Cold Spring Harbor Perspectives in Biology*, 10(6), a022608. <https://doi.org/10.1101/cshperspect.a022608>
- Grant, S. G., Jessee, J., Bloom, F. R., & Hanahan, D. (1990). Differential plasmid rescue

Bibliography

- from transgenic mouse DNAs into *Escherichia coli* methylation-restriction mutants. *Proceedings of the National Academy of Sciences of the United States of America*, 87(12), 4645–4649. <https://doi.org/10.1073/pnas.87.12.4645>
- Gryffroy, L., Ceulemans, E., Manosalva Pérez, N., Venegas-Molina, J., Jaramillo-Madrid, A. C., Rodrigues, S. D., De Milde, L., Jonckheere, V., Van Montagu, M., De Coninck, B., Vandepoele, K., Van Damme, P., & Goossens, A. (2023). Rhizogenic *Agrobacterium* protein RolB interacts with the TOPLESS repressor proteins to reprogram plant immunity and development. *Proceedings of the National Academy of Sciences*, 120(3), e2210300120. <https://doi.org/10.1073/pnas.2210300120>
- Gu, Y., Wildermuth, M. C., Chakravarthy, S., Loh, Y., Yang, C., He, X., Han, Y., & Martin, G. B. (2002). Tomato transcription factors *pti4*, *pti5*, and *pti6* activate defense responses when expressed in *Arabidopsis*. *The Plant Cell*, 14(4), 817–831. <https://doi.org/10.1105/tpc.000794>
- Gui, Y.-J., Chen, J.-Y., Zhang, D.-D., Li, N.-Y., Li, T.-G., Zhang, W.-Q., Wang, X.-Y., Short, D. P. G., Li, L., Guo, W., Kong, Z.-Q., Bao, Y.-M., Subbarao, K. V., & Dai, X.-F. (2017). *Verticillium dahliae* manipulates plant immunity by glycoside hydrolase 12 proteins in conjunction with carbohydrate-binding module 1. *Environmental Microbiology*, 19(5), 1914–1932. <https://doi.org/10.1111/1462-2920.13695>
- Guillen, K. de, Ortiz-Vallejo, D., Gracy, J., Fournier, E., Kroj, T., & Padilla, A. (2015). Structure Analysis Uncovers a Highly Diverse but Structurally Conserved Effector Family in Phytopathogenic Fungi. *PLOS Pathogens*, 11(10), e1005228. <https://doi.org/10.1371/journal.ppat.1005228>
- Guo, A.-Y., Chen, X., Gao, G., Zhang, H., Zhu, Q.-H., Liu, X.-C., Zhong, Y.-F., Gu, X., He, K., & Luo, J. (2008). PlantTFDB: A comprehensive plant transcription factor database. *Nucleic Acids Research*, 36(Database issue), D966–D969. <https://doi.org/10.1093/nar/gkm841>
- Guo, M., Kim, P., Li, G., Elowsky, C. G., & Alfano, J. R. (2016). A Bacterial Effector Co-opts Calmodulin to Target the Plant Microtubule Network. *Cell Host & Microbe*, 19(1), 67–78. <https://doi.org/10.1016/j.chom.2015.12.007>
- Haas, B. J., Kamoun, S., Zody, M. C., Jiang, R. H. Y., Handsaker, R. E., Cano, L. M., Grabherr, M., Kodira, C. D., Raffaele, S., Torto-Alalibo, T., Bozkurt, T. O., Ah-Fong, A. M. V., Alvarado, L., Anderson, V. L., Armstrong, M. R., Avrova, A., Baxter, L., Beynon, J., Boevink, P. C., ... Nusbaum, C. (2009). Genome sequence and analysis of the Irish potato famine pathogen *Phytophthora infestans*. *Nature*, 461(7262), Article 7262. <https://doi.org/10.1038/nature08358>
- Hacquard, S., Spaepen, S., Garrido-Oter, R., & Schulze-Lefert, P. (2017). Interplay Between Innate Immunity and the Plant Microbiota. *Annual Review of Phytopathology*, 55, 565–589. <https://doi.org/10.1146/annurev-phyto-080516-035623>
- Han, L., Li, Y., Wang, F.-X., Wang, W.-Y., Liu, J., Wu, J.-H., Zhong, N.-Q., Wu, S.-J., Jiao, G.-L., Wang, H.-Y., & Xia, G.-X. (2019). The Cotton Apoplastic Protein CRR1 Stabilizes Chitinase 28 to Facilitate Defense against the Fungal Pathogen *Verticillium dahliae*. *The Plant Cell*, 31(2), 520–536. <https://doi.org/10.1105/tpc.18.00390>
- Han, Q., Qi, J., Hao, G., Zhang, C., Wang, C., Dirk, L. M. A., Downie, A. B., & Zhao, T. (2020).

- ZmDREB1A Regulates RAFFINOSE SYNTHASE Controlling Raffinose Accumulation and Plant Chilling Stress Tolerance in Maize. *Plant and Cell Physiology*, 61(2), 331–341. <https://doi.org/10.1093/pcp/pcz200>
- Han, X., Altegoer, F., Steinchen, W., Binnebesel, L., Schuhmacher, J., Glatte, T., Giammarinaro, P. I., Djamei, A., Rensing, S. A., Reissmann, S., Kahmann, R., & Bange, G. (2019). A kiwellin disarms the metabolic activity of a secreted fungal virulence factor. *Nature*, 565(7741), Article 7741. <https://doi.org/10.1038/s41586-018-0857-9>
- Hanahan, D. (1983). Studies on transformation of Escherichia coli with plasmids. *Journal of Molecular Biology*, 166(4), 557–580. [https://doi.org/10.1016/S0022-2836\(83\)80284-8](https://doi.org/10.1016/S0022-2836(83)80284-8)
- Hao, D., Ohme-Takagi, M., & Sarai, A. (1998). Unique mode of GCC box recognition by the DNA-binding domain of ethylene-responsive element-binding factor (ERF domain) in plant. *The Journal of Biological Chemistry*, 273(41), 26857–26861. <https://doi.org/10.1074/jbc.273.41.26857>
- Hartmann, H. A., Kahmann, R., & Bölker, M. (1996). The pheromone response factor coordinates filamentous growth and pathogenicity in Ustilago maydis. *The EMBO Journal*, 15(7), 1632–1641. <https://doi.org/10.1002/j.1460-2075.1996.tb00508.x>
- Harvey, S., Kumari, P., Lapin, D., Griebel, T., Hickman, R., Guo, W., Zhang, R., Parker, J. E., Beynon, J., Denby, K., & Steinbrenner, J. (2020). Downy Mildew effector HaRxL21 interacts with the transcriptional repressor TOPLESS to promote pathogen susceptibility. *PLOS Pathogens*, 16(8), e1008835. <https://doi.org/10.1371/journal.ppat.1008835>
- Hashimoto, T. (2015). Microtubules in Plants. *The Arabidopsis Book / American Society of Plant Biologists*, 13, e0179. <https://doi.org/10.1199/tab.0179>
- He, B., Shi, P., Lv, Y., Gao, Z., & Chen, G. (2020). Gene coexpression network analysis reveals the role of SRS genes in senescence leaf of maize (Zea mays L.). *Journal of Genetics*, 99, 3.
- Heese, A., Hann, D. R., Gimenez-Ibanez, S., Jones, A. M. E., He, K., Li, J., Schroeder, J. I., Peck, S. C., & Rathjen, J. P. (2007). The receptor-like kinase SERK3/BAK1 is a central regulator of innate immunity in plants. *Proceedings of the National Academy of Sciences*, 104(29), 12217–12222. <https://doi.org/10.1073/pnas.0705306104>
- Heimel, K., Scherer, M., Vranes, M., Wahl, R., Pothiratana, C., Schuler, D., Vincon, V., Finkernagel, F., Flor-Parra, I., & Kämper, J. (2010). The Transcription Factor Rbf1 Is the Master Regulator for b-Mating Type Controlled Pathogenic Development in Ustilago maydis. *PLOS Pathogens*, 6(8), e1001035. <https://doi.org/10.1371/journal.ppat.1001035>
- Hemetsberger, C., Herrberger, C., Zechmann, B., Hillmer, M., & Doeblemann, G. (2012). The Ustilago maydis Effector Pep1 Suppresses Plant Immunity by Inhibition of Host Peroxidase Activity. *PLOS Pathogens*, 8(5), e1002684. <https://doi.org/10.1371/journal.ppat.1002684>
- Hemetsberger, C., Mueller, A. N., Matei, A., Herrberger, C., Hensel, G., Kumlehn, J., Mishra, B., Sharma, R., Thines, M., Hückelhoven, R., & Doeblemann, G. (2015). The fungal core effector Pep1 is conserved across smuts of dicots and monocots. *New*

Bibliography

- Phytologist*, 206(3), 1116–1126. <https://doi.org/10.1111/nph.13304>
- Hind, S. R., Strickler, S. R., Boyle, P. C., Dunham, D. M., Bao, Z., O'Doherty, I. M., Baccile, J. A., Hoki, J. S., Viox, E. G., Clarke, C. R., Vinatzer, B. A., Schroeder, F. C., & Martin, G. B. (2016). Tomato receptor FLAGELLIN-SENSING 3 binds flgII-28 and activates the plant immune system. *Nature Plants*, 2(9), Article 9. <https://doi.org/10.1038/nplants.2016.128>
- Hiratsu, K., Matsui, K., Koyama, T., & Ohme Takagi, M. (2003). Dominant repression of target genes by chimeric repressors that include the EAR motif, a repression domain, in Arabidopsis. *The Plant Journal*, 34(5), 733–739. <https://doi.org/10.1046/j.1365-313X.2003.01759.x>
- Hirota, A., Kato, T., Fukaki, H., Aida, M., & Tasaka, M. (2007). The auxin-regulated AP2/EREBP gene PUCHI is required for morphogenesis in the early lateral root primordium of Arabidopsis. *The Plant Cell*, 19(7), 2156–2168. <https://doi.org/10.1105/tpc.107.050674>
- Höfgen, R., & Willmitzer, L. (1988). Storage of competent cells for Agrobacterium transformation. *Nucleic Acids Research*, 16(20), 9877. <https://doi.org/10.1093/nar/16.20.9877>
- Holliday, R. (1961). The genetics of Ustilago maydis. *Genetics Research*, 2(2), 204–230. <https://doi.org/10.1017/S0016672300000719>
- Holliday, R. (1974). Ustilago maydis. Bacteria, Bacteriophages, and Fungi. *New York: Plenum*, 1, 575–595. https://doi.org/10.1007/978-1-4899-1710-2_31
- Hong, Z., Bednarek, S. Y., Blumwald, E., Hwang, I., Jurgens, G., Menzel, D., Osteryoung, K. W., Raikhel, N. V., Shinozaki, K., Tsutsumi, N., & Verma, D. P. S. (2003). A unified nomenclature for Arabidopsis dynamin-related large GTPases based on homology and possible functions. *Plant Molecular Biology*, 53(3), 261–265. <https://doi.org/10.1023/b:plan.0000007000.29697.81>
- Hong, Z., Geisler-Lee, C. J., Zhang, Z., & Verma, D. P. S. (2003). Phragmoplastin dynamics: Multiple forms, microtubule association and their roles in cell plate formation in plants. *Plant Molecular Biology*, 53(3), 297–312. <https://doi.org/10.1023/B:PLAN.0000006936.50532.3a>
- Hou, S., Liu, D., & He, P. (2021). Phytocytokines function as immunological modulators of plant immunity. *Stress Biology*, 1(1). <https://doi.org/10.1007/s44154-021-00009-y>
- Hu, W., Ren, Q., Chen, Y., Xu, G., & Qian, Y. (2021). Genome-wide identification and analysis of WRKY gene family in maize provide insights into regulatory network in response to abiotic stresses. *BMC Plant Biology*, 21(1), 427. <https://doi.org/10.1186/s12870-021-03206-z>
- Hu, Y., Xie, Q., & Chua, N.-H. (2003). The Arabidopsis Auxin-Inducible Gene ARGOS Controls Lateral Organ Size. *The Plant Cell*, 15(9), 1951–1961. <https://doi.org/10.1105/tpc.013557>
- Huang, C.-Y., Wang, H., Hu, P., Hamby, R., & Jin, H. (2019). Small RNAs – Big Players in Plant-Microbe Interactions. *Cell Host & Microbe*, 26(2), 173–182. <https://doi.org/10.1016/j.chom.2019.07.021>
- Hufford, M. B., Seetharam, A. S., Woodhouse, M. R., Chougule, K. M., Ou, S., Liu, J., Ricci,

- W. A., Guo, T., Olson, A., Qiu, Y., Della Coletta, R., Tittes, S., Hudson, A. I., Marand, A. P., Wei, S., Lu, Z., Wang, B., Tello-Ruiz, M. K., Piri, R. D., ... Dawe, R. K. (2021). De novo assembly, annotation, and comparative analysis of 26 diverse maize genomes. *Science*, 373(6555), 655–662. <https://doi.org/10.1126/science.abg5289>
- Hurlburt, N. K., Chen, L.-H., Stergiopoulos, I., & Fisher, A. J. (2018). Structure of the *Cladosporium fulvum* Avr4 effector in complex with (GlcNAc)₆ reveals the ligand-binding mechanism and uncouples its intrinsic function from recognition by the Cf-4 resistance protein. *PLOS Pathogens*, 14(8), e1007263. <https://doi.org/10.1371/journal.ppat.1007263>
- Hussey, P. J., Haas, N., Hunsperger, J., Larkin, J., Snustad, D. P., & Silflow, C. D. (1990). The beta-tubulin gene family in *Zea mays*: Two differentially expressed beta-tubulin genes. *Plant Molecular Biology*, 15(6), 957–972. <https://doi.org/10.1007/BF00039438>
- Hutin, M., Pérez-Quintero, A. L., Lopez, C., & Szurek, B. (2015). MorTAL Kombat: The story of defense against TAL effectors through loss-of-susceptibility. *Frontiers in Plant Science*, 6. <https://doi.org/10.3389/fpls.2015.00535>
- Iizasa, E., Mitsutomi, M., & Nagano, Y. (2010). Direct Binding of a Plant LysM Receptor-like Kinase, LysM RLK1/CERK1, to Chitin in Vitro. *The Journal of Biological Chemistry*, 285(5), 2996–3004. <https://doi.org/10.1074/jbc.M109.027540>
- Ikeda, Y., Banno, H., Niu, Q.-W., Howell, S. H., & Chua, N.-H. (2006). The ENHANCER OF SHOOT REGENERATION 2 gene in *Arabidopsis* Regulates CUP-SHAPED COTYLEDON 1 at the Transcriptional Level and Controls Cotyledon Development. *Plant and Cell Physiology*, 47(11), 1443–1456. <https://doi.org/10.1093/pcp/pcl023>
- Ito, J., Fukaki, H., Onoda, M., Li, L., Li, C., Tasaka, M., & Furutani, M. (2016). Auxin-dependent compositional change in Mediator in ARF7- and ARF19-mediated transcription. *Proceedings of the National Academy of Sciences*, 113(23), 6562–6567. <https://doi.org/10.1073/pnas.1600739113>
- James, P., Halladay, J., & Craig, E. A. (1996). Genomic libraries and a host strain designed for highly efficient two-hybrid selection in yeast. *Genetics*, 144(4), 1425–1436. <https://doi.org/10.1093/genetics/144.4.1425>
- Jashni, M. K., Dols, I. H. M., Iida, Y., Boeren, S., Beenen, H. G., Mehrabi, R., Collemare, J., & de Wit, P. J. G. M. (2015). Synergistic Action of a Metalloprotease and a Serine Protease from *Fusarium oxysporum* f. Sp. *Lycopersici* Cleaves Chitin-Binding Tomato Chitinases, Reduces Their Antifungal Activity, and Enhances Fungal Virulence. *Molecular Plant-Microbe Interactions: MPMI*, 28(9), 996–1008. <https://doi.org/10.1094/MPMI-04-15-0074-R>
- Jefferson, R. A., Kavanagh, T. A., & Bevan, M. W. (1987). GUS fusions: Beta-glucuronidase as a sensitive and versatile gene fusion marker in higher plants. *The EMBO Journal*, 6(13), 3901–3907. <https://doi.org/10.1002/j.1460-2075.1987.tb02730.x>
- Jiang, R. H. Y., Tripathy, S., Govers, F., & Tyler, B. M. (2008). RXLR effector reservoir in two *Phytophthora* species is dominated by a single rapidly evolving superfamily with more than 700 members. *Proceedings of the National Academy of Sciences*,

Bibliography

- 105(12), 4874–4879. <https://doi.org/10.1073/pnas.0709303105>
- Jones, J. D. G., & Dangl, J. L. (2006). The plant immune system. *Nature*, 444(7117), Article 7117. <https://doi.org/10.1038/nature05286>
- Juarez, M. T., Twigg, R. W., & Timmermans, M. C. P. (2004). Specification of adaxial cell fate during maize leaf development. *Development*, 131(18), 4533–4544. <https://doi.org/10.1242/dev.01328>
- Jumper, J., Evans, R., Pritzel, A., Green, T., Figurnov, M., Ronneberger, O., Tunyasuvunakool, K., Bates, R., Žídek, A., Potapenko, A., Bridgland, A., Meyer, C., Kohl, S. A. A., Ballard, A. J., Cowie, A., Romera-Paredes, B., Nikolov, S., Jain, R., Adler, J., ... Hassabis, D. (2021). Highly accurate protein structure prediction with AlphaFold. *Nature*, 596(7873), Article 7873. <https://doi.org/10.1038/s41586-021-03819-2>
- Kadota, Y., Sklenar, J., Derbyshire, P., Stransfeld, L., Asai, S., Ntoukakis, V., Jones, J. D., Shirasu, K., Menke, F., Jones, A., & Zipfel, C. (2014). Direct Regulation of the NADPH Oxidase RBOHD by the PRR-Associated Kinase BIK1 during Plant Immunity. *Molecular Cell*, 54(1), 43–55. <https://doi.org/10.1016/j.molcel.2014.02.021>
- Kagale, S., & Rozwadowski, K. (2011). EAR motif-mediated transcriptional repression in plants. *Epigenetics*, 6(2), 141–146. <https://doi.org/10.4161/epi.6.2.13627>
- Kaku, H., Nishizawa, Y., Ishii-Minami, N., Akimoto-Tomiyama, C., Dohmae, N., Takio, K., Minami, E., & Shibuya, N. (2006). Plant cells recognize chitin fragments for defense signaling through a plasma membrane receptor. *Proceedings of the National Academy of Sciences*, 103(29), 11086–11091. <https://doi.org/10.1073/pnas.0508882103>
- Kämper, J. (2004). A PCR-based system for highly efficient generation of gene replacement mutants in *Ustilago maydis*. *Molecular Genetics and Genomics: MGG*, 271(1), 103–110. <https://doi.org/10.1007/s00438-003-0962-8>
- Kämper, J., Kahmann, R., Bölker, M., Ma, L.-J., Brefort, T., Saville, B. J., Banuett, F., Kronstad, J. W., Gold, S. E., Müller, O., Perlin, M. H., Wösten, H. A. B., de Vries, R., Ruiz-Herrera, J., Reynaga-Peña, C. G., Sneltselaar, K., McCann, M., Pérez-Martín, J., Feldbrügge, M., ... Birren, B. W. (2006). Insights from the genome of the biotrophic fungal plant pathogen *Ustilago maydis*. *Nature*, 444(7115), Article 7115. <https://doi.org/10.1038/nature05248>
- Kämper, J., Reichmann, M., Romeis, T., Bölker, M., & Kahmann, R. (1995). Multiallelic recognition: Nonspecific-dependent dimerization of the bE and bW homeodomain proteins in *ustilago maydis*. *Cell*, 81(1), 73–83. [https://doi.org/10.1016/0092-8674\(95\)90372-0](https://doi.org/10.1016/0092-8674(95)90372-0)
- Kang, B.-H., Rancour, D. M., & Bednarek, S. Y. (2003). The dynamin-like protein ADL1C is essential for plasma membrane maintenance during pollen maturation. *The Plant Journal*, 35(1), 1–15. <https://doi.org/10.1046/j.1365-313X.2003.01775.x>
- Kang, Y., Jelenska, J., Cecchini, N. M., Li, Y., Lee, M. W., Kovar, D. R., & Greenberg, J. T. (2014). HopW1 from *Pseudomonas syringae* Disrupts the Actin Cytoskeleton to Promote Virulence in *Arabidopsis*. *PLoS Pathogens*, 10(6), e1004232. <https://doi.org/10.1371/journal.ppat.1004232>
- Kar, U. P., Dey, H., & Rahaman, A. (2021). Cardiolipin targets a dynamin-related protein to the nuclear membrane. *ELife*, 10, e64416. <https://doi.org/10.7554/eLife.64416>

- Karim, Md. R., Hirota, A., Kwiatkowska, D., Tasaka, M., & Aida, M. (2009). A Role for Arabidopsis PUCHI in Floral Meristem Identity and Bract Suppression. *The Plant Cell*, 21(5), 1360–1372. <https://doi.org/10.1105/tpc.109.067025>
- Kato, H., Nemoto, K., Shimizu, M., Abe, A., Asai, S., Ishihama, N., Matsuoka, S., Daimon, T., Ojika, M., Kawakita, K., Onai, K., Shirasu, K., Yoshida, M., Ishiura, M., Takemoto, D., Takano, Y., & Terauchi, R. (2022). Recognition of pathogen-derived sphingolipids in Arabidopsis. *Science*, 376(6595), 857–860. <https://doi.org/10.1126/science.abn0650>
- Kay, S., Hahn, S., Marois, E., Hause, G., & Bonas, U. (2007). A bacterial effector acts as a plant transcription factor and induces a cell size regulator. *Science (New York, N.Y.)*, 318(5850), 648–651. <https://doi.org/10.1126/science.1144956>
- Kazan, K., & Lyons, R. (2014). Intervention of Phytohormone Pathways by Pathogen Effectors. *The Plant Cell*, 26(6), 2285–2309. <https://doi.org/10.1105/tpc.114.125419>
- Ke, J., Ma, H., Gu, X., Thelen, A., Brunzelle, J. S., Li, J., Xu, H. E., & Melcher, K. (2015). Structural basis for recognition of diverse transcriptional repressors by the TOPLESS family of corepressors. *Science Advances*, 1(6), e1500107. <https://doi.org/10.1126/sciadv.1500107>
- Keon, J. P. R., White, G. A., & Hargreaves, J. A. (1991). Isolation, characterization and sequence of a gene conferring resistance to the systemic fungicide carboxin from the maize smut pathogen, Ustilago maydis. *Current Genetics*, 19(6), 475–481. <https://doi.org/10.1007/BF00312739>
- Khang, C. H., Berruyer, R., Giraldo, M. C., Kankanala, P., Park, S.-Y., Czymmek, K., Kang, S., & Valent, B. (2010). Translocation of Magnaporthe oryzae Effectors into Rice Cells and Their Subsequent Cell-to-Cell Movement[W][OA]. *The Plant Cell*, 22(4), 1388–1403. <https://doi.org/10.1105/tpc.109.069666>
- Kim, S., Kim, C.-Y., Park, S.-Y., Kim, K.-T., Jeon, J., Chung, H., Choi, G., Kwon, S., Choi, J., Jeon, J., Jeon, J.-S., Khang, C. H., Kang, S., & Lee, Y.-H. (2020). Two nuclear effectors of the rice blast fungus modulate host immunity via transcriptional reprogramming. *Nature Communications*, 11(1), Article 1. <https://doi.org/10.1038/s41467-020-19624-w>
- Koeck, M., Hardham, A. R., & Dodds, P. N. (2011). The role of effectors of biotrophic and hemibiotrophic fungi in infection. *Cellular Microbiology*, 13(12), 1849–1857. <https://doi.org/10.1111/j.1462-5822.2011.01665.x>
- Kohorn, B. D., Johansen, S., Shishido, A., Todorova, T., Martinez, R., Defeo, E., & Obregon, P. (2009). Pectin activation of MAP kinase and gene expression is WAK2 dependent. *The Plant Journal: For Cell and Molecular Biology*, 60(6), 974–982. <https://doi.org/10.1111/j.1365-313X.2009.04016.x>
- Komatsu, M., Chujo, A., Nagato, Y., Shimamoto, K., & Kyojuka, J. (2003). FRIZZY PANICLE is required to prevent the formation of axillary meristems and to establish floral meristem identity in rice spikelets. *Development*, 130(16), 3841–3850. <https://doi.org/10.1242/dev.00564>
- Kombrink, A., Rovenich, H., Shi-Kunne, X., Rojas-Padilla, E., van den Berg, G. C. M., Domazakis, E., de Jonge, R., Valkenburg, D., Sánchez-Vallet, A., Seidl, M. F., & Thomma,

Bibliography

- B. P. H. J. (2017). *Verticillium dahliae* LysM effectors differentially contribute to virulence on plant hosts. *Molecular Plant Pathology*, 18(4), 596–608. <https://doi.org/10.1111/mpp.12520>
- Koncz, C., & Schell, J. (1986). The promoter of TL-DNA gene 5 controls the tissue-specific expression of chimaeric genes carried by a novel type of *Agrobacterium* binary vector. *Molecular and General Genetics MGG*, 204(3), 383–396. <https://doi.org/10.1007/BF00331014>
- Konopka, C. A., Backues, S. K., & Bednarek, S. Y. (2008). Dynamics of Arabidopsis Dynamin-Related Protein 1C and a Clathrin Light Chain at the Plasma Membrane. *The Plant Cell*, 20(5), 1363–1380. <https://doi.org/10.1105/tpc.108.059428>
- Köster, P., DeFalco, T. A., & Zipfel, C. (2022). Ca²⁺ signals in plant immunity. *The EMBO Journal*, 41(12), e110741. <https://doi.org/10.15252/emboj.2022110741>
- Kourelis, J., & van der Hoorn, R. A. L. (2018). Defended to the Nines: 25 Years of Resistance Gene Cloning Identifies Nine Mechanisms for R Protein Function. *The Plant Cell*, 30(2), 285–299. <https://doi.org/10.1105/tpc.17.00579>
- Krishnaswamy, S., Verma, S., Rahman, M. H., & Kav, N. N. V. (2011). Functional characterization of four APETALA2-family genes (RAP2.6, RAP2.6L, DREB19 and DREB26) in Arabidopsis. *Plant Molecular Biology*, 75(1), 107–127. <https://doi.org/10.1007/s11103-010-9711-7>
- Krogan, N. T., Hogan, K., & Long, J. A. (2012). APETALA2 negatively regulates multiple floral organ identity genes in Arabidopsis by recruiting the co-repressor TOPLESS and the histone deacetylase HDA19. *Development*, 139(22), 4180–4190. <https://doi.org/10.1242/dev.085407>
- Kronstad, J. W., & Leong, S. A. (1989). Isolation of two alleles of the b locus of *Ustilago maydis*. *Proceedings of the National Academy of Sciences of the United States of America*, 86(3), 978–982. <https://doi.org/10.1073/pnas.86.3.978>
- Kronstad, J. W., & Leong, S. A. (1990). The b mating-type locus of *Ustilago maydis* contains variable and constant regions. *Genes & Development*, 4(8), 1384–1395. <https://doi.org/10.1101/gad.4.8.1384>
- Kunst, L., Klenz, J. E., Martinez-Zapater, J., & Haughn, G. W. (1989). AP2 Gene Determines the Identity of Perianth Organs in Flowers of Arabidopsis thaliana. *The Plant Cell*, 1(12), 1195–1208. <https://doi.org/10.1105/tpc.1.12.1195>
- Kunze, G., Zipfel, C., Robatzek, S., Niehaus, K., Boller, T., & Felix, G. (2004). The N terminus of bacterial elongation factor Tu elicits innate immunity in Arabidopsis plants. *The Plant Cell*, 16(12), 3496–3507. <https://doi.org/10.1105/tpc.104.026765>
- Kushnirov, V. V. (2000). Rapid and reliable protein extraction from yeast. *Yeast (Chichester, England)*, 16(9), 857–860. [https://doi.org/10.1002/1097-0061\(20000630\)16:9<857::AID-YEA561>3.0.CO;2-B](https://doi.org/10.1002/1097-0061(20000630)16:9<857::AID-YEA561>3.0.CO;2-B)
- Laemmli, U. K. (1970). Cleavage of structural proteins during the assembly of the head of bacteriophage T4. *Nature*, 227(5259), 680–685. <https://doi.org/10.1038/227680a0>
- Lanver, D., Mendoza-Mendoza, A., Brachmann, A., & Kahmann, R. (2010). Sho1 and Msb2-Related Proteins Regulate Appressorium Development in the Smut Fungus

- Ustilago maydis. *The Plant Cell*, 22(6), 2085–2101. <https://doi.org/10.1105/tpc.109.073734>
- Lanver, D., Müller, A. N., Happel, P., Schweizer, G., Haas, F. B., Franitza, M., Pellegrin, C., Reissmann, S., Altmüller, J., Rensing, S. A., & Kahmann, R. (2018). The Biotrophic Development of *Ustilago maydis* Studied by RNA-Seq Analysis. *The Plant Cell*, 30(2), 300–323. <https://doi.org/10.1105/tpc.17.00764>
- Lanver, D., Tollot, M., Schweizer, G., Presti, L., Reissmann, S., Ma, L. S., Schuster, M., Tanaka, S., Liang, L., Ludwig, N., & Kahmann, R. (2017). *Ustilago maydis* effectors and their impact on virulence. *Nature Reviews Microbiology*, 15. <https://doi.org/10.1038/nrmicro.2017.33>
- Lazar, N., Mesarich, C. H., Petit-Houdenot, Y., Talbi, N., Sierra-Gallay, I. L. de la, Zélie, E., Blondeau, K., Gracy, J., Ollivier, B., Blaise, F., Rouxel, T., Balesdent, M.-H., Idnurm, A., Tilbeurgh, H. van, & Fudal, I. (2022). A new family of structurally conserved fungal effectors displays epistatic interactions with plant resistance proteins. *PLOS Pathogens*, 18(7), e1010664. <https://doi.org/10.1371/journal.ppat.1010664>
- Lee, A. H.-Y., Hurley, B., Felsensteiner, C., Yea, C., Ckurshumova, W., Bartetzko, V., Wang, P. W., Quach, V., Lewis, J. D., Liu, Y. C., Börnke, F., Angers, S., Wilde, A., Guttman, D. S., & Desveaux, D. (2012). A Bacterial Acetyltransferase Destroys Plant Microtubule Networks and Blocks Secretion. *PLOS Pathogens*, 8(2), e1002523. <https://doi.org/10.1371/journal.ppat.1002523>
- Lee, M.-S., An, J.-H., & Cho, H.-T. (2016). Biological and molecular functions of two EAR motifs of *Arabidopsis* IAA7. *Journal of Plant Biology*, 59(1), 24–32. <https://doi.org/10.1007/s12374-016-0453-1>
- Leydon, A. R., Wang, W., Gala, H. P., Gilmour, S., Juarez-Solis, S., Zahler, M. L., Zemke, J. E., Zheng, N., & Nemhauser, J. L. (2021). Repression by the *Arabidopsis* TOPLESS corepressor requires association with the core mediator complex. *ELife*, 10, e66739. <https://doi.org/10.7554/eLife.66739>
- Li, G.-B., Fan, J., Wu, J.-L., He, J.-X., Liu, J., Shen, S., Gishkori, Z. G. N., Hu, X.-H., Zhu, Y., Zhou, S.-X., Ji, Y.-P., Pu, M., Zhao, J.-H., Zhao, Z.-X., Wang, H., Zhang, J.-W., Huang, Y.-Y., Li, Y., Huang, F., & Wang, W.-M. (2021). The Flower-Infecting Fungus *Ustilaginoides virens* Subverts Plant Immunity by Secreting a Chitin-Binding Protein. *Frontiers in Plant Science*, 12, 733245. <https://doi.org/10.3389/fpls.2021.733245>
- Li, P., & Day, B. (2019). Battlefield Cytoskeleton: Turning the Tide on Plant Immunity. *Molecular Plant-Microbe Interactions*®, 32(1), 25–34. <https://doi.org/10.1094/MPMI-07-18-0195-FI>
- Liao, Y., Smyth, G. K., & Shi, W. (2014). featureCounts: An efficient general purpose program for assigning sequence reads to genomic features. *Bioinformatics (Oxford, England)*, 30(7), 923–930. <https://doi.org/10.1093/bioinformatics/btt656>
- Liu, X., Galli, M., Camehl, I., & Gallavotti, A. (2019). RAMOSA1 ENHANCER LOCUS2-Mediated Transcriptional Repression Regulates Vegetative and Reproductive Architecture. *Plant Physiology*, 179(1), 348–363. <https://doi.org/10.1104/pp.18.00913>
- Lo Presti, L., Lanver, D., Schweizer, G., Tanaka, S., Liang, L., Tollot, M., Zuccaro, A., Reissmann, S., & Kahmann, R. (2015). Fungal Effectors and Plant Susceptibility.

Bibliography

- Annual Review of Plant Biology*, 66(1), 513–545. <https://doi.org/10.1146/annurev-arplant-043014-114623>
- Lo, S.-F., Yang, S.-Y., Chen, K.-T., Hsing, Y.-I., Zeevaart, J. A. D., Chen, L.-J., & Yu, S.-M. (2008). A Novel Class of Gibberellin 2-Oxidases Control Semidwarfism, Tillering, and Root Development in Rice. *The Plant Cell*, 20(10), 2603–2618. <https://doi.org/10.1105/tpc.108.060913>
- Long, J. A., Ohno, C., Smith, Z. R., & Meyerowitz, E. M. (2006). TOPLESS Regulates Apical Embryonic Fate in Arabidopsis. *Science*, 312(5779), 1520–1523. <https://doi.org/10.1126/science.1123841>
- Long, J. A., Woody, S., Poethig, S., Meyerowitz, E. M., & Barton, M. K. (2002). Transformation of shoots into roots in Arabidopsis embryos mutant at the TOPLESS locus. *Development*, 129(12), 2797–2806. <https://doi.org/10.1242/dev.129.12.2797>
- Lorenzo, O., Piqueras, R., Sánchez Serrano, J. J., & Solano, R. (2003). ETHYLENE RESPONSE FACTOR1 Integrates Signals from Ethylene and Jasmonate Pathways in Plant Defense. *The Plant Cell*, 15(1), 165–178. <https://doi.org/10.1105/tpc.007468>
- Love, M. I., Huber, W., & Anders, S. (2014). Moderated estimation of fold change and dispersion for RNA-seq data with DESeq2. *Genome Biology*, 15(12), 550. <https://doi.org/10.1186/s13059-014-0550-8>
- Ludwig, N., Reissmann, S., Schipper, K., Gonzalez, C., Assmann, D., Glatter, T., Moretti, M., Ma, L.-S., Rexer, K.-H., Snetselaar, K., & Kahmann, R. (2021). A cell surface-exposed protein complex with an essential virulence function in Ustilago maydis. *Nature Microbiology*, 6(6), Article 6. <https://doi.org/10.1038/s41564-021-00896-x>
- Ma, H., Duan, J., Ke, J., He, Y., Gu, X., Xu, T., Yu, H., Wang, Y., Brunzelle, J. S., Jiang, Y., Rothbart, S. B., Xu, H. E., Li, J., & Melcher, K. (2017). A D53 repression motif induces oligomerization of TOPLESS corepressors and promotes assembly of a corepressor-nucleosome complex. *Science Advances*, 3(6), e1601217. <https://doi.org/10.1126/sciadv.1601217>
- Ma, L.-S., Tsai, W.-L., Damei, F. A., Kalunke, R. M., Xu, M.-Y., Lin, Y.-H., & Lee, H.-C. (2023). Maize Antifungal Protein AFP1 Elevates Fungal Chitin Levels by Targeting Chitin Deacetylases and Other Glycoproteins. *MBio*, 14(2), e00093-23. <https://doi.org/10.1128/mbio.00093-23>
- Ma, L.-S., Wang, L., Trippel, C., Mendoza-Mendoza, A., Ullmann, S., Moretti, M., Carsten, A., Kahnt, J., Reissmann, S., Zechmann, B., Bange, G., & Kahmann, R. (2018). The Ustilago maydis repetitive effector Rsp3 blocks the antifungal activity of mannose-binding maize proteins. *Nature Communications*, 9(1), Article 1. <https://doi.org/10.1038/s41467-018-04149-0>
- Ma, Y., Yang, C., He, Y., Tian, Z., & Li, J. (2017). Rice OVATE family protein 6 regulates plant development and confers resistance to drought and cold stresses. *Journal of Experimental Botany*, 68(17), 4885–4898. <https://doi.org/10.1093/jxb/erx309>
- Ma, Z., Song, T., Zhu, L., Ye, W., Wang, Y., Shao, Y., Dong, S., Zhang, Z., Dou, D., Zheng, X., Tyler, B. M., & Wang, Y. (2015a). A Phytophthora sojae Glycoside Hydrolase 12 Protein Is a Major Virulence Factor during Soybean Infection and Is Recognized as

- a PAMP. *The Plant Cell*, 27(7), 2057–2072. <https://doi.org/10.1105/tpc.15.00390>
- Ma, Z., Song, T., Zhu, L., Ye, W., Wang, Y., Shao, Y., Dong, S., Zhang, Z., Dou, D., Zheng, X., Tyler, B. M., & Wang, Y. (2015b). A *Phytophthora sojae* Glycoside Hydrolase 12 Protein Is a Major Virulence Factor during Soybean Infection and Is Recognized as a PAMP[OPEN]. *The Plant Cell*, 27(7), 2057–2072. <https://doi.org/10.1105/tpc.15.00390>
- Macho, A. P., & Zipfel, C. (2014). Plant PRRs and the activation of innate immune signaling. *Molecular Cell*, 54(2), 263–272. <https://doi.org/10.1016/j.molcel.2014.03.028>
- Maeda, K., Nakata, T., Noda, Y., Sato-Yoshitake, R., & Hirokawa, N. (1992). Interaction of dynamin with microtubules: Its structure and GTPase activity investigated by using highly purified dynamin. *Molecular Biology of the Cell*, 3(10), 1181–1194. <https://doi.org/10.1091/mbc.3.10.1181>
- Mano, S., Nakamori, C., Kondo, M., Hayashi, M., & Nishimura, M. (2004). An Arabidopsis dynamin-related protein, DRP3A, controls both peroxisomal and mitochondrial division. *The Plant Journal*, 38(3), 487–498. <https://doi.org/10.1111/j.1365-313X.2004.02063.x>
- Marois, E., Van den Ackerveken, G., & Bonas, U. (2002). The xanthomonas type III effector protein AvrBs3 modulates plant gene expression and induces cell hypertrophy in the susceptible host. *Molecular Plant-Microbe Interactions: MPMI*, 15(7), 637–646. <https://doi.org/10.1094/MPMI.2002.15.7.637>
- Martin, M. (2011). Cutadapt removes adapter sequences from high-throughput sequencing reads. *EMBnet.Journal*, 17(1), Article 1. <https://doi.org/10.14806/ej.17.1.200>
- Martin-Arevalillo, R., Nanao, M. H., Larrieu, A., Vinos-Poyo, T., Mast, D., Galvan-Ampudia, C., Brunoud, G., Vernoux, T., Dumas, R., & Parcy, F. (2017). Structure of the Arabidopsis TOPLESS corepressor provides insight into the evolution of transcriptional repression. *Proceedings of the National Academy of Sciences of the United States of America*, 114(30), 8107–8112. <https://doi.org/10.1073/pnas.1703054114>
- Martinez, P., Dixit, R., Balkunde, R. S., Zhang, A., O’Leary, S. E., Brakke, K. A., & Rasmussen, C. G. (2020). TANGLED1 mediates microtubule interactions that may promote division plane positioning in maize. *The Journal of Cell Biology*, 219(8), e201907184. <https://doi.org/10.1083/jcb.201907184>
- Martínez-Cruz, J., Romero, D., Hierrezuelo, J., Thon, M., de Vicente, A., & Pérez-García, A. (2021). Effectors with chitinase activity (EWCAs), a family of conserved, secreted fungal chitinases that suppress chitin-triggered immunity. *The Plant Cell*, 33(4), 1319–1340. <https://doi.org/10.1093/plcell/koab011>
- Maruyama, Y., Yamoto, N., Suzuki, Y., Chiba, Y., Yamazaki, K., Sato, T., & Yamaguchi, J. (2013). The Arabidopsis transcriptional repressor ERF9 participates in resistance against necrotrophic fungi. *Plant Science*, 213, 79–87. <https://doi.org/10.1016/j.plantsci.2013.08.008>
- Masaru, O. T., & Hideaki, S. (1995). Ethylene-inducible DNA binding proteins that interact with an ethylene-responsive element. *The Plant Cell*, 7(2), 173–182.

Bibliography

- <https://doi.org/10.1105/tpc.7.2.173>
- Matei, A., Ernst, C., Günl, M., Thiele, B., Altmüller, J., Walbot, V., Usadel, B., & Doehlemann, G. (2018). How to make a tumour: Cell type specific dissection of Ustilago maydis-induced tumour development in maize leaves. *New Phytologist*, 217(4), 1681–1695. <https://doi.org/10.1111/nph.14960>
- McGrath, K. C., Dombrecht, B., Manners, J. M., Schenk, P. M., Edgar, C. I., Maclean, D. J., Scheible, W.-R., Udvardi, M. K., & Kazan, K. (2005). Repressor- and activator-type ethylene response factors functioning in jasmonate signaling and disease resistance identified via a genome-wide screen of Arabidopsis transcription factor gene expression. *Plant Physiology*, 139(2), 949–959. <https://doi.org/10.1104/pp.105.068544>
- Meng, X., & Zhang, S. (2013). MAPK Cascades in Plant Disease Resistance Signaling. *Annual Review of Phytopathology*, 51(1), 245–266. <https://doi.org/10.1146/annurev-phyto-082712-102314>
- Mentlak, T. A., Kombrink, A., Shinya, T., Ryder, L. S., Otomo, I., Saitoh, H., Terauchi, R., Nishizawa, Y., Shibuya, N., Thomma, B. P. H. J., & Talbot, N. J. (2012). Effector-mediated suppression of chitin-triggered immunity by magnaporthe oryzae is necessary for rice blast disease. *The Plant Cell*, 24(1), 322–335. <https://doi.org/10.1105/tpc.111.092957>
- Misas Villamil, J. C., Mueller, A. N., Demir, F., Meyer, U., Ökmen, B., Schulze Hüynck, J., Breuer, M., Dauben, H., Win, J., Huesgen, P. F., & Doehlemann, G. (2019). A fungal substrate mimicking molecule suppresses plant immunity via an inter-kingdom conserved motif. *Nature Communications*, 10(1), Article 1. <https://doi.org/10.1038/s41467-019-09472-8>
- Miya, A., Albert, P., Shinya, T., Desaki, Y., Ichimura, K., Shirasu, K., Narusaka, Y., Kawakami, N., Kaku, H., & Shibuya, N. (2007). CERK1, a LysM receptor kinase, is essential for chitin elicitor signaling in Arabidopsis. *Proceedings of the National Academy of Sciences*, 104(49), 19613–19618. <https://doi.org/10.1073/pnas.0705147104>
- Moffat, C. S., Ingle, R. A., Wathugala, D. L., Saunders, N. J., Knight, H., & Knight, M. R. (2012). ERF5 and ERF6 Play Redundant Roles as Positive Regulators of JA/Et-Mediated Defense against Botrytis cinerea in Arabidopsis. *PLOS ONE*, 7(4), e35995. <https://doi.org/10.1371/journal.pone.0035995>
- Mueller, A. N., Ziemann, S., Treitschke, S., Aßmann, D., & Doehlemann, G. (2013). Compatibility in the Ustilago maydis–Maize Interaction Requires Inhibition of Host Cysteine Proteases by the Fungal Effector Pit2. *PLOS Pathogens*, 9(2), e1003177. <https://doi.org/10.1371/journal.ppat.1003177>
- Mur, L. A. J., Kenton, P., Lloyd, A. J., Ougham, H., & Prats, E. (2008). The hypersensitive response; the centenary is upon us but how much do we know? *Journal of Experimental Botany*, 59(3), 501–520. <https://doi.org/10.1093/jxb/erm239>
- Nakamura, M., Naoi, K., Shoji, T., & Hashimoto, T. (2004). Low concentrations of propyzamide and oryzalin alter microtubule dynamics in Arabidopsis epidermal cells. *Plant & Cell Physiology*, 45(9), 1330–1334. <https://doi.org/10.1093/pcp/pch300>

- Navarrete, F., Gallei, M., Kornienko, A. E., Saado, I., Khan, M., Chia, K. S., Darino, M. A., Bindics, J., & Djamei, A. (2022a). TOPLESS promotes plant immunity by repressing auxin signaling and is targeted by the fungal effector Naked1. *Plant Communications*, 3(2), 100269. <https://doi.org/10.1016/j.xplc.2021.100269>
- Navarrete, F., Gallei, M., Kornienko, A. E., Saado, I., Khan, M., Chia, K.-S. S., Darino, M. A., Bindics, J., & Djamei, A. (2022b). TOPLESS promotes plant immunity by repressing auxin signaling and is targeted by the fungal effector Naked1. *Plant Communications*, 3. <https://doi.org/10.1016/j.xplc.2021.100269>
- Navarrete, F., Grujic, N., Stirnberg, A., Saado, I., Aleksza, D., Gallei, M., Adi, H., Alcântara, A., Khan, M., Bindics, J., Trujillo, M., & Djamei, A. (2021). The Pleiades are a cluster of fungal effectors that inhibit host defenses. *PLOS Pathogens*, 17(6), e1009641. <https://doi.org/10.1371/journal.ppat.1009641>
- Ngou, B. P. M., Ahn, H.-K., Ding, P., & Jones, J. D. G. (2021). Mutual potentiation of plant immunity by cell-surface and intracellular receptors. *Nature*, 592(7852), Article 7852. <https://doi.org/10.1038/s41586-021-03315-7>
- Ngou, B. P. M., Ding, P., & Jones, J. D. G. (2022). Thirty years of resistance: Zig-zag through the plant immune system. *The Plant Cell*, 34(5), 1447–1478. <https://doi.org/10.1093/plcell/koac041>
- Nickel, W., & Rabouille, C. (2009). Mechanisms of regulated unconventional protein secretion. *Nature Reviews. Molecular Cell Biology*, 10(2), 148–155. <https://doi.org/10.1038/nrm2617>
- Nogales, E. (2000). Structural Insights into Microtubule Function. *Annual Review of Biochemistry*, 69(1), 277–302. <https://doi.org/10.1146/annurev.biochem.69.1.277>
- Nogales, E., Wolf, S. G., & Downing, K. H. (1998). Structure of the $\alpha\beta$ tubulin dimer by electron crystallography. *Nature*, 391(6663), Article 6663. <https://doi.org/10.1038/34465>
- Nottensteiner, M., Zechmann, B., McCollum, C., & Hückelhoven, R. (2018). A barley powdery mildew fungus non-autonomous retrotransposon encodes a peptide that supports penetration success on barley. *Journal of Experimental Botany*, 69(15), 3745–3758. <https://doi.org/10.1093/jxb/ery174>
- O’Connell, R. J., Thon, M. R., Hacquard, S., Amyotte, S. G., Kleemann, J., Torres, M. F., Damm, U., Buiate, E. A., Epstein, L., Alkan, N., Altmüller, J., Alvarado-Balderrama, L., Bauser, C. A., Becker, C., Birren, B. W., Chen, Z., Choi, J., Crouch, J. A., Duvick, J. P., ... Vaillancourt, L. J. (2012). Lifestyle transitions in plant pathogenic *Colletotrichum* fungi deciphered by genome and transcriptome analyses. *Nature Genetics*, 44(9), Article 9. <https://doi.org/10.1038/ng.2372>
- Oh, E., Zhu, J. Y., Ryu, H., Hwang, I., & Wang, Z. Y. (2014). TOPLESS mediates brassinosteroid-induced transcriptional repression through interaction with BZR1. *Nature Communications*, 5(1), Article 1. <https://doi.org/10.1038/ncomms5140>
- Ohta, M., Matsui, K., Hiratsu, K., Shinshi, H., & Ohme-Takagi, M. (2001). Repression Domains of Class II ERF Transcriptional Repressors Share an Essential Motif for Active Repression. *The Plant Cell*, 13(8), 1959–1968. <https://doi.org/10.1105/TPC.010127>
- Okamuro, J. K., Caster, B., Villarreal, R., Van Montagu, M., & Jofuku, K. D. (1997). The

Bibliography

- AP2 domain of APETALA2 defines a large new family of DNA binding proteins in Arabidopsis. *Proceedings of the National Academy of Sciences of the United States of America*, 94(13), 7076–7081. <https://doi.org/10.1073/pnas.94.13.7076>
- Ökmen, B., Jaeger, E., Schilling, L., Finke, N., Klemd, A., Lee, Y. J., Wemhöner, R., Pauly, M., Neumann, U., & Doehlemann, G. (2022). A conserved enzyme of smut fungi facilitates cell-to-cell extension in the plant bundle sheath. *Nature Communications*, 13(1), Article 1. <https://doi.org/10.1038/s41467-022-33815-7>
- Ökmen, B., Kemmerich, B., Hilbig, D., Wemhöner, R., Aschenbroich, J., Perrar, A., Huesgen, P. F., Schipper, K., & Doehlemann, G. (2018). Dual function of a secreted fungalsin metalloprotease in Ustilago maydis. *The New Phytologist*, 220(1), 249–261. <https://doi.org/10.1111/nph.15265>
- Oliveira-Garcia, E., Tamang, T. M., Park, J., Dalby, M., Martin-Urdiroz, M., Rodriguez Herrero, C., Vu, A. H., Park, S., Talbot, N. J., & Valent, B. (2023). Clathrin-mediated endocytosis facilitates the internalization of Magnaporthe oryzae effectors into rice cells. *The Plant Cell*, koad094. <https://doi.org/10.1093/plcell/koad094>
- Otegui, M. S., Mastronarde, D. N., Kang, B.-H., Bednarek, S. Y., & Staehelin, L. A. (2001). Three-Dimensional Analysis of Syncytial-Type Cell Plates during Endosperm Cellularization Visualized by High Resolution Electron Tomography[W]. *The Plant Cell*, 13(9), 2033–2051. <https://doi.org/10.1105/tpc.13.9.2033>
- Otegui, M. S., Verbrugghe, K. J., & Skop, A. R. (2005). Midbodies and phragmoplasts: Analogous structures involved in cytokinesis. *Trends in Cell Biology*, 15(8), 404–413. <https://doi.org/10.1016/j.tcb.2005.06.003>
- Outram, M. A., Figueroa, M., Sperschneider, J., Williams, S. J., & Dodds, P. N. (2022). Seeing is believing: Exploiting advances in structural biology to understand and engineer plant immunity. *Current Opinion in Plant Biology*, 67, 102210. <https://doi.org/10.1016/j.pbi.2022.102210>
- Pathi, K. M., Rink, P., Budhagatapalli, N., Betz, R., Saado, I., Hiekel, S., Becker, M., Djamei, A., & Kumlehn, J. (2020). Engineering Smut Resistance in Maize by Site-Directed Mutagenesis of LIPOXYGENASE 3. *Frontiers in Plant Science*, 11. <https://doi.org/10.3389/fpls.2020.543895>
- Petersen, T. N., Brunak, S., von Heijne, G., & Nielsen, H. (2011). SignalP 4.0: Discriminating signal peptides from transmembrane regions. *Nature Methods*, 8(10), Article 10. <https://doi.org/10.1038/nmeth.1701>
- Petutschnig, E. K., Jones, A. M. E., Serazetdinova, L., Lipka, U., & Lipka, V. (2010). The lysin motif receptor-like kinase (LysM-RLK) CERK1 is a major chitin-binding protein in Arabidopsis thaliana and subject to chitin-induced phosphorylation. *The Journal of Biological Chemistry*, 285(37), 28902–28911. <https://doi.org/10.1074/jbc.M110.116657>
- Plant, A. R., Larrieu, A., & Causier, B. (2021). Repressor for hire! The vital roles of TOPLESS-mediated transcriptional repression in plants. *New Phytologist*, 231(3), 963–973. <https://doi.org/10.1111/nph.17428>
- Praefcke, G. J. K., & McMahon, H. T. (2004). The dynamin superfamily: Universal membrane tubulation and fission molecules? *Nature Reviews Molecular Cell Biology*,

- 5(2), Article 2. <https://doi.org/10.1038/nrm1313>
- Pré, M., Atallah, M., Champion, A., De Vos, M., Pieterse, C. M. J., & Memelink, J. (2008). The AP2/ERF Domain Transcription Factor ORA59 Integrates Jasmonic Acid and Ethylene Signals in Plant Defense. *Plant Physiology*, 147(3), 1347–1357. <https://doi.org/10.1104/pp.108.117523>
- Qi, J., Wang, J., Gong, Z., & Zhou, J.-M. (2017). Apoplastic ROS signaling in plant immunity. *Current Opinion in Plant Biology*, 38, 92–100. <https://doi.org/10.1016/j.pbi.2017.04.022>
- Qiu, X., Kong, L., Chen, H., Lin, Y., Tu, S., Wang, L., Chen, Z., Zeng, M., Xiao, J., Yuan, P., Qiu, M., Wang, Y., Ye, W., Duan, K., Dong, S., & Wang, Y. (2023). The Phytophthora sojae nuclear effector PsAvh110 targets a host transcriptional complex to modulate plant immunity. *The Plant Cell*, 35(1), 574–597. <https://doi.org/10.1093/plcell/koac300>
- Rabouille, C. (2017). Pathways of Unconventional Protein Secretion. *Trends in Cell Biology*, 27(3), 230–240. <https://doi.org/10.1016/j.tcb.2016.11.007>
- Rabouille, C., Malhotra, V., & Nickel, W. (2012). Diversity in unconventional protein secretion. *Journal of Cell Science*, 125(Pt 22), 5251–5255. <https://doi.org/10.1242/jcs.103630>
- Raffaele, S., & Kamoun, S. (2012). Genome evolution in filamentous plant pathogens: Why bigger can be better. *Nature Reviews Microbiology*, 10(6), Article 6. <https://doi.org/10.1038/nrmicro2790>
- Redkar, A., & Dohlemann, G. (2016). Ustilago maydis Virulence Assays in Maize. *Bio-Protocol Journal*, 6(6). <https://en.bio-protocol.org/en/bpdetail?id=1760&type=0>
- Redkar, A., Hoser, R., Schilling, L., Zechmann, B., Krzymowska, M., Walbot, V., & Dohlemann, G. (2015). A Secreted Effector Protein of Ustilago maydis Guides Maize Leaf Cells to Form Tumors. *The Plant Cell*, 27(4), 1332–1351. <https://doi.org/10.1105/tpc.114.131086>
- Riedl, J., Crevenna, A. H., Kessenbrock, K., Yu, J. H., Neukirchen, D., Bista, M., Bradke, F., Jenne, D., Holak, T. A., Werb, Z., Sixt, M., & Wedlich-Soldner, R. (2008). Lifeact: A versatile marker to visualize F-actin. *Nature Methods*, 5(7), 605–607. <https://doi.org/10.1038/nmeth.1220>
- Rieu, I., Eriksson, S., Powers, S. J., Gong, F., Griffiths, J., Woolley, L., Benlloch, R., Nilsson, O., Thomas, S. G., Hedden, P., & Phillips, A. L. (2008). Genetic Analysis Reveals That C19-GA 2-Oxidation Is a Major Gibberellin Inactivation Pathway in Arabidopsis. *The Plant Cell*, 20(9), 2420–2436. <https://doi.org/10.1105/tpc.108.058818>
- Robinson, M. D., McCarthy, D. J., & Smyth, G. K. (2010). edgeR: A Bioconductor package for differential expression analysis of digital gene expression data. *Bioinformatics*, 26(1), 139–140. <https://doi.org/10.1093/bioinformatics/btp616>
- Rushton, P. J., Somssich, I. E., Ringler, P., & Shen, Q. J. (2010). WRKY transcription factors. *Trends in Plant Science*, 15(5), 247–258. <https://doi.org/10.1016/j.tplants.2010.02.006>
- Saado, I., Chia, K.-S., Betz, R., Alcântara, A., Pettkó-Szandtner, A., Navarrete, F., D'Auria, J. C., Kolomiets, M. V., Melzer, M., Feussner, I., & Djamei, A. (2022). Effector-mediated relocalization of a maize lipoxygenase protein triggers susceptibility to Ustilago maydis. *The Plant Cell*, 34(7), 2785–2805. <https://doi.org/10.1093/plcell/koac105>

Bibliography

- Sakuma, Y., Liu, Q., Dubouzet, J. G., Abe, H., Shinozaki, K., & Yamaguchi-Shinozaki, K. (2002). DNA-Binding Specificity of the ERF/AP2 Domain of Arabidopsis DREBs, Transcription Factors Involved in Dehydration- and Cold-Inducible Gene Expression. *Biochemical and Biophysical Research Communications*, 290(3), 998–1009. <https://doi.org/10.1006/bbrc.2001.6299>
- Sambrook, J., Fritsch, E. F., & Maniatis, T. (1989). Molecular cloning: A laboratory manual. *Cold Spring Harbor Laboratory, Ed. 2*. [https://doi.org/10.1016/0167-7799\(91\)90068-s](https://doi.org/10.1016/0167-7799(91)90068-s)
- Sánchez-Vallet, A., Saleem-Batcha, R., Kombrink, A., Hansen, G., Valkenburg, D.-J., Thomma, B. P., & Mesters, J. R. (2013). Fungal effector Ecp6 outcompetes host immune receptor for chitin binding through intrachain LysM dimerization. *ELife*, 2, e00790. <https://doi.org/10.7554/eLife.00790>
- Schilling, L., Matei, A., Redkar, A., Walbot, V., & Doehlemann, G. (2014). Virulence of the maize smut *Ustilago maydis* is shaped by organ-specific effectors. *Molecular Plant Pathology*, 15(8), 780–789. <https://doi.org/10.1111/mpp.12133>
- Schirawski, J., Böhnert, H. U., Steinberg, G., Snetselaar, K., Adamikowa, L., & Kahmann, R. (2005). Endoplasmic Reticulum Glucosidase II Is Required for Pathogenicity of *Ustilago maydis*. *The Plant Cell*, 17(12), 3532–3543. <https://doi.org/10.1105/tpc.105.036285>
- Schirawski, J., Mannhaupt, G., Münch, K., Brefort, T., Schipper, K., Doehlemann, G., Di Stasio, M., Rössel, N., Mendoza-Mendoza, A., Pester, D., Müller, O., Winterberg, B., Meyer, E., Ghareeb, H., Wollenberg, T., Münsterkötter, M., Wong, P., Walter, M., Stukenbrock, E., ... Kahmann, R. (2010). Pathogenicity Determinants in Smut Fungi Revealed by Genome Comparison. *Science*, 330(6010), 1546–1548. <https://doi.org/10.1126/science.1195330>
- Schmitz, L., McCotter, S., Kretschmer, M., Kronstad, J. W., & Heindel, K. (2018). Transcripts and tumors: Regulatory and metabolic programming during biotrophic phytopathogenesis. *F1000Research*, 7, F1000 Faculty Rev-1812. <https://doi.org/10.12688/f1000research.16404.1>
- Schomburg, F. M., Bizzell, C. M., Lee, D. J., Zeevaart, J. A. D., & Amasino, R. M. (2003). Overexpression of a Novel Class of Gibberellin 2-Oxidases Decreases Gibberellin Levels and Creates Dwarf Plants. *The Plant Cell*, 15(1), 151–163. <https://doi.org/10.1105/tpc.005975>
- Schornack, S., van Damme, M., Bozkurt, T. O., Cano, L. M., Smoker, M., Thines, M., Gaulin, E., Kamoun, S., & Huitema, E. (2010). Ancient class of translocated oomycete effectors targets the host nucleus. *Proceedings of the National Academy of Sciences*, 107(40), 17421–17426. <https://doi.org/10.1073/pnas.1008491107>
- Schreiner, P., Chen, X., Husnjak, K., Randles, L., Zhang, N., Elsasser, S., Finley, D., Dikic, I., Walters, K. J., & Groll, M. (2008). Ubiquitin docking at the proteasome through a novel pleckstrin-homology domain interaction. *Nature*, 453(7194), Article 7194. <https://doi.org/10.1038/nature06924>
- Schurack, S., Depotter, J. R. L., Gupta, D., Thines, M., & Doehlemann, G. (2021). Comparative transcriptome profiling identifies maize line specificity of fungal effectors in the maize–*Ustilago maydis* interaction. *The Plant Journal*, 106(3), 733–

752. <https://doi.org/10.1111/tpj.15195>
- Schuster, M., Schweizer, G., & Kahmann, R. (2018). Comparative analyses of secreted proteins in plant pathogenic smut fungi and related basidiomycetes. *Fungal Genetics and Biology*, 112, 21–30. <https://doi.org/10.1016/j.fgb.2016.12.003>
- Schuster, M., Schweizer, G., Reissmann, S., & Kahmann, R. (2016). Genome editing in *Ustilago maydis* using the CRISPR-Cas system. *Fungal Genetics and Biology: FG & B*, 89, 3–9. <https://doi.org/10.1016/j.fgb.2015.09.001>
- Seitner, D., Uhse, S., Gallei, M., & Djamei, A. (2018). The core effector Cce1 is required for early infection of maize by *Ustilago maydis*. *Molecular Plant Pathology*, 19(10), 2277–2287. <https://doi.org/10.1111/mpp.12698>
- Seong, K., & Krasileva, K. V. (2021). Computational Structural Genomics Unravels Common Folds and Novel Families in the Secretome of Fungal Phytopathogen *Magnaporthe oryzae*. *Molecular Plant-Microbe Interactions®*, 34(11), 1267–1280. <https://doi.org/10.1094/MPMI-03-21-0071-R>
- Seong, K., & Krasileva, K. V. (2023). Prediction of effector protein structures from fungal phytopathogens enables evolutionary analyses. *Nature Microbiology*, 8(1), Article 1. <https://doi.org/10.1038/s41564-022-01287-6>
- Sessa, G., Meller, Y., & Fluhr, R. (1995). A GCC element and a G-box motif participate in ethylene-induced expression of the PRB-1b gene. *Plant Molecular Biology*, 28(1), 145–153. <https://doi.org/10.1007/BF00042046>
- Shi, J., Drummond, B. J., Wang, H., Archibald, R. L., & Habben, J. E. (2016). Maize and Arabidopsis ARGOS Proteins Interact with Ethylene Receptor Signaling Complex, Supporting a Regulatory Role for ARGOS in Ethylene Signal Transduction. *Plant Physiology*, 171(4), 2783–2797. <https://doi.org/10.1104/pp.16.00347>
- Shi, J., Habben, J. E., Archibald, R. L., Drummond, B. J., Chamberlin, M. A., Williams, R. W., Lafitte, H. R., & Weers, B. P. (2015). Overexpression of ARGOS Genes Modifies Plant Sensitivity to Ethylene, Leading to Improved Drought Tolerance in Both Arabidopsis and Maize[OPEN]. *Plant Physiology*, 169(1), 266–282. <https://doi.org/10.1104/pp.15.00780>
- Shi, W., Stolze, S. C., Nakagami, H., Misas Villamil, J. C., Saur, I. M. L., & Doehlemann, G. (2023). Combination of in vivo proximity labeling and co-immunoprecipitation identifies the host target network of a tumor-inducing effector in the fungal maize pathogen *Ustilago maydis*. *Journal of Experimental Botany*, erad188. <https://doi.org/10.1093/jxb/erad188>
- Shimono, M., Lu, Y.-J., Porter, K., Kvitko, B. H., Henty-Ridilla, J., Creason, A., He, S. Y., Chang, J. H., Staiger, C. J., & Day, B. (2016). The *Pseudomonas syringae* Type III Effector HopG1 Induces Actin Remodeling to Promote Symptom Development and Susceptibility during Infection1[OPEN]. *Plant Physiology*, 171(3), 2239–2255. <https://doi.org/10.1104/pp.16.01593>
- Singh, N. K., Badet, T., Abraham, L., & Croll, D. (2021). Rapid sequence evolution driven by transposable elements at a virulence locus in a fungal wheat pathogen. *BMC Genomics*, 22(1), 393. <https://doi.org/10.1186/s12864-021-07691-2>
- Skibbe, D. S., Doehlemann, G., Fernandes, J., & Walbot, V. (2010). Maize Tumors Caused by *Ustilago maydis* Require Organ-Specific Genes in Host and Pathogen. *Science*,

Bibliography

- 328(5974), 89–92. <https://doi.org/10.1126/science.1185775>
- Smertenko, A., Hewitt, S. L., Jacques, C. N., Kacprzyk, R., Liu, Y., Marcec, M. J., Moyo, L., Ogden, A., Oung, H. M., Schmidt, S., & Serrano-Romero, E. A. (2018). Phragmoplast microtubule dynamics—A game of zones. *Journal of Cell Science*, 131(2), jcs203331. <https://doi.org/10.1242/jcs.203331>
- Snetselaar, K. M., & Mims, C. W. (1992). Sporidial Fusion and Infection of Maize Seedlings by the Smut Fungus *Ustilago Maydis*. *Mycologia*, 84(2), 193–203. <https://doi.org/10.1080/00275514.1992.12026126>
- Snetselaar, K. M., & Mims, C. W. (1993). Infection of maize stigmas by *Ustilago maydis*: Light and electron microscopy. *Phytopathology (USA)*. <https://doi.org/10.1094/phyto-83-843>
- Solano, R., Stepanova, A., Chao, Q., & Ecker, J. R. (1998). Nuclear events in ethylene signaling: A transcriptional cascade mediated by ETHYLENE-INSENSITIVE3 and ETHYLENE-RESPONSE-FACTOR1. *Genes & Development*, 12(23), 3703–3714. <https://doi.org/10.1101/gad.12.23.3703>
- Solberg, N., & Krauss, S. (2013). Luciferase assay to study the activity of a cloned promoter DNA fragment. *Methods in Molecular Biology (Clifton, N.J.)*, 977, 65–78. https://doi.org/10.1007/978-1-62703-284-1_6
- Sonah, H., Deshmukh, R. K., & Bélanger, R. R. (2016). Computational Prediction of Effector Proteins in Fungi: Opportunities and Challenges. *Frontiers in Plant Science*, 7. <https://doi.org/10.3389/fpls.2016.00126>
- Southern, E. M. (1975). Detection of specific sequences among DNA fragments separated by gel electrophoresis. *Journal of Molecular Biology*, 98(3), 503–517. [https://doi.org/10.1016/s0022-2836\(75\)80083-0](https://doi.org/10.1016/s0022-2836(75)80083-0)
- Sperschneider, J., Catanzariti, A.-M., DeBoer, K., Petre, B., Gardiner, D. M., Singh, K. B., Dodds, P. N., & Taylor, J. M. (2017). LOCALIZER: Subcellular localization prediction of both plant and effector proteins in the plant cell. *Scientific Reports*, 7(1), Article 1. <https://doi.org/10.1038/srep44598>
- Sperschneider, J., Dodds, P. N., Gardiner, D. M., Manners, J. M., Singh, K. B., & Taylor, J. M. (2015). Advances and Challenges in Computational Prediction of Effectors from Plant Pathogenic Fungi. *PLOS Pathogens*, 11(5), e1004806. <https://doi.org/10.1371/journal.ppat.1004806>
- Sperschneider, J., Dodds, P. N., Singh, K. B., & Taylor, J. M. (2018). ApoplastP: Prediction of effectors and plant proteins in the apoplast using machine learning. *New Phytologist*, 217(4), 1764–1778. <https://doi.org/10.1111/nph.14946>
- Sperschneider, J., Gardiner, D. M., Dodds, P. N., Tini, F., Covarelli, L., Singh, K. B., Manners, J. M., & Taylor, J. M. (2016). EffectorP: Predicting fungal effector proteins from secretomes using machine learning. *New Phytologist*, 210(2), 743–761. <https://doi.org/10.1111/nph.13794>
- Stergiopoulos, I., & de Wit, P. J. G. M. (2009). Fungal Effector Proteins. *Annual Review of Phytopathology*, 47(1), 233–263. <https://doi.org/10.1146/annurev.phyto.112408.132637>
- Sun, X., Ma, Y., Yang, C., & Li, J. (2020). Rice OVATE family protein 6 regulates leaf angle by modulating secondary cell wall biosynthesis. *Plant Molecular Biology*, 104(3),

- 249–261. <https://doi.org/10.1007/s11103-020-01039-2>
- Sun, Y., Li, L., Macho, A. P., Han, Z., Hu, Z., Zipfel, C., Zhou, J.-M., & Chai, J. (2013). Structural Basis for flg22-Induced Activation of the Arabidopsis FLS2-BAK1 Immune Complex. *Science*, 342(6158), 624–628. <https://doi.org/10.1126/science.1243825>
- Sun, Y., Wang, Y., Zhang, X., Chen, Z., Xia, Y., Wang, L., Sun, Y., Zhang, M., Xiao, Y., Han, Z., Wang, Y., & Chai, J. (2022). Plant receptor-like protein activation by a microbial glycoside hydrolase. *Nature*, 610(7931), Article 7931. <https://doi.org/10.1038/s41586-022-05214-x>
- Takahara, H., Hacquard, S., Kombrink, A., Hughes, H. B., Halder, V., Robin, G. P., Hiruma, K., Neumann, U., Shinya, T., Kombrink, E., Shibuya, N., Thomma, B. P. H. J., & O’Connell, R. J. (2016). Colletotrichum higginsianum extracellular LysM proteins play dual roles in appressorial function and suppression of chitin-triggered plant immunity. *The New Phytologist*, 211(4), 1323–1337. <https://doi.org/10.1111/nph.13994>
- Tanaka, S., Brefort, T., Neidig, N., Djamei, A., Kahnt, J., Vermerris, W., Koenig, S., Feussner, K., Feussner, I., & Kahmann, R. (2014). A secreted Ustilago maydis effector promotes virulence by targeting anthocyanin biosynthesis in maize. *ELife*, 3, e01355. <https://doi.org/10.7554/eLife.01355>
- Tanaka, S., Schweizer, G., Rössel, N., Fukada, F., Thines, M., & Kahmann, R. (2019). Neofunctionalization of the secreted Tin2 effector in the fungal pathogen Ustilago maydis. *Nature Microbiology*, 4(2), Article 2. <https://doi.org/10.1038/s41564-018-0304-6>
- Tian, F., Yang, D.-C., Meng, Y.-Q., Jin, J., & Gao, G. (2020). PlantRegMap: Charting functional regulatory maps in plants. *Nucleic Acids Research*, 48(D1), D1104–D1113. <https://doi.org/10.1093/nar/gkz1020>
- Tollot, M., Assmann, D., Becker, C., Altmüller, J., Dutheil, J. Y., Wegner, C.-E., & Kahmann, R. (2016). The WOPR Protein Ros1 Is a Master Regulator of Sporogenesis and Late Effector Gene Expression in the Maize Pathogen Ustilago maydis. *PLoS Pathogens*, 12(6), e1005697. <https://doi.org/10.1371/journal.ppat.1005697>
- Torres, D. E., Thomma, B. P. H. J., & Seidl, M. F. (2021). Transposable Elements Contribute to Genome Dynamics and Gene Expression Variation in the Fungal Plant Pathogen Verticillium dahliae. *Genome Biology and Evolution*, 13(7), evab135. <https://doi.org/10.1093/gbe/evab135>
- Toruño, T. Y., Stergiopoulos, I., & Coaker, G. (2016). Plant-Pathogen Effectors: Cellular Probes Interfering with Plant Defenses in Spatial and Temporal Manners. *Annual Review of Phytopathology*, 54, 419–441. <https://doi.org/10.1146/annurev-phyto-080615-100204>
- Turian, G., & Hamilton, R. H. (1960). Chemical detection of 3-indolylacetic acid in Ustilago zeae tumors. *Biochimica Et Biophysica Acta*, 41, 148–150. [https://doi.org/10.1016/0006-3002\(60\)90381-4](https://doi.org/10.1016/0006-3002(60)90381-4)
- Underwood, W. (2012). The Plant Cell Wall: A Dynamic Barrier Against Pathogen Invasion. *Frontiers in Plant Science*, 3, 85. <https://doi.org/10.3389/fpls.2012.00085>
- Uribe, X., Torres, M. A., Capellades, M., Puigdomènech, P., & Rigau, J. (1998). Maize alpha-tubulin genes are expressed according to specific patterns of cell

Bibliography

- differentiation. *Plant Molecular Biology*, 37(6), 1069–1078. <https://doi.org/10.1023/a:1006067710312>
- van den Burg, H. A., Harrison, S. J., Joosten, M. H. A. J., Vervoort, J., & de Wit, P. J. G. M. (2006). Cladosporium fulvum Avr4 protects fungal cell walls against hydrolysis by plant chitinases accumulating during infection. *Molecular Plant-Microbe Interactions: MPMI*, 19(12), 1420–1430. <https://doi.org/10.1094/MPMI-19-1420>
- van der Graaff, E., Dulk-Ras, A. D., Hooykaas, P. J., & Keller, B. (2000). Activation tagging of the LEAFY PETIOLE gene affects leaf petiole development in Arabidopsis thaliana. *Development*, 127(22), 4971–4980. <https://doi.org/10.1242/dev.127.22.4971>
- van der Linde, K., Hemetsberger, C., Kastner, C., Kaschani, F., van der Hoorn, R. A. L., Kumlehn, J., & Doehlemann, G. (2012). A Maize Cystatin Suppresses Host Immunity by Inhibiting Apoplastic Cysteine Proteases. *The Plant Cell*, 24(3), 1285–1300. <https://doi.org/10.1105/tpc.111.093732>
- van der Linde, K., Mueller, A. N., Hemetsberger, C., Kashani, F., van der Hoorn, R. A. L., & Doehlemann, G. (2012). The maize cystatin CC9 interacts with apoplastic cysteine proteases. *Plant Signaling & Behavior*, 7(11), 1397–1401. <https://doi.org/10.4161/psb.21902>
- Villajuana-Bonequi, M., Matei, A., Ernst, C., Hallab, A., Usadel, B., & Doehlemann, G. (2019). Cell type specific transcriptional reprogramming of maize leaves during Ustilago maydis induced tumor formation. *Scientific Reports*, 9(1), Article 1. <https://doi.org/10.1038/s41598-019-46734-3>
- Wan, J., Tanaka, K., Zhang, X.-C., Son, G. H., Brechenmacher, L., Nguyen, T. H. N., & Stacey, G. (2012). LYK4, a Lysin Motif Receptor-Like Kinase, Is Important for Chitin Signaling and Plant Innate Immunity in Arabidopsis. *Plant Physiology*, 160(1), 396–406. <https://doi.org/10.1104/pp.112.201699>
- Wan, J., Zhang, X.-C., Neece, D., Ramonell, K. M., Clough, S., Kim, S., Stacey, M. G., & Stacey, G. (2008). A LysM Receptor-Like Kinase Plays a Critical Role in Chitin Signaling and Fungal Resistance in Arabidopsis. *The Plant Cell*, 20(2), 471–481. <https://doi.org/10.1105/tpc.107.056754>
- Wang, C., Yang, Q., & Yang, Y. (2011). Characterization of the ZmDBP4 gene encoding a CRT/DRE-binding protein responsive to drought and cold stress in maize. *Acta Physiologiae Plantarum*, 33(2), 575–583. <https://doi.org/10.1007/s11738-010-0582-y>
- Wang, D., Tian, L., Zhang, D.-D., Song, J., Song, S.-S., Yin, C.-M., Zhou, L., Liu, Y., Wang, B.-L., Kong, Z.-Q., Klosterman, S. J., Li, J.-J., Wang, J., Li, T.-G., Adamu, S., Subbarao, K. V., Chen, J.-Y., & Dai, X.-F. (2020). Functional analyses of small secreted cysteine-rich proteins identified candidate effectors in Verticillium dahliae. *Molecular Plant Pathology*, 21(5), 667–685. <https://doi.org/10.1111/mpp.12921>
- Wang, G., Yuan, Z., Zhang, P., Liu, Z., Wang, T., & Wei, L. (2020). Genome-wide analysis of NAC transcription factor family in maize under drought stress and rewatering. *Physiology and Molecular Biology of Plants*, 26(4), 705–717. <https://doi.org/10.1007/s12298-020-00770-w>
- Wang, H., Wang, S., Wang, W., Xu, L., Welsh, L. R. J., Gierlinski, M., Whisson, S. C., Hemsley, P. A., Boevink, P. C., & Birch, P. R. J. (2023). Uptake of oomycete RXLR effectors into

- host cells by clathrin-mediated endocytosis. *The Plant Cell*, koad069. <https://doi.org/10.1093/plcell/koad069>
- Wang, L., Liu, H., Zhang, M., Ye, Y., Wang, L., Zhu, J., Chen, Z., Zheng, X., Wang, Y., & Wang, Y. (2022). Microbe-derived non-necrotic glycoside hydrolase family 12 proteins act as immunogenic signatures triggering plant defenses. *Journal of Integrative Plant Biology*, 64(10), 1966–1978. <https://doi.org/10.1111/jipb.13337>
- Wang, M., Weiberg, A., & Jin, H. (2015). Pathogen small RNAs: A new class of effectors for pathogen attacks. *Molecular Plant Pathology*, 16(3), 219–223. <https://doi.org/10.1111/mpp.12233>
- Wang, N., Ryan, L., Sardesai, N., Wu, E., Lenderts, B., Lowe, K., Che, P., Anand, A., Worden, A., van Dyk, D., Barone, P., Svitashhev, S., Jones, T., & Gordon-Kamm, W. (2023). Leaf transformation for efficient random integration and targeted genome modification in maize and sorghum. *Nature Plants*, 1–16. <https://doi.org/10.1038/s41477-022-01338-0>
- Wang, S., Boevink, P. C., Welsh, L., Zhang, R., Whisson, S. C., & Birch, P. R. J. (2017). Delivery of cytoplasmic and apoplastic effectors from *Phytophthora infestans* haustoria by distinct secretion pathways. *New Phytologist*, 216(1), 205–215. <https://doi.org/10.1111/nph.14696>
- Wang, S., Chang, Y., Guo, J., & Chen, J.-G. (2007). Arabidopsis Ovate Family Protein 1 is a transcriptional repressor that suppresses cell elongation. *The Plant Journal*, 50(5), 858–872. <https://doi.org/10.1111/j.1365-313X.2007.03096.x>
- Wang, W., Vignani, R., Scali, M., Sensi, E., & Cresti, M. (2004). Post-translational modifications of alpha-tubulin in *Zea mays* L are highly tissue specific. *Planta*, 218(3), 460–465. <https://doi.org/10.1007/s00425-003-1122-4>
- Wang, Y., Pruitt, R. N., Nürnberger, T., & Wang, Y. (2022). Evasion of plant immunity by microbial pathogens. *Nature Reviews Microbiology*, 20(8), Article 8. <https://doi.org/10.1038/s41579-022-00710-3>
- Wang, Y., Xu, Y., Sun, Y., Wang, H., Qi, J., Wan, B., Ye, W., Lin, Y., Shao, Y., Dong, S., Tyler, B. M., & Wang, Y. (2018). Leucine-rich repeat receptor-like gene screen reveals that *Nicotiana* RXEG1 regulates glycoside hydrolase 12 MAMP detection. *Nature Communications*, 9(1), Article 1. <https://doi.org/10.1038/s41467-018-03010-8>
- Win, J., Chaparro-Garcia, A., Belhaj, K., Saunders, D. G. O., Yoshida, K., Dong, S., Schornack, S., Zipfel, C., Robatzek, S., Hogenhout, S. A., & Kamoun, S. (2012). Effector biology of plant-associated organisms: Concepts and perspectives. *Cold Spring Harbor Symposia on Quantitative Biology*, 77, 235–247. <https://doi.org/10.1101/sqb.2012.77.015933>
- Win, J., Morgan, W., Bos, J., Krasileva, K. V., Cano, L. M., Chaparro-Garcia, A., Ammar, R., Staskawicz, B. J., & Kamoun, S. (2007). Adaptive Evolution Has Targeted the C-Terminal Domain of the RXLR Effectors of Plant Pathogenic Oomycetes. *The Plant Cell*, 19(8), 2349–2369. <https://doi.org/10.1105/tpc.107.051037>
- World Population Prospects 2022: Summary of Results*. (n.d.). United Nations Department of Economic and Social Affairs, Population Division. Retrieved April 24, 2023, from <https://www.un.org/development/desa/pd/content/World-Population-Prospects-2022>

Bibliography

- Wu, A., Allu, A. D., Garapati, P., Siddiqui, H., Dortay, H., Zanol, M. I., Asensi Fabado, M. A., Munné Bosch, S., Antonio, C., Tohge, T., Fernie, A. R., Kaufmann, K., Xue, G. P., Mueller Roeber, B., & Balazadeh, S. (2012). JUNGBRUNNEN1, a Reactive Oxygen Species-Responsive NAC Transcription Factor, Regulates Longevity in Arabidopsis. *The Plant Cell*, 24(2), 482–506. <https://doi.org/10.1105/tpc.111.090894>
- Wu, R., & Citovsky, V. (2017). Adaptor proteins GIR1 and GIR2. II. Interaction with the co-repressor TOPLESS and promotion of histone deacetylation of target chromatin. *Biochemical and Biophysical Research Communications*, 488(4), 609–613. <https://doi.org/10.1016/j.bbrc.2017.05.085>
- Xia, Y., Ma, Z., Qiu, M., Guo, B., Zhang, Q., Jiang, H., Zhang, B., Lin, Y., Xuan, M., Sun, L., Shu, H., Xiao, J., Ye, W., Wang, Y., Wang, Y., Dong, S., Tyler, B. M., & Wang, Y. (2020). N-glycosylation shields Phytophthora sojae apoplastic effector PsXEG1 from a specific host aspartic protease. *Proceedings of the National Academy of Sciences of the United States of America*, 117(44), 27685–27693. <https://doi.org/10.1073/pnas.2012149117>
- Xu, F., Jia, M., Li, X., Tang, Y., Jiang, K., Bao, J., & Gu, Y. (2021). Exportin-4 coordinates nuclear shuttling of TOPLESS family transcription corepressors to regulate plant immunity. *The Plant Cell*, 33(3), 697–713. <https://doi.org/10.1093/plcell/koaa047>
- Xu, G., Zhong, X., Shi, Y., Liu, Z., Jiang, N., Liu, J., Ding, B., Li, Z., Kang, H., Ning, Y., Liu, W., Guo, Z., Wang, G.-L., & Wang, X. (2020). A fungal effector targets a heat shock-dynammin protein complex to modulate mitochondrial dynamics and reduce plant immunity. *Science Advances*, 6(48), eabb7719. <https://doi.org/10.1126/sciadv.abb7719>
- Yang, S., Fu, Y., Zhang, Y., Peng Yuan, D., Li, S., Kumar, V., Mei, Q., & Hu Xuan, Y. (2022). Rhizoctonia solani transcriptional activator interacts with rice WRKY53 and grassy tiller 1 to activate SWEET transporters for nutrition. *Journal of Advanced Research*, S2090-1232(22)00216-8. <https://doi.org/10.1016/j.jare.2022.10.001>
- Yip Delormel, T., & Boudsocq, M. (2019). Properties and functions of calcium-dependent protein kinases and their relatives in Arabidopsis thaliana. *New Phytologist*, 224(2), 585–604. <https://doi.org/10.1111/nph.16088>
- Yuan, M., Jiang, Z., Bi, G., Nomura, K., Liu, M., Wang, Y., Cai, B., Zhou, J.-M., He, S. Y., & Xin, X.-F. (2021). Pattern-recognition receptors are required for NLR-mediated plant immunity. *Nature*, 592(7852), Article 7852. <https://doi.org/10.1038/s41586-021-03316-6>
- Zahiri, A., Heimel, K., Wahl, R., Rath, M., & Kämper, J. (2010). The Ustilago maydis forkhead transcription factor Fox1 is involved in the regulation of genes required for the attenuation of plant defenses during pathogenic development. *Molecular Plant-Microbe Interactions: MPMI*, 23(9), 1118–1129. <https://doi.org/10.1094/MPMI-23-9-1118>
- Zang, Z., Lv, Y., Liu, S., Yang, W., Ci, J., Ren, X., Wang, Z., Wu, H., Ma, W., Jiang, L., & Yang, W. (2020). A Novel ERF Transcription Factor, ZmERF105, Positively Regulates Maize Resistance to Exserohilum turcicum. *Frontiers in Plant Science*, 11, 850. <https://doi.org/10.3389/fpls.2020.00850>
- Zeng, T., Rodriguez-Moreno, L., Mansurkhodzaev, A., Wang, P., van den Berg, W.,

- Gascioli, V., Cottaz, S., Fort, S., Thomma, B. P. H. J., Bono, J.-J., Bisseling, T., & Limpens, E. (2020). A lysin motif effector subverts chitin-triggered immunity to facilitate arbuscular mycorrhizal symbiosis. *The New Phytologist*, 225(1), 448–460. <https://doi.org/10.1111/nph.16245>
- Zhang, L., Yan, J., Fu, Z., Shi, W., Ninkuu, V., Li, G., Yang, X., & Zeng, H. (2021). FoEG1, a secreted glycoside hydrolase family 12 protein from *Fusarium oxysporum*, triggers cell death and modulates plant immunity. *Molecular Plant Pathology*, 22(5), 522–538. <https://doi.org/10.1111/mpp.13041>
- Zhang, Wu, X., Findley, S., Wan, J., Libault, M., Nguyen, H. T., Cannon, S. B., & Stacey, G. (2007). Molecular evolution of lysin motif-type receptor-like kinases in plants. *Plant Physiology*, 144(2), 623–636. <https://doi.org/10.1104/pp.107.097097>
- Zhang, Y., Behrens, I. von, Zimmermann, R., Ludwig, Y., Hey, S., & Hochholdinger, F. (2015). LATERAL ROOT PRIMORDIA 1 of maize acts as a transcriptional activator in auxin signalling downstream of the Aux/IAA gene rootless with undetectable meristem 1. *Journal of Experimental Botany*, 66(13), 3855–3863. <https://doi.org/10.1093/jxb/erv187>
- Zhou, J., & Zhang, Y. (2020). Plant Immunity: Danger Perception and Signaling. *Cell*, 181(5), 978–989. <https://doi.org/10.1016/j.cell.2020.04.028>
- Zhou, Z., Bi, G., & Zhou, J.-M. (2018). Luciferase Complementation Assay for Protein-Protein Interactions in Plants. *Current Protocols in Plant Biology*, 3(1), 42–50. <https://doi.org/10.1002/cppb.20066>
- Zhu, Z., Xu, F., Zhang, Y., Cheng, Y. T., Wiermer, M., Li, X., & Zhang, Y. (2010). Arabidopsis resistance protein SNC1 activates immune responses through association with a transcriptional corepressor. *Proceedings of the National Academy of Sciences of the United States of America*, 107(31), 13960–13965. <https://doi.org/10.1073/pnas.1002828107>
- Ziemann, S., van der Linde, K., Lahrmann, U., Acar, B., Kaschani, F., Colby, T., Kaiser, M., Ding, Y., Schmelz, E., Huffaker, A., Holton, N., Zipfel, C., & Doehlemann, G. (2018). An apoplastic peptide activates salicylic acid signalling in maize. *Nature Plants*, 4(3), 172–180. <https://doi.org/10.1038/s41477-018-0116-y>
- Zipfel, C. (2014). Plant pattern-recognition receptors. *Trends in Immunology*, 35(7), 345–351. <https://doi.org/10.1016/j.it.2014.05.004>
- Zlobin, N., Lebedeva, M., Monakhova, Y., Ustinova, V., & Taranov, V. (2021). An ERF121 transcription factor from *Brassica oleracea* is a target for the conserved TAL-effectors from different *Xanthomonas campestris* pv. *Campestris* strains. *Molecular Plant Pathology*, 22(5), 618–624. <https://doi.org/10.1111/mpp.13048>
- Zuo, W., Depotter, J. R. L., Gupta, D. K., Thines, M., & Doehlemann, G. (2021). Cross-species analysis between the maize smut fungi *Ustilago maydis* and *Sporisorium reilianum* highlights the role of transcriptional change of effector orthologs for virulence and disease. *New Phytologist*, 232(2), 719–733. <https://doi.org/10.1111/nph.17625>
- Zuo, W., Depotter, J. R. L., Stolze, S. C., Nakagami, H., & Doehlemann, G. (2023). A transcriptional activator effector of *Ustilago maydis* regulates hyperplasia in maize during pathogen-induced tumor formation (p. 2023.03.06.531288). *bioRxiv*.

Bibliography

- <https://doi.org/10.1101/2023.03.06.531288>
Zuo, W., Depotter, J. RL., & Doehlemann, G. (2020). Cas9HF1 enhanced specificity in *Ustilago maydis*. *Fungal Biology*, 124(3), 228–234.
<https://doi.org/10.1016/j.funbio.2020.02.006>
Zuo, W., Ökmen, B., Depotter, J. R. L., Ebert, M. K., Redkar, A., Misas Villamil, J., & Doehlemann, G. (2019). Molecular Interactions Between Smut Fungi and Their Host Plants. *Annual Review of Phytopathology*, 57(1), 411–430.
<https://doi.org/10.1146/annurev-phyto-082718-100139>

6 Appendix

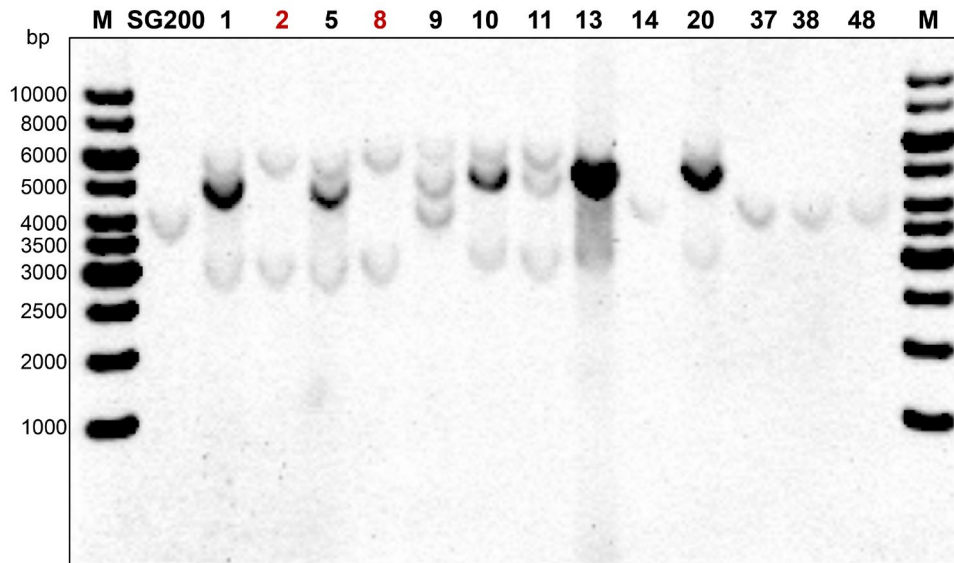


Fig. 1. Southern blot analysis of the *U. maydis* Δ Tip6 complementation strain. Genomic DNA was extracted from the indicated strains, digested with the *SacI* restriction enzymes, and separated on a 0.8% agarose gel. The Southern blot was probed with a DNA fragment specific to the *ip* locus, and hybridization was performed according to standard protocols. Lanes 1 and 16 contain a molecular weight marker (M), and lanes 2-15 correspond to the following strains: Lane 2, SG200 strain; Lanes 3-15, different transformants of Δ Tip6 complementation strains. The ladder sizes of the bands are indicated on the left. The expected sizes for the *ip* locus are SG200: 4756 bp, single integration: 3502 bp and 7014 bp, multiple integration: 3502 bp, 5760 bp and 7014 bp. Colonies 2 and 8 (shown in red font) are confirmed to have a single integration based on band size.

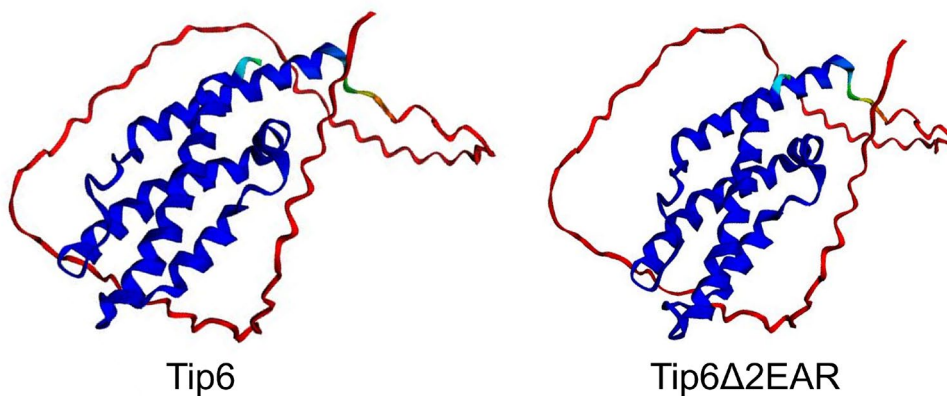


Fig. 2. AlphaFold prediction of the structure of Tip6 and Tip6 Δ 2EAR. The left panel shows the predicted structure of Tip6, and the right panel shows the predicted structure of Tip6 Δ 2EAR, a truncated version of Tip6 in which the two EAR motifs have been deleted. The predicted structures were generated using the AlphaFold protein structure prediction. The protein sequences used for the prediction of Tip6 and Tip6 Δ 2EAR included the signal peptide and the mature protein sequence, which were obtained from the EnsemblFungi database (https://fungi.ensembl.org/Ustilago_maydis).

Appendix

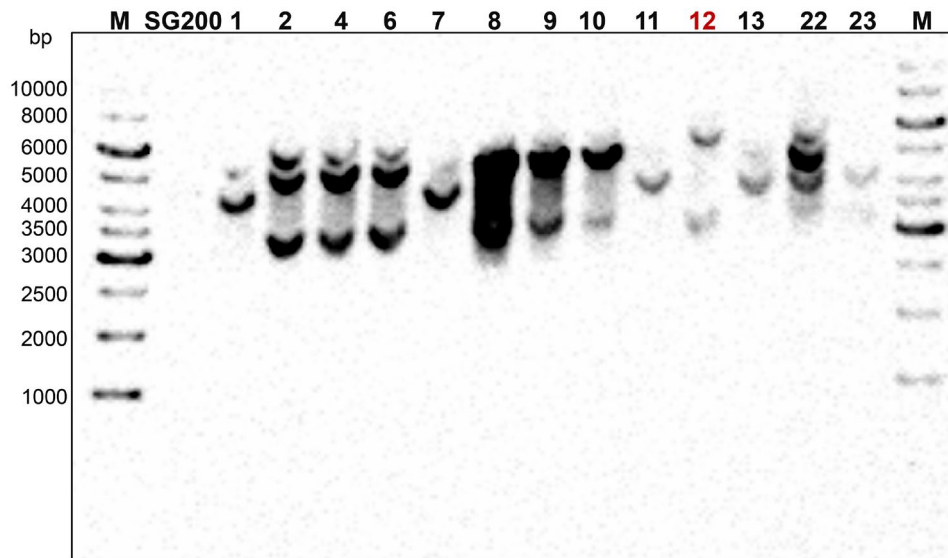


Fig. 3. Southern blot analysis of the *U. maydis* Tip6EArm complementation strain. Genomic DNA was extracted from the indicated strains, digested with the *SacI* restriction enzymes, and separated on a 0.8% agarose gel. A DNA probe specific to the *ip* locus was hybridized to the southern blot, which was performed according to standard protocols. Lanes 1 and 16 contain a molecular weight marker (M), and lanes 2-15 correspond to the following strains: Lane 2, SG200 strain; Lanes 3-15, different transformants of Tip6EArm complementation strains. The ladder sizes of the bands are indicated on the left. The expected sizes for the *ip* locus are SG200: 4756 bp, single integration: 3502 bp and 7014 bp, multiple integration: 3502 bp, 5760 bp and 7014 bp. Colonies 12 is confirmed to have a single integration based on band size.

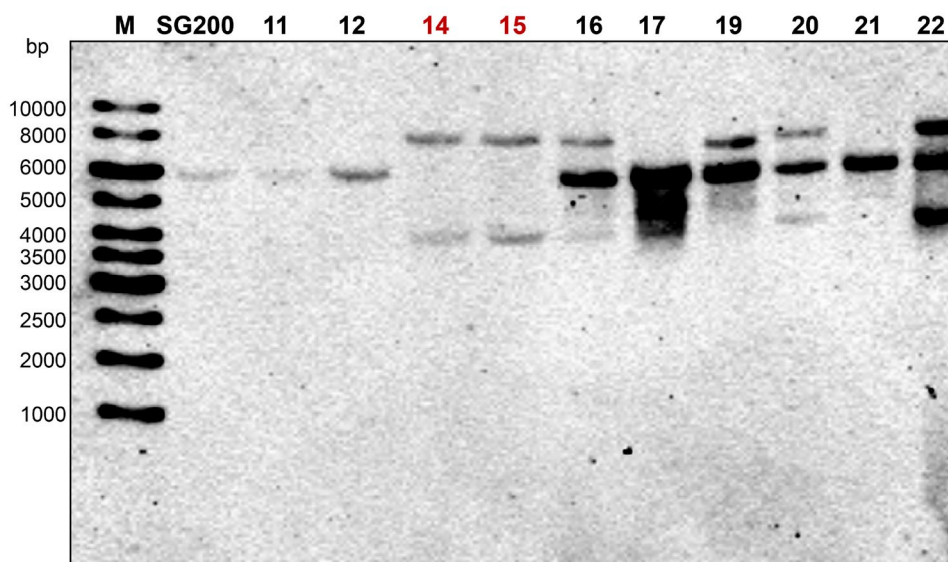


Fig. 4. Southern blot analysis of the *U. maydis* Δ UMAG_05306 complementation strain. Genomic DNA was extracted from the indicated strains, digested with the *EcorV* and *XbaI* restriction enzymes, and separated on a 0.8% agarose gel. A DNA probe specific to the *ip* locus was hybridized to the southern blot, which was performed according to standard protocols. Lane 1 contains a molecular weight marker (M), and lanes 2-12 correspond to the following strains: Lane 2, SG200 strain; Lanes 3-12, different transformants of Δ UMAG_05306 complementation strains. The ladder sizes of the bands

are indicated on the left. The expected sizes for the *ip* locus are SG200: 6112 bp, single integration: 4090 bp and 8048 bp, multiple integration: 4090 bp, 6026 bp and 8048 bp. Colonies 14 and 15 are confirmed to have a single integration based on band size.

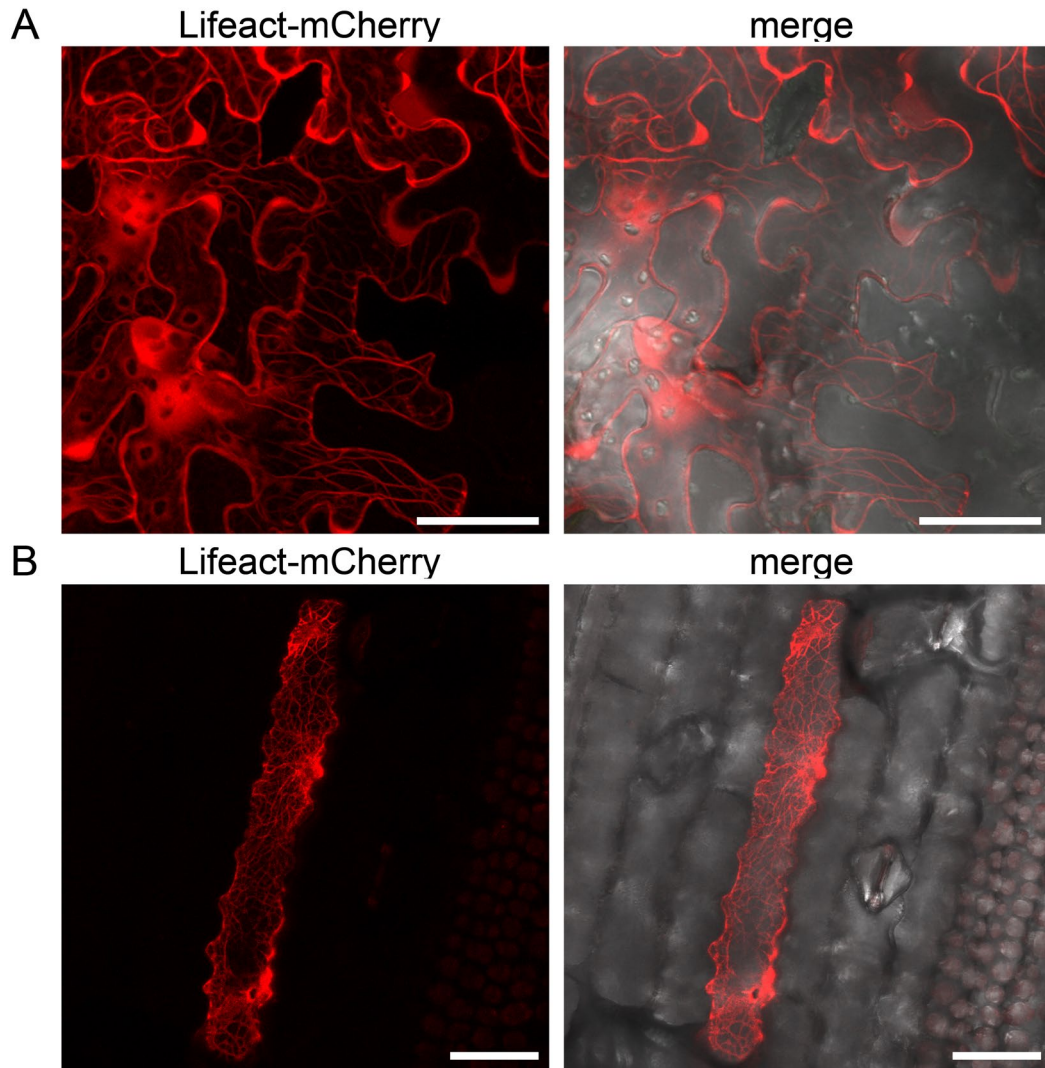


Fig. 5. Lifeact in *N. benthamiana* and *Z. mays*. **A.** Confocal image of *N. benthamiana* expressing Lifeact-mCherry. Lifeact-mCherry was expressed in *N. benthamiana* by *Agrobacterium*-mediated transformation. Scale bar, 50 μ m. **B.** Confocal image of maize expressing Lifeact-mCherry. Lifeact-mCherry was expressed in maize via biolistic bombardment. Scale bar, 50 μ m.

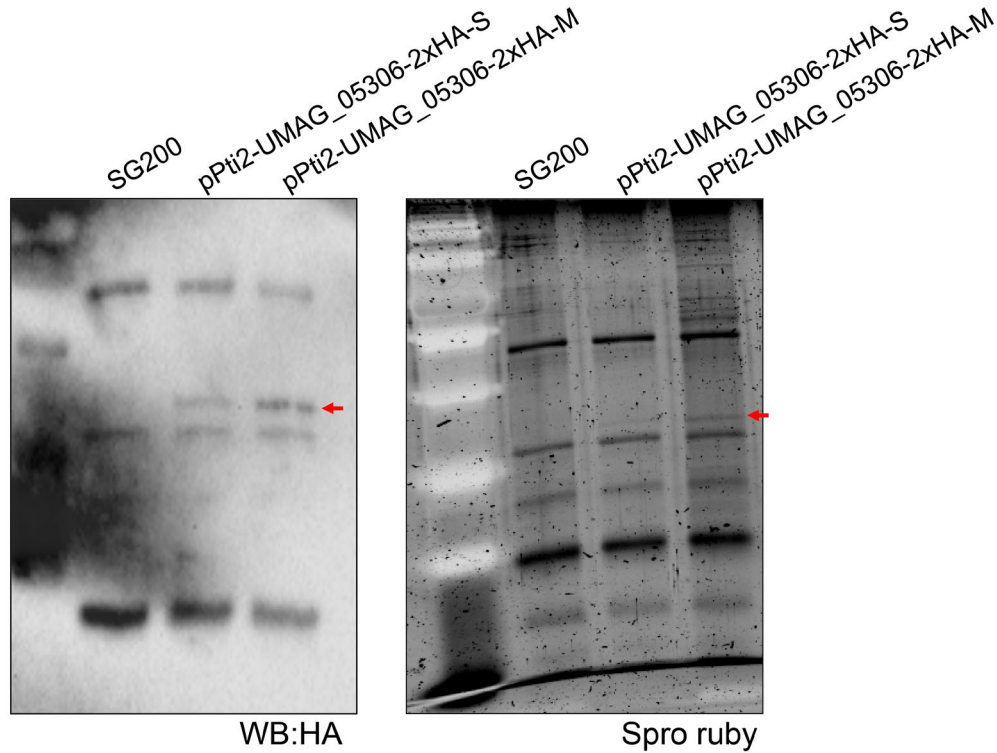


Fig. 6. Expression of UMAC_05306-2xHA in infected maize leaves. 7-day-old maize plants were infected with a Δ UMAG_05306 knockout strain expressing UMAC_05306-2xHA under the *pit2* promoter. Infected leaves were collected at 3 dpi, and total proteins were extracted and immunoprecipitated using HA magnetic beads. The resulting Western blot analysis using an anti-HA antibody and SDS-PAGE gel stained with Sypro ruby dye confirmed the expression of UMAC_05306-2xHA in infected maize leaves, with an expected size of 34.8 kDa. The S and M indicate single and multiple integration strains.

Tab. 1. Differential expression of TFs in the Δ Tip6 vs. SG200 comparison

gene	protein name	Short name	change
Zm00001eb330200	branched silkless1(EREB151)	bd1	down
Zm00001eb092300	ofp11-OVATE-transcription factor 11	ofp11	down
Zm00001eb015020	ereb26-AP2-EREBP-transcription factor 26	ereb26	down
Zm00001eb029770	arftf33-ARF-transcription factor 33	arftf33	down
Zm00001eb396160	bzip77-bZIP-transcription factor 77	bzip77	down
Zm00001eb255230	vq31-VQ motif-transcription factor31	vq31	down
Zm00001eb103460	srs2-SHI/STY (SRS)-transcription factor 2	srs2	down
Zm00001eb421530	ereb125-AP2-EREBP-transcription factor 125	ereb125	up
Zm00001eb168150	zim11-ZIM-transcription factor 11	zim11	up
Zm00001eb264150	GeBP-transcription factor 15	GeBP15	up
Zm00001eb337270	wrky80-WRKY-transcription factor 80	wrky80	up
Zm00001eb103100	dbf3-DRE-binding protein3	dbf3	up
Zm00001eb269420	dbp4-DRE-binding protein4	dbp4	up
Zm00001eb193550	ereb13-AP2-EREBP-transcription factor 13	ereb13	up
Zm00001eb373370	ereb217-AP2-EREBP-transcription factor 217	ereb217	up

Zm00001eb318900	ereb23-AP2-EREBP-transcription factor 23	ereb23	up
Zm00001eb318890	ereb36-AP2-EREBP-transcription factor 36	ereb36	up
Zm00001eb299720	nactf73-NAC-transcription factor 73	nactf73	up

Tab. 2. Differential expression of TFs in the Tip6EArm vs. SG20 comparison

gene	Protein name	Short name	change
Zm00001eb330200	branched silkless1(EREB151)	bd1	down
Zm00001eb092300	ofp11-OVATE-transcription factor 11	ofp11	down
Zm00001eb352200	glk25-G2-like-transcription factor 25	glk25	down
Zm00001eb424870	nactf15-NAC-transcription factor 15	nactf15	down
Zm00001eb058360	hagtf6-GNAT-transcription factor 6	hagtf6	down
Zm00001eb033630	bZIP-transcription factor 126	bZIP126	down
Zm00001eb100410	HSF-transcription factor 2	HSF2	down
Zm00001eb428800	hsftf20-HSF-transcription factor 20	hsftf20	down
Zm00001eb268770	MYB-transcription factor 1	MYB1	down
Zm00001eb405450	MYB-transcription factor 69	MYB69	down
Zm00001eb060160	vq11-VQ motif-transcription factor 11	vq11	down
Zm00001eb228670	mybr96-MYB-related-transcription factor 96	mybr96	down
Zm00001eb048740	zim21-ZIM-transcription factor 21	zim21	down
Zm00001eb239380	HSF-transcription factor 18	HSF18	down
Zm00001eb382780	MADS-transcription factor 47	MADS47	down
Zm00001eb418630	GeBP-transcription factor 11	GeBP11	down
Zm00001eb119420	ofp13-OVATE-transcription factor 13	ofp13	down
Zm00001eb170920	col17-C2C2-CO-like-transcription factor 17	col17	down
Zm00001eb427470	yab14-yabby14	yab14	down
Zm00001eb073550	ereb105-AP2-EREBP-transcription factor 105	ereb105	up
Zm00001eb168040	ereb106-AP2-EREBP-transcription factor 106	ereb106	up
Zm00001eb318910	ereb115-AP2-EREBP-transcription factor 115	ereb115	up
Zm00001eb156040	ereb126-AP2-EREBP-transcription factor 126	ereb126	up
Zm00001eb187190	ereb127-AP2-EREBP-transcription factor 127	ereb127	up
Zm00001eb250560	ereb16-AP2-EREBP-transcription factor 16	ereb16	up
Zm00001eb398110	ereb173-AP2-EREBP-transcription factor 173	ereb173	up
Zm00001eb021440	ereb188-AP2-EREBP-transcription factor 188	ereb188	up
Zm00001eb279090	ereb27-AP2-EREBP-transcription factor 27	ereb27	up
Zm00001eb414830	ereb51-AP2-EREBP-transcription factor 51	ereb51	up
Zm00001eb074730	ereb6-AP2-EREBP-transcription factor 6	ereb6	up
Zm00001eb103110	ereb65-AP2-EREBP-transcription factor 65	ereb65	up
Zm00001eb401290	ereb71-AP2-EREBP-transcription factor 71	ereb71	up
Zm00001eb198410	bZIP-transcription factor 81	bZIP81	up
Zm00001eb103100	dbf3-DRE-binding protein3	dbf3	up
Zm00001eb269420	dbp4-DRE-binding protein4	dbp4	up
Zm00001eb193550	ereb13-AP2-EREBP-transcription factor 13	ereb13	up
Zm00001eb373370	ereb217-AP2-EREBP-transcription factor 217	ereb217	up
Zm00001eb318900	ereb23-AP2-EREBP-transcription factor 23	ereb23	up

Appendix

Zm00001eb318890	ereb36-AP2-EREBP-transcription factor 36	ereb36	up
Zm00001eb250650	ofp23-OVATE-transcription factor 23	ofp23	up
Zm00001eb273120	Homeobox-transcription factor 81	Homeobox81	up
Zm00001eb238570	bZIP-transcription factor 89	bZIP89	up
Zm00001eb275080	WRKY-transcription factor 114	WRKY114	up
Zm00001eb163680	zhd9-ZF-HD-transcription factor 9	zhd9	up
Zm00001eb401480	bHLH-transcription factor 21	bHLH21	up
Zm00001eb186150	bbx12-b-box12(B-box zinc finger protein 20)	bbx12	up
Zm00001eb299720	nactf73-NAC-transcription factor 73	nactf73	up

Tab. 6. Oligonucleotides used in this study

Name	Sequence	Application
Um11060-F	AAGCTTCATATGCGCCGGGTGGCCTTGCATAG	Tip6C
Um11060-R1	TGCTCACCATGGAACCACTTGAACGTACGC	Tip6C
Um11060-R2	TGCTCACCATGGCGACAAGAGGCCAGGCTGTG	Tip6C
Mo11060-1F	TTGGTCTCAAATGCTACCACCTTCCAGCTC	Moclo UMAG_11060
Mo11060-1R	TTGGTCTCACCCTGTCTGCCAAAGACACC	Moclo UMAG_11060
Mo11060-2F	TTGGTCTCAAGGGTGAGAGGATCTCGCATGTA	Moclo UMAG_11060
Mo11060-2R	TTGGTCTCACGAAGCGGCCTTGTAGTTCCCTGAAGAC	Moclo UMAG_11060
MoZmTPL1-1F	TTGGTCTCAAATGAAGTACTTCGAGGAGAAG	Moclo ZmTPL1
MoZmTPL1-1R	TTGGTCTCAATACCTTCATAGAAGAAGCTTCGTATTG	Moclo ZmTPL1
MoZmTPL1-2F	TTGGTCTCAGTATCAGGTGCTCCTGTTG	Moclo ZmTPL1
MoZmTPL1-2R	TTGGTCTCACGAAGCTCTTTGGATTTGATCCGCAG	Moclo ZmTPL1
MoZmTPL2-F	TTGGTCTCAAATGACATCGCTCAGCCGTG	Moclo ZmTPL2
MoZmTPL2-R	TTGGTCTCACGAAGCTCTTTCTGGTTGGTCAGAACTT	Moclo ZmTPL2
MoZmTPL3-F	TTGGTCTCAAATGTCGTCTCTTAGCAGG	Moclo ZmTPL3
MoZmTPL3-R	TTGGTCTCACGAAGCCCTTGTTGGCTGATCAGATG	Moclo ZmTPL3
MoZmTPL4-F	TTGGTCTCAAATGGCATATAGCGCAGATGG	Moclo ZmTPL4
MoZmTPL4-R	TTGGTCTCACGAAGCTCTTTTCAGGTTGATCAGAACTT	Moclo ZmTPL4
AD-ZmTPL1-F	GTACCAGATTACGCTCATATGAAGTACTTCGAGGAGAAG	pGADT7-ZmTPL1
AD-ZmTPL1-R	GCAGCTCGAGCTCGATGGACTATCTTTGGATTTGATCCG	pGADT7-ZmTPL1
AD-ZmTPL2-F	CGTACCAGATTACGCTCATATGACATCGCTCAGCCGTG	pGADT7-ZmTPL2
AD-ZmTPL2-R	GCAGCTCGAGCTCGATGGATCATCTTTCTGGTTGGTC	pGADT7-ZmTPL2
AD-ZmTPL3-F	CGTACCAGATTACGCTCATATGTCGTCTCTTAGCAGGG	pGADT7-ZmTPL3
AD-ZmTPL3-R	GCAGCTCGAGCTCGATGGATCACCTTGTGGCTGATC	pGADT7-ZmTPL3
AD-ZmTPL4-F	CGTACCAGATTACGCTCATATGGCATATAGCGCAGATGG	pGADT7-ZmTPL4
AD-ZmTPL4-R	GCAGCTCGAGCTCGATGGATCATCTTTCAGGTTGATCAG	pGADT7-ZmTPL4
AD-ZmTPL2N-R	GCTCGAGCTCGATGGATCAACTGTTTGCTGGTGATGG	pGADT7-ZmTPL2N
AD-ZmTPL2C-F	CGTACCAGATTACGCTCATATGGCAAACAGTCCGTTACTT GG	pGADT7-ZmTPL2C
AD-ZmTPL2-CRA-F	AGGCCTGGATCCTCGCGAATGCGGTCAAAGGCTGTT	pGADT7-ZmTPL2-CRA
AD-ZmTPL2-CRA-R	ATGGTGATGATGACTAGTACTGTTTGCTGGTGATGG	pGADT7-ZmTPL2-CRA

Appendix

AD-ZmTPL2-Lish-CTLH-F	AGGCCTGGATCCTCGCGAATGACATCGCTCAGCCGTG	pGADT7-ZmTPL2-Lish-CTLH
AD-ZmTPL2-Lish-CTLH-R	ATGGTGATGATGACTAGTTTCAACAGCCTTTGACCG	pGADT7-ZmTPL2-Lish-CTLH
BD-11060-1F	CTCAGAGGAGGACCTGCATATGCTACCACCTTCCAG	pGBKT7-UMAG_11060
BD-11060-1R	CATCCTTCCCTGTCATGCTCGTTGCCAAC	pGBKT7-UMAG_11060ΔEAR1
BD-11060-2F	GAGCATGACAGGGAAGGATGGTCCGAAG	pGBKT7-UMAG_11060ΔEAR2
BD-11060-2R	CCGCTGCAGGTCGACGTCAGGCCTTGTAAGTTCCTGA	pGBKT7-UMAG_11060ΔEAR2
BD-11060m-2F	GAGCATGACGCCGATTGTCCCTCGGAAG	pGBKT7-UMAG_11060
BD-11060m-1R	CAATCCGGCGTCATGCTCGTTGCCAAC	pGBKT7-UMAG_11060
BD-Sr14941-F	CAGAGGAGGACCTGCATATGTTTACAGCGAGCGCAGCTCC	pGBKT7-Sr14941
BD-Sr14941-R	CCGCTGCAGGTCGACGTTAGGGCTTGAATTTCCCTC	pGBKT7-Sr14941
ZmTPL2m-F	CTTAGCGTCTTTGCATCCTTCAATGAGGAGTTGTTCAAGG	amplification
	AGATCGCATCGCTTCTAACCTTGTCGAAT	ZmTPL2m
ZmTPL2m-R	TTTGACAAGGTTAGAAGCGATGCGATCTCCTTGAACAAC	amplification
	TCCTCATTGAAGGATGCAAAGACGCTAAG	ZmTPL2m
ZmTPL2m-2F	AGGACCTTAGCGTCTTTG	amplification
		ZmTPL2m
ZmTPL2m-1R	CAAAGACGCTAAGGTCCTTG	amplification
		ZmTPL2m
ZmTPL2N-F	AGGCCTGGATCCTCGCGAATGGCAAACAGTCCGTTAC	pHAT2-6xHis-ZmTPL2N-6xHis
UMAG_11060-F	ATTGTACTGAGAGTGCACCATATGCGCCGGGTGGCCTT	UMAG_11060EARm-3xHA
UMAG_11060-R	AGACGGTATGCTGAACGAGCTCTGGTTCGAATCTTATG	UMAG_11060EARm-3xHA
UMAG_11060m-F	GCGGTCCAAGTACCGAAGGTGTCTTTGGAAGACAG	UMAG_11060EARm-3xHA
UMAG_11060m-R	CTGTCTTCCAAAGACACCTTCGGTACTTGGACCGC	UMAG_11060EARm-3xHA
UMAG_11060-3F	GCAAGGGAAGGATGGTC	UMAG_11060EARm-3xHA
UMAG_11060-2R	GGACCATCCTTCCCTTGC	UMAG_11060EARm-3xHA
UMAG_11060-2F	GTCCAAGTACCGAAGCTGCGGCTGCAGGTGTCTTTGGAAG	UMAG_11060EARm-3xHA
	AC	
UMAG_11060-1R	GTCTTCCAAAGACACCTGCAGCCGCAGCTTCGGTACTTGG	UMAG_11060EARm-3xHA
	AC	

Appendix

UMAG_11060-F1	ATTGTACTGAGAGTGCACCATATGCGCCGGGTGGCCTT	Nde1 site
UMAG_11060-R1	GTCTTCCAAAGACACCTGCAGCCGCAGCTTCGGTACTTGG ACC	mutation EAR1
UMAG_11060-F2	CCAAGTACCGAAGCTGCGGCTGCAGGTGTCTTTGG	mutation EAR1
UMAG_11060-R2	GGACCATCCTTCCCTTGC	mutation EAR2
UMAG_11060-F3	GCAAGGGAAGGATGGTC	mutation EAR2
UMAG_11060-R3	TCTTGGACACTTCGTCCCGGGTGCTTGGGGCACGTTG	Sac1 site
UMAG_11060-F1	CAGATTGTACTGAGAGTGCACCATATGCGCCGGGTGGCCT TGCATAGG	Nde1 site
Um05306-R2	TGCTCACCATGGGTGCGGCAAGTGCCTTGG	for complementation
Um05306-F	AAGCTTCATATGCCTGCACATCTCAACATCTG	for complementation
Um05306-R1	TGCTCACCATGGATGCCAACACGATAGTCACC	for complementation
Lifeact-F	CACTCTGTGGTCTCAAATGGGTGTGCGAGATTTGATCAAG AAATTCGAAAGCATCTCAAAGGAAGAAATGGTGAGCAAG GGCGAGGAG	Lifeact-mCherry marker
Lifeact-R	GCCACTTCGTGGTCTCAAAGCTCACTTGTACAGCTCGTCC ATGC	Lifeact marker
05306-1F	TTGGTCTCAAATGAGCGATGACGAGCTTG	Moclo UMAG_05306
05306-1R	TTGGTCTCATCGTGACGACGACGGGACAT	Moclo UMAG_05306
05306-2F	TTGGTCTCAACGACATTTGCGAAGGCTTC	Moclo UMAG_05306
05306-2R	TTGGTCTCACGAAGCAGTAGGCGGTCTGTAAGTG	Moclo UMAG_05306
ZmDRP1C-F	TTGGTCTCAAATGGCGACCATGGAGAGCCTGA	Moclo ZmDRP1C
ZmDRP1C-F	AAGGTCTCACGAAGCTTTCCATGCGACCGAGTCGAT	Moclo ZmDRP1C
ZmDRP3A-F	TTGGTCTCAAATGGCCGAAGACCACTTCTC	Moclo ZmDRP3A
ZmDRP3A-R	TTGGTCTCACGAAGCAAAACCATTGCCACTCGTTGCG	Moclo ZmDRP3A
ZmDRP4C-F	TTGGTCTCAAATGCCTAAGAAGGGTCACATGGGG	Moclo ZmDRP4C
ZmDRP4C-R	AAGGTCTCACGAAGCGATGTCACCAGCCGCGCTAA	Moclo ZmDRP4C
ZmDRP5A-F	TTGGTCTCAAATGGATAAATTGATCACCTCGTCAACAAG CTGCAGAGGGCCTGCACGGCTCTCGGCGACCAC	Moclo ZmDRP5A
ZmDRP5A-R	AAGGTCTCACGAAGCTTTGGACCATGCGACTGCATC	Moclo ZmDRP5A
ZmTub6 α -F	TTGGTCTCAAATGAGAGAGATCATCAGCATCC	Moclo ZmTub6 α
ZmTub6 α -R	TTGGTCTCACGAAGCATAGTCATCGCCCTCGTCAC	Moclo ZmTub6 α
ZmTub3 β -F	TTGGTCTCAAATGAGGGAGATCCTGCACA	Moclo ZmTub3 β
ZmTub3 β -R	TTGGTCTCACGAAGCGGCGTGCTCCTCCTCGCC	Moclo ZmTub3 β
ZmDRP5A mutant-F	TTGGTCTCAAATGGATAAATTGATCACCTCGTCAACAAG CTGCAGAGGGCCTGCACGGCTCTCGGCGACCACGGAGAGG AGAGTGCACTCCCGACGCTCACAATTGCAGAGCTGGAAAC	Moclo ZmDRP5A C- terminal
ZmDRP5A mutant-R	TTGGTCTCACGAAGCTTTGGACCATGCGACTGCATC	Moclo ZmDRP5A C- terminal

ZmDRP5A	TTGGTCTCAAATGTGGGACTCGCTGCCGGCCATC	Moclo ZmDRP5A
GTPase-F		GTPase
ZmDRP5A	TTGGTCTCACGAAGCCTTTGTTATAAGAGATTGGATCCC	Moclo ZmDRP5A
GTPase-R		GTPase
MoZmTub3 α -F	TTGGTCTCAAATGAGGGAGTGCATCTCCG	Moclo ZmTub3 α
MoZmTub3 α -R	TTGGTCTCACGAAGCGTATTCTCCTCCTCGTCAC	Moclo ZmTub3 α
UMAG_05306-F	GACGACGACAAATTAATTATGCAGTTCAGCTGCCACAC	nLuc-UMAG_05306
UMAG_05306-R	GACGCGTACGAGATCTGGCGAGTAGGCGGTCTGTAAG	nLuc-UMAG_05306
ZmDRP1C-F	GGAGGTCAGATCTCGTACATGGCGACCATGGAGAG	ZmDRP1C-cLuc
ZmDRP1C-R	GGGTGAGACCAGTTAATTTTCCATGCGACCGAGTC	ZmDRP1C-cLuc
ZmTub3 β -F	GCGGAGGTCAGATCTCGTACATGAGGGAGTGCATCTC	ZmTub3 β -cLuc
ZmTub3 β -R	GGGTGAGACCAGTTAATGTATTCTCCTCCTCGTC	ZmTub3 β -cLuc

Tip6C: Tip6 α complementation

Erklärung zur Dissertation

gemäß der Promotionsordnung vom 12. März 2020

Hiermit versichere ich an Eides statt, dass ich die vorliegende Dissertation selbstständig und ohne die Benutzung anderer als der angegebenen Hilfsmittel und Literatur angefertigt habe. Alle Stellen, die wörtlich oder sinngemäß aus veröffentlichten und nicht veröffentlichten Werken dem Wortlaut oder dem Sinn nach entnommen wurden, sind als solche kenntlich gemacht. Ich versichere an Eides statt, dass diese Dissertation noch keiner anderen Fakultät oder Universität zur Prüfung vorgelegen hat; dass sie - abgesehen von unten angegebenen Teilpublikationen und eingebundenen Artikeln und Manuskripten - noch nicht veröffentlicht worden ist sowie, dass ich eine Veröffentlichung der Dissertation vor Abschluss der Promotion nicht ohne Genehmigung des Promotionsausschusses vornehmen werde. Die Bestimmungen dieser Ordnung sind mir bekannt. Darüber hinaus erkläre ich hiermit, dass ich die Ordnung zur Sicherung guter wissenschaftlicher Praxis und zum Umgang mit wissenschaftlichem Fehlverhalten der Universität zu Köln gelesen und sie bei der Durchführung der Dissertation zugrundeliegenden Arbeiten und der schriftlich verfassten Dissertation beachtet habe und verpflichte mich hiermit, die dort genannten Vorgaben bei allen wissenschaftlichen Tätigkeiten zu beachten und umzusetzen. Ich versichere, dass die eingereichte elektronische Fassung der eingereichten Druckfassung vollständig entspricht.

Datum: 02.05.2023

Unterschrift: *Luyao Huang*

Delimitation of own contribution

I independently acquired the results presented in this study without any assistance other than that stated here. As the supervisor of this study, Prof. Dr. Gunther Döhlemann provided valuable guidance and support throughout the project. The specific experimental contributions of other individuals who participated in this study are listed below:

Dr. Weiliang Zuo generated the *U. maydis* $\Delta Tip6$ strains and the CRISPR/Cas9 plasmid vector for UMAG_05306 gene mutation.

Dr. Bilal Ökmen and Daniel Hilbig performed immunoprecipitation of GFP control and UMAG_05306-GFP in *Nicotiana benthamiana* for mass spectrometry.

Dr. Bilal Ökmen and Melanie Kastl generated plasmid vectors GST-mCherry and GST-Tip6-mCherry for protein production in *E. coli*.

Dr. Hirofumi Nakagami, Sara Christina Stolze, and Anne Harzen performed mass spectrometry protein identification and original raw data analysis. (Protein Mass Spectrometry Facility, Max-Planck Institute for Plant Breeding Research, Cologne, Germany)

Dr. Ulla Neumann performed fixation, sectioning, observation, and imaging of the transmission electron microscopy samples of UMAG_05306 and the control. (Central Microscopy, CEMIC, Max-Planck Institute for Plant Breeding Research, Cologne, Germany)

Shan Gao analyzed the raw RNA-Seq data and generated the count files used for differential gene expression analyses.

Acknowledgements

First and foremost, I would like to express my deepest gratitude to my supervisor, Prof. Dr. Gunther Döhlemann, for giving me the opportunity to join his research group and pursue my research interests. His unwavering support, expertise and constructive suggestions have helped me develop my research skills and scientific perspective. I am also grateful for his assistance in securing the necessary funding to complete my study. I would like to thank my thesis committee members, Prof. Dr. Martin Hülskamp and Dr. Takaki Maekawa, for their valuable feedback and insightful suggestions during my project discussions. I would like to express my sincere gratitude to Prof. Dr. Armin Djamei for his support and guidance during my six-week stay in his lab. I am grateful to Prof. Dr. Bart Thomma for his willingness to serve as the second reviewer on my thesis defense committee despite his busy schedule. I am also grateful to Dr. Isabell Witt from the GSfBS for facilitating informative and beneficial workshops.

Furthermore, I want to express my gratitude to all of my colleagues in the lab group for their support, advice, encouragement, and friendship throughout my study. The success of this project would not have been possible without the teamwork and collaboration of everyone involved. Particularly, I want to thank Weiliang, Wei, Sina, and Bilal for their invaluable help with project discussions, experimental suggestions, thesis revisions, and other aspects that were essential for the successful completion of my project. I am also grateful to Gudrun, Johana, Ute, Rapha and Jan for their support and guidance throughout my time in the lab.

I would like to acknowledge the financial support provided by the China Scholarship Council and the University of Cologne. These funds enabled me to pursue my research and were instrumental in the success of this thesis.

Last but not least, I want to express my heartfelt appreciation to my family and friends for their constant love, encouragement, and unwavering belief in me.

Curriculum Vitae

Luyao Huang

Born on November 7th, 1992 in Chongqing, China.

Education

10/2018-
4/2023 Doctoral program in biology at CEPLAS/University of Cologne, Germany.

Thesis topic: functionally characterize *Ustilago maydis* effectors *UMAG_11060* and *UMAG_05306*. (Supervised by Prof. Dr. Gunther Doehlemann)

09/2015-
06/2018 Master of Agriculture, major in Plant Protection, Institute of Agricultural and Biological Technology, Zhejiang University, Hangzhou, China.

Thesis topic: functional analyses of *MoCDK8* in *Magnaporthe oryzae*. (Supervised by Prof. Dr. Xiaohong Liu)

09/2011-
06/2015 Bachelor of Agriculture, major in Plant Protection, Hainan University, Haikou, China.

Thesis topic: Molecular cloning of the *CMR1* gene involved in melanin synthesis from the fungal pathogen *Colletotrichum gloeosporioides*. (Supervised by Prof. Dr. Xiaomei Liu)